REMARKS

THE CLAIM AMENDMENTS

Applicants have canceled claim 80.

Applicants have amended radical "R^2" in claims 22, 45, 48, 51-52, 54, 57-58, 60-62, 64-65, and 67-69 to further clarify the subject matter intended therein. Applicants have recited the phrase:

"CO_2H, CH_2CO_2H or C_{1-6} alkyl esters, C_{3-10} cycloalkyl esters, or cholesterol esters thereof; or primary, secondary or tertiary amides thereof; wherein suitable substituents on the nitrogen of said amides includes one or more C_{1-6} alkyl groups optionally substituted with $N(R)_2$ or 5-6 membered heterocyclic rings containing 1-2 heteroatoms; and wherein R is linear or branched C_{1-12} aliphatic;"

after the term "R^2 is" and in place of the phrase:

"i) CO_2H, or an ester, or an amide thereof; or R^2 is an isostere of said CO_2H; or
ii) CH_2CO_2H, or an ester, or an amide thereof; or R^2 is an isostere of said CH_2CO_2H"

Support for this amendment is found throughout the specification as originally filed (see, e.g., page 12, lines 26-31 and page 13, lines 1-12).

Applicants have amended radical "R^2" in claim 41 to further clarify the subject matter intended therein. Applicants have recited the phrase:

"CO_2H, or C_{1-6} alkyl esters, C_{3-10} cycloalkyl esters, or cholesterol esters thereof; or primary, secondary or tertiary amides thereof; wherein suitable substituents on the nitrogen of said amides includes one or more C_{1-6} alkyl groups optionally substituted with $N(R)_2$ or 5-6 membered heterocyclic rings containing 1-2 heteroatoms; and wherein R is linear or branched C_{1-12} aliphatic;"

after the term "wherein R^2 is" and in place of the phrase:

"CO_2H, or an ester, or an amide thereof; or R^2 is an isostere of said CO_2H."

Support for this amendment is found throughout the specification as originally filed (see, e.g., page 12, lines 26-31 and page 13, lines 1-12).

Applicants have amended claim 69 by inserting an "and" between the definition of radical R^2 and radical R^4 and R^5 to further clarify the claim.

Applicants have amended claim 79 by inserting the phrase "a caspase-mediated disease selected from" after the term "A method of treating" to clarify the type of diseases intended. Support for this amendment is found throughout the specification as originally filed (see, e.g., page 4, lines 19-22). In response to the telephonic discussion with the Examiner on 8/16/05, applicants have removed the following diseases; "an inflammatory disease, glomerulonephritis, burns, traumatic brain injury, spinalcord injury, amyotrophic lateral sclerosis, multiple sclerosis, pancreatitis, various forms of liver and renal disease, chronic active hepatitis, hepatitis B, and treatment for complications associated with coronary bypass grafts". Applicants have also recited the disease "acute renal failure" in place of the term "various forms of liver and renal disease" to further clarify the type of renal disease intended. Applicants have recited the definitions of radicals R^1, R^2, R^3, R^4, R^5, R, Z, and Y after the structure of the compound of formula I to insure all the limitations of independent claim 79 are recited.

Applicants have amended claim 81 to depend from claim 22. Therein, applicants have deleted the phrase "of formula I" and recited the phrase "according to claim 22".

None of the above amendments adds any new matter. These amendments are further discussed below in the context of the Examiner's objections and rejections.

THE OBJECTIONS

The Examiner has objected to claims 36 and 37 as being dependent upon rejected base claim 22. As discussed above, applicants have amended claim 22 to overcome the Examiner's rejection. Applicants now believe that claim 22 is in condition for allowance and that therefore claims 36 and 37, which depend therefrom, are also in condition for allowance. Therefore, applicants request that the Examiner withdraw this objection.

THE REJECTIONS

35 U.S.C. § 112, Second Paragraph

Applicants respond below to the Examiner's specific assertions using the enumeration set forth in the Office Action.

i) Claims 22 and 39-81 stand rejected under 35 U.S.C. § 112, second paragraph, as being indefinite for failing to point out and distinctly claim the subject matter of the invention. Specifically, the Examiner asserts that the definition of radical R^2 as "$-CO_2H$ or $-CH_2CO_2H$, or an ester or an amide thereof" is open-ended. As noted above, and as suggested by the Examiner, applicants have amended claims 22, 41, 45, 48, 51-52, 54, 57-58, 60-62, 64-65, and 67-69 to clarify the definition of radical R^2. Accordingly, applicants respectfully request that the Examiner withdraw this rejection.

ii) The Examiner has rejected claim independent 79 for failing to recite all the limitations of the radicals for compounds of formula I. As discussed above, applicants have amended claim 79 to recite the definitions of radicals R^1, R^2, R^3, R^4, R^5, R, Z, and Y. Therefore, claim 79, as amended, now recites all the limitations of compounds of formula I. Accordingly, applicants respectfully request that the Examiner withdraw this rejection.

iii) The Examiner has rejected claim 80 for depending from improper independent claim 79. As discussed above, applicants have canceled claim 80 thereby obviating this rejection.

35 U.S.C. § 112, First Paragraph

Claims 79-81 stand rejected for lack of enablement under 35 U.S.C. § 112, first paragraph. Specifically, the Examiner contends that the amended list of diseases in claim 79 raise additional problems. The Examiner suggests that "'inflammatory disease' embraces inflammation from any cause, not just caspase mediated ones". Likewise the Examiner contends that "pancreatitis [and] various forms of liver and renal disease" embrace diseases which result from other diseases not associated with caspases. Additionally, the Examiner acknowledged the references submitted by applicants in support of the claimed diseases. However, the Examiner could not see the authors conclusions in sixteen* of the references because only the single page abstracts were submitted. Lastly, the Examiner contends "most of the remaining papers are speculative and say that more research is required". Applicants traverse in light of the amendments discussed above and for the reasons below.

The methods of the present invention are drawn to treating diseases wherein caspase plays a regulatory role. See, e.g., specification page 4, lines 19-32, page 5, lines 1-4, page 8, lines 13-16, page 31, lines 15-21, page 37, lines 4-32, and page 38, lines 1-13 claims 79-81, as filed. Applicants have clarified this aspect of the invention in claim 79 by amending it to recite "a caspase-mediated disease selected from".

*Applicants have submitted, herewith, full copies of Exhibits 4, 7, 9-12, 15, 17, 19-21, and 23-25 in response to the Examiner's comments.

Additionally, applicants have discussed the role of caspases in inflammatory diseases (see specification at page 3, lines 1-13), in apoptotic disorders (see specification at page 1, lines 19-27), and a variety of other mammalian diseases associated with an increase in cellular apoptosis (see specification at page 4, lines 19-32 and page 5, lines 1-4). Applicants have also expressly disclosed examples of such diseases (see specification at page 37, lines 4-32 and page 38, lines 1-13).

Thus, the twin requirements of an identifiable disease state and caspase regulation underpinning such a disease state ensures that the methods of the present invention do not read on disease states implicated by non-caspase pathways.

The caspase art and applicants' specification provide ample evidence of the regulatory role of caspase in various diseases (see, e.g., Exhibits 1-42 in the December 21, 2004 response and in the specification page 2, lines 14-24, page 3, lines 5-15, page 4, lines 10-30). And, applicants have extensively demonstrated the ability of the compounds of the present invention to inhibit caspase activity, IL-1ß secretion, and Fas-induced apoptosis (see specification at page 74, lines 25-27 to page 79, line 24).

For the above reasons, one of skill in the art will readily appreciate that:

(a) the methods of claims 79-81 are drawn to a scope that is readily ascertained and encompasses disease states only associated with caspase activity; and

(b) this scope is commensurate with applicants disclosure and exemplification of caspase inhibitory activity and by the references/exhibits provided.

Furthermore, the MPEP states that "the applicant does not have to provide evidence sufficient to establish that an asserted utility is true 'beyond a reasonable doubt' In re Irons, 340 F.2d 974, 978 (CCPA 1965)." See, MPEP § 2164.07.

Based on the amendments to claim 79 discussed above, the specification as filed, the 14 full references provided herewith in support of the claimed diseases, and the evidence of record provided by applicants in their December 21, 2004 response, applicants believe they have provided credible evidence to support the claimed caspase-mediated diseases. Therefore, for all of the reasons set forth above, applicants request that the Examiner withdraw this § 112, first paragraph rejection.

CONCLUSION

Applicants respectfully request that the Examiner consider the foregoing remarks and allow the pending claims to pass to issue. Applicant's express their appreciation to the Examiner for helpful discussions during their August 16, 2005 phone conference. If it is believed that a telephone call would further expedite prosecution, the Examiner is invited to contact the undersigned at (617) 444-6467.

Respectfully submitted,

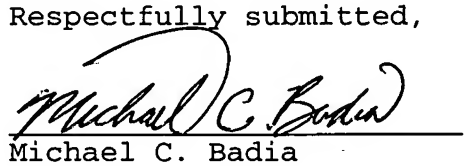

Michael C. Badia
Reg. No. 51,424
Agent for Applicants
Vertex Pharmaceuticals Inc.
130 Waverly Street
Cambridge, MA 02139-4242
Tel.: (617)444-6467
Fax.: (617)444-6483

ELSEVIER

Journal of Neuroimmunology 121 (2001) 76–78

Journal of Neuroimmunology

www.elsevier.com/locate/jneuroin

Caspase-3 activity is present in cerebrospinal fluid from patients with traumatic brain injury

Luc Härter [a,*], Marius Keel [a], Hannes Hentze [b], Marcel Leist [c], Wolfgang Ertel [a]

[a] *Department of Trauma Surgery, University Hospital Zürich, Zürich, Switzerland*
[b] *Institute of Molecular and Cell Biology, 117609 Singapore, Singapore*
[c] *H. Lundbeck A/S, 2500 Valby, Denmark*

Received 13 March 2001; received in revised form 23 July 2001; accepted 2 August 2001

Abstract

Loss of neurons after traumatic brain injury (TBI) might involve dysregulated apoptosis. Activation of caspase-3 is one hallmark of apoptosis. Therefore, caspase-3 activity (cleavage of DEVD-afc) was measured in cerebrospinal fluid (CSF) samples ($n = 113$) from 27 patients with TBI at day 1 t0 14 after trauma. Caspase-3 activity was detected in 31 (27.4%) CSF samples with highest values (> 5.5 μM/min) seen at day 2–5 after trauma. No caspase-3 activity was found in serum from patients or CSF from controls. The presence of activated caspase-3 in CSF suggests ongoing apoptotic processes during traumatic brain injury.

Keywords: Apoptosis; Neurons; Trauma; Brain; DEVD-afc; zVAD

Neuronal cell loss after traumatic brain injury (TBI) has been formerly attributed to necrosis of neurons as a result of secondary insults. More recent evidence from animal models (Rink et al., 1995) and findings in human patient tissues (Ng et al., 2000; Clark et al., 1999) point towards an involvement of apoptosis in the mechanism of neuronal destruction following TBI. Apoptosis in neurons, endothelial cells, and astrocytes is triggered through the CD95 system (Leist and Nicotera, 1998). Because high concentrations of CD95-ligand were found in cerebrospinal fluid (CSF) from patients with severe TBI (Ertel et al., 1997), this points to the involvement of apoptotic processes responsible for brain damage following TBI.

A group of intracellular cysteine proteases, called caspases has been shown to play a pivotal role in the regulation and execution of apoptosis. Within this group, caspase-3 is the main executioner protease and its activation marks a point-of-no-return in the complicated cascade of apoptosis induction. Thus, the presence of active caspase-3 is a good indicator of apoptosis. To date, it is unknown whether active caspase-3 can be released from cells dying by apoptosis into CSF following TBI.

Therefore, caspase-3 activity was examined in the CSF of 27 patients with severe TBI. All patients were treated according to our standard protocol for TBI (Stocker et al., 1995), which was approved by the University Hospital Medical Ethics Board. Three patients (11.1%) succumbed to death due to TBI. As a control, the CSF from seven patients requiring spinal anesthesia for elective orthopedic surgery (with normal CSF protein content and cell count) were included in this study after written informed consent. The control group was comparable to the trauma patients with regard to age and gender (Table 1).

CSF drained from an indwelling ventricular catheter was collected from all patients each day at 8 am between days 1 and 14 after trauma. However, in some patients, it was not possible to obtain CSF on consecutive days due to failure of the intraventricular catheter, collapsed ventricles due to extensive brain edema or death of the patient. The preflow (0,5 ml) was discarded and 1–2 ml of the sterile CSF centrifuged ($300 \times g$, 10 min, 4 °C) and then frozen immediately at −80 °C until further processing.

Caspase-3 activity in the CSF was measured by a fluorimetric assay based on the specific hydrolysis of DEVD-7-amino-4-trifluromethylcoumarin (DEVD-afc, 60 μM) in substrate buffer (50 mM HEPES, pH 7.4, 1% sucrose, 0.1% Chaps, 10 mM DDT, Thornberry, 1994). Caspase-3 activity (μM afc/min) was determined by measuring the increase of afc-fluorescence (excitation at 385 nm; fluorescence emission at 505 nm) over 30 min at 37 °C, and calculation of the afc formation/time based on an

* Corresponding author.

0165-5728/01/$ - see front matter
PII: S0165-5728(01)00409-X

Table 1
Demographic data of patients and controls

Group	n	Age[a]	Gender[b]	Mortality	AIS	ISS	GCS
Patients	27	36.1 ± 12.9	24/3	11.1%	4.8 ± 0.4	29.2 ± 11.9	7.9 ± 4.2
Controls	7	41.6 ± 9.8	6/1	–	–	–	–

AIS: abbreviated injury score (points), ISS: injury severity score (points). GCS: Glasgow coma scale (points).
[a]Mean age ± SD.
[b]Gender is given as male/female.

afc standard curve. The specificity of the assay for caspase-3 activity was confirmed by the block of fluorescence increase when samples were re-measured in the presence of the caspase inhibitors DEVD-CHO (1 μM) or zVAD-fmk (5 μM). Recovery (105 ± 10% at a mixture of sample:caspase-3 (300 μM/min) of 96:4) and sensitivity (≥ 0.5 μM/min) of the assay was regularly controlled by addition of active recombinant human caspase-3 to control CSF samples.

Caspase-3 activity was detected in 31 of 113 (27.4%) CSF samples from 20 out of 27 patients (74.1%) with TBI (Fig. 1). The highest levels of caspase-3 activity were detected between day 2 (6.5 μM/min), day 4 (5.5 μM/min) and day 5 (6.3 μM/min) after trauma and declined thereafter. In contrast to CSF from patients, caspase-3 activity was undetectable in CSF from the seven controls or in parallel serum samples from patients and controls despite addition of DTT (10 mM) to the samples which is known to reactivate caspases previously inactivated by mild oxidants or nitric oxide (NO).

The data presented here show that caspase-3 activity is present in CSF of patients with severe TBI, indicating the involvement of apoptotic processes in the brain following TBI. Undetectable caspase-3 activity in the circulation excludes secondary migration of caspase-3 through the blood–brain barrier. The identification of the mode of death in human TBI has been complicated by the fact that only post mortem material can be used where the mechanisms of death are difficult to study. Since the only form of cell death associated with caspase-3 activation is apoptosis (Leist and Jäättelä, 2001), the observation of increased activity of this protease in CSF of patients adds further evidence for the contribution of apoptosis to TBI. Thus, our results refute arguments that caspase-3 detected in post-mortem brain tissues from patients with TBI were a post-mortem artifact (Love et al., 2000).

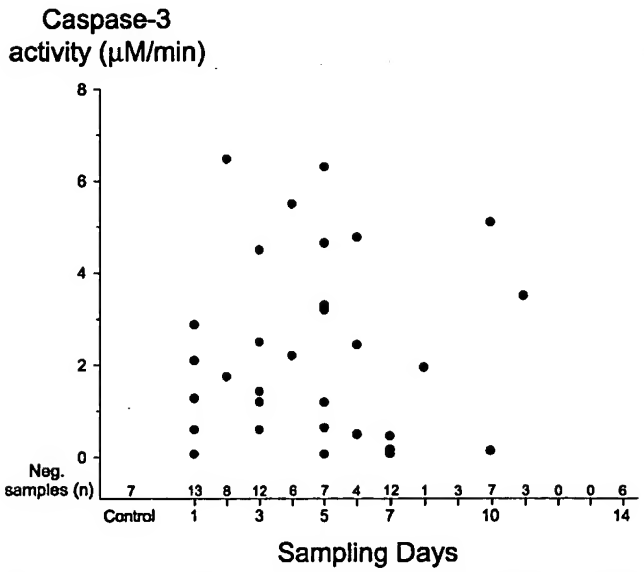

Fig. 1. Caspase-3 activity in CSF from patients with severe traumatic brain injury compared to controls. Sterile CSF was collected from patients between day 1 and 14 after trauma and from controls and immediately frozen until measurement of caspase-3 activity (μM/min).

Sampling of CSF has been used frequently as a minimally invasive method or readily available source to draw conclusions on the state of injury to the brain, and to obtain markers of predictive or diagnostic value. Besides various cytokines indicating inflammatory processes, also increased concentrations of the apoptosis-inducing CD95L have been detected (Ertel et al., 1997). This finding is now complemented by even closer evidence of ongoing apoptotic processes indicated by the release of activated caspase-3. It should be emphasized that our results do not allow localization or identification of specific cells undergoing apoptosis in the injured brain or differentiation between active involvement of caspase-3 and its release due to cell death. Although preliminary, our study demonstrates for the first time the presence of active caspase-3 in CSF from patients with severe head injuries.

Acknowledgements

We thank Heike Naumann and Andreas Rassow for expert technical assistance. This work was supported by grant 32-52932.97 from the Swiss National Science Foundation.

References

Clark, R.S., Kochanek, P.M., Chen, M., Watkins, S.C., Marion, D.W., Chen, J., Hamilton, R.L., Loeffert, J.E., Graham, S.H., 1999. Increases in Bcl-2 and cleavage of caspase-1 and caspase-3 in human brain after head injury. FASEB J. 13, 813–821.

Ertel, W., Keel, M., Stocker, R., Imhof, H.G., Leist, M., Steckholzer, U., Tanaka, M., Trentz, O., Nagata, S., 1997. Detectable concentrations

of Fas ligand in cerebrospinal fluid after severe head injury. J. Neuroimmunol. 80, 93–96.

Leist, M., Nicotera, P., 1998. Apoptosis versus necrosis: the shape of neuronal cell death. Results Probl. Cell Differ. 24, 105–135.

Leist, M., Jäättelä, M., 2001. Nat. Rev. Mol. Cell. Biol. 2 (8), 1–12.

Love, S., Barber, R., Wilcock, G.K., 2000. Neuronal death in brain infarcts in man. Neuropathol. Appl. Neurobiol. 26, 55–66.

Ng, I., Yeo, T.T., Tang, W.Y., Soong, R., Ng, P.Y., Smith, D.R., 2000. Apoptosis occurs after cerebral contusions in humans. Neurosurgery 46, 949–956.

Rink, A., Fung, K.M., Trojanowski, J.Q., Lee, V.M., Neugebauer, E., McIntosh, T.K., 1995. Evidence of apoptotic cell death after experimental traumatic brain injury in the rat. Am. J. Pathol. 147, 1575–1583.

Stocker, R., Bernays, R., Kossmann, T., Imhof, H.G., 1995. Monitoring and treatment of acute head injury. Update Intensive Care Emerg. Med. 22, 196–210.

Thornberry, N.A., 1994. Interleukin-1beta converting enzyme. Methods Enzymol. 244, 615–631.

Acta Neurol Scand 2001: 103: 255–258
Printed in UK. All rights reserved

ACTA NEUROLOGICA SCANDINAVICA
ISSN 0001-6314

Short communication

Interleukin-1β converting enzyme/Caspase-1 (ICE/Caspase-1) and soluble APO-1/Fas/CD 95 receptor in amyotrophic lateral sclerosis patients

Iłżecka J, Stelmasiak Z, Dobosz B. Interleukin-1β converting enzyme/Caspase-1 (ICE/Caspase-1) and soluble APO-1/Fas/CD 95 receptor in amyotrophic lateral sclerosis patients.
Acta Neurol Scand 2001: 103: 255–258. © Munksgaard 2001.

Objectives – The aim of the study was to investigate the role of ICE/Caspase-1 and soluble APO-1/Fas/CD 95 receptor in amyotrophic lateral sclerosis patients. *Material and methods* – The apoptosis parameters were measured by enzyme-linked immunosorbent assay (ELISA) in serum and cerebrospinal fluid from 25 amyotrophic lateral sclerosis and 15 control patients. *Results* – There has been shown a significant increase of ICE/Caspase-1 level in serum, and significant decrease of this parameter in cerebrospinal fluid from amyotrophic lateral sclerosis patients. Soluble APO-1/Fas/CD 95 level in amyotrophic lateral sclerosis patients did not differ from the control group. There was no significant correlation between clinical status, duration of amyotrophic lateral sclerosis, and levels of ICE/Caspase-1 and soluble APO-1/Fas/CD 95. *Conclusion* – Our study suggests that ICE/Caspase-1 may play a role in neurodegeneration in ALS. Due to ethical difficulties we cannot include patients suffering from progressive neurological diseases, who are a more appropriate control group for the amyotrophic lateral sclerosis patients. Therefore we are limited in drawing conclusions from the research.

J. Iłżecka, Z. Stelmasiak, B. Dobosz
Department of Neurology, Lublin Medical School, Poland

Key words: apoptosis; Caspase-1; sAPO-1; amyotrophic lateral sclerosis

Joanna Iłżecka, Department of Neurology, Lublin Medical School, Jaczewskiego 8, 20–954 Lublin, Poland

Accepted for publication December 29, 2000

It has been suggested that apoptosis may play a role in the mechanism of neurodegeneration in amyotrophic lateral sclerosis (ALS) (1). Interleukin-1β converting enzyme/Caspase-1 (ICE/Caspase-1) is a cysteine protease that shares sequence homology with the protein product of *ced-3*, the gene responsible for cell death of the *Caenorhabditis elegans*. Its homology initiated studies about the role of ICE/Caspase-1 in apoptosis (2, 3). The activation of caspases appears to play a key role in this process (4). APO-1/Fas/CD 95, a member of the tumor necrosis factor receptor superfamily, is a transmembranous protein that can transduce cell death signals via a proteolytic cascade upon cross-linking or ligand binding (5, 6). Soluble APO-1/Fas/CD 95 (sAPO-1/Fas/CD 95) is able to protect cells from Fas-mediated apoptosis (7). Triggering of CD 95 rapidly stimulates the proteolytic activity of ICE. Overexpression of ICE potentiates Fas-mediated cell death (8, 9). Determination of apoptotic parameters could help to explain the mechanism of neurodegeneration in ALS.

Material and methods

Twenty-five patients with clinically definite ALS were studied. ALS was recognized on the basis of El Escorial Criteria WFN of ALS (10). The mean duration of the disease was 1.4 years (range 3 months–4 years). According to Munsat, the ALS Health State Scale (11), the patients were divided into 4 groups: mild, moderate, severe and terminal,

and into 3 groups in dependence on time of ALS duration. Group characteristics are summarized in Table 1.

The control group consisted of 15 patients (8 males/7 females) with lumbosacral disc disease. The mean age was 55 years (range 32–69). Blood and cerebrospinal fluid were taken for examination from the patients of the control group during diagnosis. The cerebrospinal fluid was collected from a lumbar puncture performed on radiculography. Lumbosacral disc disease was confirmed by means of computer tomography or magnetic resonance imaging. The history, neurological examination and additional tests (biochemical test of blood serum, urine analysis, general examination of the cerebrospinal fluid, X-ray of the chest) allowed us to exclude other diseases which could affect the levels of ICE and sAPO-1.

The measurements were performed one time in serum and cerebrospinal fluid (CSF) from ALS and control group patients. The study was approved by the ethics committee of the Lublin Medical School.

Clinical samples were kept at 2–8°C and centrifuged rapidly before storing at −20°C to avoid loss of bioactive sAPO-1 and ICE. ICE and sAPO-1 levels were measured by sandwich enzyme-linked immunosorbent assay (ELISA) (12) using the sAPO-1/Fas ELISA and IL-1β converting enzyme (ICE/Caspase-1) ELISA (human kits from Bender MedSystems Diagnostics GmbH). Sensitivity of sAPO-1/Fas ELISA method was 20 pg/ml, and ICE/Caspase-1 ELISA method – 5 pg/ml.

For statistical analysis the Mann–Whitney *U*-test, ANOVA procedure (Kruskal–Wallis test), and Spearman rank correlation were used. *P* values <0.05 were considered significant.

Results

The mean ICE level from serum of ALS patients was significantly higher than controls ($P<0.05$), however the mean ICE level from CSF of ALS patients was significantly lower than controls ($P<0.05$). sAPO-1 levels in serum and CSF of ALS patients did not differ significantly from controls ($P>0.05$) (Table 2).

Table 1. Characteristics of ALS patients

Number of patients	25
Male/female	13/12
Age of patients	57 (34–77)
Munsat the ALS Health State Scale	
Mild	5
Moderate	7
Severe	8
Terminal	5
Time of ALS duration	
0–6 months	9
7–24 months	10
25–48 months	6

Table 2. Comparative analysis of Caspase-1 and sAPO-1 levels (pg/ml) in ALS patients with controls

Parameter	ALS patients	Controls	*P*
ICE in serum	89.3 SD 33.1	56.0 SD 14.5	0.0002*
ICE in CSF	6.36 SD 4.55	16.4 SD 9.9	0.0027*
sAPO-1 in serum	1781.6 SD 702.6	1530.2 SD 431.3	0.605
sAPO-1 in CSF	188.2 SD 36.0	184.6 SD 28.6	0.730

Mann–Whitney *U*-test. * $P<0.05$ statistical significance versus control group.

The study has shown that ICE and sAPO-1 levels in serum of ALS patients had a tendency to increase with the time of ALS duration. ICE in CSF of ALS patients has been increasing with the time of duration of ALS and with the advance of the disease, but it has been decreasing in the groups of patients with terminal clinical status and with the longest time of ALS duration. Statistical analysis showed that there was no significant correlation between clinical status, time of ALS duration, and levels of ICE and sAPO-1. The clinical status of patients and time of duration of the disease did not influence significantly ICE and sAPO-1 levels in serum and CSF of ALS patients ($P>0.05$) (Table 3).

Discussion

Experimental research conducted with the model of a transgenic SOD 1 mutant mouse and *in vitro* suggests that apoptosis may play a role in the process of the death of neurons in ALS. The mutations in Cu/Zn superoxide dismutase 1 (SOD-1) have a significant role in the pathogenesis of ALS (13). Pasinelli et al. (14) showed increased activity of ICE in motoneurons limits with expression of mutated SOD-1. ICE is activated by xanthine/xanthine oxidase which increases production and secretion of pro-interleukin 1β. Activation of ICE in SOD-1 transgenic mouse, causes changes characteristic of apoptosis process in the spinal cord area.

Table 3. Relationship of Caspase-1 and sAPO-1 levels [pg/ml] with clinical status and time of ALS duration

	Clinical status		ALS duration	
Parameter	H	*P*	H	*P*
ICE in serum	0.49	0.93	0.69	0.70
ICE in CSF	2.17	0.53	2.54	0.28
sAPO-1 in serum	0.81	0.84	1.30	0.52
sAPO-1 in CSF	0.43	0.93	1.77	0.41

H: value of Kruskal–Wallis test. $P<0.05$ statistical significance.

APO-1 can mediate cytotoxicity, and play a role in cell survival in the immune system and in the nervous system. It is presumed that in neurodegenerative diseases, among others, in ALS increased expression of CD 95–CD 95L on glial cells may lead to apoptosis (15). De la Monte et al. (16) state that death cell mechanism dependent on Fas receptor may be important in ALS. APO-1 expression increase and nuclear DNA fragmentation were shown in the motor cortex and spinal ventral horns in ALS.

Gamen et al. (17) reported that caspases play the leading role in apoptosis depending on Fas receptor. Activation of caspases takes place under the influence of the adapter protein Fas-associated death domain (FADD), as the outcome of Fas receptor stimulation by its ligand (18). This process leads to mitochondrial transmembrane potential damage. It was shown that Caspase-1-treated mitochondria release an apoptosis-inducing factor causing DNA fragmentation (19).

Caspases play an important role in the process of neurodegeneration of SOD-1 transgenic mice, which suggests that caspases inhibition may play a protective role in ALS. Intracerebroventricular administration of VAD-fmk, a caspase inhibitor, delays ALS onset and mortality (20). Milligan et al. (21) reported that peptide inhibitors of ICE proteases prevent apoptosis in motoneurons in *vivo* and in *vitro*. ICE-like proteases might affect disease progression in ALS mouse model and suggest that ICE inhibitors may be a useful treatment for ALS (22).

Vercammen et al. (23) demonstrated the existence of two different pathways originating from the Fas receptor. If one pathway is blocked by caspase inhibitors, a second leads to necrosis and oxygen radical production. That is why in ALS a combined therapy which influences different potential neurodegeneration mechanisms is most recommended.

Our study suggests that ICE may be considered when we deal with the case of the death of neurons in ALS. There are no essential differences in the levels of sAPO-1 in blood serum and in the cerebrospinal fluid of the ALS patients in comparison with the control group, but we cannot exclude that sAPO-1 receptor may play a role in the pathomechanism of the disease. No significant correlation has been found between the levels of the apoptosis parameters and the duration of the disease and the clinical state of the patients. It is difficult to interpret the findings and the conclusions are limited. We could not include into the control group the patients with other progressive neurological conditions. Due to ethical reasons we did not take the cerebrospinal fluid from them. The control group consisted of patients with lumbosacral disc disease, in whose case it was possible to take the cerebrospinal fluid during examination. In view of the fact that there is not a more appropriate control group for the ALS patients, which would be patients with progressive neurological diseases, it is difficult to say whether the findings are specific of ALS. The conclusions are also limited by a very small number of patients who took part in the research. Therefore if we want to know the potential mechanisms of the death of neurons in ALS we need further research.

References

1. Rabizadeh S, Gralla EB, Borchelt DR et al. Mutations associated with amyotrophic lateral sclerosis convert superoxide dismutase from an antiapoptotic gene to a proapoptotic gene: studies in yeast and neural cells. Proc Natl Acad Sci USA 1995;**92**:3024–8.
2. Yuan J, Shahams S, Ledoux S, Ellis HM, Horvitz HR. The *C. elegans* cell death gene *ced-3* encodes a protein similar to mammalian interleukin-1β converting enzyme. Cell 1993;**75**: 641–52.
3. Marks N, Berg MJ. Recent advances on neuronal caspases in development and neurodegeneration. Neurochem Int 1999;**35**(3):195–220.
4. Schwartz LM, Milligan CE. Cold thoughts of death: the role of ICE proteases in neuronal cell death. Trends Neurosci 1996;**19**:555–62.
5. Suda T, Takahashi T, Golstein P, Nagata S. Molecular cloning and expression of the Fas ligand, a novel member of the tumor necrosis factor family. Cell 1993;**75**:1169–78.
6. Hofmann K. The modular nature of apoptotic signaling proteins. Cell Mol Life Sci 1999;**55**:1113–28.
7. Cheng J, Zhou T, Lin C et al. Protection from Fas-mediated apoptosis by a soluble form of the Fas molecule. Science 1994;**263**:1759–62.
8. Los M, Craen M, Penning LC et al. Requirement of an ICE/CED-3 protease for Fas/APO-1-mediated apoptosis. Nature 1995;**375**:81–3.
9. Waring P, Mullbacher A. Cell death induced by the Fas/Fas ligand and its role in pathology. Immunol Cell Biol 1999;**77(4)**:312–17.
10. Brooks BR. El Escorial World Federation of Neurology criteria for the diagnosis of amyotrophic lateral sclerosis. J Neurol Sci [Suppl] 1994;**124**:96–107.
11. Riviere M, Meininger V, Zeisser P, Munsat T. An analysis of extended survival in patients with amyotrophic lateral sclerosis treated with riluzole. Arch Neurol 1998;**55**:526–8.
12. Seishima H, Takemura M, Saito K et al. Highly sensitive ELISA for soluble Fas in serum: increased soluble Fas in the elderly. Clin Chem 1996;**42**(12):1911–14.
13. Radunovic A, Leigh PN. Cu/Zn superoxide dismutase gene mutations in amyotrophic lateral sclerosis: correlation between genotype and clinical features. J Neurol Neurosurg Psych 1996;**61**:565–71.
14. Pasinelli P, Borchelt DR, Houseweart MK, Cleveland DW, Brown RH. Caspase-1 is activated in neural cells and tissue with amyotrophic lateral sclerosis-associated mutations in copper-superoxide dismutase. Proc Natl Acad Sci USA 1998;**95**(26):15763–8.
15. Becher B, Barker PA, Owens T, Antel JP. CD 95–CD 95 L: can the brain learn from the immune system? Trends Neurosci 1998;**21**(3):114–17.
16. De la Monte SM, Sohn YK, Ganju N, Wands JR. P 53 and CD 95-associated apoptosis in neurodegenerative diseases. Lab Invest 1998;**78**(4):401–11.
17. Gamen S, Anel A, Pineiro A, Naval J. Caspases are the main executioners of Fas-mediated apoptosis, irrespective of the

ceramide signaling pathway. Cell Death Differ 1998;5(3): 241–9.
18. Tatsuta T, Shivaishi A, Mountz JD. The prodomain of caspase-1 enhances Fas-mediated apoptosis through facilitation of caspase-8 activation. J Biol Chem 2000; 275:14248–54.
19. Susin SA, Zamzami N, Castedo M et al. The central executioner of apoptosis: multiple connections between protease activation and mitochondria in Fas/APO-1/CD 95- and ceramide-induced apoptosis. J Exp Med 1997;186(1): 25–37.
20. Li M, Ona VO, Guegan C et al. Functional role of caspase-1 and caspase-3 in an ALS transgenic mouse model. Science 2000;288:335–9.
21. Milligan CE, Prevette D, Yaginuma H et al. Peptide inhibitors of ICE proteases family arrest programmed cell death of motoneurons in *vivo* and in *vitro*. Neuron 1995; 15:385–93.
22. Friedlander RM, Brown RH, Gagliardini V, Wang J, Yuan J. Inhibition of ICE slows ALS in mice. Nature 1997;388 (6637):31.
23. Vercammen D, Brouckaert G, Denecker G et al. Dual signaling of the Fas receptor: initiation of both apoptotic and necrotic cell death pathways. J Exp Med 1998;188(5):919–30.

Caspase-1 Regulates the Inflammatory Process Leading to Autoimmune Demyelination[1]

Roberto Furlan,* Gianvito Martino,[2*†] Francesca Galbiati,[‡] Pietro L. Poliani,* Simona Smiroldo,[‡] Alessandra Bergami,* Gaetano Desina,*[§] Giancarlo Comi,[†] Richard Flavell,[¶] Michael S. Su,[‖] and Luciano Adorini[‡]

T cell-mediated inflammation is considered to play a key role in the pathogenic mechanisms sustaining multiple sclerosis (MS). Caspase-1, formerly designated IL-1β-converting enzyme, is crucially involved in immune-mediated inflammation because of its pivotal role in regulating the cellular export of IL-1β and IL-18. We studied the role of caspase-1 in experimental autoimmune encephalomyelitis (EAE), the animal model for MS. Caspase-1 is transcriptionally induced during EAE, and its levels correlate with the clinical course and transcription rate of proinflammatory cytokines such as TNF-α, IL-1β, IFN-γ, and IL-6. A reduction of EAE incidence and severity is observed in caspase-1-deficient mice, depending on the immunogenicity and on the amount of the encephalitogenic myelin oligodendrocyte glycoprotein (MOG) peptide used. In caspase-1-deficient mice, reduced EAE incidence correlates with defective development of anti-MOG IFN-γ-producing Th1 cells. Finally, pharmacological blockade of caspase-1 in Biozzi AB/H mice, immunized with spinal cord homogenate or MOG_{35-55} peptide, by the caspase-1-inhibitor Z-Val-Ala-DL-Asp-fluoromethylketone, significantly reduces EAE incidence in a preventive but not in a therapeutic protocol. These results indicate that caspase-1 plays an important role in the early stage of the immune-mediated inflammatory process leading to EAE, thus representing a possible therapeutic target in the acute phase of relapsing remitting MS. *The Journal of Immunology,* 1999, 163: 2403–2409.

The caspase family comprises thus far 13 different cysteine proteases that are mainly involved in the apoptotic pathway (1). Among them, caspase-1, formerly named IL-1β-converting enzyme, which is activated by caspase-11-mediated proteolytic cleavage (2), is less involved in the apoptotic cascade but is prominent in inflammation because of its pivotal role in regulating the cellular export of proinflammatory cytokines such as IL-1β. Caspase-1 is elevated in intestinal macrophages during inflammatory bowel disease (3) and in a variety of organs, including the brain, in response to bacterial LPS administration (4). Further evidence on the role played by caspase-1 in inflammation comes from studies on caspase-1-deficient (−/−) mice and caspase-1 pharmacological inhibitors. Caspase-$1^{-/-}$ mice display an alteration in the export of several proinflammatory cytokines, namely IL-1β, IL-1α, IL-6, and TNF-α, although neither IL-1α nor IL-6 nor TNF-α are substrates for caspase-1 (5). Furthermore, caspase-1 proteolytically activates IL-18, and caspase-$1^{-/-}$ mice have also reduced serum levels of IL-18 and IFN-γ in response to LPS administration (6). Caspase-$1^{-/-}$ mice are resistant to LPS-induced endotoxic shock (7) and to the induction of experimental pancreatitis (8). In vivo pharmacological inhibition of caspase-1 protects mice from TNF-α-induced liver failure (9) and collagen-induced arthritis (10).

MS[3] is an immune-mediated demyelinating disease of the CNS of unknown etiology (11). The pathological hallmark of the disease is the presence within the CNS of inflammatory infiltrates containing few autoreactive T cells and many pathogenic nonspecific mononuclear cells (12). It is currently believed that Ag-specific T cells provide the organ specificity of the pathogenic process and regulate the recirculation within the CNS of activated mononuclear cells releasing inflammatory myelinotoxic substances. These latter cells can be activated in the periphery by polyclonal inflammatory stimuli, thus determining disease recurrence (12, 13). Proinflammatory cytokines participate either in Ag-specific T cell activation or in peripheral activation of nonspecific mononuclear cells. TNF-α, IFN-γ, and IL-6 levels increase before disease relapses (13, 14). An increased number of disease relapses was observed in MS patients treated with IFN-γ (15). Moreover, TNF-α, IFN-γ, and IL-1β are present in demyelinating plaques (16), and IL-1β has been shown to be a mediator of the inflammatory process sustaining EAE, the animal model for MS (17).

We evaluated the role of caspase-1 in EAE. We found that caspase-1 mRNA blood levels parallel those of proinflammatory cytokines, such as IL-1β, IL-6, TNF-α, and IFN-γ, during EAE and peak at the time of maximal EAE severity. A reduction of EAE incidence and severity was observed in caspase-$1^{-/-}$ mice depending on the immunogenicity and on the amount of the encephalitogenic MOG peptide used. Finally, pharmacological blockade of caspase-1 reduced the incidence of EAE, induced either with SCH or MOG_{35-55} peptide, in a preventive but not therapeutic

*Experimental Neuroimmunotherapy Unit, Department of Biotechnology, and †Department of Neurology, San Raffaele Scientific Institute, Milan, Italy; ‡Roche Milano Ricerche, Milan, Italy; §Department of Neurology, Casa Sollievo della Sofferenza Scientific Institute, San Giovanni Rotondo (FG), Italy; ¶Howard Huges Medical Institute, Yale University School of Medicine, New Haven, CT 06510; and ‖Vertex Pharmaceuticals, Inc., Cambridge, MA 02139

Received for publication April 12, 1999. Accepted for publication June 10, 1999.

The costs of publication of this article were defrayed in part by the payment of page charges. This article must therefore be hereby marked *advertisement* in accordance with 18 U.S.C. Section 1734 solely to indicate this fact.

[1] This work was supported by Istituto Superiore di Sanità (Target project: Multiple Sclerosis), and Ministero dell'Università e della Ricerca Scientifica e Tecnologica.

[2] Address correspondence and reprint requests to Dr. Gianvito Martino, Department of Biotechnology-San Raffaele Scientific Institute, Via Olgettina 58, 20132 Milan, Italy. E-mail address: g.martino@hsr.it

[3] Abbreviations used in this paper: MS, multiple sclerosis; EAE, experimental autoimmune encephalomyelitis; MOG, myelin oligodendrocyte glycoprotein; SCH, spinal cord homogenate; AU, arbitrary units; p.i., postimmunization.

0022-1767/99/$02.00

protocol. These results indicate that caspase-1 plays an important role in the immune-mediated pathogenic events leading to EAE and might represent a suitable therapeutic target of the active phase of the immune-mediated inflammatory demyelination.

Materials and Methods

Mice and immunizations

Female Biozzi AB/H mice, 4–6 wk old, were purchased from Harlan U.K. (Blackthorn, U.K.). Female C57BL/6 mice, 4–6 wk old were obtained by Charles River (Calco, Italy). Female (SV129 × C57BL/6)F_1 mice, hereafter designated (SV129 × B6)F_1, 4–6 wk old, were obtained by The Jackson Laboratory (Bar Harbor, ME). Caspase-$1^{-/-}$ mice had been obtained as previously described (5). Briefly, chimeric mice were obtained by injection of embryonic stem cells, in which the caspase-1 gene was disrupted and replaced with a neomycin resistance gene cassette, into C57BL/6 blastocysts. The chimeric males were then mated with CB57BL/6 mice. Homozygous mice with two copies of the disrupted caspase-1 gene were identified by Southern blot of genomic DNA, and the absence of caspase-1 mRNA in caspase-$1^{-/-}$ mice was confirmed by RT-PCR analysis. Homozygous mice were then interbred and used for the experiments.

All animals were housed in specific pathogen-free conditions and treated according to the guidelines of the Animal Ethical Committee of our Institute. Mice were immunized with IFA (Difco, Detroit, MI) supplemented with 4 mg/ml *Mycobacterium tuberculosis* (strain H37Ra; Difco) and MOG_{35-55} (Multiple Peptide Systems, San Diego, CA), MOG_{40-55} (Roche Milano Ricerche, Milan, Italy), or SCH from Biozzi AB/H mice. Two immunization schedules were used for peptides: a single injection of 200 μg or two injections of 300 μg peptide 7 days apart. For SCH immunization, 1 mg of Ag was given twice, at days 0 and 7. All injections were followed by i.p. administration of 500 ng pertussis toxin (Sigma, St. Louis, MI) the same day and 48 h later. Body weight and clinical score (0 = healthy, 1 = flaccid tail, 2 = ataxia and/or paresis of hind limbs, 3 = paralysis of hind limbs and/or paresis of forelimbs, 4 = tetraparalysis, 5 = moribund or death) were recorded daily.

Miniosmotic pumps

Miniosmotic pumps (Alzet 2001, Alza, Palo Alto, CA) were implanted s.c. in the dorsal flank of mice. The mean fill volume of pumps was ~220 μl, and the mean pumping rate was ~1 μl/h, delivering continuously for ~10 days. Pumps were filled with 50 mg/ml of the caspase-1 inhibitor Z-Val-Ala-DL-Asp-fluoromethylketone (Bachem, Bubendorf, Switzerland) obtaining a delivery of 1.2 mg/day. Pumps were implanted 1 day before immunization (preventive protocol) or 1 week after (therapeutic protocol). Dosage of Z-Val-Ala-DL-Asp-fluoromethylketone has been deducted from previous reports showing that in vivo administration of 25–50 mg/kg of specific caspase-1 inhibitors (i.e., Z-Val-Ala-DL-Asp-fluoromethylketone, VE 13.045) completely inhibits caspase-1 enzymatic activity for several days (18, 19).

Semiquantitative RT-PCR for cytokines

Blood samples were obtained from mice by tail bleeding every week. RNA was recovered from these samples in guanidinium thiocyanate by acid phenol extraction. A T-primed first strand kit was used for the reverse transcription of total RNA into cDNA (Ready-to-go kit, Pharmacia, Uppsala, Sweden). PCR amplification (30 cycles: 1 min 95°C, 1 min 55°C, 1 min 72°C) of cDNA sequences specific for caspase-1 and cytokines was performed using 20 pmol of each primer, 200 mM concentrations of each dNTP, 25 mM KCl, 10 mM Tris-HCl (pH 8.3), 1.5 mM $MgCl_2$, and 2.5 U *Taq* polymerase. Amplified PCR products were hybridized with the specific ^{32}P-labeled oligonucleotide probe (caspase-1 and cytokines) or ^{32}P-labeled probe obtained from a plasmid containing the mouse GAPDH cDNA, followed by analysis on a PhosphorImager (Molecular Dynamics, Sunnyvale, CA; Image Quant Software, version 3.3). Values were normalized against the GAPDH gene. For interanimal comparisons, the normalized intensities were further corrected with the use of the normalized intensities of the bands resulting from RT-PCR amplification of a cDNA derived from mouse LPS-activated splenocytes (positive control). The following primers and probes were used: caspase-1 (product: 343 bp), antisense 5′-GTGTTGAAGAGCAGAAAGCA-3′, sense 5′-GAGATGGTGAAA GAGGTGAA-3′, probe 5′-TGAAAGACAAGCCCAAGG TG-3′; IL-1β (product: 563 bp), antisense 5′-CAGGACAGGTATAGATTCTTTCCTTT-3′, sense 5′-ATGGCAACTGTTCCTGAACTCAACT-3′, probe 5′-AGCTTTCAGCTCATATGGGTCCGACAGCAC-3′; IL-6 (product: 634 bp), antisense 5′-CACTAGGTTTGCCGAGTAGATCTC-3′, sense 5′-ATGAAGTTCCTCTCTGCAAGAGACT-3′, probe 5′-CTCCAGAAGAC CAGAGGAAATTTCAATAG-3′; TNF-α (product: 373 bp), antisense 5′-GTATGAGATAGCAAATGCGCTGACGGTGTGGG-3′, sense 5′-TTCTG TCTACTGAACTTCGGGGTGATCGGTCC-3′, probe 5′-GCCGTTGGC CAGGAGGGCGTTGGCGCGCTG-3′; IFN-γ (product: 450 bp), antisense 5′-ACACTGCATCTTGGCTTTGC-3′, sense 5′-CGACTCCTTTTCCGCT TCCT-3′, probe 5′-TTCTTCAGCAACAGCAAGGC-3′; GAPDH (product: 710 bp), antisense 5′-CGCATCTTCTTGTGCAGTG-3′; sense 5′-GT TCAGCTCTGGGATGAC-3′. RT-PCR results were expressed as fold induction of AU from basal levels.

Ag-specific proliferation assays

For T cell proliferation assays, draining lymph nodes were removed, and 4×10^5 lymph node cells per well were cultured in 96-well culture plates (Costar, Cambridge, MA) in synthetic HL-1 medium (Ventrex Laboratories, Portland, ME) supplemented with 2 mM L-glutamine and 50 μg/ml gentamicin (Sigma, St. Louis, MO) and serial concentrations (1, 3, 10 μM) of MOG_{40-55} peptide. Cultures were incubated for 3 days in 5% CO_2 in air and pulsed 8 h before harvesting with 1 μCi [^{3}H]TdR (40 Ci/nmol, Pharmacia Biotech, Amersham, Cologno Monzese, Italy). Incorporation of [^{3}H]TdR was measured by liquid scintillation spectrometry.

Intracytoplasmatic staining for cytokine production

Lymph node cells (6×10^5 cells/well) were cultured in 96-well culture plates in synthetic HL-1 medium with 10 μM MOG_{40-55}. After 72 h of culture cells were harvested, washed, and recultured for additional 72 h in RPMI 1640 supplemented with 2 mM L-glutamine, 50 μg/ml gentamicin, 50 μM 2-ME (Fluka Chemical, Ronkonkoma, NY), and 10% FCS (Sigma). After culture, living cells separated on a Ficoll gradient were restimulated with PMA (1 μg/ml) and ionomycin (50 ng/ml) for 4 h at 37°C, with 10 μg/ml brefeldin A (Novartis, Basel, Switzerland) added for the last 2 h to prevent egress of newly synthesized proteins from the endoplasmic reticulum. After fixation with 4% paraformaldehyde for 20 min at room temperature, cells were stained for IFN-γ and IL-4 using the method of Openshaw et al. (20) and Galbiati et al. (21). Cells were washed, preincubated for 10 min with PBS/FCS/saponin, and then incubated with FITC rat anti-mouse IFN-γ (XMG1.2, PharMingen, San Diego, CA) and PE rat anti-mouse IL-4 (11B11, PharMingen) or with isotype controls FITC- and PE-labeled rat IgG1, κ (R3-34, PharMingen). After 30 min, cells were washed twice with PBS/FCS/saponin and then with PBS containing 5% of FCS without saponin to allow membrane closure. Cell membranes were then stained with Cy-Chrome-labeled anti-CD4 (L3T4, PharMingen) for 15 min at room temperature. Analysis was performed with a FACScan flow cytometer (Becton Dickinson, Mountain View, CA) equipped with CellQuest software, and 50,000 events were acquired.

ELISA for IFN-γ secretion

IFN-γ was quantified by two-sites sandwich ELISA using polyvinyl microtiter plates (Falcon 3012) coated with AN-18.17.24 mAb in carbonate buffer as previously described (21). Samples (50 μl/well) diluted in test solution (PBS containing 5% FCS and 1 g/l phenol) were incubated together with 50 μl peroxidase-conjugated XMG1.2 mAb. After overnight incubation at room temperature, bound peroxidase was detected by 3,3′,5,5′-tetramethylbenzidine (Fluka Chemical), and adsorbance was read at 450 nm with an automated microplate ELISA reader (MR5000, Dynatech Laboratories, Chantilly, VA). IFN-γ was quantified from two to three titration points using standard curves generated by purified recombinant mouse IFN-γ, and results were expressed as cytokine concentration in ng/ml. Detection limit was 15 pg/ml.

Neuropathological features in EAE mice

At the time of sacrifice, mice were transcardially perfused with 4% paraformaldehyde. Brains and spinal cords were removed and postfixed in the same fixative for 2–4 h, washed in PBS, and then embedded in paraffin. Tissue sections were cut at 4 μm on a microtome and stained for histological examination. Hematoxylin and eosin staining was used to reveal perivascular inflammatory infiltrates, Luxol Fast Blue staining was used to reveal demyelinated areas, and Bielshowsky staining was used to detect axonal loss. Macrophages were stained using peroxidase-labeled BS-I isolectin B4 (Sigma), whereas T cells using a rat anti-CD3 Ab (pan-T cell marker; Serotec Ltd, Oxoford, U.K.) revealed using a biotin-labeled secondary anti-rat Ab (Amersham). Neuropathological findings were quantified on an average of 10 complete cross-sections of spinal cord per mouse. The number of perivascular inflammatory infiltrates was calculated and expressed as the numbers of inflammatory infiltrates per mm^2, whereas demyelinated areas and axonal loss were expressed as the percentage of

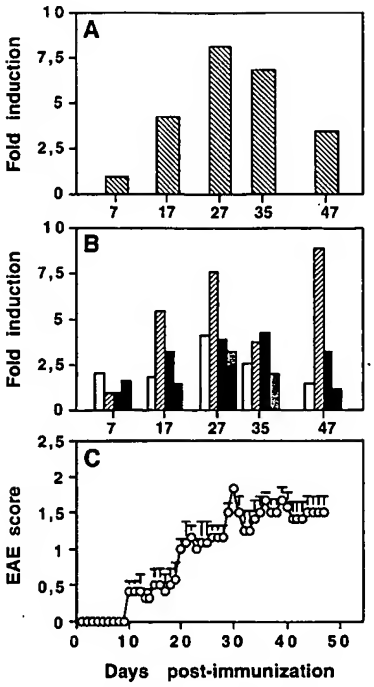

FIGURE 1. Caspase-1 and proinflammatory cytokine mRNAs are up-regulated during the course of EAE in blood from C57BL/6 mice immunized with 200 μg of MOG_{40-55}. *A*, Caspase-1 mRNA levels. *B*, mRNA levels of IL-1β (□), IL-6 (▨), IFN-γ (■), and TNF-α (▩) from the same mice. mRNA levels were measured by a semiquantitative RT-PCR on blood samples obtained from the tail vein of mice once a week. mRNA levels have been normalized against GAPDH mRNA levels and expressed as fold induction (AU increase over basal level recorded 7 days p.i.). Blood samples were obtained every week after immunization as indicated on *x*-axis. *C*, Clinical course of EAE in blood donors (n = 12 mice). Each circle represents the mean EAE score registered. Bars represent the SE.

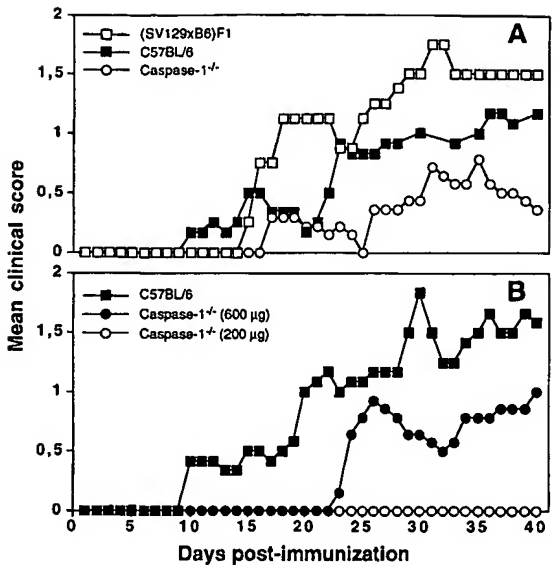

FIGURE 2. Clinical course of EAE in MOG peptide-immunized (SV129 × B6)F_1, caspase-$1^{-/-}$, and C57BL/6 mice. In caspase-$1^{-/-}$ mice, the EAE course and severity varies depending on the amount and length of the MOG peptide used. *A*, EAE immunization protocol with 200 μg MOG_{35-55} in (SV129 × B6)F_1, C57BL/6, and caspase-$1^{-/-}$ mice. Caspase-$1^{-/-}$ mice are susceptible to EAE induction but develop a less severe disease than control mice. *B*, EAE immunization protocol with 200 or 600 μg MOG_{40-55} in C57BL/6 (■ = 200 μg MOG_{40-55}) and caspase-$1^{-/-}$ mice (○ = 200 μg MOG_{40-55}; ● = 600 μg MOG_{40-55}). Immunization of caspase-$1^{-/-}$ mice with the low amount (200 μg) of the shorter peptide (MOG_{40-55}) does not lead to EAE development. Irrespective of the dose of MOG_{40-55} used, C57BL/6 mice always show a more severe EAE than do caspase-$1^{-/-}$ mice.

damaged area per mm^2 (22). T cells and macrophages were counted and expressed as the number of cells per mm^2.

Statistical analysis

Data are expressed as mean ± SE. Student's t test for unpaired data was used to compare cytokine and caspase-1 mRNA levels and the cytokine protein levels. EAE cumulative score was calculated by summing up each individual score registered in any group of mice studied during the follow-up period levels. Comparison between cumulative scores was performed using Student's t test. A χ^2 test was used to compare EAE incidence in the different groups of mice. $p < 0.05$ was considered significant.

Results

Caspase-1 mRNA is up-regulated in the course of EAE

C57BL/6 mice immunized with MOG_{40-55} were bled once a week for 5 weeks after immunization. RT-PCR was performed on blood samples to determine caspase-1, IL-1β, IL-6, TNF-α, and IFN-γ mRNA levels. Caspase-1 mRNA levels increased almost 8-fold (Fig. 1*A*) during EAE from basal levels recorded at day 7 p.i. This increase paralleled disease severity, peaking 4 wk p.i. (day 27 p.i., 52.9 ± 16.8 AU; p = 0.01 vs day 7 p.i.) (Fig. 1*A*) when EAE clinical score reached its maximum (Fig. 1*C*). Caspase-1 mRNA level increase paralleled that of the caspase-1 substrate IL-1β, which showed a 2-fold increase (day 27 p.i., 3.3 ± 0.9 AU; p = 0.03 vs day 7 p.i.) (Fig. 1*B*); IL-6 mRNA increased almost 8-fold (day 27 p.i., 15.4 ± 7.6 AU; p = 0.04) (Fig. 1*B*); TNF-α mRNA increased almost 3-fold (day 27 p.i., 12.2 ± 5.4; p = n.s. vs day 7 p.i.) (Fig. 1*B*), and IFN-γ mRNA 4-fold (day 27 p.i., 1.6 ± 0.5 AU; p = 0.02 vs day 7 p.i.) (Fig. 1*B*). These data indicate that caspase-1 is up-regulated at the transcriptional level during the course of EAE and that this up-regulation parallels that of proinflammatory cytokines such as IL-1β, IFN-γ, TNF-α, and IL-6.

Caspase-$1^{-/-}$ mice are less susceptible to EAE induction

To further explore the role of caspase-1 in EAE, we studied the susceptibility of caspase-$1^{-/-}$ mice to MOG peptide-induced EAE. We first analyzed EAE susceptibility of (SV129 × B6)F_1 and C57BL/6 mice, which have a genetic background comparable with that of the caspase-$1^{-/-}$ mice using 200 μg of MOG_{35-55}. The two groups of mice showed similar disease courses (Fig. 2*A*, Table I) confirming results previously reported (23).

To analyze EAE susceptibility in caspase-$1^{-/-}$ mice, we used two different amounts (200 μg once or 300 μg twice, 7 days apart) of two MOG overlapping peptides (MOG_{35-55} and MOG_{40-55}). MOG peptides were chosen because of their previously described difference in immunogenicity and encephalitogenicity in C57BL/6 mice (24). Low dose immunization (200 μg) with MOG_{40-55} failed to induce EAE in caspase-$1^{-/-}$ mice (0 of 12 sick animals) compared with C57BL/6 mice (11 of 12) ($p < 0.0001$) (Fig. 2*B*, Table I). Caspase-$1^{-/-}$ mice developed EAE when immunized with the low dose (200 μg) of MOG_{35-55} (Fig. 2*A*, Table I) or the high dose (600 μg) of MOG_{40-55} (Fig. 2*B*, Table I); the incidence, however, was lower and the onset delayed compared with (SV129 × B6)F_1 or C57BL/6 mice. Therefore, caspase-$1^{-/-}$ mice are less susceptible to MOG-induced EAE compared with C57BL/6 or (SV129 × B6)F_1 mice. However, caspase-$1^{-/-}$ mice can develop EAE when the immunogenicity of the encephalitogenic peptide is increased.

Table I. *EAE in (SV129 × B6)F_1, C57BL/6, and caspase-1$^{-/-}$ mice*

Mouse Strain	MOG Peptide (amount)	EAE Incidence (%)	EAE Onset (range)[a]	Maximum EAE Score (range)[b]
(SV129 × B6)F_1	MOG_{35-55} (200 μg)	4/4 (100)	20.0 ± 3.7 (16–31)	1.9 ± 0.6 (1–2.5)
C57BL/6	MOG_{35-55} (200 μg)	6/6 (100)	19.2 ± 3.0 (10–31)	1.5 ± 0.2 (1–2)
	MOG_{40-55} (200 μg)	11/12 (92)	17.3 ± 2.6 (10–30)	2.0 ± 0.1 (1.5–2.0)
Caspase-1$^{-/-}$	MOG_{40-55} (600 μg)[c]	5/7 (71)	27.8 ± 2.4 (23–34)	1.8 ± 0.4 (1.0–3.0)
	MOG_{35-55} (200 μg)	4/7 (57)	27.2 ± 3.9 (18–35)	1.9 ± 0.1 (1.5–2.0)
	MOG_{40-55} (200 μg)	0/12[d] (0)	NA[e]	NA

[a] EAE onset is expressed as day post immunization ± SE.
[b] EAE score is expressed as mean maximum score ± SE.
[c] MOG_{40-55} has been administered twice 1 wk apart (300 + 300 μg).
[d] $p < 0.0001$ vs C57BL/6 mice immunized with 200 μg MOG_{40-55}, $p = 0.03$ and $p = 0.006$ vs caspase-1$^{-/-}$ mice immunized with 200 μg MOG_{35-55} or 600 μg MOG_{40-55}, respectively.
[e] NA, not applicable.

Inhibition of the Th1 response in caspase-1-deficient mice

To elucidate the possible causes of reduced susceptibility of caspase-1$^{-/-}$ mice to EAE, we analyzed mice immunized with 200 μg of MOG_{40-55} peptide in which the most striking difference between caspase-1$^{-/-}$ and C57BL/6 was observed (Fig. 2*B*, Table I). Five caspase-1$^{-/-}$ mice and 5 C57BL/6 mice were sacrificed 10 days after immunization with MOG_{40-55}, and cells from the draining lymph nodes were obtained. Proliferation assays to MOG_{40-55} showed no impairment in the responsiveness of T cells from caspase-1$^{-/-}$ compared with C57BL/6 mice (Fig. 3*A*). We detected, however, decreased levels of IFN-γ secreted in the supernatant of MOG_{40-55} restimulated cells (Fig. 3B) from caspase-1$^{-/-}$ compared with C57BL/6 mice ($p = 0.01$). Intracytoplasmic staining for IFN-γ and IL-4 of MOG_{40-55}-restimulated cells showed reduced IFN-γ-producing cells and no induction of IL-4-producing cells (Fig. 3, *C–E*). These results suggest that cells from caspase-1$^{-/-}$ mice efficiently present the encephalitogenic peptide to T cells but are defective in Th1 development.

Caspase-1 inhibitor administration prevents but does not treat EAE

Pharmacological blockade of EAE with caspase-1 inhibitors was tested in Biozzi AB/H mice immunized with SCH or MOG_{35-55}. In Biozzi mice, SCH induces a very aggressive relapsing-remitting EAE (25), whereas MOG_{35-55} induces a more chronic progressive disease. We administered vehicle or Z-Val-Ala-DL-Asp-fluoromethylketone, a highly specific, cell-permeable, and irreversible inhibitor of caspase-1-like proteases (26) to Biozzi mice before immunization with SCH or MOG_{35-55}. Because this caspase-1 inhibitor is a peptide with a very short half-life in vivo, we implanted s.c. mini-osmotic pumps able to continuously release the inhibitor for 10 days. Continuous administration of the caspase-1 inhibitor induced a clearcut suppression of either SCH-induced or MOG_{35-55}-induced EAE compared with vehicle-treated mice (Table II). The cumulative EAE score, representing the disease burden, was significantly lower in caspase-1 inhibitor-treated mice than in vehicle-treated mice in both immunization protocols (Table II).

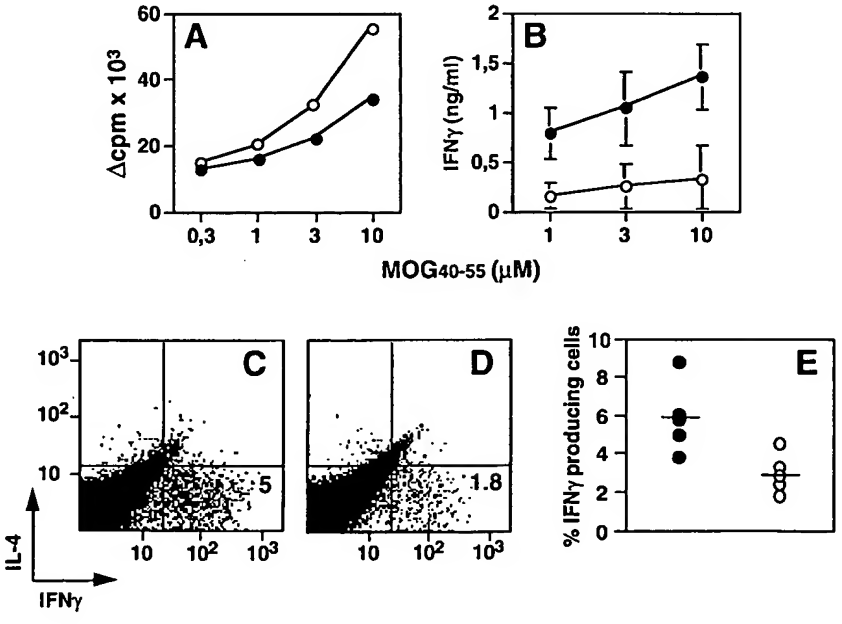

FIGURE 3. Reduced Th1 cell development in caspase-1$^{-/-}$ mice immunized with 200 μg of MOG_{40-55}. *A*, Proliferation of draining lymph nodes cells from caspase-1$^{-/-}$ (○) and C57BL/6 (●) mice restimulated in vitro with the indicated concentrations of MOG_{40-55}. The background cpm values were subtracted (Δ cpm). *B*, IFN-γ levels (±SE) in supernatants from cell cultures from caspase-1$^{-/-}$ (○) and C57BL/6 (●) in response to the indicated concentrations of MOG_{40-55}. *C*, Intracellular staining for IFN-γ and IL-4 of MOG_{40-55}-stimulated cells from a representative C57BL/6 mouse. *D*, Intracellular staining for IFN-γ and IL-4 of MOG_{40-55}-stimulated cells from a representative caspase-1$^{-/-}$ mouse. In *C* and *D*, the percentage of IFN-γ-producing cells are reported in the lower right corner. In *E*, the percentage of IFN-γ-producing cells from MOG_{40-55}-immunized C57BL/6 (●) and caspase-1$^{-/-}$ (○) mice. Each circle represents a single mouse, and mean values are indicated by the horizontal bars. Caspase1$^{-/-}$ mice display a significant ($p = 0.01$) reduction of IFN-γ production.

Table II. *EAE in Biozzi AB/H mice immunized with SCH or MOG_{35-55} and treated with vehicle or the caspase-1 inhibitor Z-Val-Ala-DL-fluoromethylketone*

Treatment Schedule[a]	EAE Incidence (%)	EAE Onset (range)[b]	Maximum EAE Score (range)[c]	Cumulative Score (days of follow-up)[d]
MOG_{35-55} (preventive)				
Vehicle	5/7	22.4 ± 2.9	2.1 ± 0.5	89.5
	(71)	(16–30)	(1–4)	(40)
Caspase-1 inhibitor	2/7	23.5 ± 5.5	2.2 ± 1.2	32
	(29)	(18–29)	(1–3.5)	(40)
SCH (preventive)				
Vehicle	10/10	14.2 ± 0.5	3.7 ± 0.2	282
	(100)	(12–16)	(1.5–5.0)	(25)
Caspase-1 inhibitor	4/10[e]	15.0 ± 0.7	3.6 ± 0.4	82[f]
	(40)	(13–16)	(2.5–4.0)	(25)
SCH (therapeutic)				
Vehicle	10/10	14.5 ± 0.6	3.8 ± 0.3	NA[g]
	(100)	(13–19)	(1.5–5.0)	
Caspase-1 inhibitor	9/10	14.3 ± 0.3	3.0 ± 0.3	NA
	(90)	(13–16)	(1.5–4.0)	

[a] Treatment was performed by implantation of mini-osmotic pumps releasing for 10 days vehicle or the caspase-1 inhibitor Z-Val-Ala-DL-fluoromethylketone (1.2 mg/day) from the day before immunization (preventive) or day 7 (therapeutic) after immunization.

[b] EAE onset is expressed as day post immunization ± SE.

[c] EAE score is expressed as mean maximum score ± SE.

[d] Cumulative score was calculated by summing up each individual score registered during the follow-up period.

[e] $p = 0.003$ vs vehicle-treated mice.

[f] $p = 0.0007$ vs vehicle-treated mice.

[g] NA, not applicable because in the therapeutic administration one mouse died during the follow-up period.

However, the mean day of onset and the mean clinical score of sick animals were comparable between groups (Table II). In the SCH-induced group, two animals for each treatment were sacrificed for neuropathology examination. Animals treated with the inhibitor had less infiltrates per mm^2 than did vehicle-treated controls (0.4 and 1.6 vs 6.6 and 3.1, respectively) (Fig. 4, *A* and *B*), less demy-

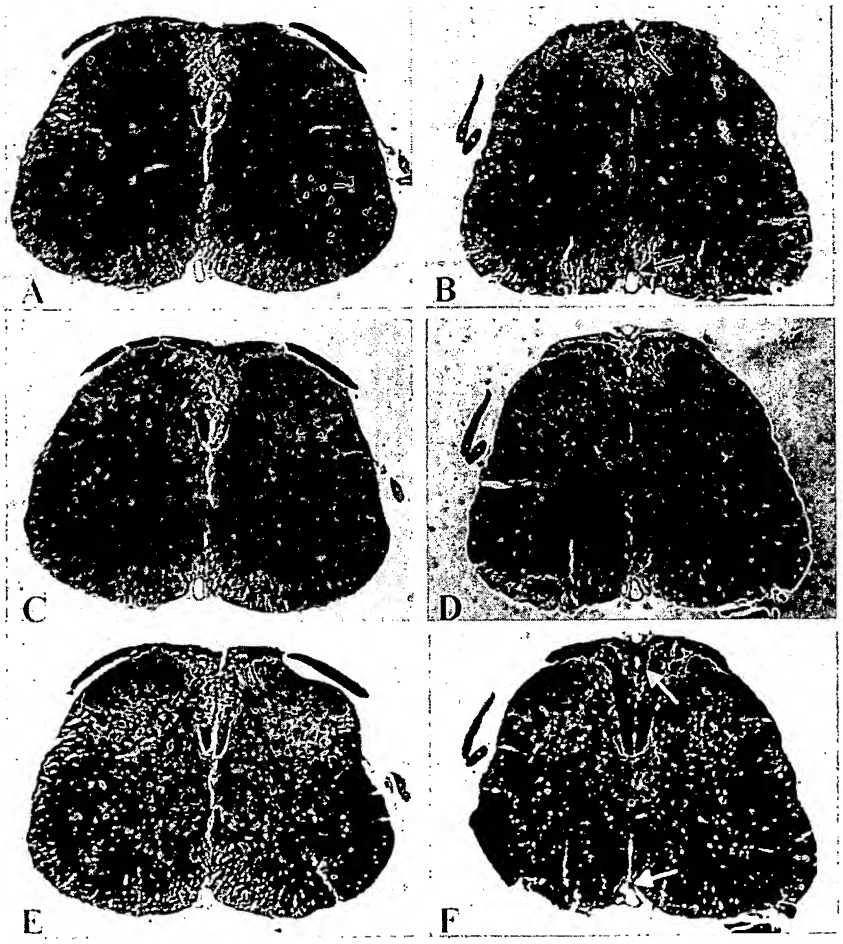

FIGURE 4. Neuropathological findings of SCH-induced EAE in two representative Biozzi mice treated with vehicle or caspase-1 inhibitor Z-Val-Ala-DL-Asp-fluoromethylketone, respectively. Spinal cord sections stained with hematoxylin and eosin (×5) are shown in *A* and *B*; perivascular infiltrates (arrowheads) are less evident in the caspase-1 inhibitor-treated (*A*) vs vehicle-treated (*B*) mouse. Spinal cord sections stained with Luxol Fast Blue (×5) are shown in *C* and *D*; demyelinated areas (arrowheads) are less prominent in the caspase-1 inhibitor-treated (*C*) vs vehicle-treated (*D*) mouse. Spinal cord sections stained with Bielshowsky staining (×5) are shown in *E* and *F*; axonal loss (arrowheads) is decreased in the caspase-1 inhibitor-treated mouse (*E*) vs the vehicle-treated (*F*) mouse. Tissue sections of each mouse are from the same spinal cord area and have been obtained serially.

elination (0.6% and 0.8% vs 9.8% and 2.2%, respectively) (Fig. 4, *C* and *D*), reduced axonal loss (0.4% and 0.6% vs 8.3% and 1.5%, respectively) (Fig. 4, *E* and *F*), less infiltrating $CD3^+$ cells/mm^2 (39.9 and 90.5 vs 291 and 138.2, respectively), and reduced numbers of infiltrating macrophages per mm^2 (21.8 and 52.5 vs 211.9 and 84.9, respectively).

By contrast, when the mini-osmotic pumps were implanted 7 days p.i. in Biozzi mice immunized with SCH, EAE development was similar in inhibitor- and vehicle-treated mice (Table II). Only 1 of the 10 mice treated with the inhibitor from 7 days p.i. did not develop a full-blown EAE. These results suggest that caspase-1 is crucial in the induction phase of EAE, when peripheral inflammation leads to the recruitment of effector cells into the CNS.

Discussion

The central role of proinflammatory cytokines in orchestrating the pathogenic process leading to EAE has been extensively studied (27–29), but few data are thus far available on the posttranslational mechanisms of regulation of cytokine secretion during this experimental autoimmune CNS-confined disease. We focused our attention on the proteolytic enzyme caspase-1, because previous studies showed that its pharmacological inhibition or its absence (i.e., deletion mutant mice) mainly affects the secretion of proinflammatory cytokines such as IL-1β, IL-1α, IL-6, TNF-α, IL-18, and IFN-γ (5–7). We found that caspase-1 transcription is up-regulated during mouse EAE, reaching a peak at maximal disease severity. This induction is higher compared with other proinflammatory cytokines previously shown to be up-regulated during EAE (27) and is similar to that found in the Lewis rat EAE (30). These data suggest that proteolytic activation of proinflammatory cytokines is a crucial step in the immune-mediated process leading to EAE.

Caspase-$1^{-/-}$ mice were susceptible to MOG peptide-induced EAE. Disease susceptibility was associated with the number of immunizations and the dose and the MHC-binding affinity of the encephalitogenic MOG-peptide. In our hands, MOG_{40-55} showed a 3-fold weaker binding (IC_{50} = 360 pM) compared with MOG_{35-55} (IC_{50} = 1 nM) to the I-A^{g7} molecule (data not shown). However, the disease induced in caspase-$1^{-/-}$ mice was always less severe then in C57BL/6 or (SV129 × B6)F_1 mice and did not develop at all when a low dose of the weaker MHC binder MOG peptide was used. The reduced EAE in caspase-1-deficient mice was not caused by inefficient Ag presentation to T cells, as shown by the Ag-specific proliferation assays, but to an impairment in Th1 cell development as indicated by the lower percentage of IFN-γ-producing cells from caspase-$1^{-/-}$ vs C57BL/6 mice. The most likely explanation of this finding possibly resides in the cleavage activity of caspase-1 on the precursor of IL-18 into its mature form (6). Although IL-18 in itself does not induce Th1 cell development (31, 32), which is mostly driven by IL-12 (33), Th1 cell development independent from IL-12 could be induced by the cooperative action of IL-18 and other factors (34). These factors may include IFN-γ itself (35) and IL-1$\alpha\beta$ (33). Thus, the simultaneous caspase-1-dependent defect in IL-18 and IL-1$\alpha\beta$ production could explain the impaired Th1 development and the reduced EAE in caspase-$1^{-/-}$ mice. A more aggressive immunization protocol, however, is able to overcome this limiting step in EAE induction, likely because other proteases may replace caspase-1 in the cleavage of pro-IL-1β and pro-IL-18.

Results obtained with caspase-1 inhibitor administration are consistent with the lower susceptibility to EAE of caspase-$1^{-/-}$ mice. The preventive administration of the caspase-1 inhibitor Z-Val-Ala-DL-Asp-fluoromethylketone dramatically reduced both relapsing-remitting or chronic-progressive EAE in two different mouse strains. However, the small proportion (35%) of mice not protected from EAE by caspase-1 inhibitor treatment developed a clinical course of EAE indistinguishable from that of controls. As in inflammatory fluids other proteases (i.e., trypsin, chymotrypsin, elastase, granzyme A) (36) can replace caspase-1 enzymatic activity, an immunization protocol able to induce a potent local inflammation may bypass its requirement. Nevertheless, recent data indicate that Z-Val-Ala-DL-Asp-fluoromethylketone is active also on other cysteine proteases involved in inflammatory reactions but not in the apoptotic cascade, such as caspases-4 and -5 (37).

Administration of Z-Val-Ala-DL-Asp-fluoromethylketone during the effector phase of SCH-induced EAE (i.e., therapeutic protocol) had no effect on the disease course and severity. These data are suggestive for a crucial role played by caspase-1 in the peripheral activation of proinflammatory cytokines during the induction phase of EAE. The lack of efficacy of caspase-1 inhibitors once the inflammatory cascade has already determined CNS infiltration and damage might be also explained by the impaired blood-brain barrier crossing of caspase-1 inhibitors (26).

In conclusion, our results indicate that caspase-1 plays a crucial role in the development of the immune-mediated inflammatory process leading to CNS demyelination. EAE development is impaired in caspase-$1^{-/-}$ mice, although the requirement for caspase-1 in the inflammatory phase of EAE can be bypassed. The role of caspase-1 in autoimmune demyelination is further corroborated by the significant reduction of EAE incidence in mice preventively treated with the caspase-1-inhibitor Z-Val-Ala-DL-Asp-fluoromethylketone. However, the inefficacy of caspase-1 inhibitors in blocking ongoing EAE suggests that this enzyme is crucial in the early phase of the inflammatory process leading to immune-mediated demyelination. Thus, caspase-1 could represent both a marker of inflammation sustaining immune-mediated demyelination and a possible therapeutic target of the acute phase of relapsing-remitting MS.

Acknowledgments

We thank Drs. Adriano Fontana, Hans-Pietro Eugster, and Hans Lassmann for helpful discussion, and Silvia Gregori for performing the MHC-binding assay.

References

1. Thornberry, N. A., and Y. Lazebnik. 1998. Caspases: enemies within. *Science 281:1312.*
2. Wang, S., M. Miura, Y. Jung, H. Zhu, E. Li, and J. Yuan. 1998. Murine caspase-11, an ICE-interacting protease, is essential for the activation of ICE. *Cell 92:501.*
3. McAlidon, M. E., C. J. Hawkey, and Y. R. Mahida. 1998. Expression of interleukin-1β and interleukin-1β converting enzyme by intestinal macrophages in health and inflammatory bowel disease. *Gut 42:214.*
4. Tingsborg, S., M. Zetterstrom, K. Alheim, H. Hasanvan, M. Schultzberg, and T. Bartfai. 1996. Regionally specific induction of ICE mRNA and enzyme activity in the rat brain and adrenal gland by LPS. *Brain Res. 712:153.*
5. Kuida, K., J. A. Lippke, G. Ku, M. W. Harding, D. J. Livingston, M. S. Su, and R. A. Flavell. 1995. Altered cytokine export and apoptosis in mice deficient in interleukin-1β converting enzyme. *Science 267:2000.*
6. Gu, Y., K. Kuida, H. Tsutsui, G. Ku, K. Hsiao, M. A. Fleming, N. Hayashi, K. Higashino, H. Okamura, K. Nakanishi, et al. 1997. Activation of interferon-γ inducing factor mediated by interleukin-1β converting enzyme. *Science 275:206.*
7. Li, P., H. Allen, S. Banerjee, and T. Seshadri. 1997. Characterization of mice deficient in interleukin-1β converting enzyme. *J. Cell. Biochem. 64:27.*
8. Norman, J., J. Yang, G. Fink, G. Carter, G. Ku, W. Denham, and D. Livingston. 1997. Severity and mortality of experimental pancreatitis are dependent on interleukin-1 converting enzyme (ICE). *J. Interferon Cytokine Res. 17:113.*
9. Rouquet, N., J. C. Pages, T. Molina, P. Briand, and V. Joulin. 1996. ICE inhibitor YVADcmk is a potent therapeutic agent against in vivo liver apoptosis. *Curr. Biol. 6:1192.*
10. Ku, G., T. Faust, L. L. Lauffer, D. J. Livingston, and M. W. Harding. 1996. Interleukin-1β converting enzyme inhibition blocks progression of type II collagen-induced arthritis in mice. *Cytokine 8:377.*
11. Martin, R., H. F. McFarland, and D. E. McFarlin. 1992. Immunological aspects of demyelinating diseases. *Annu. Rev. Immunol. 10:153.*

12. Steinman, L. 1996. A few autoreactive cells in an autoimmune infiltrate control a vast population of nonspecific cells: a tale of smart bombs and the infantry. *Proc. Natl. Acad. Sci. USA 93:2253.*
13. Martino, G., F. Grohovaz, E. Brambilla, F. Codazzi, A. Consiglio, E. Clementi, M. Filippi, G. Comi, and L. M. E. Grimaldi. 1998. Proinflammatory cytokines regulate antigen-independent T-cell activation by two separate calcium-signaling pathways in multiple sclerosis patients. *Ann. Neurol. 43:340.*
14. Beck, J., P. Rondot, L. Catinot, E. Falcoff, H. Kirchner, and J. Wietzerbin. 1988. Increased production of interferon γ and tumor necrosis factor precedes clinical manifestation in multiple sclerosis: do cytokines trigger off exacerbations? *Acta Neurol. Scand. 78:318.*
15. Panitch, H. S., R. L. Hirsch, A. S. Haley, and K. P. Johnson. 1987. Exacerbations of multiple sclerosis in patients treated with γ interferon. *Lancet 1:893.*
16. Brosnan, C. F., B. Cannella, L. Battistini, and C. S. Raine. 1995. Cytokine localization in multiple sclerosis lesions: correlation with adhesion molecule expression and reactive nitrogen species. *Neurology 45:S16.*
17. Martin, D., and S. L. Near. 1995. Protective effect of the interleukin-1 receptor antagonist (IL-1ra) on experimental allergic encephalomyelitis in rats. *J. Neuroimmunol. 61:241.*
18. Zhu, H., H. O. Fearnhead, and G. M. Cohen. 1995. An ICE-like protease is a common mediator of apoptosis induced by diverse stimuli in human monocytic THP-1 cells. *FEBS Lett. 374:303.*
19. Rodriguez, I., K. Matsuura, C. Ody, S. Nagata, and P. Vassalli. 1996. Systemic injection of a tripeptide inhibits the intracellular activation of CPP32-like proteases in vivo and fully protects mice against Fas-mediated fulminant liver destruction and death. *J. Exp. Med. 184:2067.*
20. Openshaw, P., E. E. Murphy, N. A. Hosken, V. Maino, K. Davis, K. Murphy, and A. O'Garra. 1995. Heterogeneity of intracellular cytokine synthesis at the single-cell level in polarized T helper 1 and T helper 2 populations. *J. Exp. Med. 182: 1357.*
21. Galbiati, F., L. Rogge, J. C. Guery, S. Smiroldo, and L. Adorini. 1998. Regulation of the IL-12 receptor β-2 subunit by soluble antigen and IL-12 in vivo. *Eur. J. Immunol. 28:209.*
22. Piddlesden, S. J., M. K. Storch, M. Hibbs, A. M. Freeman, H. Lassmann, and B. P. Morgan. 1994. Soluble recombinant complement receptor 1 inhibits inflammation and demyelination in antibody-mediated demyelinating experimental allergic encephalomyelitis. *J. Immunol. 152:5477.*
23. Eugster, H-P., K. Frei, M. Kopf, H. Lassmann, and A. Fontana. 1998. IL-6-deficient mice resist myelin oligodendrocyte glycoprotein-induced autoimmune encephalomyelitis. *Eur. J. Immunol. 28:2178.*
24. Mendel, I., N. Kerlero de Rosbo, and A. Ben-Nun. 1995. A myelin oligodendrocyte glycoprotein peptide induces typical chronic experimental autoimmune encephalomyelitis in H-2^b mice: fine specificity and T cell receptor Vβ expression of encephalitogenic T cells. *Eur. J. Immunol. 25:1951.*
25. O'Neil, J. K., D. Baker, A. N. Davison, K. K. Maggon, B. D. Jaffee, and J. L. Turk. 1992. Therapy of chronic relapsing experimental allergic encephalomyelitis and the role of the blood-brain barrier: elucidation by the action of Brequinar sodium. *J. Neuroimmunol. 38:53.*
26. Livingston, D. J. 1997. In vitro and in vivo studies of ICE inhibitors. *J. Cell. Biochem. 64:19.*
27. Olsson, T. 1995. Critical influences of the cytokine orchestration on the outcome of myelin antigen-specific T-cell autoimmunity in experimental autoimmune encephalomyelitis and multiple sclerosis. *Immunol. Rev. 144:245.*
28. Ewing, C., and C. C. Bernard. 1998. Insights into the aetiology and pathogenesis of multiple sclerosis. *Immunol. Cell. Biol. 76:47.*
29. Ruuls, S. R., and J. D. Sedgwick. 1998. Cytokine-directed therapies in multiple sclerosis and experimental autoimmune encephalomyelitis. *Immunol. Cell. Biol. 76:65.*
30. Jander, S., and G. Stoll. 1998. Differential induction of interleukin-12, interleukin-18 and interleukin-1β converting enzyme mRNA in experimental autoimmune encephalomyelitis of the Lewis rat. *J. Neuroimmunol. 91:93.*
31. Matsui, K., T. Yoshimoto, H. Tsutsui, Y. Hyodo, N. Hayashi, K. Hiroishi, N. Kawada, H. Okamura, K. Nakanishi, and K. Higashino. 1997. *Propionibacterium acnes* treatment diminishes $CD4^+$ $NK1.1^+$ T cells but induces type I T cells in the liver by induction of IL-12 and IL-18 production from Kupffer cells. *J. Immunol. 159:97.*
32. Robinson, D., K. Shibuya, A. Mui, F. Zonin, E. Murphy, T. Sana, S. B. Hartley, S. Menon, R. Kastelein, F. Bazan, and A. O'Garra. 1997. IGIF does not drive Th1 development but synergizes with IL-12 for interferon-γ production and activates IRAK and NFκB. *Immunity 7:571.*
33. Gately, M. K., L. M. Renzetti, J. Magram, A. S. Stern, L. Adorini, U. Gubler, and D.H. Presky. 1998. The interleukin-12/interleukin-12-receptor system: role in normal and pathologic immune responses. *Annu. Rev. Immunol. 16:495.*
34. Takeda, K., H. Tsutsui, T. Yoshimoto, O. Adachi, N. Yoshida, T. Kishimoto, H. Okamura, K. Nakanishi, and S. Akira. 1998. Defective NK cell activity and Th1 response in IL-18-deficient mice. *Immunity 8:383.*
35. Szabo, S. J., A. S. Dighe, U. Gubler, and K. M. Murphy. 1997. Regulation of the interleukin (IL)-12R beta 2 subunit expression in developing T helper 1 (Th1) and Th2 cells. *J. Exp. Med. 185:817.*
36. Fantuzzi, G., G. Ku, M. W. Harding, D. J. Livingston, J. D. Sipe, K. Kuida, R. A. Flavell, and C. A. Dinarello. 1997. Response to local inflammation of IL-1β-converting enzyme-deficient mice. *J. Immunol. 158:1818.*
37. Schulz, J. B., M. Weller, and M. A. Moskowitz. 1999. Caspases as treatment targets in stroke and neurodegenerative diseases. *Ann. Neurol. 45:421.*

ELSEVIER

Journal of the Neurological Sciences 197 (2002) 9–18

Journal of the Neurological Sciences

www.elsevier.com/locate/jns

Caspase-1 expression in multiple sclerosis plaques and cultured glial cells

Xue Ming [a,1], Weiping Li [b,1], Yasuhiro Maeda [a,b], Benjamin Blumberg [b], Sumul Raval [a], Stuart D. Cook [a,b], Peter C. Dowling [a,b,*]

[a] *Department of Neurosciences, UMDNJ-New Jersey Medical School, Newark, NJ, USA*
[b] *Neurology Service, VA New Jersey Health Care System, East Orange, NJ 07018, USA*

Received 20 July 2001; received in revised form 15 January 2002; accepted 28 January 2002

Abstract

Caspase-1 is responsible for processing inflammatory cytokines and is associated with the induction of apoptosis. Using RT-PCR, we found that caspase-1 mRNA transcripts from frozen brain extracts were significantly elevated in multiple sclerosis (MS) compared to controls. Immunohistochemical staining using a specific antiserum confirmed the marked up regulation of caspase-1 within acute and chronic MS plaques, while little staining was seen in control brains. In addition to the expected caspase-1 expression in microglia and infiltrating perivascular mononuclear cells, we found that cytoplasmic caspase-1 expression was sharply increased in the resident oligodendrocytes of MS lesions. The TUNEL reaction for fragmented DNA co-localized over an occasional caspase-1-expressing cell and large numbers of caspase-1-positive "corpses" were observed within phagocytic macrophages of an acute evolving MS lesion. Studies using an immortalized human oligodendroglial hybrid cell line exposed to cytokine challenge showed that death induction was blocked by the caspase-1-like inhibitor Z-YVAD-fmk, while the caspase-3-like inhibitor Z-DEVD-fmk was less effective. Cellular levels of procaspase-1 were reduced compared to controls in oligodendroglia induced to die by cytokine challenge, as judged by Western immunoblotting. Our results suggest that caspase-1 may play a role in the inflammatory and apoptotic processes associated with MS pathogenesis.

Keywords: Caspase-1; Multiple sclerosis; Plaques; Oligodendrocyte; Cultures

1. Introduction

Multiple sclerosis (MS) is a chronic inflammatory demyelinating disease and its neuropathology is characterized by CNS white matter plaques displaying myelin loss and gliosis [1,2]. Inflammatory cytokines such as tumor necrosis factor alpha (TNF-α), interleukin-1 beta (IL-1β), and interferon-gamma (IFN-γ) are upregulated in MS plaques [3], although the precise link between the inflammatory process and myelin sheath destruction is unclear. In previous investigations on the fate of glial cells, we identified substantial numbers of apoptotic oligodendrocytes within developing and mature MS lesions by the in situ TUNEL reaction [4,5]. We also found that glial cells in MS plaques often strongly express both Fas receptor and ligand on their plasma membrane surface, suggesting that the Fas death pathway may be active during MS lesion formation [6]. However, the precise molecules and intracellular pathways responsible for glial cell death in MS remain ill-defined.

Caspase-1, previously named interleukin-1β converting enzyme (ICE), is a cysteine protease whose proteolytic activity makes it a key molecule in myriad cellular processes, including mediation of the inflammatory response through cleavage activation of IL-1β and IFN-γ promolecules. In addition, developmental studies in the nematode *C. elegans* have shown that the caspase-1 homolog CED-3 is chief among the genes required to induce programmed cell death [7–9]. We investigated caspase-1 expression in MS white matter lesions and tested for its activation in response to death induction by cytokine stimulation on immortalized cultures of oligodendrocytes.

* Corresponding author. Neurology Service (127), Veterans Administration New Jersey Health Care System, 385 Tremont Avenue, East Orange, NJ 07018, USA. Tel.: +1-973-676-1000x3596; fax: +1-973-395-7233.

E-mail address: dowlinpc@umdnj.edu (P.C. Dowling).

[1] The first two authors contributed equally to this study.

0022-510X/02/$ - see front matter
PII: S0022-510X(02)00030-8

2. Methods

2.1. Autopsy specimens

This study was performed on frozen and paraffin-embedded formalin-fixed MS and control brains obtained from the Rocky Mountain Multiple Sclerosis Center (Englewood, CO), the MS Human Neurospecimen Bank (West Los Angeles, CA), Dr. John Prineas (UMDNJ, NJ) and St. Vincent's Hospital (New York, NY). The frozen control specimens ($n=14$) included white matter samples from chronic CNS measles virus infection (subacute sclerosing panencephalitis, SSPE; $n=9$), cerebrovascular disease ($n=2$), Parkinson's disease ($n=2$), and amyotrophic lateral sclerosis (ALS). The average postmortem interval for the MS brains ($n=18$) was 17.8 h, and five brains were obtained within 7 h of death. The paraffin-embedded fixed brains consisted of MS ($n=11$), ALS ($n=4$), cerebrovascular disease, Parkinson's disease, and AIDS-associated progressive multifocal leukoencephalopathy (PML). The disease diagnosis was established from patient clinical records and neuropathological examination.

2.2. RT-PCR and liquid hybridization

RNA was extracted from 500-mg fragments of frozen MS and control white matter by the GITC/CsCl method as previously described [10] A one-tube 50-μl RT-PCR reaction was performed in buffer containing 20 mM KCl, 6 mM $MgCl_2$, 70 mM Tris–HCl (pH 8.3), 1 mM DTT, 0.1% gelatin, 40 U RNasin, 100 U Superscript II, and 5 U of Taq polymerase (Gibco, Life Technologies, Grand Island, NY). Total RNA (3 μg) was used as template. A 50-pmol amount of caspase-1 mRNA reverse primer 5′-CATGAACACCAGGAACGTGCTGTC-3′ (position 698–722) was used for reverse transcription (15 min each at 37 and 42 °C), and an equal amount of forward primer 5′-GGAAATTACCTTAATATGCAAGAC-3′ (position 303–329) was used for PCR (50 cycles of 95, 42, and 72 °C/60 s). RT-PCR was performed to measure expression of glyceraldehyde-3-phosphate dehydrogenase (GAPDH) as an internal control of cellular mRNA levels and integrity using the reverse primer 5′-ATAGGATCCTCAGTGTAGCCCAGGATGC-3′ and the forward primer 5′-ATAAAGCTTACCATGGAGAAGGCTGG-3′ [11]. For detection and semiquantification of PCR products, oligonucleotide probes representing internal portions of the caspase-1 (5′-GTCGGCAGAGATTTATCCAA-3′; 430-bp product) and GAPDH (5′-GTGGAAGGACTCATGACCACAGTCCATGCC-3′; 508-bp product) amplicons were 5′-end-labeled with [^{32}P]-ATP using T4 polynucleotide kinase. A 1-μl aliquot of probe (150,000 cpm) was mixed with 20 μl of the PCR product in buffer containing 0.15 M NaCl and 2.5 mM EDTA, and was hybridized (5 min at 98 °C and 15 min at 25 °C). The hybridization products were analyzed by electrophoresis on a 3.5% agarose gel in 0.5 × TBE buffer. The gel was dried with a vacuum and the radioactivity of the caspase-1 and GAPDH mRNA bands was quantified by digital autoradiography and integration using a Packard Instant Imager (Packard, Meriden, CT).

2.3. Caspase-1 antigen detection by immunohistochemistry

Three-micron paraffin-embedded sections were attached to Vectabond treated slides (Vector Labs, Burlingame, CA) by heat fixation. After dewaxing and rehydration through graded alcohols, sections were washed in PBS, subjected to antigen retrieval (95 °C for 10 min) in Target Unmasking Fluid (TUF; Zymed Laboratory, South San Francisco, CA), and then incubated further in hot TUF for 10 min on the benchtop. Sections were then reacted for 2 h at room temperature with a rabbit polyclonal antiserum (R105, 1:300 dilution) that recognizes both the intact procaspase and the cleaved forms of human caspase-1 (kindly provided by Dr. Douglas K. Miller, Merck Research Laboratories). Staining was done as previously described [5,6] using standard horseradish peroxidase-conjugated avidin–biotin methods (ABC kit, Vector Labs) and visualized with the chromogen diaminobenzidine (DAB). To identify glial-specific antigens in caspase-1/DAB-stained sections, multilabeling with several fluorescent stains was performed. A goat polyclonal antibody against CNPase (a gift from Dr. T.J. Sprinkle of the Medical College of Georgia) was used to label oligodendrocytes (diluted at 1:500 and incubated for 1 h) and was visualized by an FITC-conjugated donkey anti-goat antibody (diluted at 1:600 and incubated for 30 min). A 1-h incubation with a mouse monoclonal antibody against GFAP (DAKO, Carpinteria, CA) diluted to 1:25 was used to label astrocytes and was visualized with a Cy3-conjugated rabbit anti-mouse antibody (1:500 dilution for 30 min). Finally, a biotinylated *Ricinus communis* agglutinin 1 lectin (RCA-1, Vector Labs) was used for macrophage/microglia (1:500 for 1 h) and was visualized with a Cy5-conjugated mouse anti-biotin antibody (1:500 for 30 min). All secondary antibodies were obtained from Jackson Laboratories (West Grove, PA). Omission of the primary antibody was used to control for specificity. Fluorescent-labeled sections were mounted in glycerol/PBS.

2.4. In situ TUNEL detection of apoptotic cells and co-localization with caspase-1

Cells containing fragmented DNA were labeled with digoxigenin-11-dUTP by terminal transferase (TdT) tailing, and subsequently detected by immunoperoxidase staining (Intergen ApopTag kit, Purchase, NY) [12,13]. We previously used a modification of this method on both fixed and frozen MS brain, and confirmed the specificity of this assay by demonstrating laddering in DNA extracted from TUNEL-positive frozen MS brain [5]. Immunohistochemistry for caspase-1 using DAB chromogen detection was combined

with FITC-fluorescent staining for cell-specific identification of inflammatory and glial cells. For determining the co-localization of TUNEL-positive cells with caspase-1 expression, sections were reassayed with a caspase-1 antibody (a gift from Dr. Douglas K. Miller; diluted at 1:300). A Cy3-conjugated goat anti-rabbit secondary antibody (Jackson Laboratories; diluted at 1:100 and incubated for 30 min) was used to visualize caspase-1 reactivity. The sections were then evaluated using a four-channel Zeiss Model 410 series confocal microscope.

2.5. *In vitro studies on the oligodendroglial hybrid cell line*

The MO3.13 human oligodendroglial hybrid cell line (a kind gift of Dr. P.J. Talbot, University of Quebec, Canada) was maintained in Dulbecco's modified Eagle's medium (DMEM) supplemented with 10% fetal calf serum (FCS), 100 U/ml penicillin, and 100 μg/ml streptomycin in a 5% (v/v) CO_2 incubator at 37 °C. The MO3.13 oligodendrocyte hybrid cell line was characterized by immunohistochemistry under the culture conditions described above. The cells were collected, washed in PBS, and then spun down using a cell preparation system, Cytospin 3 (Shandon, Pittsburgh, PA) onto microscope slides. After air-drying, cells were fixed in 2% formalin in PBS for 10 min at room temperature, then treated with ethanol/acetic acid at −20 °C for 5 min. The cellular endogenous peroxidase was blocked using 0.3% H_2O_2 for 10 min and 10% normal horse serum was used to block nonspecific immunoglobin binding sites. A battery of glial cell markers was employed for the immunohistochemical staining using a previously published method [6]. These markers included CNPase (a gift from Dr. Terry Sprinkle, 1:600 dilution, incubated at room temperature for 1 h.), PLP (Chemicon, 1:200, at room temperature for 1 h.), PDGFα-R (Santa Cruz Biotechnology, Santa Cruz, CA, 1:150, at 4°C overnight) and GFAP (DAKO, 1:200, at 4 °C overnight). The MBP (1:500), O1 (1:25), and A2B5 (1:25) were all gifts from Dr. Steven Pfeiffer and were incubated at 4 °C overnight. The NCTC929 connective tissue cell line was used as a negative control.

In the caspase-inhibitor blocking experiments, MO3.13 cells were preincubated with either a caspase-1-like inhibitor (Z-YVAD-fmk; Enzyme Systems, Livermore, CA) or a caspase-3-like inhibitor (Z-DEVD-fmk; Enzyme Systems) for 3 h at a dose range of 0–500 μM, and then challenged with TNF-α/IL-1β (100 and 10 ng/ml) combined with cycloheximide (5 μg/ml). Each determination was made in duplicate. Challenged cells were harvested after 24 or 48 h and assayed for Annexin V staining following the manufacturer's protocol (Vybrant™ Apoptosis Assay Kit #1, Molecular Probes, Eugene, OR). The apoptotic and viable cells were then quantified by flow cytometry (FACSCalibur, Becton-Dickinson, San Jose, CA). A comparison was made between numbers of apoptotic cells in cytokine-challenged groups and those of controls. Data were analyzed using Histogram Statistics by LYSYS II software (Becton-Dickinson) gated for 10,000 events. The experiment was replicated six times and a one-way ANOVA was used for statistical analysis.

For the lower molecular weight DNA analysis, DNA was extracted from cultured cells with 10 mM Tris–HCl (pH 8.0), 0.5% SDS, 0.1 M NaCl, and 5 mM EDTA containing 100 μg/ml of proteinase K (Sigma) for 2 h at 37 °C. Sodium chloride was added to a final concentration of 1 M, and samples were incubated overnight at 4 °C. Then the samples were centrifuged for 15 min and the supernatant was ethanol-precipitated after phenol–chloroform extraction. In order to enhance the detection system, we used a radiolabeling method that is capable of detecting very low levels of apoptotic DNA. A 1-μg sample of DNA was labeled with 0.5 μCi of [^{32}P]-labeled dATP in the presence of 10 mM Tris–HCl (pH 7.5), 5 mM $MgCl_2$, and 5 U of Klenow polymerase (Gibco). The mixture was incubated for 10 min at room temperature and then the reaction was terminated by adding EDTA to a final concentration of 10 mM. Unincorporated nucleotides were removed by a Microcon centrifugal filter device (Amicon Bioseparations, Millipore, Bedford, MA). Identical amounts of control and test DNA were electrophoresed on 1.5% agarose gels. The gels were then dried on DEAE cellulose filters and developed by autoradiography.

2.6. *Western blotting*

Cultures were lysed in radio-immuno-protein assay (RIPA) buffer containing 150 mM NaCl, 1% NP-40, 0.5% deoxycholate, 0.1% SDS, 50 mM Tris (pH 8.0), and proteinase inhibitors (2 mg/ml aprotinin, 1 mg/ml leupeptin, and 25 μg/ml phenylmethylsufonyl fluoride) at 0 °C for 30 min. The cell lysates were then incubated in 1 μl of PMSF on ice for another 30 min and centrifuged at 4 °C for 10 min. The protein concentration in the supernatant was determined by the Bio-Rad assay using BSA as the standard. A 50-μg sample of protein from cell lysates was run on a 10–20% Tris–glycine gel and transferred to a nitrocellulose membrane (Invitrogen/Novex Electrophoresis, Carlsbad, CA). The membrane was blocked for nonspecific binding in 5% milk at 4 °C overnight and washed in 1 × T–TBS (Tris-buffered saline and 0.1% Tween 20). The membranes were incubated for 1 h with a caspase-1 p20 polyclonal rabbit antibody at a 1:300 dilution (Santa Cruz Biotechnology, Cat #sc-1780). They were then rinsed three times with T–TBS and incubated with an HRP-conjugated donkey anti-rabbit secondary antibody (Amersham, Arlington Heights, IL) diluted 1:3000 for 1 h at room temperature. Immunoreactive bands were visualized by chemiluminescence using the ECL-kit (Amersham) and then exposed to Hyperfilm (Amersham). An antiserum to β-actin (Santa Cruz Biotechnology) was also tested on blots as a control for equal loading of lanes.

3. Results

3.1. Caspase-1 mRNA upregulation in MS white matter

To measure caspase-1 gene expression in white matter, RNA was extracted from the white matter of 18 MS and 14 control frozen brains and subjected to an RT-PCR assay that targeted a 420-bp segment of the caspase-1 mRNA. The PCR products were solution-hybridized with a radiolabeled oligonucleotide corresponding to an internal sequence of the amplimer and electrophoresed on agarose gels. Fig. 1A shows an autoradiograph of this gel. Caspase-1 mRNA was present in all the MS brains tested, and the bands generated from MS RNA were usually more intense than those amplified from controls. To quantify the amount of caspase-1 transcript in these samples, caspase-1 amplicon radioactivity was normalized to that of GAPDH in each extract, as is shown in the bottom panel of Fig. 1A. A graph of the normalized caspase-1 PCR product (Fig. 1B) shows significantly more caspase-1 mRNA expression in the MS group than in the control ($p<0.03$), and the average caspase-1 transcript expression in controls was half of that in MS white matter. It is important to note that the controls included white matter from nine SSPE brains (open circles) that were known from a previous study to contain large numbers of inflammatory T-cells and activated macrophage/microglia [10]. While the SSPE samples might be expected to overexpress caspase-1, the mean mRNA expression in these brains was still lower than in many MS brains.

3.2. Caspase-1 protein is upregulated in MS plaques

We next investigated caspase-1 expression and localization in MS brains by immunohistochemistry using a polyclonal antiserum that recognizes both the procaspase (uncleaved) and active tetrameric (cleaved) forms. Fig. 2 compares caspase-1 expression in normal control white

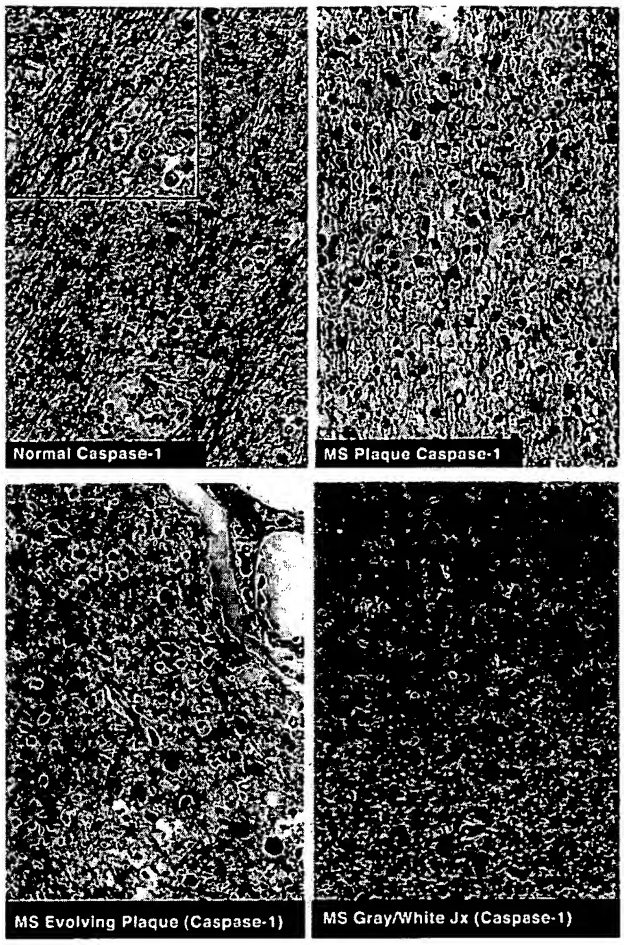

Fig. 2. Immunohistochemical study of caspase-1 expression in normal control white matter and MS plaques. Caspase-1 staining was rarely seen in normal white matter (upper left panel and enhanced inset photograph). By contrast, strong cytoplasmic caspase-1 staining was detected in many oligodendroglia, macrophage/microglia, and some enlarged reactive astrocytes of MS plaques (upper right and lower left panels). Some caspase-1-positive cells have strong nuclear staining. Neurites within another plaque located at the gray/white matter junction also stained for caspase-1 (lower right).

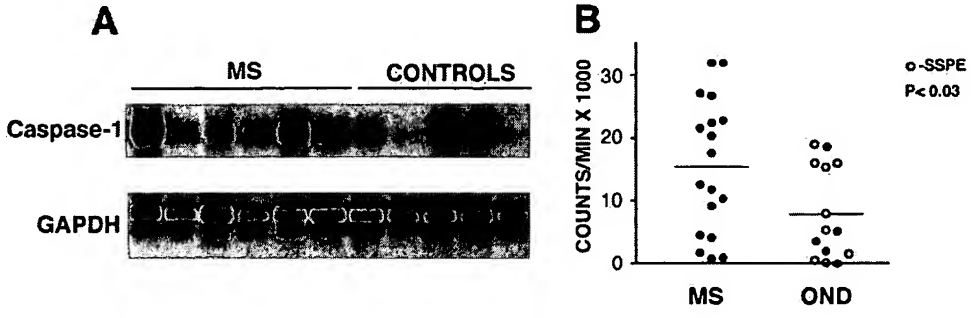

Fig. 1. Determination of caspase-1 gene expression in MS white matter and controls. (A) Semiquantitative RT-PCR and liquid hybridization for caspase-1 and control GAPDH transcripts in RNA extracts from MS and control brains. The agarose gel regions containing bands for the GAPDH and caspase-1 PCR products are shown. Lanes 1–6: MS brains. Lanes 7–11: control brains. The radioactivity of the mRNA bands was measured and caspase-1 mRNA values were normalized to those of GAPDH for each sample. (B) Graph of normalized caspase-1 gene expression in MS brain and other neurologic disease controls (OND). Mean value for each group: MS = 15,240; OND = 7818. The MS group was significantly different from the ONDs according to a Student's *t*-test ($p<0.03$). Open circles (O) represent values derived from a group of nine SSPE brains containing considerable chronic inflammation.

Table 1
Identity of caspase-1-expressing cells in MS white matter plaque

Patient number	Caspase-1-positive cells (total counted)	Oligodendrocytes (CNPase-positive)	Macrophages/microglia (RCA-1 lectin-positive)
First experiment			
Patient 1	152	44 (29%)	59 (38%)
Patient 2	148	46 (31%)	none seen (0%)
Patient 3	119	27 (23%)	47 (39%)
Patient 4	135	40 (30%)	40 (30%)
Second experiment[a]			
Patient 1	151	63 (42%)	42 (28%)
Patient 4	149	77 (52%)	42 (28%)
Average	142	50 (35%)	38 (27%)

[a] Sections from different levels of the blocks were used in the two experiments, so variation in the percentage of counted oligodendrocytes and macrophage/microglia is expected. The difference is within experimental error.

matter to that in MS brain. We found that this protein was readily detectable in most MS lesions, and that many plaques contained far more caspase-1-positive cells than control white matter. Normal white matter failed to exhibit immunoreactivity to the caspase-1 antiserum (top left panel). The inset shows an enhanced photograph of negative staining oligodendroglial cells in normal brain. The same section was subsequently reacted with CNPase to assure that the small round caspase-1-negative cells were indeed oligodendrocytes. By contrast, the MS plaques (top right and lower left panels) show strong caspase-1 staining in many cells possessing oligodendrocyte morphology. There were also caspase-1-positive astrocytes, and although most caspase staining was cytoplasmic, in some cells, prominent nuclear staining was observed. The lower right panel shows the gray/white matter junction in an MS brain where marked caspase-1 immunoreactivity was observed within nerve fibers along the plaque edge.

As previously mentioned, we superimposed fluorescent antisera specific for oligodendrocytes (CNPase) or macrophage/microglial-lineage cells (RCA-1 lectin) on sections previously subjected to caspase-1/DAB staining to determine precisely which cell types express caspase-1 in MS plaques. The experimental results are summarized in Table 1. Fig. 3 illustrates caspase-1 immunostaining at the active margin of a chronic active plaque (left panel) co-labeled with the oligodendrocyte marker CNPase (middle panel), and with the macrophage/microglia marker RCA-1 lectin (right panel). A comparison of the left and middle panels of Fig. 3 shows that caspase-1 is prominently upregulated in the cytoplasm of oligodendrocytes within the thin zone of active demyelination at the plaque margin (black arrows). Comparison of the left panel with the right panel shows that caspase-1 is also upregulated within the perivascular and parenchymal lectin-positive macrophage/microglia (white arrow) as expected. The upper region of the plaque has undergone complete myelin loss. These findings demonstrate that caspase-1 is upregulated throughout evolving early MS plaques, and that caspase-1 is also upregulated at the active margin in chronic plaques in comparison to normal brain.

The largest average number of caspase-1-positive cells belonged to the oligodendrocyte population (35%) and this was closely followed by the average in caspase-1-positive macrophages/microglia (27%, see Table 1). Cytoplasmic caspase-1 staining was often more intense in oligodendrocytes than in macrophage/microglia, and expression varied greatly among cells. GFAP-positive astrocytes usually constituted only 10–15% of caspase-1-positive cells, and their stain was also of variable intensity (data not shown).

3.3. *Macrophages engulf caspase-1-positive cell bodies in acute MS brain*

To address the possible relationship between caspase-1 expression and cell death in MS lesions, we used fluorescent

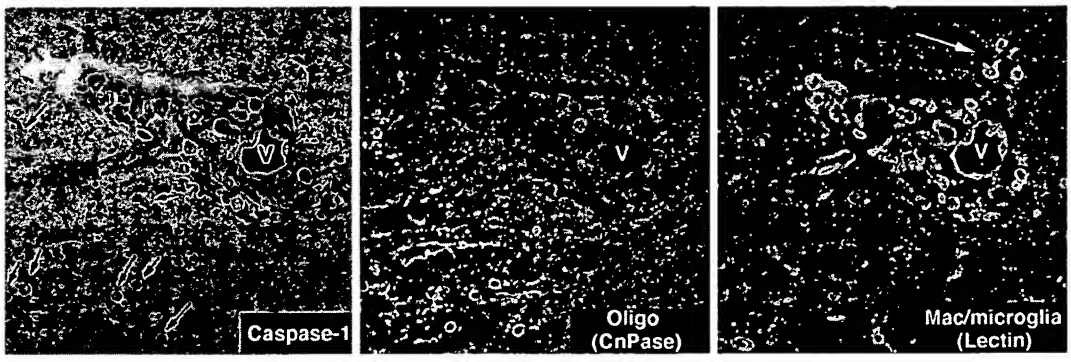

Fig. 3. Chronic MS plaque with active margin showing caspase-1 expression in oligodendrocytes and macrophage/microglia lineage cells. Left panel: Caspase-1 staining using DAB (dark cells; arrows). Arrows point to field of caspase-1-positive oligodendrocytes that are restricted to the active margin of the plaque. Additionally, many caspase-1-positive mononuclear cells are found in the perivascular infiltrate around the blood vessel (V). Middle panel: Confocal image of the same field showing FITC-labeled CNPase-positive oligodendrocytes within a partially demyelinated region of the plaque. Right panel: Confocal image of the same field now labeled with Cy5 RCA-1 lectin that shows positive macrophage/microglia around the vessel. This area of the plaque is totally devoid of myelin.

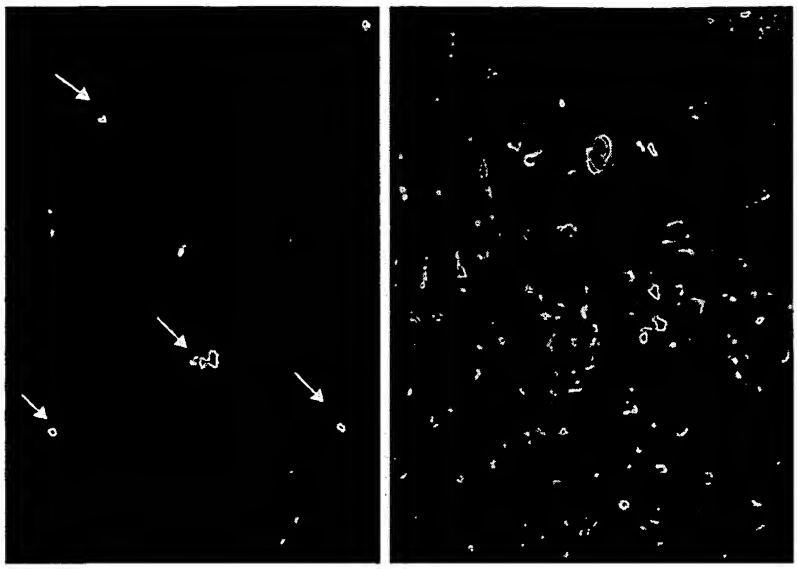

Fig. 4. Confocal fluorescent microscopic images showing FITC-labeled TUNEL-positive cells containing fragmented DNA (yellow) and Cy-3-labeled caspase-1-positive cells (red). Left panel: Arrows indicate caspase-1-positive cells with condensed TUNEL-positive nuclei. Right panel: Higher power image of two additional TUNEL-positive cells with marked expression of caspase-1.

immunohistochemistry for caspase-1 in conjunction with in situ TUNEL staining, which is a nuclear marker for fragmented DNA that is highly characteristic of cell death. Fig. 4 (left panel) shows a chronic MS plaque with many caspase-1-positive cells (red signal) and a few contain TUNEL-positive nuclei (yellow signal; arrows). In another field at higher magnification, a few cells expressing caspase-1 again labeled with the TUNEL stain (right panel). The majority of cells that stained heavily for caspase-1, however, failed to react with the TUNEL assay, indicating that increased caspase-1 expression alone is not sufficient to induce cell death.

We performed caspase-1 immunohistochemistry on an early evolving acute MS plaque where the cell death process was very aggressive, as judged by TUNEL staining. Fig. 5 shows intense caspase-1 staining (DAB) of multiple internalized cell bodies within several large phagocytic cells of this lesion. These bodies probably represent caspase-1-positive cell corpses being phagocytosed by macrophages (arrows).

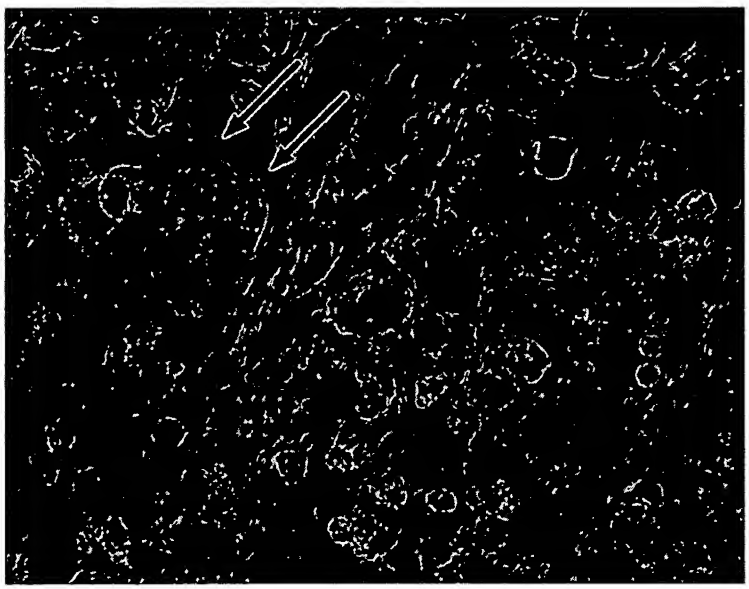

Fig. 5. Phagocytosis of caspase-1-positive cells in a very acute MS lesion. Caspase-1 immunohistochemistry (DAB chromogen, brown stain) showing highly edematous white matter and several large phagocytic cells with multiple caspase-1-positive corpses (arrows).

3.4. In vitro caspase-1 studies on oligodendrocyte hybrid cultures

The majority of MO3.13 cells expressed mature oligodendroglial cell markers including MBP, PLP, CNPase, and O1 when tested by immunohistochemistry. A small portion (up to 5%) expressed progenitor oligodendroglia markers including PDGFα-receptor and A2B5. The MO3.13 cells failed to react with the astrocyte marker GFAP. A nonneural connective tissue cell line (NCTC929) was simultaneously tested with the same marker panel and found to be nonreactive for all markers tested.

The TNF-α/IL-1β cytokine combination induced 47% of the cycloheximide-sensitized cells to die compared to control levels of 20%, as judged by flow cytometry (Fig. 6). The caspase-1-like inhibitor Z-YVAD-fmk blocked most of the cell death induced by this cytokine combination (24%), and was therefore quite effective. Fig. 6 also shows that DNA extracted from the control cells described in the experiment above contained mostly high molecular weight intact DNA and only modest amounts of the low molecular weight banding pattern that is characteristic of apoptosis. In contrast, cultures that were challenged with inflammatory cytokines showed far larger amounts of this low molecular weight banding pattern (middle lane). The companion culture treated with Z-YVAD-fmk exhibited a marked reduction in low molecular weight DNA (right lane).

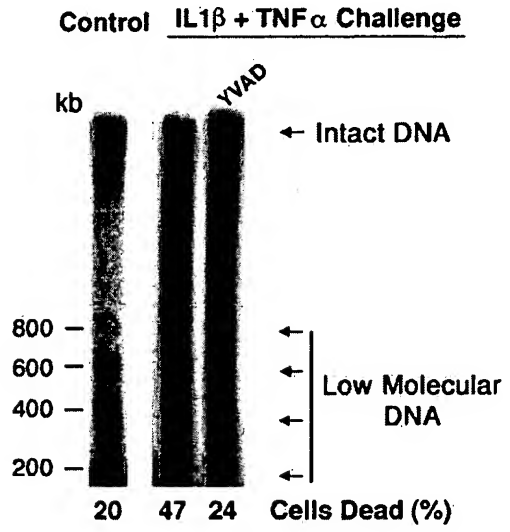

Fig. 6. Autoradiograph showing DNA analysis by 1.5% agarose gel electrophoresis. Lane 1: DNA extracted from control cells showing background apoptosis (20% cells dead). Lane 2: DNA extracted from cells exposed to cytokine challenge showing marked increase in low molecular weight DNA banding pattern (47% cells dead). Lane 3: DNA from challenged cells that were pretreated with the inhibitor Z-YVAD-fmk (60 μM). A strong low molecular weight DNA apoptotic ladder is present in the cytokine-challenged DNA, which is much less prominent in the control lane. Pretreatment with the inhibitor Z-YVAD-fmk blocks cell death, as reflected by the preservation of high molecular weight DNA species and a drop in spacers of low molecular weight. Cell death levels also dropped to 24% in the presence of the inhibitors.

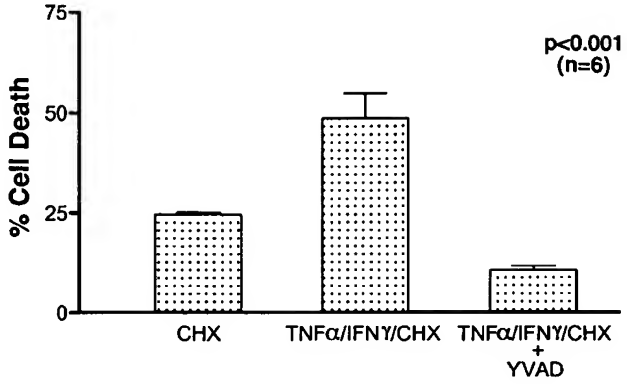

Fig. 7. Graph showing data from six independent experiments where oligodendroglial cultures were challenged with a combination of TNF-α and IFN-γ. Death induction by cytokine exposure averaged nearly 50%, and in this case, inhibition using Z-YVAD-fmk reduced the number of dead cells to less than background control values. Bars represent mean percentages of cell death ± 1 S.E.M. Data were analyzed using a one-way ANOVA ($F=495$; $p<0.001$).

Fig. 7 summarizes the in vitro results of TNF-α/IFN-γ/CHX induced cell death in six independent trials, as judged by flow cytometry using Annexin V staining. This cytokine-stimulated death was blocked by Z-YVAD-fmk, and cell death levels even dropped below the levels of CHX-treated control cultures. A one-way ANOVA showed all three groups

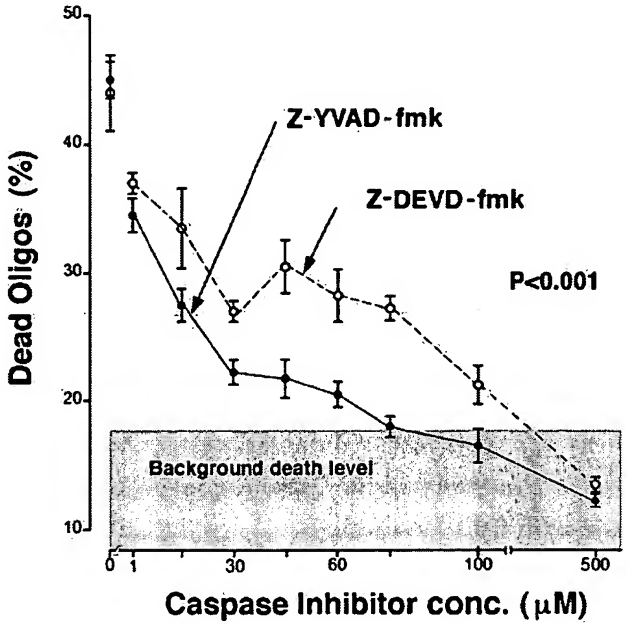

Fig. 8. Comparison of Z-YVAD-fmk and Z-DEVD-fmk dose–response curves after induction of cell death by exposure to TNF-α/IL-1β. The baseline cell death value induced after 24 h was 45% as determined by flow cytometry. Both Z-YVAD-fmk and Z-DEVD-fmk caused modest inhibition at concentrations as low as 1 μM, and both were quite effective at blocking cell death at 500 μM. Z-YVAD-fmk was more effective at blocking cell death at low concentrations (15–100 μM) than Z-DEVD-fmk. A two-way ANOVA was used for statistical analysis, and the difference between the two inhibitors was found to be highly significant ($F=163$, $p<0.001$).

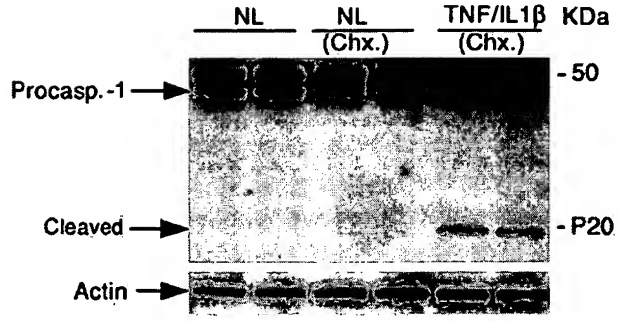

Fig. 9. Western blot showing effect of TNF-α/IL-1β activation on the immortalized MO3 oligodendrocyte culture. These immunoblots were reacted with an antibody to caspase-1 that is capable of detecting the intact promolecule and a 20-kDa cleavage activation product. The intact promolecule of caspase-1 migrates at 47 to 53 kDa depending on the cell line. The control MO3.13 cell cultures (left lanes) show a prominent caspase-1 promolecule band that is substantially reduced following exposure to TNF-α/IL-1β death induction. An activated fragment of caspase-1 is seen only in the cytokine-challenged lanes (right two lanes).

to be significantly different ($p < 0.001$), indicating that cytokine challenge resulted in increased cell death, and that Z-YVAD-fmk was highly effective in blocking this process.

We titrated the effectiveness of the two different caspase inhibitors on blocking oligodendrocyte death by determining their dose–response curves (Fig. 8). The MO3.13 cells were pretreated for 3 h with Z-YVAD-fmk or Z-DEVD-fmk at a dose range of 0–500 μM, and then challenged with 100 ng/ml of TNF-α and 10 ng/ml of IL-1β. A two-way ANOVA test was used to compare the efficacy of the two inhibitors, and Z-YVAD-fmk was found to be a more potent inhibitor of cell death than Z-DEVD-fmk ($F = 163$, $p < 0.001$). While inhibition was detectable with both Z-YVAD-fmk and Z-DEVD-fmk at a concentration of 1 μM, Z-YVAD-fmk retained increased effectiveness at much lower concentrations, indicating that Z-YVAD-fmk inhibits oligodendrocyte death induced by the cytokines in a dose-dependent manner resembling but more potent than Z-DEVD-fmk.

3.5. Caspase-1 is consumed in cytokine-challenged oligodendrocyte hybrid cells

Western blot analysis indicated that caspase-1 was activated by cytokine challenge in MO3 cells. Fig. 9 shows that challenge with TNF-α/IL-1β resulted in both a marked reduction of the procaspase-1 band compared to the control lane and the appearance of a lower molecular weight p20 cleavage activation product restricted to the cytokine-challenge lanes.

4. Discussion

A major finding in this study is that caspase-1 is commonly overexpressed in white matter oligodendrocytes of MS brain. We found that caspase-1 mRNA transcripts were significantly more abundant in MS white matter than in control brain tissue as measured by semiquantitative RT-PCR. We extended this finding at the single-cell level by using immunohistochemistry to determine the pattern of caspase-1 expression in chronic and acute MS plaques. The expression of caspase-1 was negligible in both normal control white matter and in normal appearing areas of MS brain. In contrast, a striking upregulation of caspase-1 was observed in oligodendrocytes of early evolving MS plaques, and this increased expression was often widespread throughout the lesion. In other plaques, however, positive cells were largely restricted to the active plaque margin. As expected, caspase-1 was also upregulated in infiltrating perivascular mononuclear cells and parenchymal macrophage/microglia.

Caspase-1 commonly mediates inflammatory effects through cleavage activation of the IL-1β and IFN-γ promolecules, and these inflammatory cytokines are widely distributed in MS white matter. IFN-γ and TNF-α, both toxic to oligodendrocytes in tissue culture, are produced by macrophages/microglia in the CNS of MS patients [14,15]. IFN-γ is found at the margin of active plaques, while TNF-α is prominent in macrophages at the center of lesions and in the perivascular microglia outside lesions [15]. IL-1β provokes inflammation in the CNS as demonstrated by the acute inflammation involving hemorrhage and edema observed after its injection into the brain of experimental animals [14]. Caspase-1-deficient mice have a major defect in the generation of mature IL-1β and demonstrate impaired production of IFN-γ and IFN-γ-inducing factor (IGIF), thus making them resistant to LPS-induced endotoxic shock [16–18]. These previous studies suggest that caspase-1 may play an important role in the regulation of multiple cytokines implicated in the inflammatory aspects of the MS disease process.

Recently, Furlan et al. [19] found that caspase-1 could regulate the inflammatory process leading to experimental autoimmune encephalomyelitis (EAE), an animal model of MS. In this experiment, caspase-1 mRNA blood levels parallel those of proinflammatory cytokines during EAE and peak at the time of maximal EAE severity, and a reduction of EAE incidence and severity was observed in caspase-1 knockout mice. They also found pharmacological inhibition of caspase-1 using the caspase-1-inhibitor Z-Val-Ala-DL-Asp-fluoromethylketone (Z-VADA-fmk) which could block the induction of EAE if administered early, but could not stop the latter progressive phases of the disease. This experiment clearly indicates that caspase-1 plays an important role in the early phases of the immune-mediated inflammatory process leading to EAE.

Caspase-1 is one of the few caspases with characterized activities both in the cleavage activation of proinflammatory cytokines and in apoptosis. Since caspase-1 knockout mice show no defect in development, some investigators have concluded that caspase-1 may play a redundant role in apoptosis [16]. However, one recent study has shown activation

of caspase-1 in association with apoptosis, even in the nuclei of dying cells. In Mao's report, TNF challenge of Hela cells induced apoptosis without detectable proteolytic activation of caspase-1 in the cytosol. Instead, TNF induced the translocation of procaspase-1 to the nucleus where it was proteolytically activated, releasing the intact prodomain. These findings suggest that caspase-1 may have a nuclear function in some cell types undergoing apoptosis [20], and in our experiment, a number of caspase-1-positive cells in MS plaques showed prominent nuclear expression. Other reports also indicate that caspase-1 may be implicated in cytokine-mediated glial cell death. Under some conditions, TNF induced considerable cytotoxicity in cultured oligodendrocytes. This effect was blocked by the caspase-1 inhibitor Ac-YVAD-CHO, suggesting that TNF-induced death in glial cells is mediated via a death pathway involving caspase-1 [21]. In yet another in vitro study, oligodendrocyte apoptosis was induced with a different stimulus, the neurotrophin NGF. Caspase-1 was again found to be activated in this study, as was the downstream executioner protein caspase-3 [22].

In the present study, an occasional dying TUNEL-positive cell was found in MS brain expressing large amounts of caspase-1. However, the vast majority of caspase-1-expressing cells were TUNEL-negative, so it is unclear precisely what role caspase-1 plays in the process of cell death within postmortem MS brain lesions. On the other hand, high levels of caspase-1 expression in the resident glial population at the active margin of chronic MS plaques as well as the presence of caspase-1-positive corpses within phagocytic macrophages of acute MS plaques are consistent with the operation of multiple caspase-1-mediated processes, including inflammation and perhaps apoptosis in MS lesion development.

In our in vitro studies, MO3.13 cells were used as an oligodendroglial cell model. The immortalized oligodendroglial human–human hybrid MO3.13 cell line has been utilized in previous reports to study caspase activation and apoptosis [23,24]. The cells have been shown to display several of the morphological and biochemical characteristics of human oligodendroglia [25]. We tested the cell line with a battery of glial cell markers and found that the majority of MO3.13 cells expressed markers of mature oliogodendrocytes including MBP, PLP, CNPase, and O1 antigen, and none expressed the astrocyte marker GFAP. These findings indicate that the MO3.13 cells share many of the characteristics of human oligodendrocytes. The results of our in vitro study showed that the caspase-1-like inhibitor Z-YVAD-fmk was able to block the cytotoxic effects of TNF-α/IL-1β in a dose-dependent manner. These findings suggest that caspase-1-like signaling is involved in in vitro cytokine-induced oligodendrocyte death and are strongly supported by the Western immunoblot data that revealed consumption of caspase-1 and the appearance of cleavage activation fragments in the cells subjected to death induction by TNF-α/IL-1β. While the increased expression of caspase-1 message and the caspase-1 product in MS plaques is likely associated with inflammation, the in vitro data suggest that under some circumstances, caspase-1 may be involved in the apoptosis of oligodendrocytes.

Acknowledgements

We gratefully acknowledge Dr. Douglas K. Miller from Merck Research Laboratories for his gift of caspase-1 antiserum. This work was supported in part by the L'Hommedieu Multiple Sclerosis Fund, VA Merit Review grant (#0017), National MS Society grant (RG954-A-10/1), the Kirby Fund, and the Segal Fund.

References

[1] Lassmann H. Comparative Neuropathology of Chronic Experimental Allergic Encephalomyelitis and Multiple Sclerosis. New York: Springer-Verlag, 1983. p. 47–62.
[2] Prineas JW. The neuropathology of multiple sclerosis. In: Vinken PJ, Bruyn GW, Koetsier JC, editors. Handbook of Clinical Neurology: Demyelinating Diseases, vol. 47. Amsterdam: Elsevier, 1985. pp. 213–57.
[3] Merrill JE, Benveniste EN. Cytokines in inflammatory brain lesions: helpful and harmful. TINS 1996;19:331–8.
[4] Dowling P, Bansil S, Menonna J, Husar W, Cook S. Programmed cell death in multiple sclerosis brain (abstract). Ann Neurol 1995;38:341.
[5] Dowling P, Husar W, Menonna J, Donnenfeld H, Cook S, Sidhu M. Cell death and birth in multiple sclerosis brain. J Neurol Sci 1997; 149:1–11.
[6] Dowling P, Shang G, Raval S, Menonna J, Cook S, Husar W. Involvement of the CD95(APO-1/Fas) receptor/ligand system in multiple sclerosis brain. J Exp Med 1996;184:1513–8.
[7] Ellis HM, Horvitz HR. Genetic control of programmed cell death in the nematode *C. elegans*. Cell 1986;44:817–29.
[8] Cerretti DP, Kozlosky CJ, Mosley B, et al. Molecular cloning of the interleukin-1β converting enzyme. Science 1992;256:97–100.
[9] Thornberry NA, Bull HG, Calaycay JR, et al. A novel heterodimeric cysteine protease is required for interleukin-1β processing in monocytes. Nature 1992;356:768–74.
[10] Sidhu MS, Crowley J, Lowenthal A, et al. Defective measles virus in human subacute sclerosing panencephalitis brain. Virology 1994;202: 631–41.
[11] Wesselingh SI, Power C, Glass JD, et al. Intracerebral cytokine messenger RNA expression in acquired immunodeficiency syndrome dementia. Ann Neurol 1993;33:576–82.
[12] Schmitz G, Walter T, Seibl R, Kessler C. Nonradioactive labeling of oligonucleotides in vitro with the hapten digoxigenin by tailing with terminal transferase. Anal Biochem 1991;192:222–31.
[13] Gavrieli Y, Sherman Y, Ben-Sasson SA. Identification of programmed cell death in situ via specific labeling of nuclear DNA fragmentation. J Cell Biol 1992;119:493–501.
[14] Brosnan CF, Cannella B, Battistini L, Raine CS. Cytokine localization in multiple sclerosis lesions: correlation with adhesion molecule expression and reactive nitrogen species. Neurology 1995;45:S16–21.
[15] Vartanian T, Li Y, Zhao M, Stefansson K. Interferon-γ-induced oligodendrocyte cell death: implication for the pathogenesis of multiple sclerosis. Mol Med 1995;3:732–43.
[16] Li P, Allen H, Banerjee S, et al. Mice deficient in IL-1β-converting enzyme are defective in production of mature IL-1β and resistant to endotoxic shock. Cell 1995;80:401–11.
[17] Ghayur T, Banerjee S, Hugunin M, et al. Caspase-1 processes IFN-

gamma-inducing factor and regulates LPS-induced IFN-gamma production. Nature 1997;386:619–23.

[18] Gu Y, Kuida K, Tsutsue H, et al. Activation of interferon-γ inducing factor mediated by interleukin-1β converting enzyme. Science 1997; 275:206–9.

[19] Furlan R, Martino G, Galbiati F, et al. Caspase-1 regulates the inflammatory process leading to autoimmune demyelination. J Immunol 1999;163:2403–9.

[20] Mao PL, Jiang Y, Wee BY, Porter AG. Activation of caspase-1 in the nucleus requires nuclear translocation of pro-caspase-1 mediated by its prodomain. J Biol Chem 1998;273:23621–4.

[21] Hisahara S, Shoji SI, Okano H, Miura M. Caspase-1/CED-3 family executes oligodendrocyte apoptosis by tumor necrosis factor. J Neurochem 1997;69:10–20.

[22] Gu C, Casaccia-Bonnefil P, Srinivasan A, Chao MV. Oligodendrocyte apoptosis mediated by caspase activation. J Neurosci 1999;19:3043–9.

[23] Craighead M, Pole J, Waters C. Caspases mediate C2-ceramide-induced apoptosis of the human oligodendroglial cell line, MO3.13. Neurosci Lett 2000;278:125–8.

[24] Craighead MW, Tiwari P, Keynes RG, Waters CM. Human oligodendroglial cell line, MO3.13, can be protected from apoptosis using the general caspase inhibitor zVAD-FMK. J Neurosci Res 1999;57:236–43.

[25] McLaurin J, Trudel GC, Shaw IT, Antel JP, Cashman NR. A human glial hybrid cell line differentially expressing genes subserving oligodendrocyte and astrocyte phenotype. J Neurobiol 1995;26:283–93.

Differential proteolytic activity and induction of apoptosis in fibrous versus atheromatous plaques in carotid atherosclerotic disease

Theresa Jacob, PhD,[a] Enrico Ascher, MD,[a] Anil Hingorani, MD,[a] Yevgeniy Khandros,[a] Boris Tsemekhin, MD,[a] Linda Zeien, MD,[b] and Yilmaz Gunduz, MD,[a] *Brooklyn, NY*

Purpose: Atherosclerotic plaque instability may be a contributing factor to plaque complications, such as rupture, thrombosis, and embolization. Of the two types of plaques, atheromatous and fibrous, the atheromatous type has been reported to be vulnerable and unstable. This instability may be related to changes in the cell cycle and extracellular matrix degradation. Apoptosis may weaken the plaque structurally. In addition, alteration of the cellular component may lead to imbalances in associated proteolytic activity. Our study was designed to compare the two types of plaques in terms of apoptosis, apoptosis-inducing factors, namely Fas/CD95/APO-1 and CPP-32/YAMA/caspase-3, and proteolytic activity.

Methods: Carotid artery plaques were obtained from patients undergoing endarterectomy and were classified as either atheromatous or fibrous on the basis of established criteria. Histologic study included hematoxylin and eosin staining, Verhoeff's van Gieson elastin staining, and trichrome staining. Detection of apoptosis was performed with the TUNEL assay. Immunohistochemical studies were performed to localize the expression of CPP-32/YAMA and Fas/CD95. Gelatin gel zymography was used to compare proteolytic activity levels in the two types of plaque.

Results: Apoptosis was significantly higher ($P < .001$) in atheromatous plaques (4.90% ± 1.27% [SEM]) as compared with fibrous plaques (0.86% ± 0.46% [SEM]). Zymography demonstrated elevated levels of proteinases in atheromatous plaques. Immunohistochemistry revealed significant increases in the expression of Fas/CD95 ($P < .04$) and CPP-32/YAMA ($P < .001$) in atheromatous plaques as compared with that in fibrous plaques.

Conclusions: This is the first study comparing molecular factors that render atheromatous plaques more susceptible to rupture than fibrous plaques. The higher number of apoptotic cells seen in atheromatous plaques as compared with fibrous plaques could contribute to their greater instability. Immunoreactivity to cytoplasmic death domain, Fas/CD95 and CPP-32/YAMA, a prominent mediator of apoptosis, was consistent with the numbers of apoptotic cells detected. The increased levels of proteolytic activity in atheromatous plaques may make these plaques more prone to rupture. These data identifying some of the molecular events and biochemical pathways associated with plaque vulnerability may help in the development of new strategies to prevent plaque rupture. (J Vasc Surg 2001;33:614-20.)

In carotid atherosclerotic disease, fibrous and atheromatous plaques have exhibited different levels of stability.[1-3] Fibrous plaque is made up of more than 70% collagen-rich tissue that is thought to stabilize and prevent rupture,[4] whereas atheromatous plaques, characterized by having high lipid content, thin fibrous cap, and abundant macrophages, are known for their instability.[5] Although data support the clinical differences between these two types of plaques, few studies have investigated the different types of plaques by use of modern biochemical and molecular biological techniques.

Previous studies by us, as well as by others,[6,7] have demonstrated increased levels of apoptosis and signaling molecules of the apoptotic cascade in atherosclerotic plaques as compared with normal arterial tissue. Specifically, changes in the expression of the members of the Bcl-2 family, p53, MDM2, CPP-32, and cyclin D1 have been reported.[6-9] It has been proposed that apoptosis, especially of the smooth muscle cells (SMCs) in the fibrous cap and the underlying media, weakens the plaque structurally to the point of rupture whereas death of macrophages and that of other cells contribute to the formation of soft plaque cores and therefore make them vulnerable.[10-12] However, the magnitude of apoptosis and the signaling molecules involved in apoptosis in fibrous versus atheromatous plaques have not been examined.

Plaque rupture may also be affected by the stability of extracellular matrix (ECM). Remodeling of the arterial

From the Division of Vascular Surgery[a] and the Department of Pathology,[b] Maimonides Medical Center.

Competition of interest: nil.

Supported by a grant from Maimonides Research and Development Foundation.

Presented at the Annual Meeting of Society for Clinical Vascular Society, Rancho Mirage, Calif, March 18, 2000.

Reprint requests: Enrico Ascher, MD, Division of Vascular Surgery, Maimonides Medical Center, 4802 10th Ave, Brooklyn, NY 11219.

0741-5214/2001/$35.00 + 0 24/6/111802
doi:10.1067/mva.2001.111802

ECM[13] occurs during all phases of human atherosclerosis and is a process regulated at the levels of both synthesis and degradation of matrix components. The macrophages and T-cells associated with chronic inflammation are known to secrete cytokines that can stimulate the production of metalloproteinases in the neighboring SMCs and endothelial cells. Elevated levels of proteolytic activity can cause an increase in ECM degradation and affect plaque stability.[14-20] However, there is no report comparing proteolytic activity in vulnerable atheromatous plaques and stable fibrous plaques.

This study was performed to determine potential factors that may predispose atheromatous and fibrous plaques to rupture. Degree of apoptosis, along with the levels of known inducers of apoptosis, Fas/CD95/APO-1 and CPP-32/YAMA/caspase-3, were compared between the two types of plaque. Proteolytic activity was examined in fibrous and atheromatous plaques with the goal of observing differences that may explain varying plaque stability between fibrous and atheromatous plaques.

MATERIALS AND METHODS

Patients. Two hundred consecutive patients, admitted for primary carotid endarterectomy to the vascular surgery division of Maimonides Medical Center between April 1998 and February 1999 were considered for this study. Institutional Review Board approval was obtained for procurement of specimens, and all patients gave informed written consent for the study. These carotid endarterectomy specimens were stained by hematoxylin and eosin and screened for type of plaque by an anatomic pathologist (L.Z.) blinded to the clinical symptoms and identity of each patient. Only five of the specimens were found to be fibrous, whereas the rest were atheromatous by standard criteria.[17,20] The definition of fibrous plaque was a complete lack of histologically identifiable atheroma (macrophages and cholesterol). These plaques were made up of only fibrous tissue. The five fibrous plaques and eight randomly selected atheromatous plaques were chosen for the study.

Preoperative imaging. All patients underwent preoperative carotid artery duplex ultrasound scanning. Carotid artery duplex scanning was performed by registered vascular technologists at a laboratory accredited by the Intersocietal Commission for the Accreditation of Vascular Laboratories, as part of the preoperative evaluation of these patients. The common carotid, internal carotid, and external carotid arteries were scanned bilaterally for the presence of occlusion or stenosis.[21-23] The arteries were scanned in transverse and longitudinal sections with B-mode and color-flow imaging. Local percent stenosis was estimated as a 10% interval, that is, 60% to 70%. This interval reading accounted for measurement error and variability.[24] Velocity criteria were used to confirm these data. The University of Washington criterion was used to corroborate stenosis > 50% with a peak systolic velocity more than 125 cm/s.[21] An end-diastolic velocity of 100 cm/s[25,26] was used to corroborate severe stenosis > 70%. All patients who underwent carotid endarterectomy had > 60% stenosis. None of the lesions were identified as ulcerated or inhomogeneous by duplex scanning.

Tissue specimens. Carotid artery plaques were obtained immediately after endarterectomy. All operations were performed with standard surgical techniques and minimal manipulation of the specimen. One half of each specimen was fixed in paraformaldehyde and embedded in paraffin, whereas the remainder was snap-frozen immediately in liquid nitrogen and stored at −70°C until extraction.

Histologic study. Paraffin-embedded tissues were sectioned transversely at 5-μm thickness and mounted on 3-aminopropyltriethoxysilane–coated slides. Five random sections from each specimen were used for analysis. In addition to routine hematoxylin and eosin staining used to select specimens for the study, Gomori's one-step trichrome staining was performed to differentiate between collagen and smooth muscle fibers, and Verhoeff's van Gieson elastic tissue staining was performed to observe the elastin network in the specimens.

DNA in situ end-labeling. Detection of apoptosis in the carotid artery plaques was performed with terminal deoxynucleotidyl transferase (TdT)–mediated digoxigenin-deoxyuridinetriphosphate (dUTP) nick end-labeling of free 3′ OH DNA termini of fragmented DNA present in the apoptotic cells (TUNEL), with the ApopTag kit (Intergen, Purchase, NY) as previously described.[29] The tissue sections were deparaffinized, rehydrated, and incubated in 3% citric acid to remove calcium vesicles. Nuclei were stripped of proteins by incubation with 20 μg/mL proteinase K (Oncor, Gaitherburg, Md) for 15 minutes at 45°C. After equilibration in buffer for 5 minutes, sections were covered with reaction buffer containing TdT enzyme and digoxigenin-dUTP and incubated in humidifying chambers for 1 hour at 37°C. One negative control slide (per batch) was incubated in the absence of TdT enzyme. Positive control used was tumor tissue. After end-labeling, the slides were immersed in stop-wash buffer for 20 minutes at 37°C. Blocking solution containing anti-digoxigenin antibody (sheep polyclonal) conjugated to fluorescein was applied on tissue and incubated for 30 minutes at 37°C in humidifying chambers. The antibody solution was washed away with three changes of phosphate-buffered saline solution for 5 minutes each. End-labeling was visualized after counterstaining with propidium iodide and observing the fluorescence under a Zeiss Axiophot fluorescence microscope (Carl Zeiss, Inc, Thornwood, NY).

Immunohistochemistry. The primary antibodies used in this study were mouse monoclonal antibodies for CPP-32 and Fas (DAKO, Carpenteria, Calif). Formalin-fixed paraffin-embedded tissue sections were deparaffinized and rehydrated. Antigen retrieval was performed by heat treatment at 95°C with 0.01 mol/L citrate buffer, pH 6.0. After the endogenous peroxidase activity was quenched with 0.3% hydrogen peroxide, the tissue sections were incubated with primary antibodies CPP-32 at 1:200 dilution and Fas at a dilution of 1:200 for 1 hour at room temperature. Sections were incubated with biotinylated

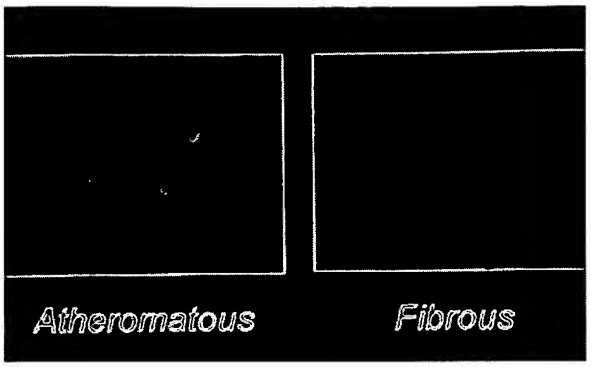

Fig 1. Apoptosis in fibrous and atheromatous plaque. Yellow-green fluorescence represents TUNEL-positive apoptotic bodies against red background of propidium iodide counterstained nuclei of nonapoptotic cells. (Original magnification ×1000.)

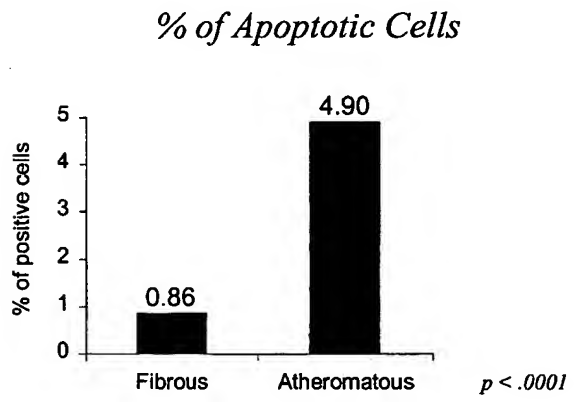

Fig 2. Apoptosis in fibrous and atheromatous plaque. Differences in incidence of apoptosis between fibrous and atheromatous plaque. Cumulative data of all atheromatous and fibrous plaques were obtained. Number of apoptotic cells per thousand cells were counted manually at high-power magnification (original magnification ×1000) for each specimen (random fields were selected).

secondary antibody for 30 minutes at room temperature. The bound primary antibodies were detected with the LSAB2-HorseRadishPeroxidase detection system (DAKO). The peroxidase reaction was developed with diaminobenzidine tetrachloride to produce a brown color at sites of immunoreactivity. Subsequently, the slides were counterstained with Mayers' hematoxylin for 1.5 minutes. Tumor tissue was used as a positive control. The primary antibody was omitted and substituted with an unrelated antibody at the same dilution to check the specificity of the immunohistochemical reactions.

Quantification. Cells only positively stained by TUNEL and containing apoptotic bodies were referred to as "apoptotic cells." Thus, multiple criteria were used to identify apoptotic cells: TUNEL staining and morphologic markings including chromatin condensation. Cells with these features have been confirmed to be apoptotic with electron microscopic analysis in previous studies by us[28] and by others.[29] The number of apoptotic cells per thousand cells were counted manually at high-power magnification (×1000) for each specimen (random fields were selected). The apoptotic index was calculated as the number of apoptotic cells divided by the total number of cells times 100. Cells positive for Fas and CPP-32 were counted manually at original magnification × 400. Cells with no nuclear staining, positive nuclear staining, and cytoplasmic staining were quantified in six random fields per section. Five sections per specimen were analyzed. The number of positive cells is presented as a percentage of the total.

Protein extraction and estimation. Tissue samples were minced and homogenized in salt buffer (50 mmol/L Tris HCl pH 7.5; 2 mol/L NaCl; 0.02% Na Azide). After centrifugation, the supernatants were dialyzed against 0.05 mol/L Tris HCl pH 7.9 overnight at 4°C. Total protein in the dialysate was determined by use of the Pierce protein microassay kit (Pierce Chemical Co, Rockford, Ill) as per the manufacturer's instructions.

Zymography. Proteolytic activity in the extracts was identified by use of substrate gels containing gelatin. Extracts with equalized amounts of protein were mixed in sample buffer in 1:2 ratio and 30 μL loaded on 10% polyacrylamide gels impregnated with gelatin (1 mg/mL) (BioRad, Hercules, Calif). Electrophoresis was performed under nonreducing conditions and at a constant voltage of 100 V. The gels were renatured for 30 minutes at room temperature and developed overnight in a 37°C water bath. The zymograms were stained in 0.5% (wt/vol) Coomassie blue for 20 minutes. Destaining was performed in 40% methanol and 10% acetic acid in distilled water until gelatinolytic activity was seen as clear bands against a background of stained gelatin. Polyacrylamide gel electrophoresis under reducing conditions was used to evaluate protein content.

Statistical analysis. The clinical data, risk factors, and histologic and immunohistochemical findings were analyzed with the Student t test and χ^2. The Fisher exact test was used to compare the results obtained in the different groups. Statistical analyses were performed with. Winks 4.21 program (Texasoft, Cedar Hill, Tex) and Instat 2.05a programs (Graphad, San Diego, Calif).

RESULTS

Patient demographics

There were seven men and six women with ages ranging from 63 to 85 years (mean, 73.6 ± 1.9 years). Eight of the patients had symptoms (history of stroke, transient ischemic attack, or amaurosis fugax), whereas five were symptom free. Patient demographics, risk factors, and clinical symptoms are given in Table I. None of the women were receiving hormone replacement therapy.

Histologic study

Fibrous plaques were observed to contain more smooth

Table I. Clinical risk factors

	Atheromatous (n = 8)		*Fibrous (n = 5)*		
	Asymptomatic (n = 3)	*Symptomatic (n = 5)*	*Asymptomatic (n = 3)*	*Symptomatic (n = 2)*	P *value*
Age ± SEM (y)	72.7 ± 2.9	73.2 ± 3.6	69.7 ± 3.2	82 ± 2	NS
Male/female (7:6)	2:1	3:2	1:2	2:0	0.67
Diabetes mellitus (n = 4)	0	2	2	0	0.56
Hypertension (n = 5)	1	3	0	1	0.44
Tobacco (n = 7)	0	4	1	2	0.6

P values compare atheromatous with fibrous plaque.

Table II. Histopathogic findings

	Atheromatous (n = 8)		*Fibrous (n = 5)*	
	Asymptomatic (n = 3)	*Symptomatic (n = 5)*	*Asymptomatic (n = 3)*	*Symptomatic (n = 2)*
Plaque rupture	1	2	—	—
Cap thinning	2	2	—	—
Plaque necrosis	1	2	—	—
Cap foam cells	2	1	—	—
Macrophages	2	4	—	—
Intraplaque fibrin	—	1	—	—
Intraplaque hemorrhage	3	3	1	—

muscle cells (identified with anti-alpha actin staining and morphologic study) than atheromatous plaques. Verhoeff's elastin staining and trichrome staining also showed a more developed extracellular matrix in atheromatous plaques than in fibrous plaques. The histopathologic findings in the patient groups are summarized in Table II.

Apoptosis detection

We observed that most of TUNEL-positive cells occur within the inflammatory regions of atheromatous plaques, composed mostly of macrophages, smaller number of T lymphocytes, and few B lymphocytes (data not shown). The atheromatous plaques contained 4.9% ± 1.27% TUNEL-positive apoptotic cells as compared with 0.86% ± 0.46% cells in the fibrous plaques ($P < .001$). In the atheromatous plaques, TUNEL-positive cells were most predominant in the lipid core, followed by the fibrous cap and the plaque shoulder region. There were fewer apoptotic cells in the medial layers. On the other hand, fibrous plaque demonstrated an even or scattered distribution of the less than 1% TUNEL-positive cells (Figs 1 and 2). The apoptotic index in the symptomatic group was 3.26, and that in the asymptomatic group was 3.45 ($P = .47$). There was no correlation of apoptosis with the degree of stenosis.

Immunohistochemical localization of the expression of mediators of apoptosis

CPP-32/YAMA. Cells expressing CPP-32 were preferentially located in areas of atheromatous plaques that had increased evidence of apoptosis, namely lipid core, fibrous cap, and shoulder region. In the atheromatous plaque, 20.3% ± 1.78% of the cells were CPP-32 positive, whereas in the fibrous plaque, significantly fewer cells were positive (11.7%; $P < .001$) (Fig 3).

Fas. There were 17.5% ± 2.35% of positive cells in the atheromatous plaques and no reactivity in the fibrous plaques ($P < .04$). This correlated with the apopotic cell death observed in serial sections of these specimens (Fig 3). We could quantify the immunoreactivity to this inducer of apoptosis, although the specimens demonstrated weakly positive staining results.

Zymography. Zymograms with extracts used from carotid artery plaque specimens demonstrated proteolytic activity. However, there was increased gelatinolytic activity in the atheromatous plaques as compared with the fibrous samples. The activities ranged from 68-94 kDa (Fig 4); however, the band intensities were not quantified.

Clinicopathologic correlation

With the risk factors analyzed, diabetes mellitus, hypertension, and smoking (Table I), no correlation could be established between plaque type and clinical symptoms. Patients who had quit smoking were considered as positive for tobacco use.

DISCUSSION

The data from this study suggest significant differences in the apoptotic cascade in between atheromatous and fibrous carotid artery plaques. We have observed greater numbers of apoptotic cells in atheromatous plaques as compared with fibrous plaques. Programmed cell death in the atheromatous plaques was mainly found

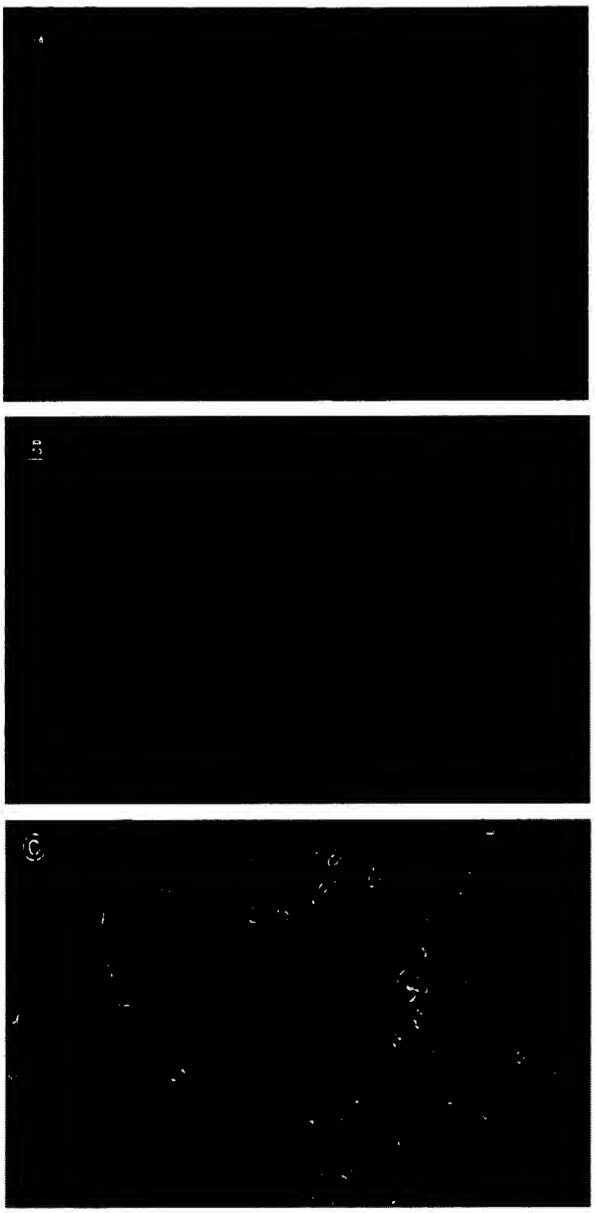

Fig 3. A, Immunohistochemical localization of CPP-32 in atheromatous plaques. Note positive staining (brown) for CPP-32. (Original magnification ×400.) **B,** Immunohistochemical localization of Fas in atheromatous plaques. Note positive staining result *(brown)* for Fas. (Original magnification ×400.) **C,** Negative control. (Original magnification ×400.)

within regions of inflammatory cell infiltration. In contrast, apoptotic cells in fibrous plaques were distributed throughout the whole plaque. Therefore, they may not be able to undermine or compromise plaque stability.[6,7] In addition, programmed cell death of SMCs may lead to imbalances in secretion of proteases associated with them,[29] whereas cell debris of dead macrophages and other cells may contribute to gruel formation. It has been suggested that the death of SMCs can be detrimental for plaque stability because most of the interstitial collagen fibers that are important for the tensile strength of the fibrous cap are produced by SMCs.[30] Because SMCs and macrophages have been characterized as the key cell types involved with matrix turnover, a high degree of apoptosis in atheromatous plaques may account for their relative instability when compared with fibrous plaques.

The apoptosis observed by TUNEL assay identifies DNA fragmentation that occurs at the final phase of the apoptotic cascade. Kockx and Herman[30] found that during TUNEL assay if aspecific labeling is avoided, as in this study, the percentage of apoptosis was low in atheromatous plaques. The half-life of apoptotic cells is only a few hours. Even a low incidence of apoptosis has great cell kinetic significance because the short duration of the apoptotic process makes it histologically inconspicuous. Previous reports have emphasized that a small proportion of apoptotic cells visualized in tissue sections can represent a considerable magnitude of cell loss.[7,11,31]

Cysteine protease CPP-32/YAMA is an inducer for mammalian programmed cell death and is an early marker of apoptosis.[32] Our data demonstrate decreased immunopositivity for CPP-32 in fibrous plaques. The fact that cells expressing CPP-32 are preferentially present in the lipid core, fibrous cap, and shoulder regions lends credence to the finding of a significant number of apoptotic cells in these regions. CPP-32 has been shown to lead to apoptosis by cleaving and deactivating poly (ADP-ribose) polymerase, an enzyme required for DNA repair and genome integrity.[32] Recent studies have demonstrated the expression of CPP-32 in apoptotic cells of carotid artery plaques.[9] Our data not only corroborate these findings but also show differential expression of CPP-32 in the two types of plaques studied.

Fas is a cellular death domain protein that is activated by Fas ligand in the apoptotic pathway.[33,34] The positive expression of Fas/CD95 in atheromatous plaques, as compared with its negative immunoreactivity in fibrous plaques, was consistent with the greater numbers of apoptotic cells observed in these plaques. Because fibrous plaques demonstrated no detectable immunopositivity for Fas, even after repeated immunohistochemical staining, it is possible that cells in the fibrous plaques do not go through the same apoptotic pathway as those in atheromatous plaques. In the atheromatous plaques, Fas seemed to colocalize with inflammatory cells in the necrotic core. Scant expression of Fas may be expected because these cells are either absent or present in small numbers in fibrous plaques.

Atherosclerotic plaque stability also may depend on the structural integrity of its extracellular matrix skeleton. We observed increased proteolytic activity in atheromatous plaque as compared with fibrous plaques. Reduction of ECM, compromising plaque stability, may result from either decreased synthesis of ECM by SMCs or its

increased breakdown by proteolytic enzymes produced by macrophages and other cells in the arterial wall. The loss of SMCs could lead to imbalances in the secretion of metalloproteinases and possibly other associated proteases. Matrix metalloproteinases have been shown to destabilize the atherosclerotic plaques through proteolytic activity, leading to degradation of the ECM.[13-17,20,35] Evidence exists that proinflammatory molecules stimulate the secretion of metalloproteinases.[17,19,35] Plaques with reduced tensile strength have been shown to have greater density of metalloproteinase-producing macrophages. This directly correlates with reduced collagen and elastin content.[19] In view of the fact that atheromatous plaques have large amounts of macrophages present in the lipid core as compared with fibrous plaques, it was hypothesized and confirmed by our data that atheromatous plaques have increased levels of proteolytic activity. Zymography demonstrated elevated proteolytic activity in the atheromatous plaques, and the activities were in the 68- to 94-kDa range. This observation is comparable to that of several previous studies identifying these activities to correspond to those of metalloproteinase (MMP)-2 and -9 active and latent forms. Because the numbers in this study are small, we have not attempted to correlate our data with instability such as cap thinning, plaque necrosis, and hemorrhage.

The presence of tissue inhibitors of metalloproteinases (TIMPs) in the specimens was not examined. Fabunmi et al[18] reported that plaques contained abundant amounts of TIMP-1, TIMP-2, and TIMP-3 and that macrophages and SMCs express these factors. Inflammatory molecules augment the levels of TIMP-1 and TIMP-3 but not of TIMP-2, suggesting that TIMPs in the plaques and in the arterial wall counteract MMP activity to influence plaque stability. Thus the role of TIMPs may be a confounding factor that deserves consideration.

The screening of 200 carotid endarterectomy specimens demonstrated that most of the plaques were of the rupture-prone atheromatous type. Conversely, it must be noted that there was no significant difference in programmed cell death between asymptomatic and symptomatic plaques. This may be due to the small numbers of patients. However, this finding is in accordance with those reported previously, which indicated that no correlation could be established between clinical symptoms and specific histologic and biochemical characteristics of the plaque. Other investigators have found no differences between asymptomatic and symptomatic groups with respect to plaque hemorrhage, the presence of a necrotic core, smooth muscle infiltration, and plaque type (fibrous, calcified, or necrotic).[1,3] Recently, another group found significantly elevated levels of MMP 9 but not MMPs 1, 2, or 3 in carotid artery specimens, but only in the patients with symptoms within 1 month of surgery.[14] This suggests that although plaque composition and structure may determine whether a plaque would be symptomatic, other factors such as heterogeneity, changes in physical characteristics of the plaque in response to hemodynamic forces, or a combination of factors may play a significant role.

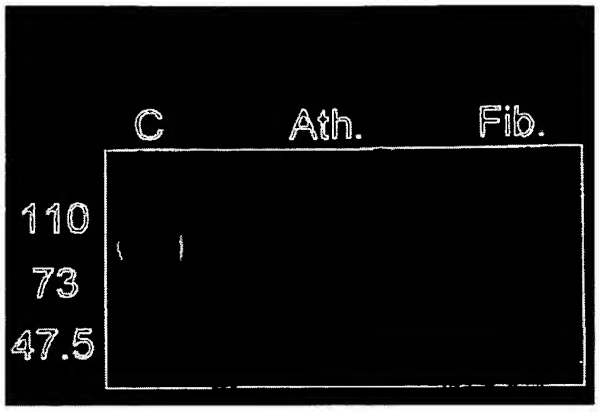

Fig 4. Gelatin zymography of atheromatous and fibrous plaque extracts. (Representative zymogram with one atheromatous specimen extract and one fibrous specimen extract. A total of five atheromatous plaques and five fibrous plaques were analyzed.) Note prominent bands of gelatinolytic activity in atheromatous plaque. Molecular weights are shown on the left. *C,* Positive control; *Ath,* atheromatous; *Fib,* fibrous. Activities ranged from 68 to 94 kDa.

The pathogenesis of intraplaque events in atherosclerotic carotid artery plaques remains a matter of debate. Our data indicate that plaque instability may be caused by programmed cell death of SMCs and inflammatory cells along with ECM degradation. The clear differences in the degree of apoptosis, level of expression of mediators of apoptosis and proteolytic activity between the two groups may be correlated with plaque vulnerability. The challenge remains to further elucidate molecular events and the mechanisms involved to develop future modalities for prevention of plaque rupture.

REFERENCES

1. Carr S, Farb A, Pearce WH, Virmani R, Yao JST. Atherosclerotic plaque rapture in symptomatic carotid artery stenosis. J Vasc Surg 1996;23:755-66.
2. Ross R. The pathogenesis of atherosclerosis: a perspective for the 1990s. Nature 1993;362:801-9.
3. Feeley TM, Leen EJ, Colgan MP, Moore DJ, Hourihane DO, Shanik GD. Histologic characteristics of carotid artery plaque. J Vasc Surg 1991;13:719-24.
4. Falk E, Shah PK, Fuster V. Coronary plaque disruption. Circulation 1995;92:657-71.
5. Milei J, Parodi JC, Alonso GF, Barone A, Grana D, Matturfi L. Carotid rapture and intraplaque hemorrhage: immunophenotype and role of cells involved. Am Heart J 1998;136:1096-105.
6. Kockx MM, De Meyer GR, Muhring J, Jacob W, Bult H, Herman AG. Apoptosis and related proteins in different stages of human atherosclerotic plaques. Circulation 1998;97:2307-15.
7. Konstadoulakis MM, Kymionis GD, Karagiani M, Katergianakis V, Doundoulakis N, Pararas V, et al. Evidence of apoptosis in human carotid atheroma. J Vasc Surg 1998;27:733-9.
8. Ihling C, Haendeler J, Menzel G, Hess RD, Fraedrich G, Schaefer

HE, et al. Co-expression of p53 and MDM2 in human atherosclerosis: implications for the regulation of cellularity of atherosclerotic lesions. J Pathol 1998;185:303-12.
9. Mallat Z, Ohan J, Leseche G, Tedgui A. Colocalization of CPP-32 with apoptotic cells in human atherosclerotic plaques. Circulation 1997;96:424-8.
10. Björkerud S, Björkerud B. Apoptosis is abundant in human atherosclerotic lesions, especially in inflammatory cells (macrophages and T cells), and may contribute to the accumulation of gruel and plaques instability. Am J Pathol 1996;149:367-80.
11. Isner JM, Kearney M, Bortman S, Passeri J. Apoptosis in human atherosclerosis and restenosis. Circulation 1995;91:2703-11.
12. Bennet M, Evan GI, Schwartz SM. Apoptosis of human vascular smooth muscle cells derived from normal vessels and coronary atherosclerotic plaques. J Clin Invest 1995;95:2266-74.
13. Galis ZS, Sukhova GK, Lark MW, Libby P. Increased expression of matrix metalloproteinases and matrix degrading activity in vulnerable regions of human atherosclerotic plaques. J Clin Invest 1994;94: 2493-503.
14. Loftus IM, Naylor AR, Goodall S, Crowther M, Jones L, Bell PR, et al. Increased matrix metalloproteinase-9 activity in unstable carotid plaques. Stroke 2000;31:40-7.
15. Nikkari ST, OBrien KD, Ferguson M, Hatsukami T, Welgus HG, Alpers CE, et al. Interstitial collagenase (MMP-1) expression in human carotid atherosclerosis. Circulation 1995;92:1393-8.
16. Henney AM, Wakeley PR, Davies MJ, Foster K, Hembry R, Murphy G, et al. Localization of stromeslysin gene expression in atherosclerotic plaques by in situ hybridization. Proc Natl Acad Sci U S A 1991;88:8154-8.
17. Moreno PR, Falk E, Palacios IF, Newell JB, Fuster V, Fallon JT. Macrophage infiltration in acute coronary syndromes—implications for plaque rapture. Circulation 1994;90:775-8.
18. Fabunmi RP, Sukhova GK, Sugiyama S, Libby P. Expression of tissue inhibitor of metalloproteinase-3 in human atheroma and regulation in lesion-associated cells. Circ Res 1998;83:270-8.
19. Shah PK, Falk E, Badimon JJ, Fernandez Ortiz A, Mailhac A, Villareal Levy G, et al. Human monocyte-derived macrophages induce collagen breakdown in fibrous caps of atherosclerotic plaques. Circulation 1995;92:1565-9.
20. Sukhova GK, Schonbeck U, Rabkin E, Schoen FJ, Poole AR, Billinghurst RC, et al. Evidence for increased collagenolysis by interstitial collagenases-1 and -3 in vulnerable human atheromatous plaques. Circulation 1999;99:2503-9.
21. Strandness DE Jr. Duplex scanning in vascular disorders. New York: Raven Press; 1993.
22. Salles-Cunha S, Andros G. Atlas of duplex ultrasonography. Pasadena: Appleton Davies, Inc; 1988, p.3-48.
23. Beebe HG, Salles Cunha SX, Scissons RP, Dosick SM, Whalen RC, Gale SS, et al. Carotid arterial ultrasound scan imaging: a direct approach to stenosis measurement. J Vasc Surg 1999;29:838-44.
24. Salles-Cunha S. Internal carotid artery ultrasonography: a technical perspective. Vascular Ultrasound Today, Lesson 4, Volume 4, 1999, 5.
25. Hood DB, Mattos MA, Mansour A, Ramsey DE, Hodgson KJ, Barkmeier LD, et al. Prospective evaluation of new duplex criteria to identify 70% internal carotid artery stenosis. J Vasc Surg 1996;23:254-61.
26. AbuRahma AF, Robinson PA, Strickler DL, Alberts S, Young L. Proposed new duplex classification for threshold stenoses used in various symptomatic and asymptomatic carotid endarterectomy trials. Ann Vasc Surg 1998;12:349-58.
27. Scheinman M, Ascher E, Kallakuri S, Hingorani A, Gade P, Sherman M, et al. P53 gene transfer to the injured rat carotid artery promotes apoptosis. Surgery 1999;126:863-8.
28. Li Y, Sharov VG, Jiang N, Zaloga C, Sabbah HN, Chopp M. Ultrastructural and microscopic evidence of apoptosis after middle cerebral occlusion in the rat. Am J Pathol 1995;146:1045-51.
29. Henderson EL, Geng YJ, Sukhova GK, Whittemore AD, Knox J, Libby P. Death of smooth muscle cells and expression of mediators of apoptosis by T lymphocytes in human abdominal aortic aneurysms. Circulation 1999;99:96-104.
30. Kockx MM, Herman AG. Apoptosis in atherosclerosis: beneficial or detrimental? Cardiovasc Res 2000;45:736-46.
31. Arends MJ, McGregor AH, Wyllie AH. Apoptosis is inversely related to necrosis and determines net growth in tumors bearing constitutively expressed myc, ras, and HPV oncogenes. Am J Pathol 1994;144: 1045-57.
32. Tewari M, Quan LT, ORourke K, Desnoyers S, Zeng Z, Beidler DR, et al. Yama/CPP32β, a mammalian homolog of CED-3, is a CrmA-inhibitable protease that cleaves the death substrate poly(ADP-ribose) polymerase. Cell 1995;81:801-9.
33. Sata M, Walsh K. Oxidized LDL activates Fas-mediated endothelial cell apoptosis. J Clin Invest 1998;102:1682-9.
34. Itoh N, Yonehara S, Ishii A, Yonehara M, Mizushima S, Sameshima M, et al. The polypeptide encoded by the cDNA for human cell surface antigen Fas can mediate apoptosis. Cell 1991;66:233-41.
35. Rajavashisth TB, Xu XP, Jovinge S, Meisel S, Xu XO, Chai NN, et al. Membrane type 1 matrix metalloproteinase expression in human atherosclerotic plaques: evidence for activation by proinflamatory mediators. Circulation 1999;99:3101-9.

Submitted Mar 27, 2000; accepted Sep 15, 2000.

ELSEVIER SCIENCE
www.elsevier.com/locate/cardiosur

Cardiovascular Surgery, Vol. 9, No. 4, pp. 319–328, 2001

0967-2109/01 $20.00

PII: S0967-2109(00)00125-3

Expression of apoptosis-related proteins and structural features of cell death in explanted aortocoronary saphenous vein bypass grafts

A.Y. Wang*, Y.V. Bobryshev*, S.M. Cherian*, H. Liang*, D. Tran*, S.J. Inder*, R.S.A. Lord*, K.W.S. Ashwell† and A.E. Farnsworth‡

**Surgical Professorial Unit, St Vincent's Hospital, Victoria Street, Darlinghurst, Sydney, NSW 2010, Australia and †School of Anatomy, The University of New South Wales, Sydney, NSW 2052, Australia and ‡Department of Cardiothoracic Surgery, St Vincent's Hospital, Sydney, NSW 2010, Australia*

This study aimed to investigate the features of cell death occurring in aortocoronary saphenous vein bypass grafts. Human aortocoronary saphenous vein bypass grafts with angiographic luminal stenosis of >75% were explanted from 14 patients at redo coronary artery bypass grafting. Proteins associated with apoptotic pathways were identified immunohistochemically using antibodies to Bcl-2, Fas, BAX, p53 and CPP32. Cells undergoing DNA fragmentation were identified by terminal deoxynucleotidyl transferase-mediated dUTP nick end labeling (TUNEL). DNA synthesis was investigated using the antibody to proliferating cell nuclear antigen (PCNA). Ultrastructural features of cell death were examined by electron microscopy. Anti-apoptotic (Bcl-2) and pro-apoptotic (Bax, p53, CPP32 and Fas) proteins were expressed throughout the graft wall, but marked differences in the characteristics of cell death were noted between atherosclerotic and non-atherosclerotic areas of the intima. In atherosclerotic areas, pro-apoptotic proteins were widely expressed, but ultrastructural analysis failed to identify cells showing typical features of apoptosis. In these areas, necrotic cells were frequently observed, with negative correlation of Bcl-2 expression with TUNEL. Pro-apoptotic proteins showed no correlation with TUNEL. In contrast, in non-atherosclerotic areas of vein grafts, the expression of both anti-apoptotic (Bcl-2) and pro-apoptotic proteins (p53, Bax and CPP32) correlated with TUNEL. In atherosclerotic areas, non-atherosclerotic intimal areas, and in the underlying media, the numbers of TUNEL+ cells correlated with PCNA positivity. Ultrastructurally, apoptotic bodies and features of necrosis were observed in non-atherosclerotic areas of grafts. The present observations indicate that in atherosclerotic areas, cell death occurs mainly by necrosis, while in non-atherosclerotic areas, cell death occurs by both necrosis and apoptosis. An imbalance between DNA fragmentation and DNA synthesis may contribute to graft instability and failure.

Keywords: apoptosis, atherosclerosis, cell death, coronary artery disease, necrosis, saphenous vein bypass grafts

Correspondence to: Dr Yuri V. Bobryshev. Tel: +61-2-9361-2354; fax: +61-2-9360-4424; e-mail: spu@stvincents.com.au

Introduction

The long-term usefulness of aortocoronary saphenous vein bypass grafts (ASVBGs) used as conduits in coronary artery bypass grafting (CABG) is limited by a disease complex [1–4] comprised of intimal hyperplasia and atherosclerosis [5,6], with both processes related to cell death.

Cell death is a significant event in graft preservation [7, 8] and rejection [9–15], being recognized as a contributing factor to the failure of various grafts, including cardiac [16–18], neuronal [15], hepatic [14], renal [19] and pancreatic [20] transplants. Cell death has also been noted in vascular diseases [13, 21–25]. Specifically, apoptosis (programmed cell death) has been observed in transplant rejection [9–14] and has recently been reported as an important contributor to the formation of primary atheromas, restenotic lesions [26–29], and in experimental atherosclerotic models [30–34].

The present study aimed to investigate the structural features of cell death in ASVBGs using immunohistochemical markers and electron microscopy.

Materials and methods

This study was approved by the Institutional Review Board of the St Vincent's Hospital, Sydney, Australia. Informed consent was obtained from all patients prior to collection of specimens and the materials collected in accordance with the principles outlined in the Declaration of Helsinki [35].

Specimen collection and clinical data

Human aortocoronary saphenous vein bypass grafts with luminal stenosis of >75% as demonstrated by angiography, were explanted from 14 patients at redo coronary artery bypass graft operation at the St Vincent's Hospital, Sydney. The patients (11 male and 3 female) were aged between 51 and 75 yr (mean age 66.6 yr) with the graft implant time ranging from 8 to 22 yr (mean 12.9 yr). The clinical details of patients are summarized in *Table 1*. Some of the grafts have been examined previously for the presence of dendritic cells [36]. However, in this study, different segments of the grafts were used and were processed separately. Ten segments of normal long saphenous veins were harvested from patients undergoing femoro-popliteal bypass graft operation that served as a control to compare the degree of histological alteration occurring in stenotic saphenous vein bypass grafts.

Tissue preparation

Areas of macroscopic luminal stenosis affecting explanted vein grafts were identified and divided into two segments: one to undertake immunohistochemistry, and the other for electron microscopy. Normal veins were similarly divided into two segments. For immunohistochemical analysis, the segments were fixed in 10% neutral buffered formalin and embedded in paraffin. Consecutive parallel sections of 5 μm thickness were cut and air-dried. Sections were stained with haematoxylin and eosin for routine histological examination. For transmission electron microscopic analysis, adjacent segments were fixed in 2.5% glutaraldehyde in 0.1 M phosphate buffered saline (pH 7.4).

Histology and selection of graft areas for further quantitative analysis

Routine microscopic examination of vein grafts demonstrated two distinct forms of graft occlusion: four out of the 14 grafts (29%) resulted from an organized fibrotic thrombus, while the remaining (71%) were due to the development of atherosclerotic lesions associated with mural thrombosis. For quantitative analysis, six specific areas within each graft were identified and analyzed. These included areas of hyperplastic intima affected by atherosclerosis evidenced by the presence of foam cells. The non-atherosclerotic intima was classified into two, namely, the cellular and acellular areas. Acellular areas were those that consisted primarily of extracellular connective tissue matrix that contained less than 35 cells per microscopic field of 200×200 μm^2 examined at ×400 magnification. Cellular areas were those that contained larger numbers of intimal cells in comparison to acellular areas, with lower extracellular matrix content. Cellular and acellular areas of the media were similarly selected. Areas of neovascularization in the media were also analyzed.

Immunohistochemical examination for the expression of apoptosis-related proteins

Apoptosis-related proteins, including anti-apoptotic (Bcl-2) and pro-apoptotic (Fas, p53, BAX and caspase-3) proteins were detected using monoclonal antibodies to Bcl-2, Fas, p53, and BAX, and polyclonal antibody to CPP32 (that labels caspase-3). The working concentrations of the antibodies are detailed in *Table 2*.

Immunohistochemical analysis was carried out using the standard avidin–biotin complex (ABC) immunoperoxidase technique [37]. Deparaffinized sections were treated by boiling in citrate buffer (pH 6.0) to retrieve antigenicity. All sections were blocked with 3% hydrogen peroxide (peroxidase blocking) prior to staining. Sections to be stained with the antibody to CPP32 were additionally blocked with 1% normal goat serum (protein blocking). After washing in Tris-buffered saline (TBS, pH 7.6), sections were incubated in the primary antibody for 60 min, followed by incubation

Table 1 Clinical characteristics of aortocoronary saphenous vein bypass grafts[a]

Patient	Sex	Age	1st surgery	2nd surgery	Mean graft implant time (years)	Hypercholesterolaemia
1	M	73	1989	1999	10	−
2	F	71	1989	1999	10	+
3	M	74	1988	1999	11	+
4	M	74	1978	1999	21	+
5	F	71	1991	1999	8	−
6	M	75	1983	1999	16	−
7	M	69	1986	1998	12	−
8	M	64	1985	1998	13	+
9	F	55	1988	1998	10	−
10	M	51	1987	1998	11	+
11	M	52	1990	1998	8	+
12	M	64	1982	1998	16	+
13	M	70	1985	1998	13	+
14	M	69	1977	1999	22	+

[a]Hypercholesterolaemia: +indicates serum cholesterol level >5.5 mmol/l; −indicates serum cholesterol level <5.5 mmol/l

Table 2 Antibodies used in the study

Designation	Type[a]	Clone	Specificity	Source	Working dilution
PCNA	M	PC10	Proliferating cell nuclear antigen	DAKO	1:50
sma	M	ASM-1	Smooth muscle α-actin (smooth muscle cells)	Novocastra	1:25
CD68	M	PG-M1	CD68 (macrophages/monocytes)	DAKO	1:50
CD3	P	-	CD3 (T cells)	DAKO	1:500
Fas	M	FAS9	FAS receptor	Zymed	1:100
P53	M	DO-1	Transcription factor p53	Immunotech	1:50
BAX	M	2D2	Human BAX protein	Zymed	1:50
Bcl-2	M	Bcl2-100	Bcl-2 oncogene	Zymed	1:50
CPP-32	P	-	Caspase-3	DAKO	1:50

[a]M - monoclonal antibody; P - polyclonal antibody

in the appropriate secondary antibody (horse anti-mouse, Vector BA-2000 or goat anti-rabbit, Vector BA-1000) for 20 min, and finally with ABC (Elite Vector PK-6100) for 30 min. The immunological reaction was visualized by treating in 3,3′-diaminobenzidine (DAB) solution for 2 min, which gave a brown colouration. Sections were counterstained with Mayer's haematoxylin. For negative control, the primary antibody was omitted or the sections treated with an immunoglobulin fraction of suitable non-immune serum as a substitute for the primary antibody. No positive staining was observed in any of the negative control sections. Sections were examined under an Olympus microscope at ×100 and ×400 magnifications.

In situ analysis of DNA fragmentation

In situ detection of DNA fragments using TUNEL is commonly used to investigate apoptosis [38, 39]. During apoptosis, cleavage of genomic DNA yields double-stranded, low molecular weight DNA fragments along with single strand breaks ('nicks') of high molecular weight DNA. TUNEL labels these DNA strand breaks with modified nucleotides [38, 39]. However, TUNEL may not only label the early stage of orderly DNA fragmentation in apoptosis, but also the nuclear breakdown during the later stages of necrosis [38, 40]. Hence, although the demonstration of DNA fragmentation in atherosclerotic plaques may provide direct evidence for the presence of degenerating cells, it does not completely discriminate between apoptotic and necrotic cell degeneration [38, 40]. To overcome this uncertainty, in the present study we employed TUNEL labelling to localize and quantify cells dying both by apoptosis and necrosis with an in situ death detection kit (1684817, Boehringer Mannheim), and the differentiation carried out by electron microscopy. Deparaffinized sections were rehydrated, following which they were incubated with proteinase K (20 μg/ml in 10m M Tris/HCl, pH 7.4) for 15 min and washed with TBS. DNA fragments were labelled

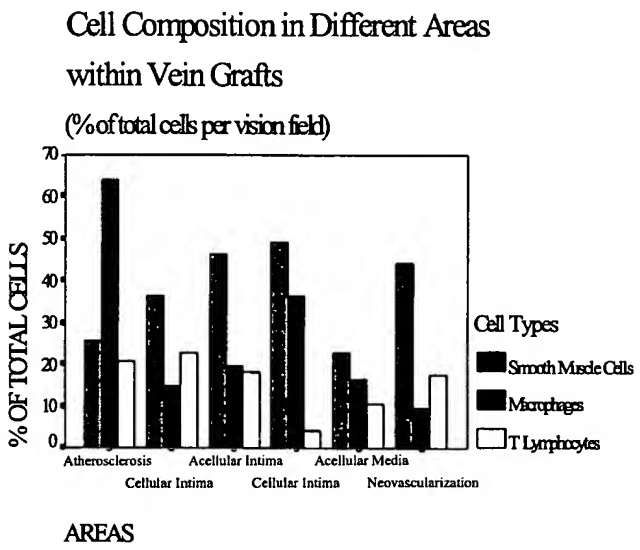

Figure 1 Cell composition in different areas of aortocoronary saphenous vein bypass grafts

with fluorescein-dUTP. The terminal transferase and the labelled DNA fragments were detected with alkaline phosphatase (AP)-conjugated antibody against fluorescein. Fast red was used as the substrate solution, rendering a pink colour to labelled nuclei.

Immunohistochemical analysis of DNA synthesis

DNA synthesis was identified using the monoclonal antibody to proliferating cell nuclear antigen (anti-PCNA), employing the ABC immunoperoxidase technique [37] as described earlier.

Identification of different cell types

Cell type specific antibodies, including anti-CD68 (to identify macrophages), anti-CD3 (T-lymphocytes) and anti-α-SMA (smooth muscle actin to identify smooth muscle cells), were used. The working concentrations of the antibodies are detailed in *Table 2*.

Quantification and statistics

In every specimen, the expression of apoptosis-related proteins, the numbers of TUNEL+ cells, PCNA+ cells, and the cellular composition were evaluated on consecutive sections in each of the six areas, namely (1) atherosclerotic areas, (2) cellular and (3) acellular non-atherosclerotic hyperplastic intima, (4) cellular and (5) acellular areas of the media, and (6) areas of neovascularization in the media. In each area, the total cell number and the number of cells stained by peroxidase/AP (brown/pink staining) were counted at a high magnification (×400) in five randomly chosen fields from each section. The average cell counts of the cellular

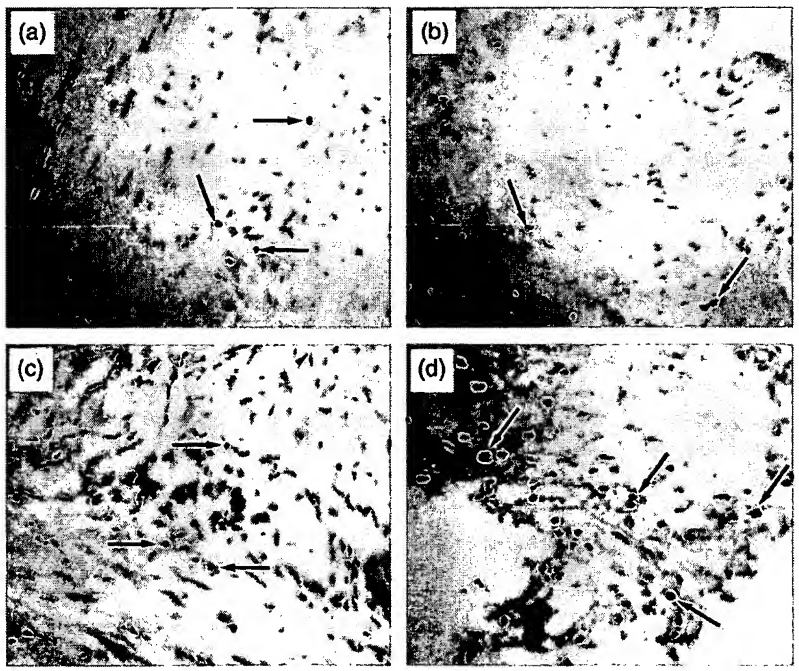

Figure 2 Apoptosis-related protein (p53, Bax) expressions in non-atherosclerotic intima (A,C) and atherosclerotic areas (B,D) of aortocoronary saphenous vein bypass grafts. ABC immunoperoxidase technique, counterstained with Mayer's haematoxylin. (A,B,C,D) ×100

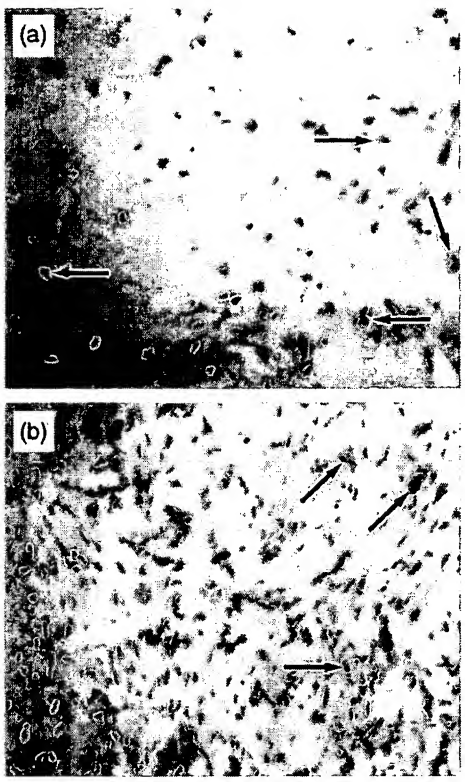

Figure 3 DNA fragmentation (A) and DNA synthesis (B) in aortocoronary saphenous vein bypass grafts. Numerous TUNEL+ (A) and PCNA+ (B) cells are evident in the cellular intima. (A): TUNEL immunoreactivity in the non-atherosclerotic cellular intima. (B): PCNA positivity around inflammatory infiltrates at the base of the non-atherosclerotic cellular intima. TUNEL — In Situ Death Detection Kit, AP; PCNA — ABC immunoperoxidase technique. Counterstaining with Mayer's haematoxylin. (A,B) ×100

and acellular intima in each specimen were taken to be the count of the intima for that specimen for each variable. Similarly, the average values of the cellular and acellular media were taken to be the count of the media for that specimen for each variable. All variables were presented as a percentage of the total number of cells in that area.

Differences in mean were determined by the Student's *t*-test. A value of $P<0.05$ was considered significant. Correlation between groups was determined by Pearson's rank correlation coefficient. SPSS program (version 7.0, Educational Edition) was used to obtain statistical calculations.

Electron microscopy

For ultrastructural analysis, the specimens were cut transversely into small pieces of 2–3 mm through all the layers of the vessel (tunica intima, media and adventitia), and postfixed in 1% osmium tetroxide. Specimens were dehydrated in graded ethanol before embedding in Araldite resin. Semithin sections were stained with Toluidine blue, and analysed for selecting areas for ultrathin sectioning. Ultrathin sections stained with uranyl acetate and lead citrate were examined with the aid of a Hitachi H7000 electron microscope at an accelerating voltage of 75 kV.

Results

Cellular density

In general, the cellular density was higher in the intima than in the media. In atherosclerotic plaques, cells of macrophage origin (CD68+) were the major cell type (mean 63.89±4.95%, range 33.3–87.0%; *Figure 1*) with most exhibiting a foam cell appearance. The percentages of T-lymphocytes and smooth muscle cells in plaques varied from 0 to 45.8% (mean 20.73±3.24%), and from 0 to 65.4% (mean 25.51±5.66%) respectively (*Figure 1*). In non-atherosclerotic intimal areas, smooth muscle cells were the predominant cell type (mean 41.23±3.00%, range 19.7–68.9%; *Figure 1*). Similarly, in the media, smooth muscle cells were the major cell type (mean 39.82±4.57%, range 1.0–68.1%; *Figure 1*).

Expression of apoptosis-related proteins

Anti-apoptotic (Bcl-2) and pro-apoptotic (p53, Fas, Bax and CPP-32) proteins were expressed in all areas of grafts. A high level of Bcl-2 positivity was found in atherosclerotic plaques (mean 35.32±9.00%, range 0–90.5%), approximately 6.1 times higher than in the adjacent intima (mean 5.68±2.1%; range 0–20.0%) and media (mean 5.8±1.38%, range 0–14.8%). p53 expression was localized in cellular areas of the intima [mean 22.64±3.95%, range 2.2–44.0%; *Figure 2(A)*]. High levels of p53 immunostaining were also observed in the atherosclerotic areas [mean 19.06±5.48%, range 0–42.2%; *Figure 2(B)*] and were four times higher than that in the media (mean 4.64±1.45%, range 0–13.5%). Bax immunoreactivity was most prominent in the non-atherosclerotic cellular intima [mean 52.17±7.19%, range 0.7–91.8%; *Figure 2(C)*]. In atherosclerotic areas, its expression was 40.36±4.10% [range 24.5–70.4%; *Figure 2(D)*], while in the media, only 11.05±2.8% of cells expressed Bax (range 0.3–26.1%). CPP32+ cells were mostly located in the cellular intima (mean 32.18±5.13%, range 8.1–61.0%). In atherosclerotic areas, 28.85±2.41% of cells showed positivity (range 11.4–38.7%), while the least expression of CPP32 was observed in the media (mean 8.42±2.61%, range 0–23.0%). In all areas of grafts, Fas expression was lower when compared to all other pro-apoptotic proteins, being 5.57±2.94% (range 0–33%) in atherosclerotic areas, 3.81±1.87% (range 0–17.5%) in the non-atherosclerotic intima, and <0.01% in the media.

In control veins, the expression of all apoptosis-related proteins that were studied was either absent or very low (<0.5%).

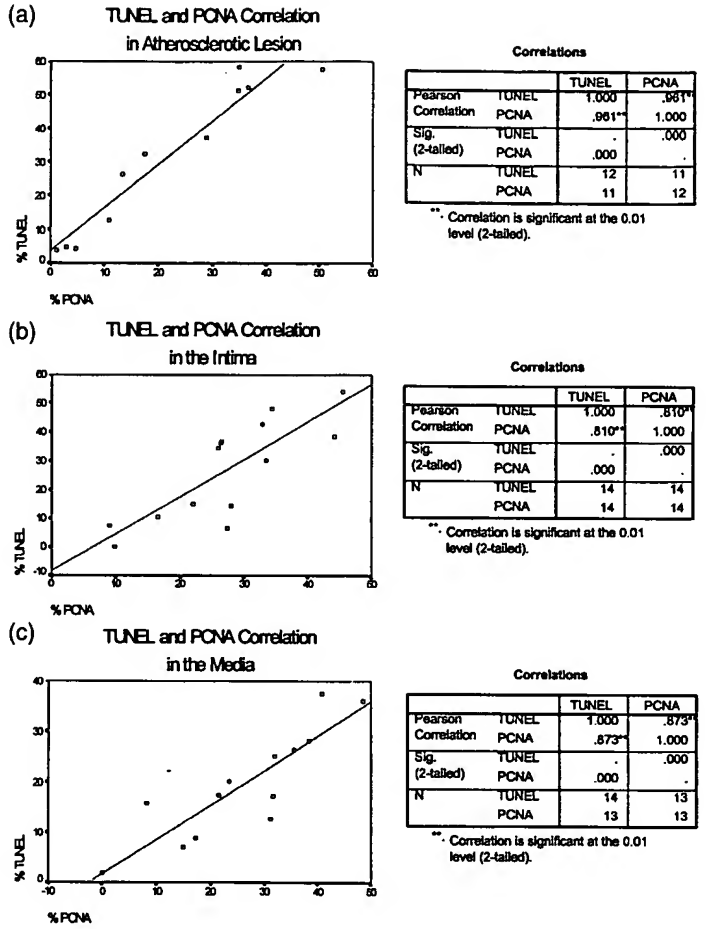

Figure 4 Correlations between TUNEL+ and PCNA+ cells in atherosclerotic areas (A), the intima (B) and the media (C) of aortocoronary saphenous vein bypass grafts, using Pearson correlation coefficient and Student's *t*-test. *P* values <0.05 were taken as being significant

TUNEL+ cells and PCNA+ cells

TUNEL+ cells were distributed unevenly throughout the graft wall. 28.67±6.56% of cells stained positive for TUNEL in atherosclerotic areas (range 1.0–58.4%). Aggregates of TUNEL+ cells were mostly present around the necrotic core and these aggregates were usually localized only at one pole rather than being evenly distributed around the necrotic core. There were approximately 1.6 times higher numbers of TUNEL+ cells in the non-atherosclerotic intima [mean 27.01±4.63%, range 3.0–54.3%; *Figure 3(A)*] than in the media (mean 18.73±2.94%, range 2.0–37.7%). In control veins, very scarce or no TUNEL-labelled nuclei were detected (<0.01%).

DNA synthesis as demonstrated by PCNA expression in control veins was either absent or very rare (<0.01%), while in the vein grafts, a large number of cells were PCNA+ [*Figure 3(B)*]. In atherosclerotic areas, the number of PCNA+ cells ranged from 0 to 69.5% (mean 25.55±6.04%). The non-atherosclerotic intima had a slightly greater proportion of PCNA+ cells than the media (27.26±2.56% in the intima vs 24.41±3.75% in the media). Most PCNA+ cells were located in areas of neovascularization in the media (mean 53.00±7.18%, range 6.3–77.9%) where the percentage of PCNA+ cells was approximately twice as high as that in the intima and media.

Correlation between TUNEL+ cells, PCNA+ cells and apoptosis-related protein expression

The number of TUNEL+ cells strongly correlated to the number of PCNA+ cells in atherosclerotic areas [$r = 0.961$, $P<0.001$; *Figure 4(A)*] and in the non-atherosclerotic intima [$r = 0.810$, $P<0.001$; *Figure 4(B)*]. Similarly, there was positive correlation between TUNEL and PCNA immunoreactivities in the media [$r = 0.873$, $P<0.001$; *Figure 4(C)*]. However, no correlation was noted between the number of TUNEL+ and PCNA+ cells in areas of neovascularization. In these areas, DNA synthesis was notably

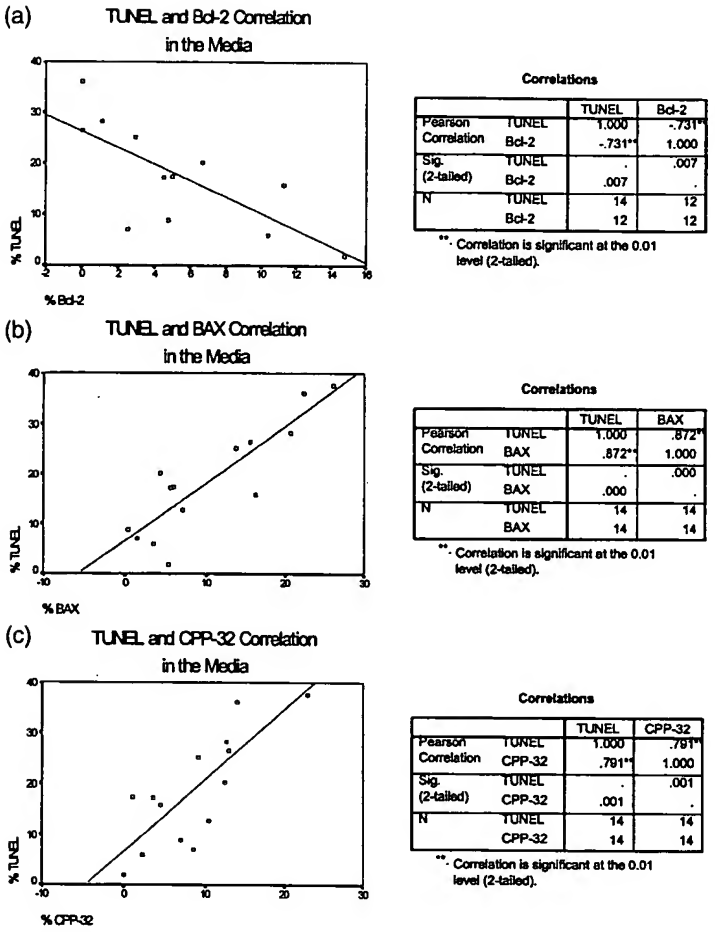

Figure 5 Correlations between TUNEL+ cells and apoptosis-related protein expressions in different areas within aortocoronary saphenous vein bypass grafts. Negative correlations between TUNEL and Bcl-2 positivities were observed in the media (A). In contrast, TUNEL correlated directly with Bax (B) and CPP-32 (C) in the media. *P* values <0.05 were taken as being statistically significant

higher in comparison to all other areas, but only few cells undergoing DNA fragmentation were observed.

Strong negative correlation was observed between Bcl-2+ cells and TUNEL+ cells in atherosclerotic areas ($r = -0.671$, $P<0.05$). A strong positive correlation was observed between the numbers of TUNEL+ cells and p53+ cells in cellular areas of the intima ($r = 0.736$, $P<0.005$). In the media, there was negative correlation between TUNEL+ cells and Bcl-2+ cells [$r = -0.731$, $P<0.007$; *Figure 5(A)*], while TUNEL+ cells correlated positively with both Bax+ cells [$r = 0.872$, $P<0.001$; *Figure 5(B)*] and CPP32+ cells [$r = 0.791$, $P<0.001$; *Figure 5(C)*].

Electron microscopic analysis

Ultrastructural analysis of atherosclerotic and non-atherosclerotic intima of grafts demonstrated large number of cells showing signs of cellular destruction that included features of perinuclear membrane rupture, plasmalemmal degeneration, and oedema of the cytoplasm [*Figure 6(A,B)*]. In non-atherosclerotic areas within the hyperplastic intima as well as in the underlying media, some cells contained condensed and fragmented chromatin within the intact cytoplasm [*Figure 7(A)*]. In other cells, the entire cytoplasm including the chromatin was fragmented [*Figure 7(B)*]. In these cells, the cytoplasmic fragments were surrounded by an intact membrane and contained intact mitochondria [*Figure 7(B)*]. Accumulation of these nuclear remnants and cytoplasmic fragments within macrophages was observed in the hyperplastic non-atherosclerotic intima [*Figure 8(A,B)*]. In contrast, no chromatin fragmentation and no formation of apoptotic bodies were observed in atherosclerotic areas.

Discussion

The present immunohistochemical observations demonstrated that pro-apoptotic proteins were

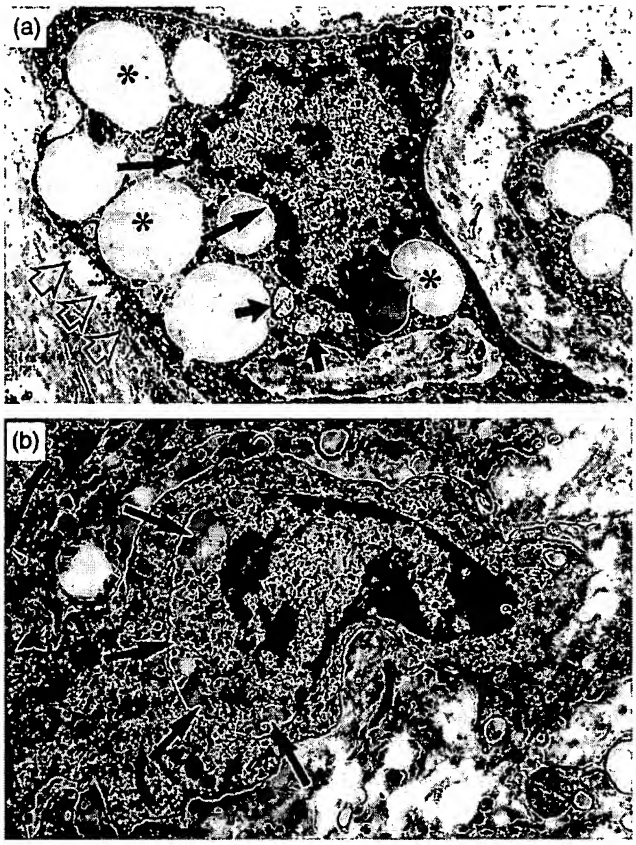

Figure 6 Necrotic alteration in cells located in atherosclerotic areas of aortocoronary saphenous vein bypass grafts. (A): Destructive changes in the nuclear membrane (large solid arrows) and their plasmalemma (open arrows) in a foam cell. Small solid arrows show swollen mitochondria containing destroyed cristae. 'Lipid droplets' are marked by asterisks. (B): Destruction of the nuclear membrane and distortion of the chromatin within a cell which is characterized by the presence of intact cytoplasm. Electron micrographs. Magnifications ×7100; ×9600

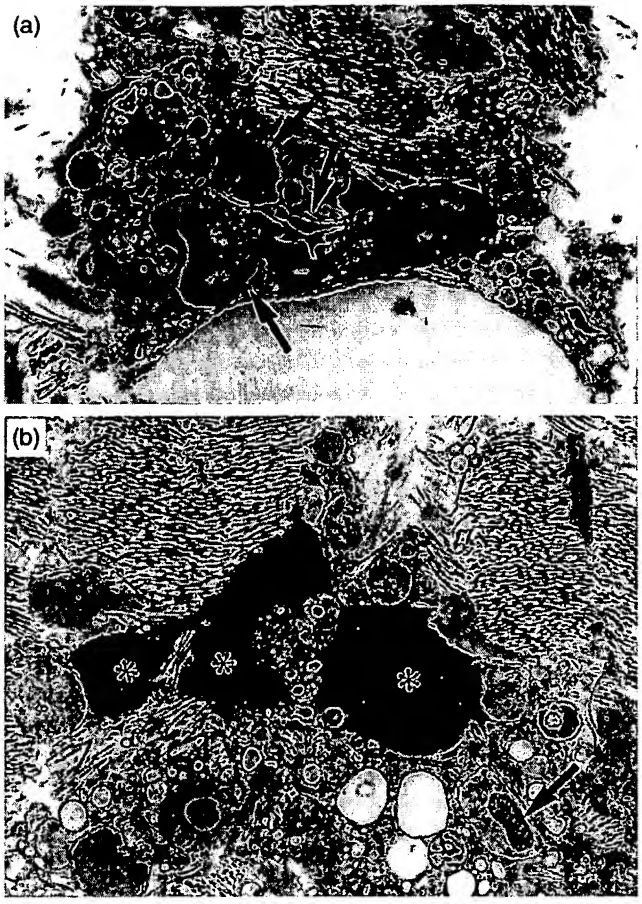

Figure 7 Apoptotic alterations of cells located in the deep portion of the hyperplastic intima of aortocoronary saphenous vein bypass grafts. (A): Condensation and fragmentation of chromatin (arrows) in a cell which is characterized by intact cytoplasm. (B): Fragmentation of condensed chromatin (asterisks) and fragmentation of the cytoplasm. Note that cytoplasmic fragments are surrounded by an intact membrane and are located in the extracellular intimal matrix. An intact mitochondrion in a cytoplasm fragment is shown by arrow. Electron micrographs. Magnifications: ×7100; ×9600

widely expressed in stenotic saphenous vein bypass grafts and corresponded to DNA fragmentation as assessed by the TUNEL method. Statistical analysis showed a positive correlation between cell death and DNA synthesis ($P<0.001$). In primary atherosclerosis, the degree of cell death relates to the disease state [41, 42] with the percentage of TUNEL+ cells ranging from 2 to 40% [41, 42]. In the present analysis, 10 of 14 grafts (71%) failed due to long-term atherosclerotic degeneration complicated by thrombosis. In these grafts, TUNEL-positivity in atherosclerotic areas was relatively high.

The percentage of PCNA+ cells in vein grafts was higher when compared to that of primary atheromas [43]. The high numbers of TUNEL+ cells and PCNA+ cells observed in our study suggests an increased cell turnover in vein grafts. This increase in cell turnover may contribute towards the accelerated atherosclerotic changes, leading to eventual graft failure. The incidence of cell death was noted to be higher in atherosclerotic areas when compared to the non-atherosclerotic intima, implying that cell death may contribute to graft instability due to the formation and enlargement of acellular necrotic cores.

The micro-environmental factors that initiate cell death in atherosclerosis are unclear. Our study clearly demonstrated that large numbers of TUNEL+ cells were located near the necrotic core of atherosclerotic lesions. Ultrastructural observation of typical necrotic (hypoxic) features suggests that oxidative stress, responsible for the generation of oxidized lipids and free radicals in the plaque, may be involved in the initiation of cell death in the graft wall. PCNA+ cells exceeded the number of TUNEL+ cells by two-fold and was markedly higher than in the primary atheroma. This is probably associated with vein graft arterialization and DNA syn-

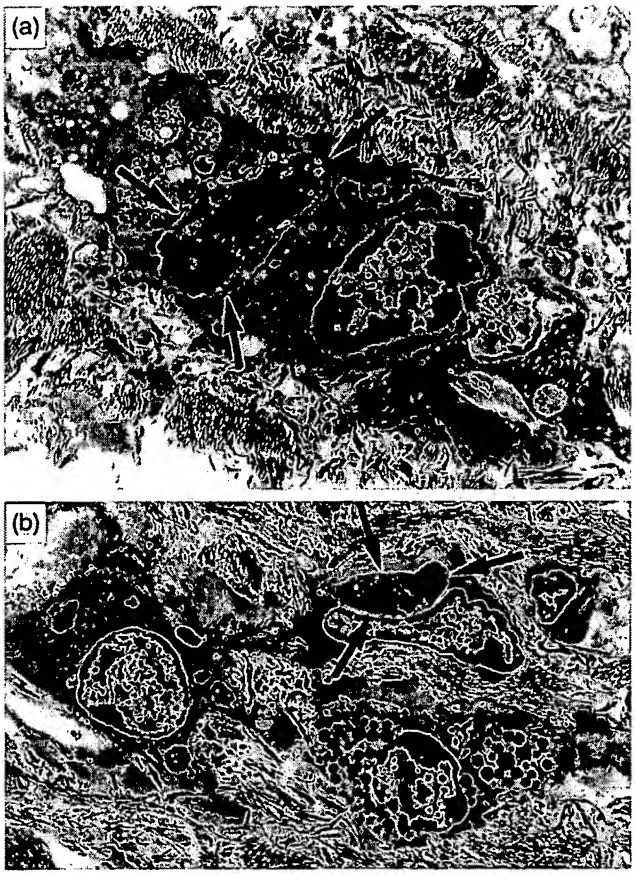

Figure 8 Cell remnants (apoptotic bodies) (arrows) within macrophages in the deep portion of the hyperplastic intima in aortocoronary saphenous vein bypass grafts (A,B). Electron micrographs ×7100; ×4200

thesis in the medial smooth muscle cells, further contributing to graft instability and enhancing failure.

In the media, typical ultrastructural features of both apoptosis and necrosis were evident. Both Bax+ and CPP32+ cells strongly correlated with TUNEL+ cells. However, the extent of these pro-apoptotic protein expressions was generally lower than the TUNEL-positivity. Anti-apoptotic protein (Bcl-2) expression correlated inversely with TUNEL+ cells, while p53 expression, although present, showed no correlation with TUNEL+ cells, suggesting that there exists a complex interaction between pro- and anti-apoptotic proteins that may regulate apoptotic pathways in the vein graft.

Conclusion

The aetiology of long-term ASVBG failure is probably multifactorial and is yet to be fully determined [6]. Our observations indicate that DNA fragmentation and synthesis in both atherosclerotic and non-atherosclerotic areas of vein grafts are higher when compared to normal saphenous veins. In atherosclerotic areas of stenotic saphenous vein bypass grafts, cell death occurs mostly by necrosis despite a high expression of pro-apoptotic proteins. In non-atherosclerotic areas of the grafts, including the hyperplastic intima and the media, cell death occurs by apoptosis and necrosis.

Acknowledgements

The research was supported by the St Vincent's Clinic Foundation, Sydney, Australia

References

1. Flemma, R. J., Mullen, D. C. and Lepley, D., Aortocoronary vein bypass grafting. In *Vascular Grafts*, eds P. N. Sawyer and M. J. Kaplitt. Appleton Century Crofts, New York 1978.
2. Szilagyi, D. E., Atherogenesis in venous bypass grafts. In *Vascular Grafts*, eds P. N. Sawyer and M. J. Kaplitt. Appleton Century Crofts, New York 1978.
3. Kirklin, J. K. and Barrat-Boyes, B. G., Ischaemic heart disease. In. *Cardiac Surgery*, Vol. 1 Churchill Livingston, Edinburgh,. 1993.
4. Cambria, R. P. and Abbott, W. M., Translocated autogenous vein grafts. In., *Vascular Surgery*, Vol. 1 W. B. Saunders Company, Sydney 1989.
5. Nielsen, T. G., Laursen, H., Gronholdt, M. L. *et al*, Histopathological features of in situ vein bypass stenoses. *European Journal of Vascular and Endovascular Surgery*, 1997, 14 492–498.
6. Motwani, J. G. and Topol, E. J., Aortocoronary saphenous vein graft disease: pathogenesis, predisposition, and prevention. *Circulation*, 1998, 97 916–931.
7. Meyer, D., Baumgardt, S., Lofeler, S. *et al*, Apoptosis in combined liver/small bowel transplantation. *Transplantation Proceedings*, 1998, 30 2588.
8. Schierle, G. S., Hansson, O., Leist, M. *et al*, Caspase inhibition reduces apoptosis and increases survival of nigral transplants. *Nature Medicine*, 1999, 5 97–100.
9. Cagiannos, C., Zhong, R., Zang, Z. *et al*, Effect of major histocompatibility complex expression on murine intestinal graft survival. *Transplantation*, 1998, **66** 1369–1374.
10. Hayakawa, K., Sato, H., Aoyagi, T. *et al*, Apoptosis in acute cellular rejection in murine renal allotransplantation. *Transplantation Proceedings*, 1998, 30 2944–2946.
11. Hayashi, M., Martinez, O. M., Krams, S. M. *et al*, Characterization of allograft rejection in an experimental model of small intestinal transplantation. *Journal of Gastrointestinal Surgery*, 1998, 2 325–332.
12. Kageyama, Y., Li, X. K., Suzuki, S. *et al*, Apoptosis is involved in acute cardiac allograft rejection in rats. *Annals of Thoracic Surgery*, 1998, **65** 1604–1609.
13. Kirsch, G. M., Kearsey, J., Butr, T. *et al*, Medial smooth muscle cell loss in arterial allografts occurs by cytolytic cell induced apoptosis. *European Journal of Cardiothoracic Surgery*, 1998, **14** 89–96.
14. Krams, S. M. and Martinez, O. M., Apoptosis as a mechanism of tissue injury in liver allograft rejection. *Seminars in Liver Disease*, 1998, **18** 153–167.
15. Boonman, Z. and Isacson, O., Apoptosis in neuronal development and transplantation: role of caspases and trophic factors. *Experimental Neurology*, 1999, **156** 1–15.
16. Vriens, P. W., Blankenberg, F. G., Stoot, J. H. *et al*, The use of technetium Tc 99m annexin V for in vivo imaging of apoptosis during cardiac allograft rejection. *Journal of Thoracic and Cardiovascular Surgery*, 1998, **116** 844–853.
17. Fandrich, F., Dresske, B., Lin, X. *et al*, Allopeptide-mediated expression of endothelial Fas-ligand (CD95L) in long-term tolerized heterotopic rat heart grafts. *Transplantation Proceedings*, 1999, **31** 1558–1559.

18. Koglin, J., Granville, D. J., Glysine-Jensen, T. *et al*, Attenuated acute cardiac rejection in NOS2 −/− recipients correlates with reduced apoptosis. *Circulation*, 1999, **99** 836–842.
19. August, C., Schmid, K. W., Dietl, K. H. *et al*, Prognostic value of lymphocyte apoptosis in acute rejection of renal allografts. *Transplantation*, 1999, **67** 581–585.
20. Rabinovitch, A., Suarez-Pinzon, W., Trynadka, K. *et al*, Transfection of human pancreatic islets with an anti-apoptotic gene (Bcl-2) protects beta-cells from cytokine-induced destruction. *Diabetes*, 1999, **48** 1223–1229.
21. Johnson, T. M., Epstein, S. E. and Finkel, T., Apoptosis in vascular disease: opportunities for genetic therapeutic intervention. *Seminars in Interventional Cardiology*, 1996, **1** 195–202.
22. Bennett, M. R., Apoptosis in vascular disease. *Transplantation Immunology*, 1997, **5** 184–188.
23. Maclouf, J., Folco, G. and Patrono, C., Eicosanoids and isoeicosanoids: constitutive, inducible and transcellular biosynthesis in vascular disease. *Thrombosis and Haemostasis*, 1998, **79** 691–705.
24. Murakami, K., Kawase, M., Kondo, T. *et al*, Cellular accumulation of extravasated serum protein and DNA fragmentation following vasogenic edema. *Journal of Neurotrauma*, 1998, **15** 825–835.
25. Pollman, M. J., Hall, J. L., Mann, M. J. *et al*, Inhibition of neointimal cell bcl-x expression induces apoptosis and regression of vascular disease. *Nature Medicine*, 1998, **4** 222–227.
26. Isner, J. M., Kearney, M., Bortman, S. *et al*, Apoptosis in human atherosclerosis and restenosis. *Circulation*, 1995, **91** 2703–2711.
27. Crisby, M., Kallin, B., Thyberg, J. *et al*, Cell death in human atherosclerotic plaques involves both oncosis and apoptosis. *Atherosclerosis*, 1997, **130** 17–27.
28. Lutgens, E., de Muinck, E. D., Kitslaar, P. J. *et al*, Biphasic pattern of cell turnover characterizes the progression from fatty streaks to ruptured human atherosclerotic plaques. *Cardiovascular Research*, 1999, **41** 473–479.
29. Kearney, M., Pieczek, A., Haley, L. *et al*, Histopathology of instent restenosis in patients with peripheral artery disease. *Circulation*, 1997, **95** 1998–2002.
30. Kockx, M. M., de Meyer, G. Y., Bult, H. *et al*, Distribution of cell replication and apoptosis in atherosclerotic plaques of cholesterol-fed rabbits. *Atherosclerosis*, 1996, **120** 115–124.
31. Harada, K., Chen, Z., Ishibashi, S. *et al*, Apoptotic cell death in atherosclerotic plaques of hyperlipidemic knockout mice. *Atherosclerosis*, 1997, **135** 235–239.
32. Kockx, M. M., de Meyer, G. R., Buyssens, N. *et al*, Cell composition, replication, and apoptosis in atherosclerotic plaques after 6 months of cholesterol withdrawal. *Circulation Research*, 1998, **83** 378–387.
33. Lutgens, E., Daemen, M., Kockx, M. M. *et al*, Atherosclerosis in APOE*3-Leiden transgenic mice: from proliferative to atheromatous stage. *Circulation*, 1999, **99** 276–283.
34. Shindo, J., Ishibashi, T., Yokoyama, K. *et al*, Granulocyte–macrophage colony-stimulating factor prevents the progression of atherosclerosis via changes in the cellular and extracellular composition of atherosclerotic lesions in watanabe heritable rabbits. *Circulation*, 1999, **99** 2150–2156.
35. World Medical Association Inc World Medical Association Declaration of Helsinki. Recommendations guiding physicians in biomedical research involving human subjects. *Cardiovascular Research*, 1997, **35** 2–3.
36. Cherian, S. M., Bobryshev, Y. V., Inder, S. J. *et al*, Involvement of dendritic cells in long-term aortocoronary saphenous vein bypass graft failure. *Cardiovascular Surgery*, 1999, **7** 508–518.
37. Hsu, S. M., Raine, L. and Fanger, H., Use of avidin–biotin–peroxidase complex (ABC) in immunoperoxidase techniques: a comparison between ABC and unlabelled antibody (PAP) procedures. *Journal of Histochemistry and Cytochemistry*, 1981, **29** 577–580.
38. Kressel, M. and Groscurth, P., Distinction of apoptotic and necrotic cell death by in situ labeling of fragmented DNA. *Cell Tissue Research*, 1994, **278** 549–556.
39. Gavrieli, Y., Sherman, Y. and Ben-Sasson, S. A., Identification of programmed cell death in situ via specific labeling of nuclear DNA fragmentation. *Journal of Cell Biology*, 1992, **119** 493–501.
40. Kimura, K., Sasano, H., Shimosegawa, T. *et al*, Ultrastructural and confocal laser scanning miroscopic examination of TUNEL-positive cells. *Journal of Pathology*, 1997, **181** 235–242.
41. Kockx, M. M., Apoptosis in the atherosclerotic plaque: quantitative and qualitative aspects. *Arteriosclerosis Thrombosis and Vascular Biology*, 1998, **18** 1519–1522.
42. Kockx, M. M. and Herman, A. G., Apoptosis in atherogenesis: implications for plaque destabilization. *European Heart Journal*, 1998, **19** (Suppl G) G23–G28.
43. Rekhter, M. D. and Gordon, D., Active proliferation of different cell types, including lymphocytes, in human atherosclerotic plaques. *American Journal of Pathology*, 1995, **147** 668–677.

Paper accepted 18 September 2000

Circulation
scientific sessions Pre-Session Symposia American Heart Association

(*Circulation.* 2001;104:I-233.)

Thoracic Transplantation and Ventricular Assist Devices

Quantitative Myocardial Cytokine Expression and Activation of the Apoptotic Pathway in Patients Who Require Left Ventricular Assist Devices

Emma J. Birks, MRCP; Najma Latif, PhD; Virginia Owen, PhD; Christopher Bowles, PhD; Leanne E. Felkin, BS; Anthony J. Mullen, BS; Asghar Khaghani, FRCS; Paul J.R. Barton, PhD; Julia M. Polak, DSc; John R. Pepper, FRCS; Nicholas R. Banner, FRCP; Magdi H. Yacoub, FRS, DSc

National Heart and Lung Institute at Imperial College School of Medicine (E.J.B., V.O., C.B., L.E.F., A.J.M., A.K., P.J.R.B., J.R.P., N.R.B., M.H.Y.), Royal Brompton and Harefield Hospital, Harefield, Middlesex; and Royal Postgraduate Medical School at Imperial College School of Medicine (J.M.P.), Hammersmith Hospital, London, UK.

Correspondence to Magdi Yacoub, FRS, Professor of Cardiothoracic Surgery, Heart Science Centre, Royal Brompton and Harefield Hospital, Harefield, Middlesex UB96JH, United Kingdom. E-mail

emmabirks@hotmail.com

Abstract

▲ Top
▪ Abstract
▼ Introduction
▼ Methods
▼ Results
▼ Discussion
▼ References

Background— Molecular mechanisms underlying the deterioration of patients undergoing LV assist device (LVAD) implantation remain poorly understood. We studied the cytokines tumor necrosis factor (TNF)-α and interleukin (IL)-1ß and IL-6 and the terminal stage of the apoptotic pathway in patients with decompensating heart failure who required LVAD support and compared them with patients with less severe heart failure undergoing elective heart transplantation.

Methods and Results— Myocardial and serum samples from 23 patients undergoing LVAD implantation were compared with those from 36 patients undergoing elective heart transplantation. Myocardial TNF-α mRNA (1.71-fold; $P<0.05$) and protein (3.43±0.19 versus 2.95±0.10 pg/mg protein; $P<0.05$) were elevated in the LVAD patients. Immunocytochemistry demonstrated TNF expression in the myocytes. Serum TNF-α was also elevated (12.5±1.9 versus 4.0±0.4 pg/mL; $P<0.0001$) in the LVAD patients. IL-6 mRNA (2.57-fold higher; $P<0.005$) and protein (27.83±9.35 versus 4.26±1.24 pg/mg protein; $P<0.001$) were higher in the LVAD candidates, as was serum IL-6 (79.3±23.6 versus 7.1±1.6 pg/mL; $P<0.0001$). Interleukin-1ß mRNA expression was 9.78-fold higher in the LVAD patients ($P<0.001$). iNOS mRNA expression was similar to that in advanced heart failure patients and was not further elevated in the LVAD patients. Levels of procaspase-9 (8.02±0.91 versus 6.16±0.43 oligodeoxynucleotide [OD] units; $P<0.01$), cleaved caspase-9 (10.02±1.0 versus 7.34±0.40 OD units; $P<0.05$), intact and spliced DFF-45 (4.58±0.75 versus 2.84±0.23 OD units; $P<0.05$) were raised in LVAD patients, but caspase-3 and human nuclease CPAN were not.

Conclusions— Elevated TNF-α, IL-1ß, and IL-6 and alterations in the apoptotic pathway were found in the myocardium and elevated TNF-α and IL-6 in serum of deteriorating patients who required LVAD support. These occurrences may have therapeutic implications and influence the timing of LVAD insertion.

Key Words: heart-assist device • interleukins • heart failure • nitric oxide synthase

Introduction

▲ Top
▲ Abstract
▪ Introduction
▼ Methods
▼ Results
▼ Discussion
▼ References

Left ventricular assist devices (LVADs) have become an established treatment for patients with severe heart failure. Molecular mechanisms underlying the decompensation of heart failure remain poorly understood. Understanding the mechanisms involved may help with decisions about timing of LVAD implantation and identifying new therapeutic targets in advanced heart failure.

Expression of the proinflammatory cytokine tumor necrosis factor (TNF)-α has been described in patients with chronic heart failure both in serum and myocardium,[1–5] and serum levels have been found to correlate with functional status.[2] TNF-α has been shown to produce myocardial depression both in in vitro and in vivo models.[2,3,6] Interleukin (IL)-6 also is elevated in myocardium and serum of patients with heart failure, and levels correlate with poor functional status.[1,3,7,8] IL-1ß is known to cause myocardial depression in vivo[9,10] and acts synergistically with TNF-α,[10] but its role in heart failure is unclear.

TNF-α and IL-1ß can activate inducible nitric oxide synthase (iNOS), and their negative inotropic effect can be mediated through iNOS induction.[11] iNOS expression has been described in patients with heart failure.[4] iNOS is a potent producer of nitric oxide, which can have a negative inotropic effect. TNF-α and IL-1ß also can induce apoptosis of cardiac myocytes,[12,13] whereas IL-6 has antiapoptotic effects.[14,15]

Apoptosis is tightly regulated by the caspases, which initially are translated as inactive proenzymes and are subsequently cleaved to become active. In the end stage of the apoptotic pathway, release of cytochrome c from the mitochondrion activates procaspase-9 to caspase-9, which, in turn, activates procaspase-3 to caspase-3. Caspase-3 activates DNA fragmentation factor, a heterodimer[16] that consists of the active capase-activated nuclease (CPAN)/DFF-40 complex, a 40-kDa nuclease, and DFF-45, its 45-kDa inhibitor. Caspase-3 cleaves DFF-45 from the CPAN/DFF-40–DFF-45 complex[16,17] and generates the functionally active CPAN nuclease, which induces chromatin condensation and DNA fragmentation.[18] Poly(ADP-ribose) polymerase (PARP), a DNA repair enzyme, is inactivated by caspase-3, which contributes to the demise of the cell. Our group and others have previously demonstrated evidence of activation of the apoptotic pathway in advanced heart failure.[19,20]

These mechanisms all could contribute to decompensation of patients with advanced heart failure, who then require LVAD support. To investigate this hypothesis, we have quantified myocardial TNF-α, IL-1ß, and IL-6 expression; circulating TNF-α, its receptors, and IL-6; and myocardial expression of iNOS and of caspases in the terminal stage of the apoptotic pathway in patients who require insertion of an LVAD and compared them with patients with stable advanced heart failure awaiting heart transplantation. Our aim was to characterize better patients for which the findings could have implications for their management and to help to understand factors that could influence progression of heart failure.

Methods

▲ Top

Patients

▲ Abstract
▲ Introduction
▪ Methods
▼ Results
▼ Discussion
▼ References

Protocol for the present study was approved by the Royal Brompton and Harefield Research Ethics Committee. Informed consent was obtained from each patient.

LVAD Patients

The present study included 23 consecutive patients who required LVAD implantation because of deteriorating clinical status with evidence of secondary organ dysfunction in the context of low cardiac output (cardiac index <1.8), despite having been given appropriate medical treatment (including inotropes and intra-aortic balloon pump).

Serum markers were studied in all 23 patients (male, n=20; female, n=3; age range, 14 to 58 years; mean age 37±3.1 years). Patients were diagnosed as having dilated cardiomyopathy (n=17), ischemic heart disease (IHD; n=2), IHD with postinfarct ventriculoseptal defect rupture (n=2), postpartum cardiomyopathy (n=1), or congenital heart disease (n=1). All were patients in New York Heart Association (NYHA) class IV and had deteriorated over a period of 3.2±0.6 days. Mean pulmonary capillary wedge pressure (PCWP) was 26.0±2.1 mm Hg. Mean LV end diastolic diameter (LVEDD) was 73.8±6.0 mm, and LV end-systolic diameter (LVESD) was 68.6±6.3 mm. Blood was collected from each patient immediately before insertion of the device.

Myocardial markers were studied in the first 13 of 23 patients (male, n=10; female, n=3; age range, 14 to 58 years; mean age, 35.5±4.1 years). These patients were diagnosed as having dilated cardiomyopathy (n=11), ischemic heart disease with postinfarct ventriculoseptal defect rupture (n=1), or postpartum cardiomyopathy (n=1). All were in NYHA class IV with a history of deterioration over a period of 2.3±0.6 days. Mean PCWP was 27.3±2.5 mm Hg. Mean LVEDD was 75.5±7.9 mm, and LVESD was 64.8±9.8 mm. A core of myocardium from the apex of the LV was taken at the time of LVAD insertion, instantly frozen in liquid nitrogen, and stored at -80°C for subsequent analysis.

Heart Failure Patients

Patients with less-severe heart failure who were undergoing heart transplantation and did not meet our criteria for LVAD implantation acted as controls. Serum markers were studied in 17 patients (men, n=14; women, n=3; age range, 22 to 64 years; mean age, 46.1±3.3 years). NYHA class was III in 13 and IV in 4. Patients were diagnosed as having dilated cardiomyopathy (n=9), ischemic heart disease (n=7), or postpartum cardiomyopathy (n=1). Mean PCWP was 25.4±2.2 mm Hg, mean LVEDD was 70±2 mm, and mean LVESD was 61.2±3 mm.

Myocardial markers were studied in 36 patients (male, n=30; female, n=6; mean age, 46±3.4 years). NYHA class was III in 31 and IV in 5. Patients were diagnosed as having dilated cardiomyopathy (n=18), ischemic heart disease (n=15), postpartum cardiomyopathy (n=2), or myocarditis (n=1). Mean PCWP was 21.9±1.5 mm Hg, mean LVEDD was 71.4±2.6 mm, and mean LVESD was 62.6+2.5 mm. A sample of LV near the apex was taken at the time of transplantation, instantly frozen in liquid nitrogen, and stored at -80°C for subsequent analysis.

For all LVAD and heart failure patients, blood was spun within 4 hours of collection at 2500 rpm for 10 minutes, and serum supernatant was stored at -40°C for analysis.

Methods

Cytokines

Real-Time Quantitative Reverse Transcription-Polymerase Chain Reaction

TNFα, IL-1ß, IL-6, and iNOS mRNA were detected[21] by polymerase chain reaction (PCR) amplification, quantified by 5' nuclease assay with fluorescence-labeled TaqMan probes and analyzed by use of real-time quantitative PCR as follows. Total RNA was extracted by use of Qiagen Inc RNeasy minicolumns and eluted in diethylpyrocarbonate-treated dH_2O. RNA quality and quantity was assessed by EtBr-agarose gel electrophoresis and by relative absorbance at 260 versus 280 nm. cDNA was synthesized from 150 ng of total RNA by use of the PE Biosystems reverse-transcriptase kit with random hexamer primers. Reactions were diluted to 100 μL. Primers and TaqMan probes for human IL-6 and iNOS were designed. Primer Express software (PE Biosystems) was used to design the IL-6 probe from a published mRNA sequence (EMBL/GenBank accession No. M54894), which gave an amplicon size of 96 bp with the TaqMan probe straddling the exon-exon junction (forward primer [Tm=58°C], 5'-TGACAAACAAATTCGGTACATCCT-3'; reverse primer [Tm=60°C], 5'-AGTGCCTCTTTGCTGCTTTCAC-3'; TaqMan probe [Tm=68°C] 5'-TTACTCTTGTTACATGTCTCCTTTCTCAGGGCTG-3'). The iNOS probe designed was 5'-CACCATAAGGCCAAAGGGATTTTAACTTGCAG-3' (Tm=70°C), the forward primer was 5'-AGCGGGATGACTTTCCAAGA-3' (Tm=58°C), and the reverse primer was 5'-TAATGGACCCCAGGCAAGATT-3' (Tm=59°C).

Perkin-Elmer primers and TaqMan probes for TNF-α and IL-ß were used. PCR reactions were performed by use of an ABI-prism 7700 sequence detector. PCR amplifications were performed in a 25-mL volume that contained a 2.5-mL cDNA template in 2x PCR Master Mix (PE Biosystems) at 50°C for 2 minutes and 95°C for 10 minutes followed by 40 cycles of 95°C for 15 s and 60°C for 1 minute. Results were analyzed by use of Sequence Detection Software (PE Biosystems), and the level of expression of TNF-α, IL-1ß, IL-6, and iNOS mRNA was normalized to 18S rRNA as outlined in User Bulletin No. 2 provided by Perkin-Elmer.

Myocardial Immunoassay

Protein was extracted from myocardial tissue. Protein preparations were made by homogenizing myocardial biopsies in 20 mmol/L of HEPES and 1.5 mmol/L of EDTA solution that contained protease inhibitors aprotinin, leupeptin, DTT, and phenylmethylsulfonyl fluoride. Concentrations of TNF-α and IL-6 were determined by use of commercially available immunoassay kits (Quantikine HS, R&D Systems).

Immunocytochemistry

Immunocytochemistry was performed on formalin-fixed paraffin-embedded sections to localize TNF-α and iNOS expression. Avidin-biotin-peroxidase complex method was used. Endogenous peroxidase was blocked with a solution of 0.03% vol/vol hydrogen peroxide in methanol for 20

minutes. After incubation with normal goat serum (1:30 for 30 minutes), sections were incubated overnight at 4°C with primary rabbit antibodies to TNF-α (Antigenex America Inc) diluted 1:100 and incubated overnight with primary rabbit antibodies to iNOS (Transduction Labs) diluted 1:400. Immunoreaction sites were visualized by use of appropriate biotinylated secondary antibodies and the avidin-biotin-peroxidase complex procedure (Vector Labs). Peroxidase activity was revealed with a solution of diaminobenzidine as chromogen with 0.2% vol/vol hydrogen peroxide in PBS to produce a brown reaction product and sections counterstained with Harris' hematoxylin. Controls consisted of replacement of primary antibodies with nonimmune rabbit serum. Staining was graded 0 to 3 by two blinded independent observers.

Serum Immunoassay

Measurements of TNF-α, its receptors TNF-R1 and TNF-R2 and IL-6 were performed by use of commercially available immunoassay kits (Quantikine HS, R&D Systems).

Apoptotic Pathway

SDS-PAGE and Western Blotting

Myocardial tissue was homogenized in 1% SDS, 40 mmol/L phenylmethylsulfonyl fluoride, and total protein homogenates (30 μg) separated on 12%-T SDS-PAGE gels with a 3%-T stacking gel. Gels were equilibrated for 30 minutes in transfer buffer (20 mmol/L Tris base and 150 mmol/L glycine) and electrophoretically transferred to supported nitrocellulose (Hybond C Super) at 500 mA for 1 hour.

Detection of Cellular Proteins

Nitrocellulose membranes were blocked with 3% non-fat dried milk in PBS that contained 0.05% Tween 20 for 1 hour and then probed with primary antibodies against caspase-9, caspase-3, and substrates (PARP and DFF; Santa-Cruz Biotechnology). After they were washed, blots were incubated for another 1 hour in horseradish peroxidase-conjugated secondary antibodies (Dako). Protein bands were visualized by use of the Supersignal Ultra chemiluminescence substrate (Pierce).

Stripping Membranes

To stain tubulin after probing, blots were incubated in stripping solution (100 mmol/L 2-mercaptoethanol, 2% vol/vol SDS, and 62.5 mmol/L Tris-chloride; pH 6.7) for 30 minutes at 56° C. Membranes were washed and probed by use of tubulin with secondary horseradish peroxidase-conjugated antibodies. Reactive bands were detected as before.

Densitometry

Levels of expression of the procaspases, active caspases, and their substrates as assessed by immunoreactivity on ECL films was quantitated by laser densitometry and standardized to tubulin reactivity in each respective lane. Densitometric analysis was performed with Quant One software on a SunSparc station.

Cell Culture

Human U-937 myeloid leukemic cell line, treated separately with TNF-α at 4 mg/mL or staurosporine 1 μmol/L for 4 hours, and Jurkat T lymphoblastoid cell line, treated with 1 μmol/L

of staurosporine for 6 hours, were used as positive controls.

Statistical Analysis

Variables are expressed as mean±SEM. Significance was assessed on grouped data with either Student's *t* test or nonparametric Mann-Whitney *U* test. A *P* value <0.05 was considered significant.

Results

▲ Top
▲ Abstract
▲ Introduction
▲ Methods
▪ Results
▼ Discussion
▼ References

Cytokines

Myocardium

Tumor Necrosis Factor-α

TNF-α mRNA expression in myocardium of LVAD patients at time of implantation was 1.71-fold higher than in stable advanced heart failure patients (*P*<0.05, Figure 1A). TNF-α protein content in myocardium of LVAD candidates (3.43±0.19 pg/mg protein) was also higher than in advanced heart failure (2.95±0.10 pg/mg protein; *P*<0.05, Figure 1B). Myocardial TNF-α protein was slightly higher in those who died after LVAD implantation (3.57±0.2 pg/mg protein) compared with those who survived >1 year (3.1±0.2 pg/mg protein), although this did not reach statistical significance (*P*=NS).

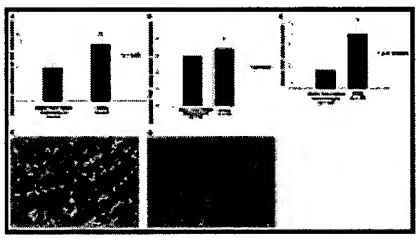

View larger version (39K):
[in this window]
[in a new window]

Figure 1. Advanced heart failure patients awaiting transplantation vs deteriorating patients undergoing LVAD implantation: A, myocardial TNF-α mRNA measured by quantitative real-time RT-PCR; B, myocardial TNF protein. Immunocytochemistry demonstrates greater TNF-α expression in myocytes from deteriorating patients who require LVAD (C) than from those in stable heart failure (D). E, Serum TNF-α. Tx indicates transplantation.

TNF-α Immunocytochemistry

TNF-α expression was immunolocalized predominantly to cardiac myocytes, although expression also was seen in endothelial cells and vascular smooth muscle cells of blood vessels. Myocyte expression of TNF-α in the LVAD candidates was significantly greater (mean score, 1.75±0.20) than in advanced heart failure patients (mean score, 1.1±0.16; *P*<0.05, Figures 1C and 1D).

Interleukin-6

IL-6 mRNA expression in myocardium at time of LVAD implantation was 2.57-fold higher than in stable advanced heart failure patients (*P*<0.005, Figure 2A). Myocardial IL-6 protein content also was significantly higher in LVAD candidates (27.83±9.35 pg/mg protein) compared with advanced heart failure patients (4.26±1.24 pg/mg protein; *P*<0.001, Figure 2B). Myocardial IL-6 protein was significantly higher in those who died after LVAD implantation (38.94±12.34 pg/mg

protein) compared with those who survived >1 year (5.60±1.64 pg/mg protein; $P<0.005$). These deaths occurred in patients who were on the device; no transplant-related deaths occurred).

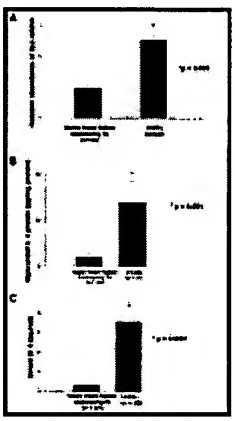

View larger version (12K):
[in this window]
[in a new window]

Figure 2. Advanced heart failure patients awaiting transplantation vs deteriorating patients undergoing LVAD implantation: A, myocardial IL-6 mRNA measured by quantitative real-time RT-PCR; B, myocardial IL-6 protein content; C, serum IL-6.

Interleukin-1ß

IL-1ß mRNA expression was 9.78-fold higher in LVAD candidates than in stable advanced heart failure patients (9.78±0.36 versus 1±0.23; $P<0.001$, Figure 3). IL-1ß was 1.4-fold higher in those who died after LVAD implantation than in those that survived, but this did not reach statistical significance.

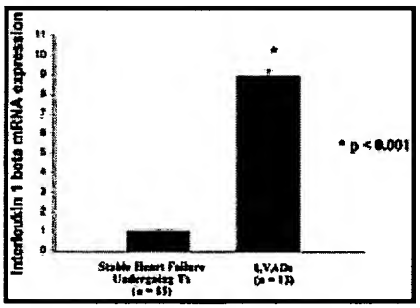

View larger version (12K):
[in this window]
[in a new window]

Figure 3. Myocardial IL-1ß mRNA levels in advanced heart failure patients awaiting transplantation vs deteriorating patients undergoing LVAD implantation.

Inducible Nitric Oxide Synthase

iNOS mRNA expression in LVAD candidates (0.81±0.19) was elevated to a level similar to that seen in advanced heart failure (1±0.27), but iNOS mRNA was no higher in deteriorating patients compared with heart failure patients (Figure 4A).

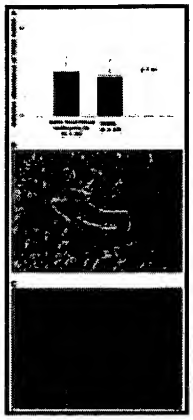

View larger version (52K):
[in this window]
[in a new window]

Figure 4. A, Myocardial iNOS mRNA levels in deteriorating patients undergoing LVAD implantation are no higher than in stable advanced heart failure patients awaiting transplantation. B, Immunocytochemistry showing strong iNOS expression in blood vessels of many of the LVAD patients with slightly greater myocyte expression than in (C) advanced heart failure patients.

iNOS Immunocytochemistry

Significantly more iNOS expression was seen in blood vessels of the LVAD candidates (vascular smooth muscle staining, 1.75±0.19 versus 0.75±0.17; $P<0.005$, Figures 4B and 4C), and slightly more iNOS staining was seen in myocytes of LVAD candidates (2.35±0.15 versus 1.93±0.13; which only just reached statistical significance; $P<0.05$).

Serum

Serum TNF-α

Serum TNF-α was significantly higher in LVAD candidates (12.5±1.9 pg/mL, n=23) compared with stable advanced heart failure patients (4.0±0.4 pg/mL, n=17; $P<0.0001$, Figure 1E).

Serum TNF-R1 and TNF-R2

No significant difference was seen between serum TNF-R1 levels in LVAD candidates (2.9±0.6 ng/mL, n=23) and stable advanced heart failure patients (2.8±0.3 ng/mL, n=17; P=NS). Serum TNF-R2 levels also were no higher in LVAD candidates (6.9±1.1 ng/mL, n=23) than in advanced heart failure patients (9.0±0.8 ng/mL, n=17; P=NS).

Serum IL-6

Serum IL-6 was higher in LVAD candidates (79.3±23.6 pg/mL, n=23) than in advanced heart failure patients (7.1±1.6 pg/mL, n=17; $P<0.0001$; Figure C).

Apoptosis

Caspase-9

Caspase-9 antibody recognizes the intact 46- to 48-kDa protein and the cleaved 37-kDa subunit. Levels of 46-kDa procaspase-9 were higher in LVAD candidates (8.02±0.91 oligodeoxynucleotide [OD] units) than in advanced heart failure patients (6.16±0.43 OD units; $P<0.01$, Figure 5A). Expression of 37-kDa cleaved caspase-9 was significantly higher in LVAD candidates (10.02±1.0 OD units) than in stable heart failure patients (7.34±0.40 OD units;

$P<0.05$, Figure 5B).

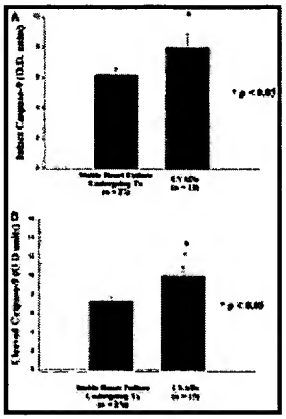

View larger version (14K):
[in this window]
[in a new window]

Figure 5. Expression of procaspase-9 and cleaved caspase-9 in stable advanced heart failure patients awaiting transplantation vs deteriorating patients undergoing LVAD implantation.

Caspase-3

Caspase-3 antibody recognizes the intact 32-kDa protein and the 2 cleaved subunits of 11 and 20 kDa. Levels of procaspase-3 were not higher in LVAD patients (9.62±0.5 OD units) than in advanced heart failure patients (9.78±0.5 OD units; P=NS).

Poly(ADP-Ribose) Polymerase

PARP antibody recognizes both full-length 116-kDa protein and the cleaved 85-kDa fragment. Levels of intact PARP were not significantly higher in LVAD candidates (0.37±0.08 OD units) than in stable advanced heart failure patients (0.27±0.05 OD units).

DFF-45

DFF-45 antibody (K-17) recognizes the intact 45-kDa inhibitor, the spliced 35-kDa product, and the cleaved 12-kDa product. Levels of intact DFF-45 were significantly higher in LVAD patients (10.86±0.91 OD units) than in advanced heart failure patients (8.91±0.38 OD units; $P<0.05$). The spliced 35-kDa product also was significantly higher in LVAD candidates (4.58±0.75 OD units) than in advanced heart failure patients (2.84±0.23 OD units; $P<0.05$).

CPAN

Levels of CPAN were not significantly higher in the LVAD candidates (2.04±0.5 OD units) than in advanced heart failure patients (2.57±0.23 OD units; P=NS).

Discussion

▲ Top
▲ Abstract
▲ Introduction

The present study has shown, for the first time, the specific pattern of increased expression of cytokines (Figure 6) together with alterations in the apoptotic

▲ Methods
▲ Results
▪ Discussion
▼ References

pathway of the myocardium and serum of deteriorating patients who require implantation of an LVAD. We have shown elevated levels of myocardial TNF-α, IL-1ß, and IL-6 (Figure 6) in these patients compared with patients who have less severe heart failure, are undergoing transplantation, and have elevated levels of circulating TNF-α and IL-6. Elevated myocardial expression of caspase-9 and DFF-45, but not caspase-3 and CPAN, in the final stage of the apoptotic pathway also was demonstrated.

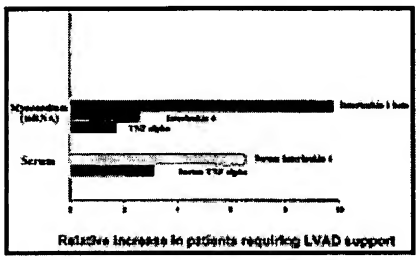

View larger version (15K):
[in this window]
[in a new window]

Figure 6. Pattern of increased cytokine expression in myocardium and serum of deteriorating patients requiring LVAD implantation.

An estimated 5 million people in the United States and 600 000 in the United Kingdom have heart failure. Mortality level for NYHA class III and IV heart failure is ≈40%. The situation is currently worsened by the decreasing supply of donor organs. When heart failure patients deteriorate, insertion of an LVAD can be lifesaving. Early implantation of the device is beneficial to outcome; hence, finding clinical and molecular markers is important for the identification of patients at high risk of deterioration so that corrective action can be taken earlier.

We used real-time PCR to measure myocardial cytokine levels because it is a new, quantitative, highly reliable method. We chose to compare deteriorating patients to those in a stable heart failure group without using a donor control group as we have previously shown increased cytokine expression after brain death in donor hearts.[21] The 13 patients in whom myocardial markers were measured had clinical parameters that showed them to be representative of the total group of patients. Limitation of tissue did not allow measurement of myocardial markers in all 23 patients.

In the present study, we found elevated levels of TNF-α mRNA and protein in the myocardium of deteriorating patients who required LVAD insertion. TNF-α is known to be elevated in heart failure,[1–5] and levels are known to correlate with NYHA functional class.[2] Infusion of TNF-α into rats at levels similar to levels present in end-stage heart failure results in depression of LV function, myocyte shortening, and LV dilatation.[6] A recent study has shown increased myocardial TNF-α with the progression of heart failure.[5] Therefore, TNF-α may be a useful marker of deterioration in these patients and also may be involved pathologically in the cause of the deterioration. In our present study, immunocytochemistry demonstrated TNF-α expression in

cardiac myocytes, and cardiac myocytes are known to be able to produce large amounts of TNF-α.[22] TNF-α acts on 2 cell-surface receptors, TNF-R1 and TNF-R2, which are thought to mediate and regulate most of the effects of TNF-α.[23] These receptors are shed as soluble forms that are thought to act as buffers to neutralize the cytotoxic activity of TNF-α.[24] The elevation of serum TNF-α in the LVAD patients in our present study was not accompanied by a rise in TNF receptors. This suggests that the increased TNF-α might not be neutralized by its receptors and, thus, may be able to act pathologically.

We have found elevated IL-6 mRNA and protein in the myocardium and elevated IL-6 in the serum of deteriorating patients who required LVAD insertion in the present study. IL-6 is known to be elevated in patients with heart failure, and raised levels correlate with decreased functional class, low ejection fraction, and poor prognosis.[1,3,7,8] A recent study has shown increased myocardial IL-6 expression with progression of heart failure.[5] Although IL-6 is known to increase with norepinephrine levels,[7] none of the patients in the present study were on norepinephrine at the time of LVAD insertion. Thus, use of norepinephrine is unlikely to be the cause of elevated IL-6 in the present study. IL-6 can be negatively inotropic, and transgenic mice overexpressing the IL-6 gene develop ventricular hypertrophy and increased heart size.[25] Of the deteriorating patients who underwent LVAD insertion in our present study, myocardial IL-6 protein expression was higher in those who died after the LVAD was implanted. Hence, IL-6 may be a good marker of deterioration and may be involved pathologically in deterioration (although elevation of IL-6 in the patients who died could imply irreversibility).

IL-1ß negatively affects myocardial function[9,10] and was 9-fold higher in the myocardium of deteriorating compared with stable patients (Figure 6). To our knowledge, this is the first time IL-1ß has been shown to be elevated in the myocardium of patients with heart failure and to be quantitatively increased in deteriorating patients. IL-1ß may be a useful marker of deterioration and may be involved in its pathogenesis.

Both TNF-α and IL-1ß induce iNOS expression, and both together act synergistically.[10,11] Therefore, we investigated iNOS expression in these patients and found that although iNOS was elevated to a level similar to that seen in advanced heart failure patients, iNOS mRNA expression was not higher in deteriorating compared with stable patients. This suggests that iNOS is not the mechanism through which these 2 cytokines act in these patients. Immunocytochemistry showed elevated iNOS protein expression in myocytes, which suggests a possible increase at the translational level. However, this barely reached statistical significance. Given that immunocytochemistry alone is not a reliable quantitative method, we feel that these results should be interpreted with caution. Immunocytochemistry demonstrated strong iNOS staining in the vascular smooth muscle cells of intracardiac blood vessels of many LVAD candidates, which suggests that increased nitric oxide release occurs in blood vessels of deteriorating patients, which could contribute to their hypotensive state.

Both TNF-α and IL-1ß can induce apoptosis,[12,13] whereas IL-6 tends to inhibit it.[14,15] We examined expression of caspases in the terminal stage of the apoptotic pathway to see whether they were elevated in deteriorating patients. Levels of procaspase-9 and activated, cleaved caspase-9 were elevated in these patients, but caspase-3 levels were not, which suggests a negative feedback mechanism at the level of caspase-3. Furthermore, levels of intact DFF-45 (inhibitor of DFF-45/CPAN) also were elevated, as was the cleaved 35-kDa product, but levels of the nuclease CPAN were not. Again, this occurrence suggests a negative feedback mechanism. IL-6 can increase BclxL and signal transducer and activator of transcription-3 (STAT-3).[14,15] Thus, IL-6 tends to be antiapoptotic. Given that we have demonstrated it to be elevated in these patients, IL-6 may be part of the negative feedback mechanism. However, it is likely that several molecules are involved in both positive and negative feedback in the apoptotic pathway in these patients. Further investigation is required. For example, nuclear factor-κB expression is induced by TNF-α and IL-1ß, is known to inhibit apoptosis, and is likely to be a potentially important mechanism. Lack of significant elevation in all of the terminal markers of apoptosis is difficult to explain and could be due to a negative feedback mechanism. Alternatively, our methods may have failed to detect a rise in these markers, or it may be that activation of the apoptotic pathway is not an important contributing mechanism to deterioration in these patients.

In conclusion, the present study has shown a specific pattern of cytokine elevation (Figure 6), alterations to caspases in the final stage of the apoptotic pathway of myocardium, and elevated levels of circulating cytokines in deteriorating patients who require LVAD insertion. Quantitative real-time RT-PCR demonstrated a 9-fold increase in IL-1ß mRNA expression, elevated myocardial TNF-α and IL-6 mRNA and protein, and raised serum TNF-α and IL-6 in deteriorating patients. iNOS was elevated to levels similar to those of heart failure, but no further elevation occurred in the deteriorating patients, which suggests that iNOS is unlikely to be the pathway through which TNF-α and IL-1ß act in these patients. Increased iNOS vascular smooth muscle expression was seen in blood vessels, which may contribute to the hypotension observed in these patients. Elevations were seen in procapase-9, cleaved caspase-9, and intact and cleaved DFF-45 of the final part of the apoptotic pathway but not in caspase-3 and CPAN, which suggests that some negative feedback mechanisms are occurring in these patients that need further investigation.

These cytokines might be useful markers for the earlier detection of patients likely to need LVAD implantation. Serial serum cytokine measurements, supplemented if necessary by myocardial biopsy, could augment hemodynamic data and detect decompensation at an earlier stage.

Furthermore, blocking cytokine production may have the potential to prevent disease progression. Pentoxifylline is a xanthine derivative that suppresses or reduces production of TNF-α and is thought to act at the mRNA level. Our study suggests that administration of pentoxifylline to patients with end-stage heart failure potentially could prevent or reverse their deterioration. Etanercept is a p75 TNF-R fusion protein that binds to TNF-α, functionally inactivating it, which also may be effective for prevention of decompensation of such patients. Both of these drugs

previously have been shown to produce clinical improvement in patients with less severe heart failure. Our present study suggests that IL-6 antagonists also potentially may prevent disease progression, as might IL-1 antagonists and specific caspase inhibitors, such as caspase-9 inhibitors. These approaches need to be investigated.

Acknowledgments

We thank the British Heart Foundation for their support. Emma J. Birks was supported by the British Heart Foundation (project grant No. 96152), Dr Barton by a British Heart Foundation Senior Research Fellowship, and Dr Yacoub as a British Heart Foundation Professor of Cardiothoracic Surgery. We thank Mahrokh Nohadani for her help.

References

▲ Top
▲ Abstract
▲ Introduction
▲ Methods
▲ Results
▲ Discussion
▪ References

1. Birks EJ, Yacoub MH. The role of nitric oxide and cytokines in heart failure. *Coronary Artery Dis.* 1997; 8: 389–402.[Medline]
2. Torre-Amione G, Kapiada S, Benedict C, et al. Proinflammatory cytokine levels in patients with depressed left ventricular ejection fraction: a report from the Studies Of Left Ventricular Dysfunction (SOLVD). *J Am Coll Cardiol.* 1996; 27: 1201–1206.[Medline]
3. Lommi J, Pulkki P, Koskinen P, et al. Haemodynamic, neuroendocrine and metabolic correlates of circulating cytokine concentrations in congestive heart failure. *Eur Heart J.* 1997; 18: 1620–1625.[Abstract]
4. Habib FM, Springall DR, Davies GJ, et al. Tumour necrosis factor and inducible nitric oxide synthase in dilated cardiomyopathy. *Lancet.* 1996; 347: 1151–1155.[Medline]
5. Kubota T, Miyagishima M, Alvarez et al. Expression of proinflammatory cytokines in the failing human heart: comparison of recent-onset and end-stage congestive heart failure. *J Heart Lung Transplant.* 2000; 19: 819–824.[Medline]
6. Bozkurt B, Kribbs SB, Clubb FJ, et al. Pathophysiologically relevant concentrations of tumor necrosis factor-α promote left ventricular dysfunction and remodeling in rats. *Circulation.* 1998; 97: 1382–1391.[Abstract/Free Full Text]
7. Tsutamoto T, Hisanaga T, Wada A, et al. Interleukin-6 spillover in the peripheral circulation increases with the severity of heart failure, and the high plasma level of interleukin-6 is an important prognostic predictor in patients with congestive heart failure. *J Am Coll Cardiol.* 1998; 31: 391–398.[Medline]
8. Plenz G, Song ZF, Reichenberg S, et al. Left-ventricular expression of interleukin-6 messenger-RNA higher in dilated than in ischemic cardiomyopathy. *Thorac Cardiovasc Surg.* 1998; 46: 213–216.[Medline]
9. Hosenpud JD, Campbell SM, Mendelson DJ. Interleukin-1-induced myocardial depression in an isolated beating heart preparation. *J Heart Transplant.* 1989; 8: 460–464.[Medline]
10. Cain BS, Meldrum DR, Dinarello CA, et al. Tumour necrosis factor-α and interleukin-1ß synergistically depress human myocardial function. *Crit Care Med.* 1999; 27: 1309–1318. [Medline]
11. Schulz R, Panas DL, Catena R, et al. The role of nitric oxide in cardiac depression induced by interleukin-1 beta and tumour necrosis factor-alpha. *Br J Pharmacol.* 1995; 114: 27–34.

[Abstract]

12. Ing DJ, Zang J, Dzau VJ, et al. Modulation of cytokine-induced cardiac myocyte apoptosis by nitric oxide, Bak, and Bcl-x. *Circ Res.* 1999; 84: 21–33.[Abstract/Free Full Text]
13. Krown KA, Page MT, Nguyen C, et al. Tumour necrosis factor alpha-induced apoptosis in cardiac myocytes: involvement of the sphingolipid signaling cascade in cardiac cell death. *J Clin Invest.* 1996; 98: 2854–2865.[Abstract/Free Full Text]
14. Schwarze MM, Hawley RG. Prevention of myeloma cell apoptosis by ectopic bcl-2 expression or interleukin 6-mediated up-regulation of bcl-xL. *Cancer Res.* 1995; 55: 2262–2265.[Abstract]
15. Fukada T, Hibi M, Yamanaka Y, et al. Two signals are necessary for cell proliferation induced by a cytokine receptor gp130: involvement of STAT3 in anti-apoptosis. *Immunity.* 1996; 5: 449–460.[Medline]
16. Liu X, Zou H, Slaughter C, et al. DFF, a heterodimeric protein that functions downstream of caspase-3 to trigger DNA fragmentation during apoptosis. *Cell.* 1997; 89: 175–184. [Medline]
17. Tang D, Kidd VJ. Cleavage of DFF-45/ICAD by multiple caspases is essential for its function during apoptosis. *J Biol Chem.* 1998; 273: 28549–28552.[Abstract/Free Full Text]
18. Halenbeck R, MacDonald H, Roulston A, et al. CPAN, a human nuclease regulated by the caspase-sensitive inhibitor DFF45. *Curr Biol.* 1998; 8: 537–540.[Medline]
19. Narula J, Pandey P, Arbustani E, et al. Apoptosis in heart failure: release of cytochrome c from mitochondria and activation of caspase-3 in human cardiomyopathy. *Proc Natl Acad Sci, U S A.* 1999; 96: 8144–8149.[Abstract/Free Full Text]
20. Latif N, Khan M, Birks E, et al. Upregulation of the bcl-2 family of proteins in end stage heart failure. *J Am Coll Cardiol.* 2000; 35: 1769–1777.[Medline]
21. Birks EJ, Burton PB, Owen V, et al. Elevated tumor necrosis factor-alpha and interleukin-6 in myocardium and serum of malfunctioning donor hearts. *Circulation.* 2000; 102 (suppl 3): III-352–III-358.
22. Kapadia S, Lee J, Torre-Amione G, et al. Tumor necrosis factor-α gene and protein expression in adult feline myocardium after endotoxin administration. *J Clin Invest.* 1995; 96: 1042–1052.[Medline]
23. Torre-Amione G, Kapadia S, Lee J, et al. Expression and functional significance of tumor necrosis factor receptors in human myocardium. *Circulation.* 1995; 92: 1487–1493. [Abstract/Free Full Text]
24. Kapadia S, Torre-Amione G, Yokoyama T, et al. Soluble tumor necrosis factor binding proteins modulate the negative inotropic effects of TNF-α in vitro. *Am J Physiol.* 1995; 37: H517–H525.
25. Hirota H, Yoshida K, Kishimoto T, et al. Continuous activation of gp130, a signal-transducing receptor component for interleukin 6-related cytokines, causes myocardial hypertrophy in mice. *Proc Natl Acad Sci U S A.* 1995; 92: 4862–4866.[Abstract]

J Mol Cell Cardiol 34, 165–174 (2002)
doi:10.1006/jmcc.2001.1498, available online at http://www.idealibrary.com on IDEAL®

Apoptosis and Post-infarction Left Ventricular Remodeling

Alfonso Baldi[1]*, Antonio Abbate[2]*, Rossana Bussani[3], Giuseppe Patti[2], Rosetta Melfi[2], Anna Angelini[1], Aldo Dobrina[2], Raffaele Rossiello[1], Furio Silvestri[3], Feliciano Baldi[1] and Germano Di Sciascio[2]

[1]*Department of Biochemistry and Biophysics, "F. Cedrangolo", Section of Pathologic Anatomy, Second University of Naples, Naples, Italy,* [2]*Department of Cardiovascular Sciences, University Campus Bio-Medico, Rome, Italy and* [3]*Department of Pathologic Anatomy, University of Trieste, Trieste, Italy*

(Received 7 August 2001, accepted for publication 31 October 2001)

A. Baldi, A. Abbate, R. Bussani, G. Patti, R. Melfi, A. Angelini, A. Dobrina, R. Rossiello, F. Silvestri, F. Baldi and G. Di Sciascio. Apoptosis and Post-infarction Left Ventricular Remodeling. *Journal of Molecular and Cellular Cardiology* (2002) 34, 165–174. Apoptosis is a common pathological feature in acute myocardial infarction (AMI), however, its role in the later phases (>10 days) of AMI and in post-infarction left ventricular remodeling has not been characterized. The aim of the study was to identify signs of ongoing cell apoptosis late post AMI. Sixteen hearts were collected at autopsy from subjects 12 to 62 days after the onset of AMI. *In situ* end-labeling of DNA fragmentation (TUNEL) and co-staining with caspase-3 were performed. Double-positive cells were defined as apoptotic and the apoptotic rate was calculated. Values are expressed as median and interquartile range. Co-stainings with muscle-actin, splicing factor (SC35), PCNA, *bax* and *bcl-2* were also performed. Apoptotic rates at site of infarction [25.4% (17.0–28.4%)] were significantly higher *v* those at remote regions [0.7% (0.5–0.8%); $P<0.001$] and significantly correlated to left ventricular longitudinal and transverse diameters [$r=+0.70$ ($P=0.016$) and $r=+0.63$ ($P=0.004$) respectively]. Moreover, in subjects with persistently occluded infarct-related artery (14 cases) there was a significantly higher apoptotic rate at the site of infarction compared to those (2 cases) with patent artery [26.0% (21.9–28.5%) *v* 4.5% (0.6% and 8,4%);$P=0.033$]. A significantly greater *bax* immuno-reactivity close to the infarction *v* remote areas was found ($P<0.001$). High grade apoptosis is present at sites of infarction in the later phases post AMI. This is more evident if the infarct-related artery is persistently occluded and signs of ventricular remodeling are present. These data may provide an explanation of progressive late left ventricular dysfunction.

Key Words: Apoptosis; Myocardial infarction; Remodeling; Caspase-3; *bax*; *bcl2*.

Introduction

Apoptosis, or programmed cell death, is an energy-requiring and highly regulated process involved in development, homeostasis and senescence. Apoptosis is triggered by the activation of intracellular signalling pathways associated with the condensation of chromatin into crescentic caps of nuclear DNA at the periphery. Apoptotic cells then undergo extracellular degeneration or phagocytosis by macrophages without eliciting an inflammatory reaction.[1] It is acknowledged that apoptosis contributes both to homeostasis and human diseases. As such, it has been recognized as a key process in the adaptations of the cardiovascular system to its continuously changing demands.[2,3] Recently, it has been implicated as a fundamental pathogenetic mechanism in a variety of diseases including acute myocardial infarction (AMI), and post-ischemic and idiopathic dilated cardiopathy.[4–10] New techniques,

* The first two authors contributed equally to the realization of this manuscript.
Please address all correspondence to: Dr Alfonso Baldi, Via G. Orsi, 25, 80128 Naples, Italy. Fax: +39-081-5569693. E-mail: alfonsobaldi@tiscalinet.it

0022–2828/02/020165+10 $35.00/0

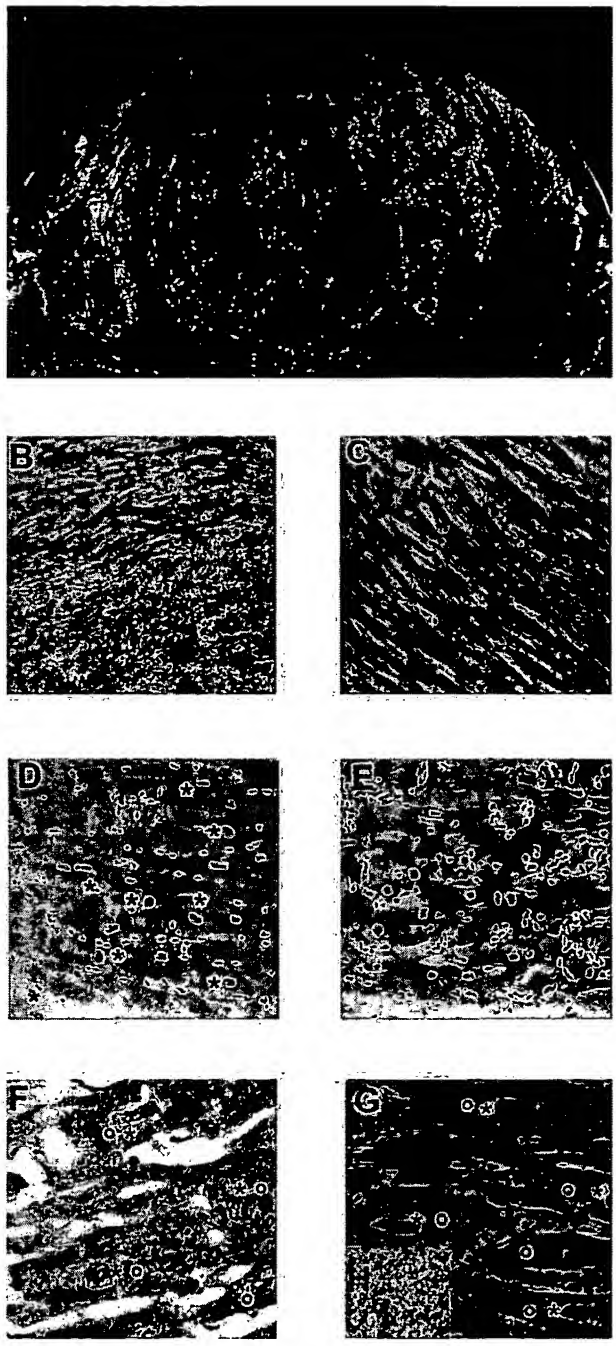

Figure 1 (A) Sampling of the different specimens, at a site of recent infarction (arrow) and at sites remote from it (*), in an examined heart collected from a 82-year old subject with a history of anterior and septal AMI (15 days earlier). AMI, Acute myocardial infarction. (B) Hematoxylin/Van Gieson. Site of recent infarction: reparative fibrosis, newly sprouted vessels and granulation tissue (original magnification × 500). (C) Hematoxylin/Van Gieson. Region remote from the infarcted area (original magnification × 500). (D) TUNEL staining. Region of the left ventricle at the site of infarction: several TUNEL-positive cells are shown (*) (original magnification × 500; lightly counterstained with hematoxylin). (E) TUNEL staining. Region of the left ventricle remote from the infarcted area: no TUNEL-positive cells are detected (original magnification × 500; lightly counterstained with hematoxylin). (F) Double staining: nuclear staining for TUNEL (*) and cytoplasmic staining for muscle-actin (○). TUNEL-positive cells co-express muscle-actin (original magnification × 600; AEC, lightly counterstained with hematoxylin). (G) Double staining: nuclear staining for TUNEL (*) and cytoplasmic staining for Caspase-3 (○). Great majority of TUNEL-positive cells co-express caspase-

especially the *in situ* end-labeling of DNA fragmentation (TUNEL), have enabled an easy qualitative and quantitative evaluation of apoptotis in tissues and proposed a re-interpretation of previously acquired concepts.[4–11] In particular, in AMI a greater incidence of apoptosis *v* necrosis has been reported in experimental models[5] and confirmed in humans,[6,10] with a particular localization at the borders of infarction. However, the incidence of apoptosis in the later phase post AMI (up to 60 days) in humans and its role in determining post-infarction left ventricular (LV) remodeling have not been characterized to date. The primary goal of our study was to evaluate ongoing myocardiocyte apoptosis in these phases and the secondary objective was to investigate its correlation with signs of LV remodeling and infarct-related artery (IRA) patency. To this aim, pathological examination of human hearts late post AMI was performed using TUNEL combined with additional stainings for muscle actin and for markers of cell death mediators (caspase-3, *bax* and *bcl-2*), DNA synthesis (PCNA) and transcription activity (RNA splicing factor SC-35).

Materials and Methods

Selection of the samples

Sixteen hearts were collected at autopsy (University of Trieste and Second University of Naples, Italy) from subjects who died 12 to 62 days after the onset of MI, median interval 23 days. All subjects were hospitalized before death, and none of them suffered from a re-infarction, as indicated by clinical data and serial CK and CK-MB determination. The cause of death was trauma in 4 cases while congestive heart failure and comorbidities were present in the rest. Features of cardiogenic shock or prolonged i.v. inotropic support were not described in the clinical charts. Clinical and demographic characteristics of the subjects are shown in Table 1.

Pathological examination

Autopsy was performed within 30 hours after death in all cases. Gross examination of the hearts was performed to measure LV parameters and to define the infarcted area and the IRA. LV transverse and longitudinal diameters were measured at the atrioventricular section. The LV free wall thickness was measured at the median third of the posterior wall. Tissue specimens (125–1000 mm^3) were obtained at sites of myocardial infarction and in regions of the left ventricle remote from the infarcted area supplied by a patent coronary artery [Figure 1(A)]. Specimens were fixed in 10% paraformaldehyde in 0.1 M buffer. Different sections were processed for each specimen. Morphologic analysis of tissue structure, cellular and nuclear integrity and inflammatory infiltrates was performed by light-microscopy after dehydration, embedding in paraffin and staining.

Table 1 Clinical and demographic characteristics

Number of subjects	16
Median age (years)	73
Range	(60–96)
Male sex	12 (75%)
Recent AMI	16
(≤2 months)	(100%)
Median time post AMI (days)	23
Range	(12–62)
Previous old AMI	8
(>6 months)	(50%)
Left ventricular dysfunction	13
(LVEF <45%)	(81%)

AMI, acute myocardial infarction; LVEF, Left ventricular ejection fraction.

TUNEL assay

TUNEL reaction was performed using the peroxidase-based Apoptag kit (Oncor, Gaithersburg, MD, USA). TUNEL positive cells were detected with diaminobenzidine and H_2O_2 according to the supplier's instructions. Moreover, in order to optimize the procedure, we applied the modifications to the protocol suggested by Saraste.[12] The experiment was repeated on different sections for each specimen (two to four). One hundred random fields (×250) per section were analyzed (12.5 mm^2).

Immunocytochemistry

Several series of TUNEL-stained sections, as well as consecutive deparaffinized and dried sections were

3. (original magnification ×600; AEC, lightly counterstained with hematoxylin). (H) Caspase-3 immunohistochemical staining of human lymph nodes as a positive control. Strong immunoreactivity for activated caspase-3 in the apoptotic-prone germinal center B-lymphocytes of a lymph node is clearly visible (original magnification ×500; AEC, lightly counterstained with hematoxylin).

subsequently stained for different markers. All the sections were heated in a microwave oven twice for 5 min at 700 W in citrate buffer (pH 6), then incubated with antibodies against muscle actin (mouse monoclonal anti-human actin HHF35 from DAKO, CA, USA; dilution 1:50), caspase-3 (rabbit polyclonal anti-human caspase-3 from Upstate Biotechnology, NY, USA; dilution 1:100), PCNA (mouse monoclonal anti-human PCNA PC10 from DAKO; dilution 1:100) and splicing factor (mouse monoclonal anti-splicing factor SC-35 from Sigma, Milan, Italy; dilution 1:200), and visualized by the streptavidin-biotin system (DAKO), using either 3-amino-9-ethylcarbazide (AEC) or diaminobenzidine (DAB) as the final chromogen. The optimal working dilutions were defined on the basis of titration experiments. Negative controls for each tissue section were prepared by leaving out the primary antibodies, which resulted in a complete disappearance of the nuclear staining for the antibodies used, indicating the non-interference of TUNEL with the secondary antibodies. Immunoreactivity (positive/negative) for each staining coincided between pairs of identical nuclei of myocytes on mirror sections. Positive controls were run with each set of slides. Immunocytochemistry for *bax* protein and *bcl-2* were also performed using specific antibodies (mouse monoclonal anti-human *bax* sc-7480 and mouse monoclonal anti-human *bcl-2* sc-7382 from Santa Cruz, CA, USA; at a dilution 1:100). Immunoreactivity for these two antigens was quantitated as percentage of positive cells per field ($\times 250$).

Apoptotic rate

Myocardiocytes were defined as apoptotic if co-localization of markers of DNA fragmentation (TUNEL) and cell death effectors (caspase-3) was evident. The apoptotic rate (AR), expressed as a ratio of number of myocardiocytes co-expressing TUNEL and caspase-3 positivity on nucleated cells per field ($\times 250$) at light microscopy, was calculated and compared in different specimens by two separate observers (A.B. and A.A.) in a double blind fashion. Consensus on the percentage of TUNEL positive cells was reached in all cases.

Statistical analysis

For statistical analysis, the software SPSS 10.0 for Windows (SPSS, Chicago, IL, USA) was used.

Table 2 Gross pathology characteristics

Weight (g) median	540
Interquartile range	(480–565)
Transverse diameter (mm) median	128
Interquartile range	(124–139)
Longitudinal diameter (mm) median	104
Interquartile range	(102–110)
LV posterior wall thickness (mm) median	15
Interquartile range	(12–16)
Previous old AMI (>6 months)	8 (50%)
Significant multivessel coronary disease	8 (50%)
Persistently occluded IRA	14 (88%)

AMI, acute myocardial infarction; IRA, infarct-related artery; LV, left ventricle.

Quantitative results were expressed as median and interquartile range. Non-parametric tests were used to compare AR among different regions of each subject (Wilcoxon test for paired data) and among different subjects (*U* Mann–Whitney for non-paired data). Correlation between variables was determined by Spearman rank test, *r* values represent correlation coefficients. *P* values ≤ 0.05 were considered significant.

Results

Gross pathology and light-microscopy examination

Table 2 summarizes the gross pathology characteristics of the hearts. Median transverse and vertical diameters were 128 mm and 104 mm respectively. Posterior wall thickness was 15 mm. In six cases of posterior AMI those values were not included for further analysis. In fourteen cases (88%) an occluded IRA was found, while in the remaining two cases (12%) the IRA was found to be patent.

Areas of scarring consistent with previous necrotic cell death were demonstrable in the infarcted area. At light-microscopy signs suggestive of ongoing necrosis (i.e. nuclear or cytoplasmic abnormalities, evidence of cell rupture) were absent in all examined sections while reparative fibrosis and newly sprouted capillaries were present, and typical post-infarction granulation tissue was evident [Fig. 1(B)]. Muscle damage was not present in specimens derived from the same subjects at areas remote from the infarction [Fig. 1(C)]. These areas

Table 3 Correlation between TUNEL staining and Caspase-3, SC-35 and PCNA. (Median value and interquartile range)

TUNEL + cells (%)	30 (20–34)
Caspase-3 + (%)	85 (83–88)
SC35 + (%)	10 (4–12)
PCNA + (%)	0.7 (0.01–1.1)
Caspase-, SC35-, PCNA- (%)	5 (2–12)

appeared normal at gross anatomy and light-microscopy and a patent related coronary was identified.

TUNEL assay and immunocytochemistry for caspase-3, PCNA and SC-35

TUNEL assay in myocardial specimens collected at the site of infarction showed a high rate of positive cells in all examined fields [Fig. 1(D)], while in regions remote from the infarcted area TUNEL positive cells were rare [Fig. 1(E)]. Light-microscopy examination of consecutive sections from the specimens with immunocytochemistry was performed for muscle actin. The great majority of TUNEL positive cells co-stained was for muscle actin, thus showing to be myocardiocytes [Fig. 1(F)]. Interstitial and inflammatory cells were were not included in the cell count.

Table 3 summarizes data showing correlation between TUNEL staining and immunocytochemistry for caspase-3, PCNA and SC-35. A high percentage of the TUNEL positive cells [median 85% (83–88%)] were overexpressing caspase-3 [Fig. 1(G)]. About 5% of caspase-3 expressing cells did not show positivity at TUNEL, and were not considered apoptotic. Non-apoptotic myocardiocytes at the site of infarction, as well as in regions remote from the infarction, were mostly negative for caspase-3 or contained only weak immunoreactivity. Staining of a lymph node is shown as a control for the specificity of the immunohistochemical reaction for the activated caspase-3. The typical strong immunoreactivity for activated caspase-3 in the apoptosis-prone germinal center B-lymphocytes is clearly visible [Fig. 1(H)].

TUNEL-positive myocardiocytes were mostly negative for PCNA and SC-35 immunocytochemistry [Figures 2(A) and 2(B); Table 3]. None of the myocardiocytes (0%) which expressed co-localization of TUNEL and caspase-3 were positive for PCNA or SC-35.

Apoptotic rate

The rate of apoptotic myocardiocytes was significantly higher at sites of infarction [25.4% (17.0–28.4%)] *v* remote regions [0.7% (0.5–0.8%), $P<0.001$] [Fig. 3(A)]. In two hearts of subjects with patent IRA the AR was significantly lower (0.6% and 8.4%) compared to those with a persistently occluded IRA [26.0% (21.9–28.5%), $P=0.033$] [Fig. 3(B)]. Moreover, the AR at the site of infarction was found to be positively correlated to signs of LV remodeling, LV longitudinal ($r=+0.70$, $P=0.016$) [Fig. 3(C)] and transverse diameter ($r=+0.63$, $P=0.004$) [Fig. 3(D)]. Not considering data from six subjects who had posterior wall infarctions, AR remote from infarction showed a mild correlation with the LV posterior wall thickness ($r=-0.64$, $P=0.06$) [Fig. 3(E)].

AR in hearts of subjects with a traumatic death (four cases, 25%; AR 27.2%) was similar to the AR in the others (12 cases, 75%; AR 25.2%; $P=0.8$). No statistically significant difference was found comparing AR in those patients who died within 23 days after AMI (median value) *v* the others (27.3% *v* 25.4%; $P=0.85$).

Immunocytochemistry for *bax* and *bcl-2*

Bax protein expression within the myocardium showed a similar localization of TUNEL with a significantly higher number of myocardiocytes expressing intense *bax* immunoreactivity in the cytoplasm at site of infarction [52.2% (34.3–58.0%)] *v* remote area [2.5% (0.7–3.4%), $P<0.001$] [Fig. 2(C)]. In Figure 2(D) a control for *bax* immunoreactivity on a lymph node is shown. Most cells within the germinal center of the lymph node were positive for *bax* expression, while the majority of cells within the interfollicular zone were negative.

Compared to *bax* expression *bcl-2* appeared only slightly overexpressed in the infarcted site [2.1% (1.4-4%)] *v* the remote site [0.5% (0.2–1.0%), $P=0.16$] [Fig. 2(E)].

Discussion

To the best of our knowledge, this is the first report in humans of persisting myocardiocyte death due to apoptosis late post AMI. Necrosis is known to cause an important loss of myocardiocytes, with attendant ventricular dysfunction and heart failure post AMI. Previous studies indicate that myocardial

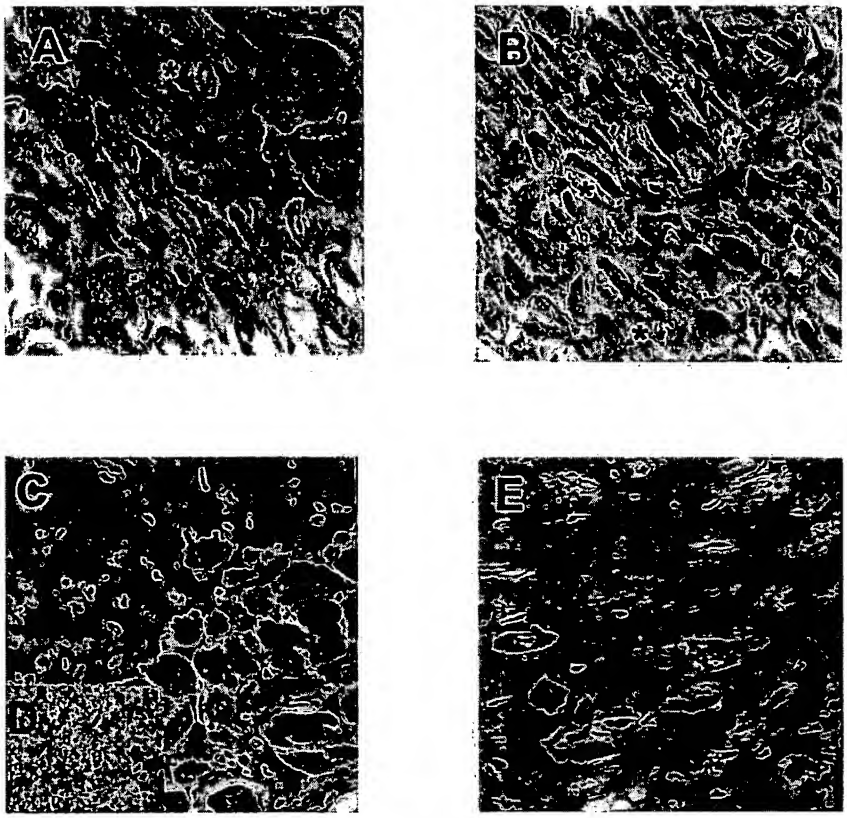

Figure 2 (A) Double staining for TUNEL and PCNA. Rare TUNEL-positive cells express PCNA. A double-positive cell is shown (*) (original magnification × 500; AEC, lightly counterstained with hematoxylin). (B) Double staining for TUNEL and SC-35. A small portion of TUNEL-positive cells express SC-35. Double-positive cells are shown (*) (original magnification × 500; AEC, lightly counterstained with hematoxylin). (C) Dark-brown positive *Bax* immunoreactivity is evident in the cytoplasm of myocardiocytes close to the infarcted area (original magnification × 500; DAB, lightly counterstained with hematoxylin). (D) Positive control for *bax* immunostaining in the germinal center of a lymph node (original magnification × 500; DAB, lightly counterstained with hematoxylin). (E) A case of *bcl-2* immunohistochemical staining of salvaged tissues surrounding the infarcted areas. Few *bcl-2* positive myocardiocytes close to the infarcted area are detected (original magnification × 500; DAB, lightly counterstained with hematoxylin).

apoptosis may be as important as necrosis in determining myocardiocyte loss in the early phases of AMI.[5,6,10] In particular, an apoptosis/necrosis ratio close to 30:1 was described in experimental AMI models in rats.[5] These data were confirmed in humans[6,10] by the examination of hearts of patients who died within 10 days post AMI, with a preferential localization of apoptotic myocytes at the borders of the infarcted site. A reduction of the apoptotic rate post AMI was described, but no direct observation after the tenth day was reported. In our study a persistent myocardiocyte loss due to apoptosis late post AMI is suggested by the presence of an elevated rate of myocardiocytes positive for TUNEL and caspase-3 immunocytochemistry. Apoptosis appears highly selective for myocardiocytes and localized to the infarcted area. The persistence of viable cells next to apoptotic ones shows the gradual incidence of the event compared to the abrupt onset observed with necrosis. The absence of ongoing necrosis enhances the specificity of TUNEL examination. However, current opinions regarding the association between apoptosis and necrosis support a possible common feature of cell death beginning as apoptosis and ending as secondary necrosis.[1,4,13,14]

Apoptosis and post-infarction left ventricular remodeling

The presence of apoptosis late post AMI suggests a possible relation with the progression of LV dysfunction sometimes observed in the later phases post AMI. In fact, an increased AR up to 232-fold in the hearts of patients with end-stage heart failure[7,8] has been described. Saraste *et al.*[9] reported

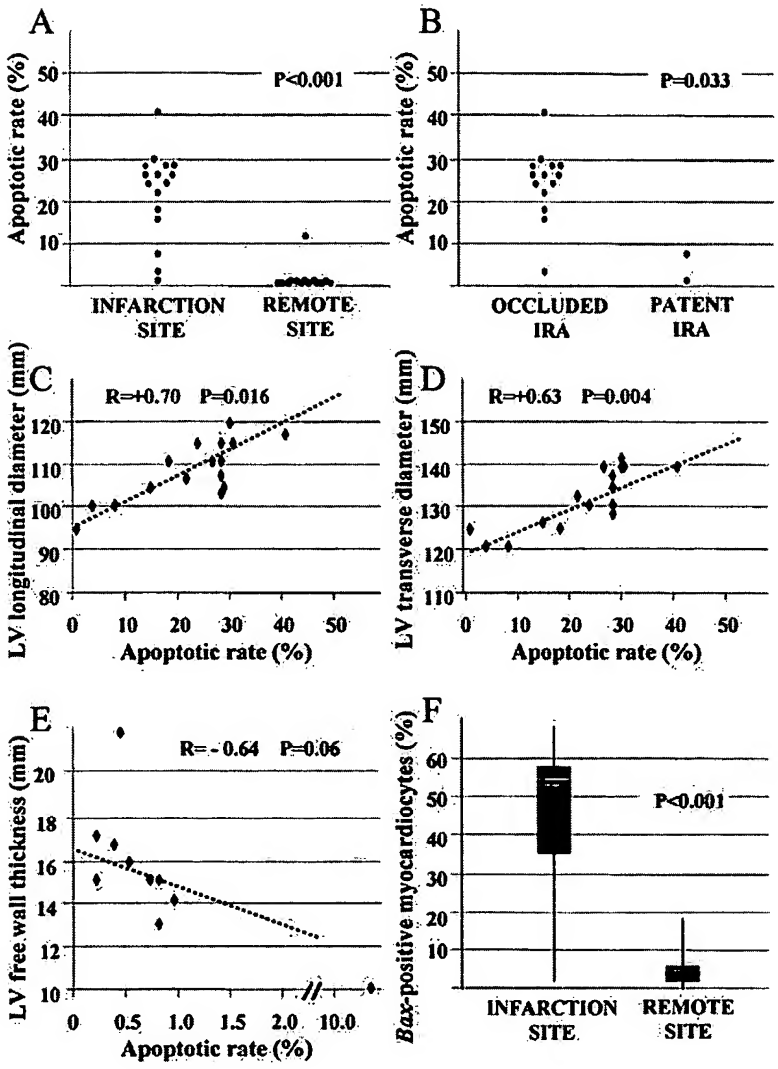

Figure 3 (A) Apoptotic rate at the site of the infarction and at regions remote from it. (B) Significantly lower AR at the site of infarction in two hearts with patent IRA (infarct-related artery) *v* those hearts with persistently occluded IRA. (C) Correlation between AR at the site of infarction and left ventricular (LV) longitudinal diameter. (D) Correlation between AR at the site of infarction and left ventricular (LV) transverse diameter. (E) Correlation between AR at site remote from the infarction (LV posterior wall) and LV wall thickness. (F) Significantly greater *bax* immuno-reactivity in the cytoplasm of myocardiocytes close to the infarction *v* remote area. AR, apoptotic rate; IRA, infarct-related artery; LV, left ventricular.

a significantly higher AR vs controls in explanted failing human heart, with a significant correlation between the AR and the severity of clinical manifestations and the rapidity of progression of heart failure in patients with ischemic heart disease. Their data also confirmed a higher AR in proximity of infarcted sites, and the highest value observed (14%) was in a subject with an AMI within the preceding year.[9] Most of the subjects in our series showed some degree of LV dysfunction before death, and AR correlated with macroscopic signs of post-infarction LV remodeling (LV dilatation and LV free wall thinning). Similar data were recently described in rats.[15] In regions remote from the infarction an AR of 0.7% was observed, although significantly lower than the AR at the site of AMI, it appears to be substantially greater than the rate described among control samples by others.[9,10] These data may support a role for apoptosis in regions remote from acute ischemic insult to promote LV re-

modeling in response to increased mechanical stress.[15–17]

Moreover, "the open-artery hypothesis", improved LV function in the long term post AMI deriving from a patent IRA[18] – was already formulated in the early 1990s, but the underlying mechanisms were not clear. In our specimens, a patent IRA was associated with a lower AR at the site of infarction. Therefore, the benefit observed with late coronary revascularization could be due to inhibition of apoptosis and prevention of LV remodeling, even if a cause–effect link between persistent IRA occlusion and apoptosis late post AMI cannot be supported by these data. However studies of delayed coronary revascularization have already shown their clinical efficacy, predicting full recovery at site of infarction and overall survival benefits.[19,20]

Demonstration of apoptosis

Some authors have suggested a lack of specificity of TUNEL on human hearts[13,21,22] whereas others have strongly supported its accuracy.[11,12] Kanoh *et al.* described TUNEL-positive myocardiocytes in hearts with dilated cardiomyopathy as living cells with increasing activity of DNA repair rather than apoptotic cells.[21] While a strict relation between PCNA and TUNEL was present in their data, in our cases most of the TUNEL-positive myocardiocytes were PCNA-negative and therefore could not be considered cells with intense DNA synthesis. On the other hand, while it has been suggested that RNA synthesis and splicing interferes with TUNEL detecting apoptosis,[22] TUNEL-positive cells were mostly negative for SC35 in our data. The association of TUNEL and high expression of caspase-3 in over 80% of TUNEL-positive myocardiocytes further supports the definition of apoptotis. As a central mediator of apoptosis in mammalian cells, caspase-3 induces caspase-activated DNase activation which leads to DNA fragmentation and also cleaves cytoskeletal proteins, leading to significant alteration of the cytoskeleton and cell death, even in the absence of DNA fragmentation.[23,24] The apoptotic activity of caspase depends mostly on post-transcriptional events, however, increases in the mRNA levels have been associated with apoptosis.[25] It has been shown that high immunohistochemical expression of caspase-3 is present in cells undergoing apoptosis,[26] co-localization of caspase-3 and TUNEL staining has been detected in neurons and myocardiocytes undergoing apoptosis[23,27] and even if the antibody used for caspase-3 in our study recognized both the precursor and the p20 subunit, it was recently demonstrated that high caspase-3 immunostaining with this antibody corresponded mostly to increased expression of the activated form of caspase-3.[23] Moreover, *bax* expression appeared substantially higher in infarcted *v* remote areas, with a high *bax/bcl-2* ratio. *Bax*'s pro-apoptotic activity depends on its ability to form heterodimers with the inhibitor of apoptosis *bcl-2*. The ratio of *bcl-2* to bax expression determines survival or death after an apoptotic stimulus[28,29] and different site-dependent expression of *bcl-2* and *bax* within the heart has been described.[30]

The AR may appear overestimated. It has been suggested that even a much lower apoptotic rate (<1%) in the hearts of subjects with heart failure would lead to a loss of more than 25% of myocardiocytes during the first year.[31] Notably, the time required for the *in vivo* formation of apoptotic bodies and their removal has not been determined in the heart, and is currently unknown whether apoptosis persists chronically or if its incidence decreases during the healing process. In our specimens, AR was calculated on a small quantity of myocardium, localized in regions of recent infarction in a definite time frame. In fact, the rate tended to decrease, reaching normal levels (<1%) as the samples were taken further away from the infarcted area and subjects with previous (>6 months) AMI had a much lower apoptotic rate at the infarcted site (A. Baldi and A. Abbate, unpublished data, 2000). Further studies on the dynamics of myocardiocyte apoptosis are necessary to define the impact of calculated AR on effective myocardiocyte loss over time.

Conclusions

Myocardial apoptosis is present late post AMI and may be related to progressive ventricular dysfunction by a cause-effect link. It may therefore be considered part of the cellular and topographic rearrangements (i.e. cell hypertrophy, elongation, side-to-side slippage) in LV remodeling. These data deserve further investigation, discussion and confirmation in appropriate studies targeted to analyze this interesting cause-effect relation. Recent studies raised the possibility of the regeneration of myocardiocytes at the site of infarction in hearts with AMI[32] and suggested that the balance between cell death and regeneration may determine whether LV remodeling occurs after AMI. PCNA-positive

myocardiocytes in our samples may indicate regenerating myocardiocytes, with active DNA synthesis, as described by Beltrami *et al.*[32] *In vivo* diagnosis of apoptosis appears a promising feature[33] and interestingly, in experimental models, anti-apoptotic therapy (i.e. treatment with ZVAD-fmk,[34] a broad caspase inhibitor) reduced infarct size, enzyme leakage and remodeling, thus opening new avenues in the diagnosis and treatment of ischemic heart disease.

Acknowledgements

The authors thank Dr G. Condorelli (Thomas Jefferson University, Philadelphia), Dr S. Miccadei (Regina Elena Cancer Institute, Rome) and Dr L. M. Biasucci (Catholic University of Rome) for their suggestions and critical review of the manuscript, and Mr T. Battista for his skilful technical assistance.

References

1. Searle J, Kerr JFR, Bishop CH. Necrosis and apoptosis: distinct modes of cell death with fundamentally different significance. *Pathol Annu* 1982; 17: 229–259.
2. Watanabe M, Choudhry A, Berlan M, Singal A, Siwik E, Mohr S, Fisher SA. Developmental remodeling and shortening of the cardiac outflow tract involves myocyte programmed cell death. *Development* 1998; 125: 3809–3820.
3. Cheng W, Li B, Kajstura J, Li P, Wolin MS, Sonnenblick E, Hintze TH, Olivetti G, Anversa P. Stretch-induced programmed myocyte cell death. *J Clin Invest* 1995; 96: 2247–2259.
4. Haunstetter A, Izumo S. Apoptosis. Basic mechanisms and implications for cardiovascular disease. *Circ Res* 1998; 82: 1111–1129.
5. Kajstura J, Cheng W, Reiss K, Clark WA, Sonnenblick EH, Krajewski S, Reed JC, Olivetti G, Anversa P. Apoptotic and necrotic myocyte cell deaths are independent contributing variables of infarct size in rats. *Lab Invest* 1996; 74: 86–107.
6. Veinot JP, Gattinger DA, Fliss H. Early apoptosis in human myocardial infarcts. *Hum Pathol* 1997; 28: 485–492.
7. Narula J, Haider N, Virmani R, DiSalvo TG, Kolodgie FD, Hajjar RJ, Schmidt U, Semigran MJ, Dec GW, Khaw BA. Apoptosis in myocytes in end-stage heart failure. *N Engl J Med* 1996; 335: 1182–1189.
8. Olivetti G, Abbi R, Quaini F, Kajstura J, Cheng W, Nitahara JA, Quaini E, Di Loreto C, Beltrami CA, Krajewski S, Reed JC, Anversa P. Apoptosis in the failing human heart. *N Engl J Med* 1997; 336: 1131–1141.
9. Saraste A, Pulkki K, Kallajoki M, Heikkila P, Laine P, Mattila S, Neiminen NS, Parvinen M, Voipio-Pulkki LM. Cardiomyocyte apoptosis and progression of heart failure to transplantation. *Eur J Clin Invest* 1999; 29: 380–386.
10. Olivetti G, Quaini F, Sala R, Lagrasta C, Corradi D, Bonacina E, Gambert SR, Cigola E, Anversa P. Acute myocardial infarction in humans is associated with activation of programmed myocyte cell death in the surviving portion of the heart. *J Mol Cell Cardiol* 1996; 28: 2005–2016.
11. James TN. Homage to James B Herrick: a contemporary look at myocardial infarction and sickle-cell heart disease, the 32nd Annual Herrick lecture of the council of Clinical Cardiology of the American heart Association. *Circulation* 2000; 101: 1874–1887.
12. Saraste A. Morphologic criteria and detection of apoptosis. *Herz* 1999; 24: 189–195.
13. Ohno M, Takemura G, Ohno A, Misao J, Hayakawa Y, Minatoguchi S, Fujiwara T, Fujiwara H. "Apoptotic" myocytes in infarct area in rabbit hearts may be oncotic myocytes with DNA fragmentation. *Circulation* 1998; 98: 1422–1430.
14. Buja LM, Entman M. Modes of myocardial cell injury and cell death in ischemic heart disease. *Circulation* 1998; 98: 1355–1357.
15. Palojoki E, Saraste A, Eriksson A, Pulkki K, Kallajoki M, Voipio-Pulkki LM, Tikkanen I. Cardiomyocyte apoptosis and ventricular remodeling after myocardial infarction in rats. *Am J Physiol – Heart Circ Physiol* 2001; 280: H2726–H2730.
16. Sam F, Sawyer DB, Chang DL, Eberli FR, Ngoy S, Jain M, Amin J, Apstein CS, Colucci WS. Progressive left ventricular remodeling and apoptosis late after myocardial infarction in mouse heart. *Am J Physiol – Heart Circ Physiol* 2000; 279: H422–H428.
17. Condorelli G, Morisco C, Stassi G, Notte A, Farina F, Sgaramella G, de Rienzo A, Roncarati R, Trimarco B, Lembo G. Increased cardiomyocyte apoptosis and changes in proapoptotic and antiapoptotic genes bax and bcl-2 during left ventricular adaptations to chronic pressure overload in the rat. *Circulation* 1999; 99: 3071–3078.
18. Kim CB, Braunwald E. Potential benefits of late reperfusion of infarcted myocardium: the open artery hypothesis. *Circulation* 1993; 88: 2426–2436.
19. Pizzetti G, Belotti G, Margonato A, Cappelletti A, Chierchia SL. Coronary recanalization by elective angioplasty prevents ventricular dilation after anterior myocardial infarction. *J Am Coll Cardiol* 1996; 28: 837–845.
20. Lancellotti P, Albert A, Berthe C, Pierard LA. Full recovery of contraction late after acute myocardial infarction: determinants and early predictors. *Heart* 2001; 85: 521–526.
21. Kanoh M, Takemura G, Misao J, Hayakawa Y, Aoyama T, Nishigaky K, Noda T, Fujiwara T, Fukuda K, Minatoguchi S, Fujiwara H. Significance of myocytes with positive DNA *in situ* nick end-labeling (TUNEL) in hearts with dilated cardiomyopathy. No apoptosis but DNA repair. *Circulation* 1999; 99: 2757–2764.
22. Kockx MM, Muhring J, Knaapen MW, de Meyer G. RNA synthesis and splicing interferes with DNA *in situ* end labeling techniques used to detect apoptosis. *Am J Pathol* 1998; 152: 885–888.

23. Nakajima W, Ishida A, Lange MS, Gabrielson KL, Wilson MA, Martin LJ, Blue ME, Johnston MV. Apoptosis has a prolonged role in the neurodegeneration after hypoxic ischemia in the newborn rat. *J Neurosci* 2000; 20: 7994–8004.
24. Sakahira H, Enari M, Nagata S. Cleavage of CAD inhibitor in CAD activation and DNA degradation during apoptosis. *Nature* 1998; 391: 96–99.
25. Kondo S, Barna BP, Morimura T, Takeuchi J, Yuan J, Akbasak A, Barnett GH. Interleukin-1β-converting enzyme mediates cisplatin-induced apoptosis in malignant glioma cells. *Cancer Res* 1995; 55: 6166–6171.
26. Krajewska M, Wang HG, Krajewski S, Zapata JM, Shabaik A, Gascoyne R, Reed JC. Immunohistochemical analysis of *in vivo* patterns of expression of CPP32 (caspase-3), a cell death protease. *Cancer Res* 1997; 57: 1605–1613.
27. Black SC, Huang JQ, Rezaiefar P, Radinovic S, Eberhart A, Nicholson DW, Rodger IW. Co-localization of the cysteine protease caspase-3 with apoptotic myocytes after *in vivo* myocardial ischemia and reperfusion in the rat. *J Mol Cell Cardiol* 1998; 30: 733–742.
28. Oltvai ZN, Milliman CL, Korsmeyer SJ. Bcl-2 heterodimerizes *in vivo* with a conserved homolog, bax, that accelerates programmed cell death. *Cell* 1993; 74: 609–619.
29. Hanada M, Aime-Sempe C, Sato T, Reed JC. Structure–function analysis of bcl-2 protein: identification of conserved domains important for homodimerization with bcl-2 and heterodimerization with bax. *J Biol Chem* 1995; 270: 11962–11969.
30. Misao J, Hayakawa Y, Ohno M, Kato S, Fujiwara T, Fujiwara H. Expression of bcl-2 protein, an inhibitor of apoptosis, and bax, an accelerator of apoptosis, in ventricular myocytes of human hearts with myocardial infarction. *Circulation* 1996; 94: 1506–1512.
31. Feuerstein G, Ruffolo RR, Yue T. Apoptosis and congestive heart failure. *Trends Cardiovas Med* 1997; 7: 249–255.
32. Beltrami AP, Urbanek K, Kajstura J, Yan SM, Finato N, Bussani R, Nadal-Ginard B, Silvestri F, Leri A, Beltrami CA, Anversa P. Evidence that human cardiac myocytes divide after myocardial infarction. *N Engl J Med* 2001; 344: 1750–1757.
33. Hofstra L, Liem IH, Dumont EA, Boersma HH, van Heerde WL, Doevendans PA, De Muinck E, Wellens HJ, Kemerink GJ, Reutelingsperger CP, Heidendal GA. Visualisation of cell death *in vivo* in patients with acute myocardial infarction. *Lancet* 2000; 356: 209–212.
34. Yaiota H, Ogawa K, Machara K, Maruyama Y. Attenuation of ischemia/reperfusion injury in rats by a caspase inhibitor. *Circulation* 1998; 97: 276–281.

ELSEVIER

Alcohol 27 (2002) 63–68

ALCOHOL

Ethanol, oxidative stress, and cytokine-induced liver cell injury

Jan B. Hoek*, John G. Pastorino

Alcohol Research Center, Department of Pathology, Anatomy and Cell Biology, Thomas Jefferson University, JAH Room 269, 1020 Locust Street, Philadelphia, PA 19107, USA

Received 23 November 2001; received in revised form 7 February 2002; accepted 9 February 2002

Abstract

Both clinical findings and results of experiments with animal models of alcoholic hepatitis have shown the importance of cytokine-mediated cell–cell interactions in the onset of ethanol-induced liver damage. Proinflammatory cytokines, such as tumor necrosis factor-alpha (TNF-α), interleukin (IL)-1beta (IL-1β), and interleukin-6, are released from Kupffer cells or infiltrating neutrophils and macrophages and elicit defensive responses in parenchymal cells, including activation of apoptosis. Reactive oxygen species (ROS) and reactive nitrogen species (RNS), generated in response to cytokine-induced stress signals in parenchymal cells and also by activation of Kupffer cells and inflammatory cells, further mobilize cellular defense mechanisms. When these defensive responses are overwhelmed cells may die by necrosis, further stimulating inflammatory responses and infiltration of neutrophils. Chronic ethanol intake (i.e., many years of heavy alcohol use in human patients, several weeks or months in experimental animals) enhances the damaging consequences of these events through a variety of mechanisms. The formation of cytokines in the liver is stimulated by increasing circulating levels of endotoxin and by enhancing the responsiveness of Kupffer cells to such stimuli. In addition, ethanol promotes oxidative stress, both by increased formation of ROS and by depletion of oxidative defenses in the cell. Furthermore, liver cells from ethanol-treated animals are more susceptible to the cytotoxic effects of TNF-α and other cytokines than cells from control animals. Mitochondria play a critical role in the apoptotic response, and alterations in mitochondrial function after chronic ethanol treatment may contribute to enhanced cell death by apoptosis or necrosis. How the shift in the balance of cytokine-induced defensive and damage responses in hepatocytes contributes to the liver injury that occurs in alcoholic hepatitis remains poorly characterized and should be a rewarding area for future studies.

Keywords: Ethanol; Cytokines; Alcoholic liver disease; Oxidative stress; Mitochondria; Apoptosis

1. The role of cytokines and oxidative stress in the onset of alcoholic liver disease

Alcoholic hepatitis and other forms of alcoholic liver disease (ALD) are major complications of chronic excessive ethanol intake[1]. However, the mechanisms underlying ethanol-induced hepatotoxicity are complex and remain poorly understood. In recent years, a significant role for proinflammatory cytokines such as tumor necrosis factor-alpha (TNF-α), in the onset of liver disease, has been indicated both by clinical observations of an enhanced circulating level of TNF-α and other cytokines in patients with ALD and by results of studies with animal models of alcohol-induced liver damage [reviewed in McClain et al. (1999); Thurman et al. (1999); Tilg & Diehl (2000)]. For instance, results of animal studies on an intragastric ethanol-feeding model have shown that treatment with neutralizing antibodies to TNF-α suppresses ethanol-induced liver damage (Iimuro et al., 1997). Depletion of Kupffer cells, a major source of TNF-α and other cytokines, prevents liver damage in this model (Adachi et al., 1994) and also suppresses ethanol-induced microvesicular and macrovesicular steatosis in an oral ethanol-feeding model (Järveläinen et al., 2000). Activation of Kupffer cells results from exposure to endotoxin, which derives from the cell wall material of Gram-negative bacteria in the gut. An elevated circulating endotoxin level has been detected in heavy drinkers (Bode et al., 1987), as well as in

* Corresponding author. Tel.: +1-215-503-5016; fax: +1-215-923-2218.

E-mail address: Jan.Hoek@mail.tju.edu (J.B. Hoek).

Editor: T.R. Jerrells

[1] The term "chronic excessive alcohol intake" is used somewhat loosely in this review to indicate prolonged heavy alcohol use, in human beings generally involving many years of daily alcohol use in excess of approximately 100 g/day. In studies on experimental animals, chronic ethanol treatment generally involves prolonged (i.e., periods ranging from 3 weeks to several months) dietary treatment in which ethanol constitutes as much as 36% of total calories (with carbohydrate or fat substituting for ethanol in pair-fed control animals) and daily ethanol intake is >10–12 g/kg/day. By contrast, in studies on isolated cells in culture, chronic ethanol treatment usually involves treating the cells with ethanol concentrations ranging from 20 to 100 mM for periods of 24 to 48 h.

0741-8329/02/$ – see front matter
PII: S0741-8329(02)00215-X

experimental animals after chronic ethanol administration (Nanji et al., 1994). This is thought to be caused by increased permeability of the intestinal wall, but an increase in bacterial flora and a reduced capacity for endotoxin scavenging may also result from chronic ethanol intake. Kupffer cells respond to the endotoxin challenge by producing a battery of cytokines and chemokines, including TNF-α, interleukin (IL)-1β, IL-6, and prostaglandin E_2 (McClain et al., 1999; Thurman et al., 1999). However, the liver damage caused by ethanol treatment in the intragastric feeding model is not mimicked by a sustained (for up to 4 weeks) infusion of endotoxin at levels considerably higher than those attained during ethanol feeding (Järveläinen et al., 1999), although ethanol intake increased hepatic necrosis caused by an acute endotoxin challenge of 24 h (Bhagwandeen et al., 1987). Thus, chronic ethanol treatment must exert effects downstream of the endotoxin-activated Kupffer cell response. In fact, there is good evidence that ethanol treatment changes the response of Kupffer cells and monocytes to endotoxin, resulting in an enhanced production of TNF-α and other cytokines (McClain et al., 1999).

Cytokines and chemokines released by Kupffer cells exert a range of autocrine and paracrine effects that initiate defense responses in the liver, but also promote infiltration of inflammatory leukocytes and activate oxidative burst responses, accompanied by a further release of cytokines and degradative proteins. These complex cascades result in a vicious cycle of acute challenges to liver cells by oxidative stress and cytotoxic signals that can overwhelm cellular defense mechanisms. How well the liver parenchymal cells handle these challenges will ultimately determine to what extent liver damage results.

However, an increased production of TNF-α and other proinflammatory cytokines cannot adequately explain the increased tissue damage in heavily drinking human patients and in animal models of chronic ethanol exposure. The parenchymal cells of the liver also change their response to TNF-α. Normally, TNF-α is not cytotoxic for liver cells. Although TNF-α can initiate a battery of intracellular pathways that lead to cell death by apoptosis or necrosis, the cells also activate cytoprotective signals that suppress the deleterious effects of TNF-α (Fig. 1). Characteristically,

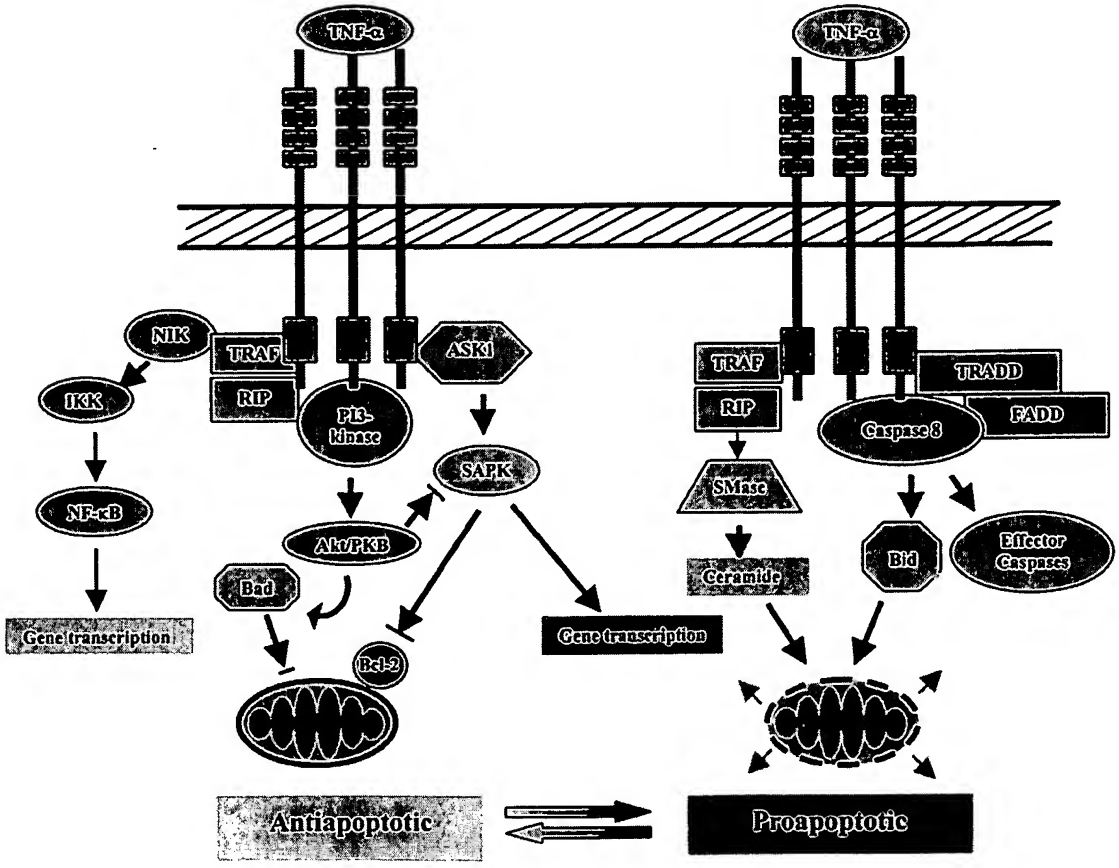

Fig. 1. Signaling pathways of the tumor necrosis factor-alpha receptor promoting proapoptotic and antiapoptotic responses. Akt/PKB = Protein kinase B; ASK1 = apoptosis signal-regulating kinase 1; Bad = Bcl-2-associated death protein; Bcl-2 = B-cell lymphoma-2 protein; Bid = Bcl-2-interacting death protein; FADD = Fas-activated death domain protein; IKK = inhibitor kappa B kinase; NF-κB = nuclear factor kappa B; NIK = nuclear factor–inducing kinase; PI3-kinase = 1-phosphatidylinositol 3-kinase; RIP = receptor-interacting protein; SAPK = stress-activated protein kinase; SMase = sphingomyelinase; TNF-α = tumor necrosis factor-alpha; TRADD = tumor necrosis factor receptor-associated death domain protein; TRAF = tumor necrosis factor receptor-associated factor.

TNF-α and IL-6 are essential ingredients to initiate the onset of liver regeneration. Chronic ethanol treatment results in an impaired regenerative response in rats and mice through mechanisms that involve defects in the early response to these cytokines (Chen et al., 1997; Yang et al., 1998). Hence, changes in the signaling machinery activated by TNF-α (or other cytokines) may occur in the liver cells after chronic ethanol treatment; such changes may cause these cells to be more sensitive to the cytotoxic actions of TNF-α than in control animals.

2. Signaling pathways that mediate the cellular effects of TNF-α

Tumor necrosis factor-alpha acts on liver cells through two types of plasma membrane receptors: p55 [type 1 tumor necrosis factor receptor (TNFR1)] and p75 [type 2 tumor necrosis factor receptor (TNFR2)]. In liver cells, TNFR1 predominates and results of studies on TNF receptor knockout mice indicate that TNFR1 is required for ethanol-induced liver damage (Yin et al., 1999). The TNFR1 is the prototype of a family of receptors that also includes the Fas receptor and the nerve growth factor receptor. Binding of TNF-α to TNFR1 induces receptor trimerization and activation, mediated by association of the receptor with a variety of signaling proteins that interact with specific protein domains on its intracellular tail, as illustrated in Fig. 1 [see Locksley et al. (2001) for a recent review].

The best characterized signaling system activated by TNF-α involves proteins that bind through the death domain, a protein domain found in a variety of signaling proteins involved in activation of the apoptotic machinery. Proteins such as TNF receptor-associated death domain protein (TRADD) and Fas-activated death domain protein (FADD) activate caspase 8, an upstream signaling caspase protein that initiates the proteolytic activation of a variety of effector proteins, including other caspases, as well as the proapoptotic Bcl-2 family protein Bid (Yin, 2000). The active, truncated form of Bid (t-Bid) acts on mitochondria to cause mitochondrial outer membrane permeabilization. This permits the release of numerous proapoptotic factors stored in the mitochondrial intermembrane space, which, together with the effector caspases, initiate the program of nuclear chromatin condensation and degradation that is characteristic of apoptosis (Kroemer & Reed, 2000).

TNF-α binding to TNFR1 also activates other signaling pathways that may promote cell death. For instance, the binding of a complex of receptor-interacting protein (RIP), a death domain serine–threonine kinase, and TNF receptor-associated factor 2 (TRAF2), an adapter protein that interacts with the activated receptor, causes activation of sphingomyelinases with formation of ceramide. This mediator may act on mitochondria to promote the mitochondrial permeability transition (MPT), a process that involves opening of a large proteinaceous pore across both inner and outer membranes (Bernardi et al., 2001). This is associated with a loss of mitochondrial energization, swelling of the matrix, and rupture of the outer membrane, again accompanied by the release of numerous proapoptotic factors. In addition, TNF-α activates different stress-activated protein kinase (SAPK) cascades in liver cells, resulting in the stimulation of p38 mitogen-activated protein kinase (MAPK) and Jun N-terminal kinase (JNK) (Wajant et al., 2001). Both affect the sensitivity of mitochondria to proapoptotic stimuli: JNK by phosphorylation of antiapoptotic proteins, such as Bcl-2 and Bcl-X_L, and p38 MAPK by enhancing the effects of the proapoptotic Bcl-2 family protein Bax.

At the same time, TNFR1 activation initiates cytoprotective responses in hepatocytes through other signaling cascades. Prominent is the activation of nuclear factor-kappa B (NF-κB), through a pathway that probably also involves TRAF2 and RIP, activating a protein kinase cascade that results in the phosphorylation and degradation of the NF-κB inhibitory protein I-κB (Wajant et al., 2001). This enables NF-κB to migrate to the nucleus and activate the transcription of a variety of genes, such as inhibitor of apoptosis (IAP) 1 and 2, the products of which suppress the activation of caspases through the death pathway. Hence, these protective actions are prevented when gene transcription or protein synthesis is inhibited. Additional protection probably comes from a TNFR1-stimulated cascade that results in activation of 1-phosphatidylinositol 3-kinase (PI3-kinase), the polyphosphoinositide products of which cause activation of protein kinase B (Akt/PKB). The Akt/PKB phosphorylates and inactivates Bad, another proapoptotic protein of the Bcl-2 family that acts through its interaction with mitochondria (Pastorino et al., 1999b). Hence, the initiation of the apoptotic program in a particular cell eminently depends on the appropriate balance of a variety of signaling cascades, and the balance of downstream actions of these cascades seems to target the mitochondria, which act as a master switch for the apoptotic machinery.

3. Ethanol treatment enhances the susceptibility of cells to TNF-α by mechanisms that involve the mitochondrial permeability transition

There is considerable evidence that ethanol treatment preconditions hepatocytes to shift the balance of cytoprotective and cytotoxic actions initiated by TNF-α (or other cytokines), thereby impairing the appropriate response of the cell to toxic challenges. Results of studies in our laboratory have demonstrated that hepatocytes isolated from rats that received an ethanol-containing liquid diet for 6 to 8 weeks are susceptible to TNF-α-induced cytotoxicity in a dose- and time-dependent manner, even in the absence of inhibitors of transcription or protein synthesis (Pastorino & Hoek, 2000). Importantly, the effect of ethanol treatment does not fully mimic the effect of inhibitors of protein synthesis, and the TNF-α-induced cytotoxicity does not involve activation of caspase 8. Thus, the pathways involved in TNF-α-mediated cell death that are active in ethanol-treated hepatocytes seem to bypass the classical death domain signaling cascade. This

is compatible with a role for other TNF-α-induced cytotoxic signaling pathways (e.g., those depending on TNF-α-induced ceramide formation) (Garcia-Ruiz et al., 1997).

The cytotoxicity associated with TNF-α treatment of hepatocytes obtained from ethanol-fed animals involves the early loss of mitochondrial function, as demonstrated by mitochondrial depolarization and the release of cytochrome c from the mitochondrial cell fraction to the cytosol, which occurs well before the loss of cell integrity is evident. The decline in the mitochondrial membrane potential is due to the mitochondrial permeability transition, and inhibition of this process with cyclosporin A prevents the TNF-α-induced cell death (Pastorino & Hoek, 2000). In previous studies from our laboratory, we had demonstrated that mitochondria obtained from ethanol-fed rats are more susceptible to undergo the permeability transition in response to a wide variety of challenges (Pastorino et al., 1999a). Hence, the effects of ethanol treatment may be a reflection of its effects on mitochondria.

Deterioration of liver mitochondrial function after chronic ethanol treatment has been well documented (Cunningham et al., 1990). Oxidative phosphorylation is impaired because of a defect in the synthesis of mitochondrially encoded proteins. Although this defect is not usually evident in limiting the energy supply in the liver and ATP levels are maintained under normal conditions, it may be more difficult for the cell to respond appropriately to stress conditions that place high demands on the mitochondrial bioenergetic capacity. In addition, ethanol treatment induces changes in mitochondrial membrane structure (Rottenberg et al., 1984) that have been reported to account for defective mitochondrial uptake of glutathione and a decline in its defense capacity against oxidative stress (Fernandez-Checa et al., 1997). This could further enhance the onset of the mitochondrial permeability transition under conditions of oxidative challenge (Higuchi et al., 2001).

The effects of chronic ethanol treatment on mitochondrial function may also include alterations in the upstream signaling pathways that mediate the protective or damaging effects of TNF-α. The onset of the mitochondrial permeability transition is controlled by a variety of proapoptotic and antiapoptotic signals that have an impact on the components of the permeability transition pore complex. For instance, results of preliminary studies indicate that inhibition of MAPK cascades that control the balance of proapoptotic and antiapoptotic proteins interacting with mitochondria could prevent the TNF-α-induced onset of the mitochondrial permeability transition in hepatocytes obtained from ethanol-fed rats (unpublished observations, J. G. Pastorino, 2001). Hence, the changes in susceptibility to TNF-α cytotoxic signals probably reflect multiple levels of adaptive (or maladaptive) effects of chronic ethanol treatment.

4. Is ethanol metabolism required for the ethanol-induced sensitization of hepatocytes to TNF-α?

The liver is the major site of ethanol oxidation, and the results of numerous studies attest to the potential damage elicited by metabolites of ethanol [e.g., through the formation of acetaldehyde and the oxidative stress generated by ethanol oxidation through cytochrome P450 isoforms, specifically cytochrome P450-2E1 (CYP2E1)] (Lieber, 1997). However, ethanol also exerts direct effects on membranes and proteins. For example, a variety of ion channels, neurotransmitter receptors, and signaling proteins are affected by ethanol binding to hydrophobic protein domains (Covarrubias et al., 1995; Seiler et al., 2000; Wick et al., 1998; Wilkemeyer et al., 2000). Hence, we have analyzed to what extent ethanol enhances the cytotoxic effects of TNF-α in HepG2 cells, a hepatoma-derived cell line that has been reported to lack detectable alcohol dehydrogenase and CYP2E1 activities (Clemens et al., 1995; Wu & Cederbaum, 1996). Even in this cell line, we observed an ethanol-induced enhancement of TNF-α-induced cell death with characteristics that were similar to those obtained with hepatocytes isolated from ethanol-fed rats (Pastorino & Hoek, 2000). Notably, activation of the death domain signaling pathways resulting in caspase 8 activation was not required for TNF-α-induced cytotoxicity, but early activation of the mitochondrial permeability transition was essential. Ethanol did not exert its effects acutely, but required preincubation of the cells for 48 h or longer. Thus, it seems that ethanol treatment induces changes in cellular defense mechanisms that control the balance of proapoptotic and antiapoptotic proteins acting on mitochondria. Oxidative stress markedly enhances the potentiation by ethanol of cytotoxic responses to TNF-α. HepG2 cells that were transfected with CYP2E1, when treated with ethanol for 48 h, were killed at much lower TNF-α concentrations and over shorter periods than were mock-transfected control cells. These effects were completely reversed by the antioxidant ebselen (Pastorino & Hoek, 2000). However, ebselen-treated cells still showed the slower onset potentiation by ethanol of TNF-α-induced cytotoxicity, similar to the TNF-α-induced cell killing in wild-type HepG2 cells. Hence, oxidative stress initiated by ethanol oxidation through CYP2E1 promoted the effects of ethanol, but it is not essential for its enhancement of TNF-α-mediated cell death.

These findings do not necessarily imply that cellular stress signaling pathways are not involved in the effects of ethanol on untransfected HepG2 cells. As we pointed out earlier, a decreased capacity to respond to a variety of stress conditions may result directly from the ethanol-induced deterioration of mitochondrial function, but might also be due to an enhancement of upstream signaling cascades that transmit the stress signals to the mitochondria. In either case, the mechanisms underlying these actions of ethanol remain to be determined. Further studies are required, both at the level of isolated cells and in cell culture model systems to understand better the mechanisms by which ethanol treatment interferes with the TNF-α signaling machinery. We also need to understand how these signaling pathways contribute to the progressive tissue damage that is associated with alcoholic hepatitis in the intact tissue.

5. Apoptosis and necrosis in alcoholic liver disease

How relevant are the studies on ethanol-mediated enhancement of the cell death response induced by TNF-α in isolated hepatocytes or HepG2 cells for understanding the mechanism by which ethanol treatment in vivo promotes liver damage? Ethanol-dependent liver damage is typically associated with tissue necrosis and infiltration of neutrophils and other inflammatory cells. The results of our studies on isolated hepatocytes and HepG2 cells show that TNF-α induces a mixed pattern of cell death, as detected by a fluorescence-activated cell sorter (FACS) with the use of fluorescence markers for apoptosis and necrosis. Some cells display the hallmarks of apoptosis, with characteristics of caspase activation, DNA laddering, and chromatin condensation, and other cells show evidence of necrosis (Pastorino & Hoek, 2000). However, it is difficult to predict how the liver cells will respond in the integrated tissue context, in which they are challenged simultaneously by multiple other cytokines, by ROS and RNS, and by other products derived from activated neutrophils and other inflammatory cells.

The apoptotic response is a defense mechanism by which the tissue disposes of unwanted or damaged cells. However, as illustrated in Fig. 2, if conditions are unfavorable for completion of the program (e.g., in the face of overwhelming cell damage or when the energy supply is inadequate for sustaining the process), cells may default to a necrotic form of cell death, which fails to show apoptotic characteristics (Leist et al., 1997). There is considerable discussion whether apoptosis occurs as an integral part of the response of the tissue to the damage associated with alcoholic hepatitis or other liver failure (Casey et al., 2001; Kanzler & Galle, 2000). However, the boundaries between apoptotic and necrotic forms of cell death are not always all that sharp, and the activation of the apoptotic cell-death program may well contribute substantially to a predominantly necrotic pattern of damage. Whether cells ultimately die by apoptosis or necrosis may depend on secondary factors determined by local conditions in the tissue.

Could these local conditions also account for the predominantly centrilobular necrosis that is characteristic of ALD? A variety of factors have been suggested to cause centrilobular tissue damage, including the prevalence of CYP2E1 expression in the pericentral region of the liver (Buhler et al., 1992) or the lower oxygen tension and transient hypoxia that would occur locally (Arteel et al., 1997). Either of these factors could substantially impede the gradual progression of the ordered sequence of events in apoptosis and enhance a shift toward necrosis. The mobilization of infiltrating neutrophils and monocytes that is triggered by the release of IL-8 and other chemokines requires necrotic cell death, and, therefore, a cascade of deleterious consequences would be triggered by a local shift toward necrotic forms of cell death.

As in politics, all final decisions are local.

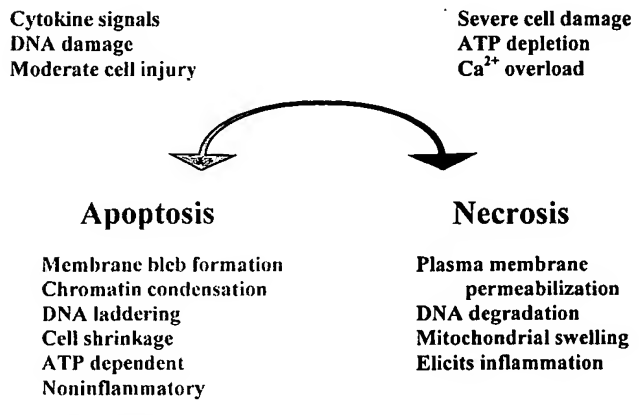

Fig. 2. Balance between apoptosis and necrosis in response to damage signals.

Acknowledgments

The work from our laboratory discussed in this overview was supported by grants AA07186, AA10968, AA08714, and AA00330 of the National Institute on Alcohol Abuse and Alcoholism.

References

Adachi, Y., Bradford, B. U., Gao, W., Bojes, H. K., & Thurman, R. G. (1994). Inactivation of Kupffer cells prevents early alcohol-induced liver injury. *Hepatology 20*, 453–460.

Arteel, G. E., Iimuro, Y., Yin, M., Raleigh, J. A., & Thurman, R. G. (1997). Chronic enteral ethanol treatment causes hypoxia in rat liver tissue in vivo. *Hepatology 25*, 920–926.

Bernardi, P., Petronilli, V., Di Lisa, F., & Forte, M. (2001). A mitochondrial perspective on cell death. *Trends Biochem Sci 26*, 112–117.

Bhagwandeen, B. S., Apte, M., Manwarring, L., & Dickeson, J. (1987). Endotoxin induced hepatic necrosis in rats on an alcohol diet. *J Pathol 152*, 47–53.

Bode, C., Kugler, V., & Bode, J. C. (1987). Endotoxemia in patients with alcoholic and non-alcoholic cirrhosis and in subjects with no evidence of chronic liver disease following acute alcohol excess. *J Hepatol 4*, 8–14.

Buhler, R., Lindros, K. O., Nordling, A., Johansson, I., & Ingelman-Sundberg, M. (1992). Zonation of cytochrome P450 isozyme expression and induction in rat liver. *Eur J Biochem 204*, 407–412.

Casey, C. A., Nanji, A., Cederbaum, A. I., Adachi, M., & Takahashi, T. (2001). Alcoholic liver disease and apoptosis. *Alcohol Clin Exp Res 25*, 49S–53S.

Chen, J., Bao, H., Sawyer, S., Kunos, G., & Gao, B. (1997). Effects of short and long term ethanol on the activation of signal transducer and activator transcription factor 3 in normal and regenerating liver. *Biochem Biophys Res Commun 239*, 666–669.

Clemens, D. L., Halgard, C. M., Miles, R. R., Sorrell, M. F., & Tuma, D. J. (1995). Establishment of a recombinant hepatic cell line stably expressing alcohol dehydrogenase. *Arch Biochem Biophys 321*, 311–318.

Covarrubias, M., Vyas, T. B., Escobar, L., & Wei, A. (1995). Alcohols inhibit a cloned potassium channel at a discrete saturable site. Insights into the molecular basis of general anesthesia. *J Biol Chem 270*, 19408–19416.

Cunningham, C. C., Coleman, W. B., & Spach, P. I. (1990). The effects of chronic ethanol consumption on hepatic mitochondrial energy metabolism. *Alcohol Alcohol 25*, 127–136.

Fernandez-Checa, J. C., Kaplowitz, N., Garcia-Ruiz, C., Colell, A., Miranda, M., Mari, M., Ardite, E., & Morales, A. (1997). GSH transport in mitochondria: defense against TNF-induced oxidative stress and alcohol-induced defect. *Am J Physiol 273*, G7–G17.

Garcia-Ruiz, C., Colell, A., Mari, M., Morales, A., & Fernandez-Checa, J. C. (1997). Direct effect of ceramide on the mitochondrial electron transport chain leads to generation of reactive oxygen species. Role of mitochondrial glutathione. *J Biol Chem 272*, 11369–11377.

Higuchi, H., Adachi, M., Miura, S., Gores, G. J., & Ishii, H. (2001). The mitochondrial permeability transition contributes to acute ethanol-induced apoptosis in rat hepatocytes. *Hepatology 34*, 320–328.

Iimuro, Y., Gallucci, R. M., Luster, M. I., Kono, H., & Thurman, R. G. (1997). Antibodies to tumor necrosis factor-α attenuate hepatic necrosis and inflammation caused by chronic exposure to ethanol in the rat. *Hepatology 26*, 1530–1537.

Järveläinen, H. A., Fang, C., Ingelman-Sundberg, M., & Lindros, K. O. (1999). Effect of chronic coadministration of endotoxin and ethanol on rat liver pathology and proinflammatory and anti-inflammatory cytokines. *Hepatology 29*, 1503–1510.

Järveläinen, H. A., Fang, C., Ingelman-Sundberg, M., Lukkari, T. A., Sippel, H., & Lindros, K. O. (2000). Kupffer cell inactivation alleviates ethanol-induced steatosis and CYP2E1 induction but not inflammatory responses in rat liver. *J Hepatol 32*, 900–910.

Kanzler, S., & Galle, P. R. (2000). Apoptosis and the liver. *Semin Cancer Biol 10*, 173–184.

Kroemer, G., & Reed, J. C. (2000). Mitochondrial control of cell death. *Nat Med 6*, 513–519.

Leist, M., Single, B., Castoldi, A. F., Kuhnle, S., & Nicotera, P. (1997). Intracellular adenosine triphosphate (ATP) concentration: a switch in the decision between apoptosis and necrosis. *J Exp Med 185*, 1481–1486.

Lieber, C. S. (1997). Role of oxidative stress and antioxidant therapy in alcoholic and nonalcoholic liver diseases. *Adv Pharmacol 38*, 601–628.

Locksley, R. M., Killeen, N., & Lenardo, M. J. (2001). The TNF and TNF receptor superfamilies: integrating mammalian biology. *Cell 104*, 487–501.

McClain, C. J., Barve, S., Deaciuc, I., Kugelmas, M., & Hill, D. (1999). Cytokines in alcoholic liver disease. *Semin Liver Dis 19*, 205–219.

Nanji, A. A., Khettry, U., & Sadrzadeh, S. M. (1994). Lactobacillus feeding reduces endotoxemia and severity of experimental alcoholic liver disease. *Proc Soc Exp Biol Med 205*, 243–247.

Pastorino, J. G., & Hoek, J. B. (2000). Ethanol potentiates tumor necrosis factor-α cytotoxicity in hepatoma cells and primary rat hepatocytes by promoting induction of the mitochondrial permeability transition. *Hepatology 31*, 1141–1152.

Pastorino, J. G., Marcinkeviciute, A., Cahill, A., & Hoek, J. B. (1999a). Potentiation by chronic ethanol treatment of the mitochondrial permeability transition. *Biochem Biophys Res Commun 265*, 405–409.

Pastorino, J. G., Tafani, M., & Farber, J. L. (1999b). Tumor necrosis factor induces phosphorylation and translocation of BAD through a phosphatidylinositide-3-OH kinase-dependent pathway. *J Biol Chem 274*, 19411–19416.

Rottenberg, H., Waring, A., & Rubin, E. (1984). Alcohol-induced tolerance in mitochondrial membranes. *Science 223*, 193–194.

Seiler, A. E., Henderson, A., & Rubin, R. (2000). Ethanol inhibits insulin receptor tyrosine kinase. *Alcohol Clin Exp Res 24*, 1869–1872.

Thurman, R. G., Bradford, B. U., Iimuro, Y., Frankenberg, M. V., Knecht, K. T., Connor, H. D., Adachi, Y., Wall, C., Arteel, G. E., Raleigh, J. A., Forman, D. T., & Mason, R. P. (1999). Mechanisms of alcohol-induced hepatotoxicity: studies in rats. *Front Biosci 4*, e42–e46.

Tilg, H., & Diehl, A. M. (2000). Cytokines in alcoholic and nonalcoholic steatohepatitis. *N Engl J Med 343*, 1467–1476.

Wajant, H., Henkler, F., & Scheurich, P. (2001). The TNF-receptor-associated factor family: scaffold molecules for cytokine receptors, kinases and their regulators. *Cell Signal 13*, 389–400.

Wick, M. J., Mihic, S. J., Ueno, S., Mascia, M. P., Trudell, J. R., Brozowski, S. J., Ye, Q., Harrison, N. L., & Harris, R. A. (1998). Mutations of γ-aminobutyric acid and glycine receptors change alcohol cutoff: evidence for an alcohol receptor? *Proc Natl Acad Sci U S A 95*, 6504–6509.

Wilkemeyer, M. F., Sebastian, A. B., Smith, S. A., & Charness, M. E. (2000). Antagonists of alcohol inhibition of cell adhesion. *Proc Natl Acad Sci U S A 97*, 3690–3695.

Wu, D., & Cederbaum, A. I. (1996). Ethanol cytotoxicity to a transfected HepG2 cell line expressing human cytochrome P4502E1. *J Biol Chem 271*, 23914–23919.

Yang, S. Q., Lin, H. Z., Yin, M., Albrecht, J. H., & Diehl, A. M. (1998). Effects of chronic ethanol consumption on cytokine regulation of liver regeneration. *Am J Physiol 275*, G696–G704.

Yin, M., Wheeler, M. D., Kono, H., Bradford, B. U., Gallucci, R. M., Luster, M. I., & Thurman, R. G. (1999). Essential role of tumor necrosis factor α in alcohol-induced liver injury in mice. *Gastroenterology 117*, 942–952.

Yin, X. M. (2000). Bid, a critical mediator for apoptosis induced by the activation of Fas/TNF-R1 death receptors in hepatocytes. *J Mol Med 78*, 203–211.

Inflammation, Vol. 22, No. 6, 1998

MEDIATORS OF MICROVASCULAR INJURY IN DERMAL BURN WOUNDS

Z. B. RAVAGE, H. F. GOMEZ,
B. J. CZERMAK, S. A. WATKINS, and G. O. TILL

University of Michigan Medical School
Ann Arbor, Michigan 48109-0602

Abstract—In previous studies we have demonstrated that second-degree thermal injury of skin in rats leads to secondary effects, such as systemic complement activation, C5a-mediated activation of blood neutrophils, their adhesion-molecule-guided accumulation in lung capillaries and the development of acute pulmonary injury, largely caused by neutrophil-derived toxic oxygen metabolites. In the dermal burn wound, however, pathophysiologic events are less well understood. The injury is fully developed at four hours post-burn. To further elucidate the pathogenesis of the "late phase" dermal vascular damage, rats were depleted of neutrophils or complement by pretreatment with rabbit antibody against rat neutrophils or with cobra venom factor, respectively. In other experiments, rats were treated with blocking antibodies to IL-6, IL-1, and TNFα immediately following thermal burning or were pretreated with hydroxyl radical scavengers (dimethyl sulfoxide, dimethyl thiourea). Extravasation of ^{125}I-labeled bovine serum albumin into the burned skin was studied, as well as, skin myeloperoxidase levels. The studies revealed that, like in secondary lung injury, neutrophils and toxic oxygen metabolites, are required for full development of microvascular injury. In contrast, however, development of dermal vascular damage in thermally injured rats was not affected by complement depletion. Our data suggest that the development of microvascular injury in the dermal burn wound is complement-independent, involves the pro-inflammatory cytokines IL-1, TNFα and IL-6, and may result from reactive oxygen metabolites generated by neutrophils accumulating in the burn wound.

INTRODUCTION

There have been significant advances in recent years in the treatment and care of burn patients. Therapies such as topical antibiotic administration, early debridement and grafting of affected areas and vast improvements in intensive care management have contributed to a marked increase in survival rates (1). Despite this progress, the pathophysiology of the burn wound is still not fully understood. Second-degree dermal burn wounds provide an interesting point of investigation as this type of trauma results in extensive tissue damage not only locally, but

0360-3997/98/1200-0619$15.00/0

in distant organs, as well. The systemic effects occur in cases with extensive thermal trauma, but can be seen even in burn injuries covering only one quarter of the total body surface area (TBSA). In a second-degree thermal injury model in rats involving 25–30% TBSA, secondary lung injury has been observed. Till, et al. (1983) described systemic complement activation, as detected by reductions in hemolytic activity of individual complement components (C3, C4, C6) and crossed immunoelectrophoresis analysis of the conversion of serum C3 (2). Chemotaxis assays showed C5a-mediated activation of blood neutrophils to occur, as well. Secondary accumulation of polymorphonuclear leukocytes (PMN) has been shown to occur in lung tissues, followed by development of acute pulmonary injury, related to production of neutrophil-derived toxic oxygen metabolites (2). Employing the same animal model of dermal burn injury, PMN influx into lung tissues was reduced substantially (up to 77%) using antibodies to adhesion molecules (LFA-1, Mac-1, ICAM-1, E and L-selectin) (3).

The process of local edema formation in the burn wound appears to be more complex, as it involves both the direct effect of heat and the consequences of inflammatory mediators locally generated in response to the thermal insult. It has been shown that under conditions of limited thermal, chemical or physical trauma, two waves of increased vascular permeability occur in the skin (4). The "early phase" of increased permeability—approximately one hour after thermally injury—was shown to develop as a result of complement activation with anaphylatoxin release and mast cell secretion of histamine. This lead to an enhancement of xanthine oxidase activity and increased production of oxygen radicals, damaging endothelial cells (5). This one hour injury has been shown to be neutrophil independent (6).

The pathophysiology of "late phase" dermal microvascular injury (at approximately four hours post-burn) is less well understood. The delay in onset of this injury would indicate that a series of elaborate events must take place before maximal tissue damage is achieved. Recent data from our group suggest that, in contrast to the "early phase" edema formation, blood neutrophils are involved in the pathogenesis of the "late phase" injury. Since antibodies to neutrophils, as well as, to E- and L-selectin and ICAM-1 were shown to effectively reduce vascular leakage in the dermal burn wound at four hours post-burn (3), we sought to clarify the mechanism for neutrophil recruitment and infiltration by focusing on the upstream inflammatory mediators that may regulate these events. The current studies were designed to elucidate the role of the cytokines IL-6, IL-1 and TNFα, as well as complement, and to further clarify the role of neutrophils in the development of microvascular injury in the second-degree, "late phase" dermal burn wound. Here, we present evidence which demonstrates that the four hour burn injury is complement independent, involves the proinflammatory cytokines IL-6, IL-1 and TNFα and may result from the tissue-damaging effects of neutrophil-derived reactive oxygen species.

MATERIALS AND METHODS

Animal Model of Thermal Injury

The experimental burn model used in the present study has been described previously (2, 6, 7). Adult male, specific pathogen-free Long-Evans rats (300–350 g, Harlan Sprague-Dawley, Indianapolis, Indiana) were used in all experiments. Ketamine hydrochloride (100 mg/kg body weight) (Fort Dodge Laboratories, Fort Dodge, Iowa) and xylazine (13 mg/kg body weight) (Bayer Corporation, Shawnee Mission, Kansas) were administered intraperitoneally and intramuscularly, respectively, throughout the experiment. This ensured that the animals were properly anesthetized for the entire procedure, from the induction of the burn injury to the time of sacrifice. The skin over the lumbrosacral and dorsal flank areas was shaved and exposed to 70°C water for 30 s. This resulted in a deep second-degree skin burn involving 25 to 30% of the total body surface area. Animals were sacrificed at 4 h by cervical dislocation. Control animals were exposed to 22°C water. All experiments were in accord with the standards in *The Guide for the Care and Use of Laboratory Animals*, and were supervised by veterinarians from the Unit for Laboratory and Animal Care of the University of Michigan Medical School.

Measurement of Microvascular Injury. Local microvascular injury was assessed by measurement of extravasation of radiolabeled bovine serum albumin (^{125}I-BSA) into the burned skin. Immediately prior to thermal injury, burn or sham-treated animals received an intravenous injection of 0.5 μCi of ^{125}I-BSA in 0.5 ml sterile phosphate buffered saline (PBS). Using a template, four uniform skin samples, each one square inch in size, were excised from the burned area on each animal. For calculations of the permeability index, the amount of radioactivity (^{125}I-BSA) in skin biopsies was compared to the amount of radioactivity present in 1.0 ml of blood obtained from the inferior vena cava at the time of sacrifice (4 h).

Measurement of Skin Myeloperoxidase (MPO) Content. Local accumulation of neutrophils was assessed by measurement of myeloperoxidase in skin biopsies. Animals received burn or sham treatment as described above. At time of sacrifice (4 h), four 4 mm punch biopsies from standardized areas of the wound were taken from each animal and instantly frozen in liquid nitrogen. The biopsies were homogenized in 500 μl of PBS pH 7.4, containing 0.1% Tween 20, sonicated on ice and insoluble material removed by centrifugation at 3000 rpm for 10 min. 5 μl of tissue extract (PBS pH 7.4 and 0.1% Tween 20) were incubated with 100 μl of 2,2'-Azino-di-[3-ethylbenzthiozoline sulfonate (6)] diammonium salt solution (ATBS substrate) (Boehringer Mannheim, BIOCHEMICA, Germany) and the maximum velocity of the substrate/MPO chromogenic reaction (Vmax) measured by monitoring the 96 well low-protein binding flat bottom plates (Corning Glass Works, Corning, New York) at 405 nm over a two minute period (BioTek Elx808 microplate reader) (BIO-TEK Instruments, INC., Winooski, Vermont). Kinetic calculations were performed using KC3 software (BIO-TEK Instruments, Inc.). MPO concentrations in samples were determined using a standard curve of purified MPO (CALBIOCHEM, San Diego, California). MPO values are reported as units of activity/biopsy.

Interventional Studies

Cytokine Blockade. Irrelevant IgG antibody, anti-mouse IL-6 polyclonal antibody, and anti-rat IL-1β monoclonal antibody were obtained from R&D Systems, Minneapolis, Minnesota. Anti-rat TNFα polyclonal antibody were purchased from PeproTech, INC., Rocky Hill, New Jersey. In

each case, antibodies were given in a total amount of 500 μg per animal, in 0.5 ml sterile PBS, administered intravenously in two equal doses at 30 and 120 min post-burn.

Complement Depletion. Cobra venom factor (CVF) was purified from crude lyophilized cobra venom (Naja naja kaouthia) (Sigma Chemical Company, St. Louis, Missouri) by ion exchange chromatography and gel filtration (8). Complement depletion was achieved by serial intraperitoneal injections of 4 X 20 units CVF in 12 h intervals, resulting in undetectable levels of serum hemolytic complement activity (CH50 Assay). The experiments were performed 12 h after the final injection of CVF.

C5a Blockade. Isolation of polyclonal antibody to C5a was performed as described by Mulligan, et al. (9). Briefly, animals were immunized with rat C5a. Obtained serum was IgG purified by acid elution of Sepharose G beads (Pharmacia Biotech AB, Uppsala, Sweden), followed by extensive dialysis against PBS. Characterization of the anti-rat C5a antibody was performed by immunoprecipitation and Western blot analysis showing a single band at 14 kDa. This antibody was given in a total amount of 400 μg per animal, administered intravenously in two equal doses at 30 and 120 min post-burn.

Neutrophil Depletion. Neutrophil depletion was induced by the intraperitoneal injection of 1.0 ml of rabbit antiserum to rat PMN (Accurate, Westbury, New York) 16 h prior to the experiment. This procedure reduced neutrophil counts in peripheral blood by >90 percent.

Hydroxyl Radical Scavenger Administration. Dimethyl thiourea (DMTU) (Sigma Chemical Co.) (1000 mg/kg body weight) in 1.0 ml sterile PBS was injected intraperitoneally 10 min prior to thermal injury. Dimethyl sulfoxide (DMSO) (Sigma Chemical Co.) (500 μg) in 1.0 ml sterile PBS was injected intraperitoneally 10 min prior to thermal injury. The effectiveness of the chosen concentrations of scavengers was demonstrated in earlier studies (7).

Statistical Analysis. Data sets were analyzed using one-way ANOVA. Individual group means were compared with the Tukey multiple comparison test. All values were expressed as mean $\pm$ *SEM*. Significance was assigned where $P < 0.05$. For percentage change between groups, values obtained from negative controls were subtracted from each data point. Statistical analysis was performed using SigmaStat 2.0 (Jandel Scientific Software, San Rafael, California).

RESULTS

Protective Effects of Neutrophil Depletion in Dermal Burn Injury. Neutropenia was achieved by intraperitoneal injection of antiserum to rat PMN. Extravasation of ^{125}I-bovine serum albumin into the skin 4 h after thermal trauma was used to measure tissue injury. The results of neutropenia on the development of increased vascular permeability in the skin are shown in Figure 1. Negative controls had a permeability index of 0.049 $\pm$ 0.039. Neutrophil depletion was associated with a 58% ($P < 0.001$) attenuation of the dermal vascular permeability four hours after thermal injury (permeability index of 0.405 $\pm$ 0.038 in neutrophil depleted rats versus an index of 0.898 $\pm$ 0.039 in nontreated rats). Thus, availability of PMNs seems to be required for the full development of dermal microvascular injury four hours after thermal trauma.

Failure of Complement Depletion to Protect Against Dermal Microvascular Injury. Complement depletion was induced with CVF as described above. Extravasation of ^{125}I-bovine serum albumin into the skin four hours after ther-

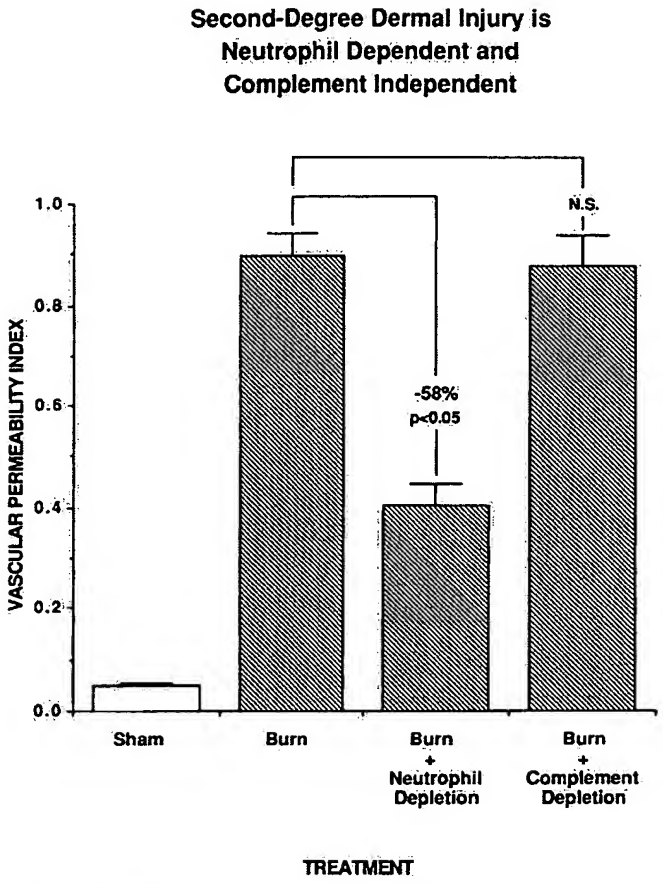

Fig. 1. Effects of complement depletion and neutrophil depletion on dermal vascular injury 4 h after thermal trauma to skin as measured by leakage of ^{125}I-labeled bovine serum albumin. For each vertical bar, $N = 4$.

mal trauma was used to assess tissue injury. The results of complement depletion on the development of increased vascular permeability in the skin are shown in Figure 1. Complement depleted rats had a permeability index of 0.88 ± 0.065 versus an index of 0.898 ± 0.039 in non-treated rats (PN.S). Thus, complement depletion was not associated with a significant reduction in dermal vascular permeability compared with positive controls.

Failure of C5a Blockade to Protect Against Dermal Microvascular Injury. In the presence of antibody to C5a, vascular permeability index was calculated. Anti-C5a-treated rats had an index of 0.89 ± 0.054, as compared with an index of

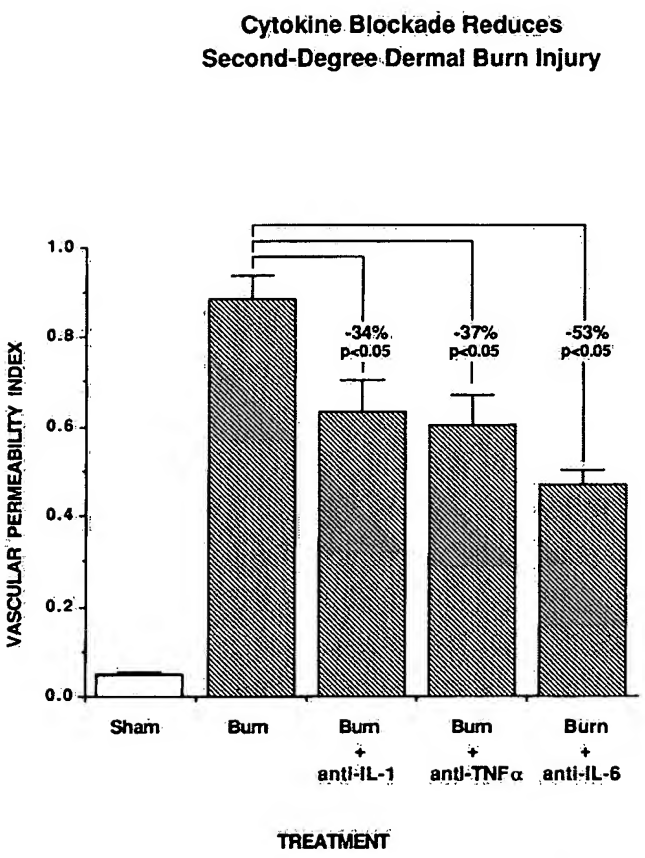

Fig. 2. Effects of cytokine blockade on dermal vascular injury 4 h after thermal trauma to skin as measured by leakage of ^{125}I-labeled bovine serum albumin. For each vertical bar, n = 5 or higher.

and 0.89 ± 0.047 in positive controls (PN.S.). C5a blockade was not associated with a significant reduction in dermal vascular permeability compared with positive controls. Thus, C5a does not seem to be required for dermal microvascular injury four h after thermal trauma, providing further evidence that development of the "late phase" burn wound is complement independent.

Protective Effects of Cytokine Blockade Against Dermal Microvascular Injury. Protection against increased vascular permeability in skin 4 h after thermal injury was evaluated through the use of blocking antibodies to cytokines. Vascular permeability index was calculated as described above. The negative control skin permeability index was 0.049 ± 0.002; this value increased to 0.885 ± 0.048 in positive controls, as shown in Figure 2. Treatment with anti-IL-6 was

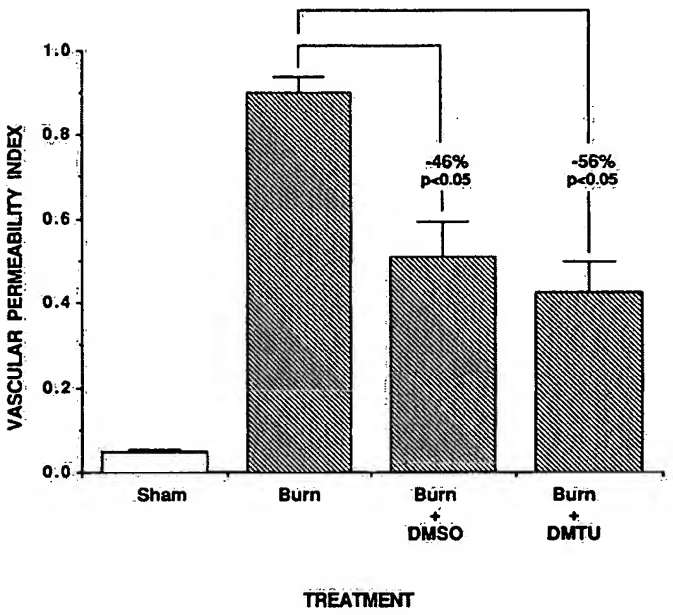

Fig. 3. Effects of hydroxyl radical scavengers on dermal vascular injury 4 h after thermal trauma to skin as measured by leakage of ^{125}I-labeled bovine serum albumin. For each vertical bar, $n = 4$.

associated with a 53% ($P < 0.001$) reduction in dermal vascular permeability to 0.47 ± 0.031. Treatment with antibody to IL-1 resulted in a decrease of dermal vascular permeability by 34% ($P < 0.001$) to a value of 0.63 ± 0.068. Similarly, animals treated with anti-TNFα had a mean dermal vascular permeability index of 0.60 ± 0.068, which was 37% ($P < 0.001$) lower than the positive control group. Thus, dermal microvascular injury at four hours after thermal trauma requires the cytokines IL-6, IL-1 and TNFα for full development.

Protective Effects of Hydroxyl Radical Scavengers in the Skin Burn Wound. The effects of hydroxyl radical scavengers on vascular permeability in skin 4 h after thermal injury was assessed by determination of vascular permeability index. The data are shown in Figure 3. Treatment with dimethyl thiourea (DMTU) was associated with a 56% ($P < 0.001$) reduction in vascular perme-

Table 1. Protection Against Neutrophil Influx into Thermally Injured Skin

Treatment	No. of animals	MPO Value (x ± SEM)	Significance (P values)	Change (%)[a]
None	4	23.81 ± 0.20	<0.001	
anti-IL-6	4	8.70 ± 0.81	<0.001	−67
anti-IL-1	4	9.34 ± 1.60	<0.001	−64
anti-TNFα	4	7.41 ± 0.11	<0.001	−73
anti-PMN	4	6.94 ± 0.33	<0.001	−75

[a]For percentage change between groups, values obtained from negative controls were subtracted from each data point.

ability as compared to the positive controls (0.426 ± 0.070 for DMTU treated rats, 0.898 ± 0.039 in non-treated rats). Treatment with dimethyl sulfoxide (DMSO) resulted in a 46% ($P < 0.001$) reduction in dermal vascular permeability (0.508 ± 0.081 with DMSO treatment, 0.898 ± 0.039 without). Thus, blockade of hydroxyl radicals results in a marked protective effect on dermal microvascular injury four hours after thermal trauma, indicating an important role for these radicals in the "late phase" local burn injury.

Role of PMN in the Dermal Burn Wound. Skin samples from injured animals treated with irrelevant antibodies or specific antibodies directed against the cytokines IL-6, IL-1 and TNFα or against rat PMNs were collected and assessed for MPO activity as a measure of tissue accumulation of neutrophils. Negative control animals showed values of MPO content of 1.31 ± 0.019, increasing to 23.8 ± 0.20 in samples from positive controls. The results of interventional studies of vascular leakage (Figure 1) were noticeably similar to PMN accumulation in these treatment groups (Table 1). Anti-IL-6 treated animals showed a MPO value of 8.7 ± 1.6 which represents a 67% ($P < 0.001$) reduction in PMN accumulation. Anti-IL-1-treated animals showed a 64% ($P < 0.001$) decrease in MPO value to 9.3 ± 3.2. Anti-TNFα-treated animals displayed an MPO value of 7.4 ± 0.23, a reduction of 73% ($P < 0.001$) as compared to positive controls. As would be expected, neutrophil depletion resulted in a 75% ($P < 0.001$) reduction in MPO value to 6.9 ± 0.66. Therefore, blockade of IL-6, IL-1 and TNFα greatly reduced tissue MPO activity, demonstrating a clear requirement for these cytokines in neutrophil accumulation during the "late phase" dermal burn injury.

DISCUSSION

Our data indicate that development of the late phase of microvascular leakage (four h post-burn) in thermally injured rat skin requires the pro-inflammatory

cytokines IL-6, IL-1 and TNFα. The ability of blocking antibodies to each of the aforementioned cytokines to attenuate both vascular injury and polymorphonuclear leukocyte (PMN) influx into the burn wound suggests that these cytokines represent upstream mediators in this inflammatory process. These cytokines may affect vascular endothelial cells (EC), which are known to actively participate in the development of inflammatory reactions by controlling fluid leakage and promoting adhesion and activation of leukocytes, or target PMN. With regard to IL-1 and TNFα, there is a large body of evidence detailing the ability of these cytokines to activate EC to synthesize and express adhesion molecules (10–14). The adhesion molecules ICAM-1 and E- and L-selectin have previously been shown to be required for full development of vascular injury in the "late phase" edema formation of thermally injured rat skin (3). In addition, IL-1 and TNFα have been shown to induce cellular production of IL-6 (15, 16).

There are several ways in which IL-6 may exert pro-inflammatory effects on increased vascular permeability and PMN influx in acute local thermal injury. There is in vitro evidence that IL-6 increases endothelial permeability by rearranging actin filaments and by changing the shape of endothelial cells (17). Biffl, et al., have demonstrated that with platelet-activating factor, IL-6 potentiates PMN priming and delays PMN apoptosis (18, 19), both effects which contribute to PMN-mediated tissue damage. Furthermore, Mullen et al. demonstrated that IL-6 is capable of interacting synergistically with TNFα to augment the effect of TNFα on PMN phagocytosis and superoxide production in vitro (20). The authors hypothesized IL-6 to be a more distal mediator of the cytokine cascade, which may modulate an inflammatory response to trauma initiated by other, more proximal cytokines. This supports our data which show IL-6 blockade to be the most effective of the cytokine interventions in reducing dermal vascular injury after thermal trauma. Lastly, expression of ICAM-1 on myocytes is induced by IL-6 in a cardiac ischemia/reperfusion injury model (21). Given the established role of ICAM-1 and E- and L-selectin in the development of "late phase" edema in thermally injured skin, it is possible that IL-6 may exert a similar effect on EC in the pathogenesis of burns, resulting in increased PMN recruitment and infiltration into injured tissues.

PMN depletion resulted in a significant decrease in both vascular leakage and PMN accumulation in skin at 4 h. This is in contrast to the 1 h burn wound for which PMN involvement was not required (7). The delay in burn wound edema formation may be explained by the time necessary for the cytokine cascade to cause expression of adhesion molecules in the injured skin and activate PMNs. The notion that increased tissue damage then results from PMN-derived reactive oxygen species is supported by our data showing the ability of hydroxyl radical scavengers in these experiments to reduce vascular injury. The fact that PMN depletion, or any of the other interventions, was only able to result in a maximum reduction of approximately 60% in vascular leakage is most likely

due to the possibility that a large percentage of injury and cell death (approximately 40%) is directly heat-related. A similar phenomenon was observed in the assay of skin MPO content.

It is known that the burn model utilized in these experiments produces systemic complement activation that initiates a series of events leading to the "early phase" edema formation in the burned skin. Interestingly, neither complement depletion nor C5a blockade was able to attenuate local vascular permeability at four hours. In this case, the effects of cytokines and PMNs may be able to produce maximal injury even in the absence of complement. Another possibility is that the role of complement is fulfilled in the early phase, whereas the late phase is more dependent on the ensuing inflammatory reaction. Despite the fact that our data does not support a role for complement in the "late phase" burn wound, a complete lack of involvement of complement components cannot be stated. Recently, studies have revealed local complement production in numerous and varied tissues in an ischemia/reperfusion injury in rabbit (22). Complement proteins may be present in thermally injured tissue and contributing to the development of the 4 h injury, but were not effectively blocked by our antibody to C5a or were able to be produced in significant amounts in skin, though serum complement levels were undetectable following treatment with CVF. Administered in one dose immediately prior to induction or thermal trauma, 400 μg of anti-C5a was able to slightly, though not significantly, reduce vascular leakage at four hours (data not shown).

We therefore conclude that the development of the "late phase" dermal vascular injury following thermal trauma to the skin is largely mediated by the pro-inflammatory actions of cytokines, in particular IL-6. IL-6 may modulate the effects of TNFα and IL-1, resulting in EC expression of E- and L-selectin and ICAM-1. IL-6 also may act directly on EC to alter cell structure and/or promote upregulation of adhesion molecules. PMN-generated reactive oxygen species appear to be responsible for the local tissue damage. Complement does not appear to play a significant role, if any, in the pathogenesis of the "late phase" second-degree burn wound.

REFERENCES

1. MANN, R. and D. HEIMBACH. 1996. Prognosis and treatment of burns. *West. J. Med.* **165**:215–220.
2. TILL, G. O., C. BEAUCHAMP, D. MENPACE, W. TOURTELLOTTE Jr., R. KUNKEL, K. J. JOHNSON, and P. A. WARD. 1983. Oxygen radical dependent lung damage following thermal injury of rat skin. *J. Trauma.* **23**:269–273.
3. MULLIGAN, M. S., G. O. TILL, C. W. SMITH, D. C. ANDERSON, M. MIYASAKA, T. TAMATANI, R. F. TODD, III, T. B. ISSEKUTZ, and P. A. WARD. 1994. Role of leukocyte adhesion molecules in lung and dermal vascular injury after thermal trauma of skin. *Am. J. Pathol.* **144**:1008–1015.

4. DEMLING, R. H. 1985. Burns. *N. Engl. J. Med.* **313:** 1389–1398.
5. FREIDL, H. P., G. O. TILL, O. TRENTZ, and P. A. WARD. 1989. Roles of histamine, complement and xanthine oxidase in thermal injury of skin. *Am. J. Pathol.* **135:**203–217.
6. TILL, G. O., L. S. GUILDS, M. MAHROUGUI, H. P. FREIDL, O. TRENTZ, and P. A. WARD. 1989. Role of xanthine oxidase in thermal injury of skin. *Am. J. Pathol.* **135:**195–202.
7. TILL, G. O., J. R. HATHERILL, W. W. TOURTELLOTTE, M. J. LUTZ, and P. A. WARD. 1985. Lipid peroxidation and acute lung injury after thermal trauma to skin: Evidence of a role for hydroxyl radical. *Am. J. Pathol.* **135:**195–202.
8. BALLOW, M. and C. G. COCHRANE. 1969. Two anti-complementary factors in cobra venom. Hemolysis of guinea pig erythrocytes by one of them. *J. Immunol.* **103:**944–952.
9. MULLIGAN, M. S., E. SCHMID, B. BECK-SCHIMMER, G. O. TILL, H. P. FRIEDL, R. B. BRAUER, T. E. HUGLI, M. MIYASAKA, R. L. WARNER, K. J. JOHNSON, and P. A. WARD. 1996. Requirement and role of C5a in Acute Lung Inflammatory Injury in Rats. *J. Clin. Invest.* **98:**503–512.
10. PROBER, J. S. and R. S. COTRAN. 1990. The role of endothelial cells in inflammation. *Transplantation.* **50:**537–544.
11. BEVILACQUA, M. P., J. S. PROBER, D. L. MENDRICK, R. S. COTRAN, and M. A. GIMBRONE, JR. 1987. Identification of an inducible endothelial-leukocyte adhesion molecule. *Proc. Natl. Acad. Sci. U.S.A.* **84:**9238–9242.
12. BEVILACQUA, M. P., S. STENGELIN, M. A. GIMBRONE, and B. SEED. 1989. Endothelial leukocyte adhesion molecule 1: An inducible receptor for neutrophils related to complement regulatory proteins and lectins. *Science 243:*1160–1165.
13. OSBORN, L., C. HESSION, R. TIZARD, C. VASSALLO, S. LUHOWSKYJ, G. CHI-ROSSO, and R. LOBB. 1989. Direct expression cloning of vascular cell adhesion molecule 1, a cytokine-induced endothelial protein that binds to lymphocytes. *Cell* **60:**577–584.
14. DUSTIN, M. A. and T. A. SPRINGER. 1988. Lymphocyte function-associated antigen-1 (LFA-1) interaction with intercellular adhesion molecule-1 (ICAM-1) is one of at least three mechanisms for lymphocyte adhesion to cultures endothelial cells. *J. Cell Biol.* **107:**321–331.
15. CONTENT, J., L. DE WIT, P. POUPART, G. OPDENAKKER, J. VAN DAMME, and A. BILLIAU. 1985. Induction of a 26-kDa-protein mRNA in human cells treated with and interleukin-1-related, leukocyte-derived factor. *Eur. J. Biochem.* **152:**253–257.
16. KASID, A., E. P. DIRECTOR, and S. A. ROSENBERG. 1989. Regulation of interleukin-6 (IL-6) by IL-2 and TNF-α in human peripheral blood mononuclear cells. *Ann. N.Y. Acad. Sci.* **557:**564–566.
17. MARUO, N., I. MORITA, M. SHIRAO, and S. MUROTA. 1992. IL-6 increases endothelial permeability in vitro. *Endocrinology* **131:**710–714.
18. BIFFL, W. L., E. E. MOORE, F. A. MOORE, V. S. CARL, F. J. KIM, and R. J. FRANCIOSE. 1994. Interleukin-6 potentiates neutrophil priming with platelet-activating factor. *Arch. Surg.* **129:**1131–1136.
19. BIFFL, W. L., E. E. MOORE, F. A. MOORE, and C. C. BARNETT. 1996. Interleukin-6 delays neutrophil apoptosis via a mechanism involving platelet-activating factor. *J. Trauma* **40:**575–579.
20. MULLEN, P. G., A. C. J. WINDSOR, C. J. WALSH, A. A. FOWLER, III, and H. J. SUGARMAN. 1995. Tumor necrosis factor-α and IL-6 selectively regulate neutrophil function in vitro. *J. Surg. Res.* **58:**124–130.
21. YOUKER, K., C. W. SMITH, D. C. ANDERSON, D. MILLER, L. H. MICHAEL, R. D. ROSSEN, and M. L. ENTMAN. 1992. Neutrophil adherence to isolated adult cardiac myocytes: Induction by cardiac lymph collected during ischemia and reperfusion. *J. Clin. Invest.* **89:**602–609.
22. YASOJIMA, K., K. S. KILGORE, R. A. WASHINGTON, B. R. LUCCHESI, and P. L. MCGEER. 1998. Complement gene expression by rabbit heart: Upregulation by ischemia and reperfusion. *Circ. Res.* **82:**1224–1230.

PATHOLOGY ONCOLOGY RESEARCH Vol 6, No 2, 2000

10.1053.paor.2000.0262 available online at http://www.idealibrary.com on IDEAL

ARTICLE

Apoptosis-related Proteins, BCL-2, BAX, FAS, FAS-L and PCNA in Liver Biopsies of Patients with Chronic Hepatitis B Virus Infection

Ji í EHRMANN Jr,[1] Dana GALUSZKOVÁ,[2] Ji í EHRMANN,[2] Ivo KR ,[2] V ra JEZDINSKÁ,[1] Bo ivoj VOJT EK,[3] Paul G MURRAY,[4] Zden k KOLÁ [1]

[1]Institute of Pathology & Centre of Molecular Biology and Medicine, Laboratory of Molecular Pathology, Faculty of Medicine, [2]Second Department of Internal Medicine, Faculty of Medicine, Palack University, Olomouc, Czech Republik, [3]Masaryk Memorial Hospital, Brno, Czech Republik, [4]Division of Biomedical Sciences, School of Health Sciences, University of Wolverhampton, Wolverhampton, United Kingdom

While the elimination of hepatitis B virus (HBV) is a common phenomenon at the end of the acute phase of disease, the persistence of HBV is characteristic for chronic hepatitis (CHB). Recent evidence indicates that the elimination of HBV is achieved by FAS/FAS-L induced apoptosis of infected hepatocytes. The aim of this study was to test the hypothesis that HBV persistence in the hepatocytes of CHB patients is due to the delayed onset of apoptosis caused by altered FAS/FAS-L interactions between lymphocytes and hepatocytes. The expression of FAS, FAS-L, BAX, BCL-2, ICE and PCNA in the liver biopsies of 55 patients (14 HBsAg positive, 20 patients with alcoholic hepatopathy, 21 patients with other hepatopathies) was tested by immunohistochemistry. Apoptosis of hepatocytes was evaluated by morphological as well as by TUNEL method. The results were correlated with a grading/staging score and analysed statistically using a one way analysis of variance and the Duncan test. Significantly higher numbers of BAX positive hepatocytes were observed in HBsAg positive patients when compared to control groups. Similarly, both BAX and FAS positive lymphocytes were more frequent in HBsAg positive patients. FAS-L positive lymphocytes and hepatocytes were numerous in all patient groups. Increased numbers of BAX positive hepatocytes in CHB may reflect the increased readiness of these cells to undergo apoptosis. However, the increased numbers of both BAX and FAS positive lymphocytes in CHB suggest that these cells may be particularly sensitive to FAS-L mediated apoptosis potentially resulting in lowered viability of these lymphocytes. This may explain, at least in part, the defective removal of virus-infected cells in chronic hepatitis. However, we cannot rule out the possibility that survival of hepatocytes during CHB may be due to other mechanisms such as defects in apoptosis activation triggered by CD40, defects involving DNase and/or other caspases downstream in the apoptotic cascade within these cells, or to defects in CTL function. (Pathology Oncology Research Vol 6, No 2, 130–135, 2000)

Keywords: apoptosis, hepatitis B virus, FAS, FAS-L

Introduction

It is generally accepted that the hepatitis B virus (HBV) does not directly cause the pathological effects of acute and chronic necrotizing inflammatory liver disease. This conclusion is supported by the fact that HBV infection in approximately 90–95% of cases results in transient liver disease followed by viral clearance.[18,51] It is evident that an immune response mediated by cytotoxic T lymphocytes (CTLs), either by the elaboration of various cytokines, or by direct interaction of these cells with HBsAg-positive hepatocytes, is primarily responsible for the associated liver disease.[3,11,16,17,19,25,31,35,38,41,43,44] There are two separate mechanisms by which CTLs induce apoptosis in target cells. The first of these involves the perforin-granzyme pathway leading to secretion of the lytic protein, perforin, and of various serine proteases (granzymes), each of which

Received: Febr 28, 2000; *accepted:* April 20, 2000

Correspondence: Ji í EHRMANN jr., M.D.; Institute of Pathology & Laboratory of Molecular Pathology CMBM; Faculty of Medicine, Palack University; Hn votínská 3; Olomouc, CZ, 775 15; Tel: 00420/68/5632455; Fax: 00420/68/5632966; E-mail: erman@tunw.upol.cz

 1219-4956/00/020130+06 $ 12.00/0

is stored in specific CTL granules and the consecutive release of which induces DNA fragmentation.[5,28,45] The second mechanism involves interaction between the FAS ligand and it's cell surface receptor, FAS. Both FAS and FAS ligand are members of the TNF receptor and ligand superfamily[6,34] and their interaction leads to the initiation of apoptosis by the activation of various caspases.[10,30,37] It has been suggested that the interaction between FAS ligand, expressed on activated CTLs, and FAS protein located on HBV-infected hepatocytes, plays an essential role in the development of acute and fulminant hepatitis[24,42] or cirrhosis.[13] However, other proteins may mediate the control of apoptosis. Among these the Bcl-2 gene family are one of the most important. Members of this family are either inducers (BAX, BAD, BAK, BID, BIK, BCL-X_S) or inhibitors (BCL-2, BCL-X_L) of apoptosis.[14,26,39] It has recently been shown that BCL-2 expression by mouse hepatocytes protects them from FAS-mediated apoptosis, suggesting the potential for alternative approaches to the prevention of hepatic failure due to viral hepatitis in man.[27]

Chronic hepatitis associated with viral persistence and potentially serious complications such as cirrhosis and hepatocellular carcinoma develops in 5–10% of patients infected with HBV. A number of viruses, including HBV, have developed strategies that enable them to persist inside host cells and escape immune control. Clonal deletion of virus-specific T cells, mutation of viral gene regions encoding epitopes critical for T cell recognition, inhibition of intracellular antigen processing and induction of T cell anergy,[36] are among the most important. Another mechanism, the maintenance of an immunoprivileged state within infected hepatocytes might be relevant to the long-term survival of HBV. FAS/FAS ligand interactions could play an important role in this process by the induction of apoptosis and the elimination of FAS-bearing CTLs,[15,47] as has been demonstrated in the prevention of graft rejection,[4,49] in testicular and melanoma cells[20,50] and in hepatocellular carcinoma cells.[46]

The role of FAS in chronic hepatitis has been studied by Mochizuki et al,[32] who showed that FAS expression by hepatocytes closely correlated with the activity of viral hepatitis in patients infected with HBV. However, with exception of the study of Luo et al[29] who detected FAS-L protein in hepatocytes and infiltrating lymphocytes in the HBV-related chronic liver disease, there are no data on the expression of the FAS ligand during chronic HBV infection. We can speculate that an increase in the FAS ligand expression by HBV-infected hepatocytes could contribute to the development of an immunoprivileged state by the induction of apoptosis in FAS bearing CTLs. To support this hypothesis and to enhance understanding of the FAS/FAS ligand role in HBV infected hepatocytes we analyzed by immunohistochemistry the expression of BCL-2 and BAX proteins in chronic HBV infection in relation to FAS/FAS-L expression. We also assessed proliferative activity by analysis of PCNA expression and the frequency of apoptosis. Furthermore, we compared the results with expression of the same proteins in patients with alcoholic and other hepatopathies.

Materials and Methods

Formalin fixed, paraffin-embedded liver biopsies from 14 HBsAg seropositive patients, 20 patients with alcoholic hepatopathy and 21 patients with other hepatopathies were used for the immunohistochemical detection of FAS, FAS-L, BCL-2, BAX, ICE and PCNA. Histopathological grading and staging were performed according to Ishak et al.[23] The presence of HBsAg in hepatocytes was also detected by histochemical means (Orcein stain). At the time of biopsy all patients were tested for serum levels of alanine aminotransferase (ALT), aspartate aminotransferase (AST), gamma-glutamyltransferase (GMT), alkaline phosphatase (ALP) and for prothrombin time (Quick), albumin (ALB) and total serum protein (TSP).

A standard immunoperoxidase technique using biotinylated secondary anti-mouse or anti-rabbit antibodies, followed by streptavidin peroxidase[9] was used for the immunohistochemical detection of PCNA, BCL-2, BAX, ICE, FAS and FAS-L proteins (see *Table 1*). The primary antibody was omitted from negative controls. As positive controls we used anaplastic astrocytoma stained with anti-PCNA, follicular lymphoma stained with anti-BAX and anti-BCL-2, bile ducts stained with anti-FAS and activated CTLs in hepatitis stained with anti FAS-L. The grade of immunopositivity in each case was scored semi-quantitatively at a magnification of 400x in the following range: 0=10% of cells positive; I=11–29% cells positive; II=30–59% cells positive; III=60% or more cells positive. The immunopositivity score was verified by measurement of the percentage of positive cells within specimens using the computerised image analysis system LUCIA M (Laboratory Imaging, Prague). A case was classified as positive if the percentage of positive cells was greater than 11% (grade score I–III). The expression of proteins was assessed in both hepatocytes and lymphocytes. Determination of apoptosis was achieved by the use of TUNEL kit for *in situ death*

Table 1 **Primary antibodies**

Antigen (clone)	*Dilution*	*Antigen retrieval*	*Source*
PCNA (PC10)	prediluted	yes (3 x 5 min.)	MOÚ Brno
BCL-2 (124)	1 : 20	yes (2 x 5 min.)	Dako
BAX (N-20)	1 : 40	No	Santa Cruz
FAS (N-18)	1 : 50	No	Santa Cruz
FAS-L (N-20)	1 : 50	No	Santa Cruz
ICE p10 (C-20)	1 : 50	yes (1 x 5 min.)	Santa Cruz

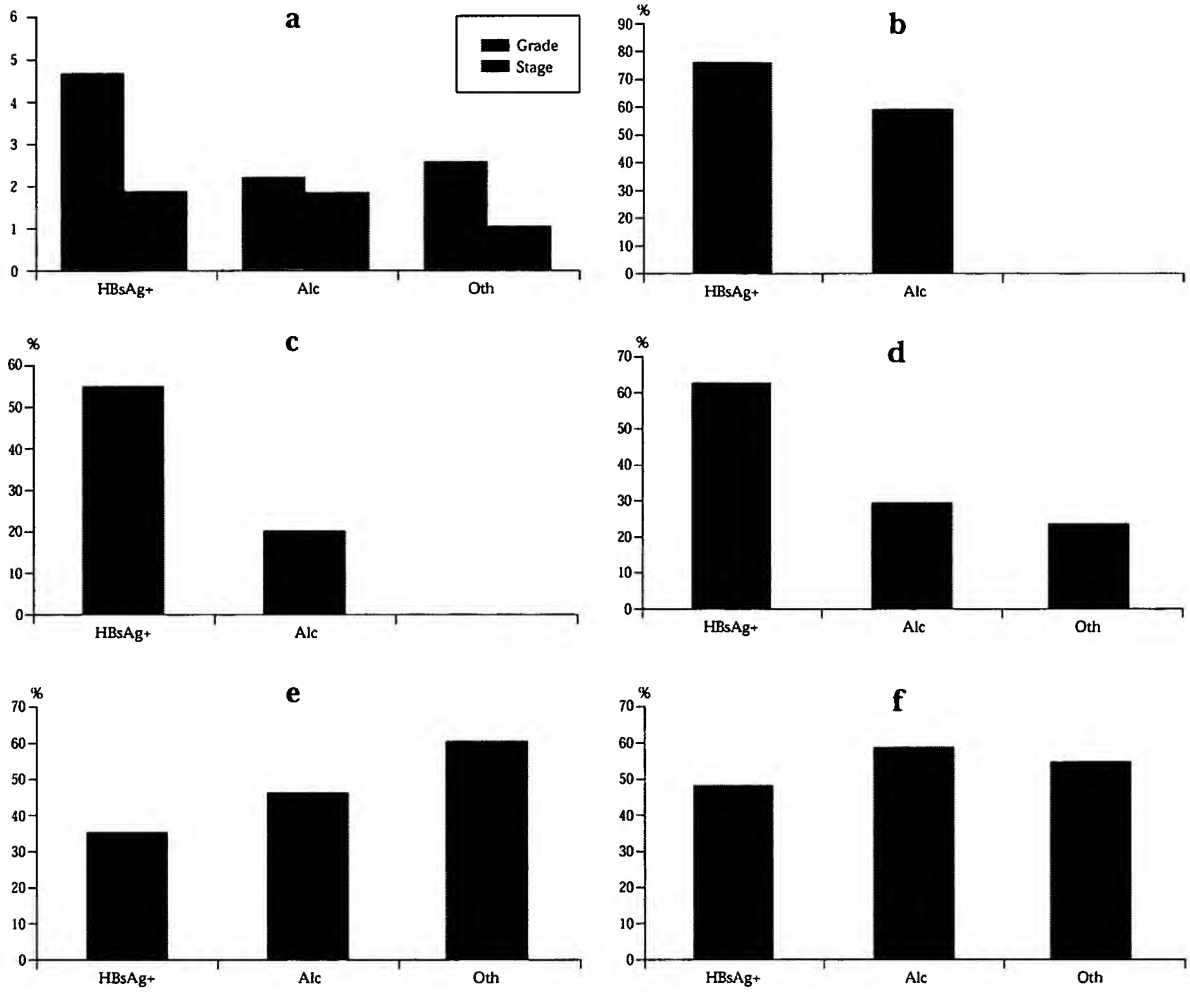

Figure 1. Statistically significant differences observed between patient groups; a) Grade/stage of disease (according to Ishak); b) percentage of BAX positive hepatocytes and; c) infiltrating lymphocytes within patient groups d) percentage of FAS positive infiltrating lymphocytes. e) Percentage of FAS-L positive hepatocytes and f) lymphocytes. Abbreviations; Alc = alcoholic hepatopathy; Oth = Other hepatopathies.

detection (Roche, cat. No. 1 684 809). The tissue samples were firstly digested by proteinase K for elimination of the DNA masking nucleoproteins. By the use of TdT (terminal deoxunucleotidyl transferase) the biotinylated deoxyuridin was incorporated into the DNA break points and then visualized using the avidin-peroxidase system. The cells were estimated at a magnification of 400x with an eyepiece microsquare micrometer (Olympus Optical). Tunel index (TI) was estimated as a percentage of TUNEL positive cells. The results of HBsAg-positive patients, those with alcoholic hepatopathy and patients with other hepatopathies were compared with the biochemical data and with the grade and stage. Statistical analysis was performed using a one way analysis of variance, by multifactorial range analysis (Duncan test) and by the Chi-square test.

Results

HBsAg-positive patients were characterised by a significantly higher grade score than the other groups (average score 4.79 in the HBsAg-positive group, versus 2.35 in patients with alcoholic hepatopathy, and 2.43 in those with non-specific hepatopathies, p=0.02) (*Figure 1a*). BCL-2 expression in hepatocytes as well as in adjacent lymphocytes of all groups was generally low (47 negative cases, 87%), whereas the levels of PCNA expression in hepatocytes was comparatively high (33 positive cases, 60%) (*Figure 2*). The expression of ICE was absent both in hepatocytes and lymphocytes in virtually all cases.

We found significantly higher numbers of BAX positive hepatocytes (11/14 cases, 78% versus 12/20 cases, 60%)

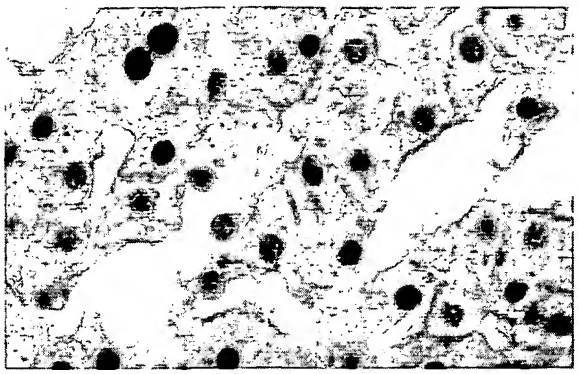

Figure 2. PCNA expression in hepatocytes from a HBsAg positive patient.

and lymphocytes (8/14 cases, 57% versus 4/16 cases, 25%) from the HBsAg-positive group ($p<0.01$) compared to patients with alcoholic hepatopathy. There were also significantly higher numbers of FAS positive lymphocytes in the HBsAg-positive group (9/14 cases, 64%, $p<0.05$) (*Figure 1b-d, Figure 3*). FAS-L positive hepatocytes and lymphocytes were relatively frequent in all patient groups (31/55 cases- 56%) and no significant difference in these numbers was observed (*Figures 1e-f*).

We also analysed the relationship between expression of the various apoptosis regulating genes in all patients. In hepatocytes the number of BAX and PCNA positive cells was positively correlated (coeff. 0,31, $p=0.02$), as were the number of BAX and FAS positive cells (coeff. 0,54, $p<0.001$), and the number of PCNA and FAS-L positive cells (coeff. 0,49, $p<0.001$). However, there was an inverse relationship between the number of BAX and BCL-2 positive cells (coeff. 0,39, $p<0.001$).

The TUNEL index (TI) of hepatocytes was higher in the HbsAg-positive group (20,7 %) compared to group with non-specific hepatopathies (12,8 %) and to group with alcoholic hepatopathy (4,4 %), however, these results were statistically non significant.

The cohort of patients was also divided into two groups according to Ishak`s grade (grade score >4; grade score <4) and stage (stage >3, stage <3). Liver biochemistry correlated well with grade and stage (increased ALT in 14/18 cases of high grade, 77% versus 19/37cases of low grade, 45%; increased AST in 14/18 of high grade cases, 77% versus 14/37 cases of low grade, 37%) (*Figure 4*), however we did not find any correlation between grade or stage and expression of apoptosis regulating genes (data not shown).

Discussion

Recent work suggests that, in patients with chronic hepatitis B (CHB), treatment by interferon can stimulate a specific CTL response that leads to viral clearance and resolution of disease.[40] There is growing evidence to implicate FAS/FAS-L interactions as important mediators of apoptosis in a variety of situations including graft rejection, tumors, autoimmune diseases and inflammation.[4,7,12,20,34,46,47,49,50] The Fas ligand is expressed on activated CTLs and induces apoptosis in FAS bearing cells.[48] This mechanism is believed to operate in hepatitis B virus infection where it is responsible for the associated liver disease and is supported by studies on HbsAg transgenic mice where FAS dependent apoptosis by CTLs induces acute liver disease.[35,43] Therefore, defects in FAS/FAS-L proteins might be relevant to the persistence of HBV in hepatocytes during CHB. In addition, FAS-ligand bearing hepatocytes in CHB may also induce apoptosis in CTLs expressing FAS. Such a mechanism may contribute to CTL escape of Hepatitis B virus infected hepatocytes.

At the present time an adequate in vitro model for the study of the possible involvement of the FAS ligand in the development of chronic hepatitis B does not exist. There-

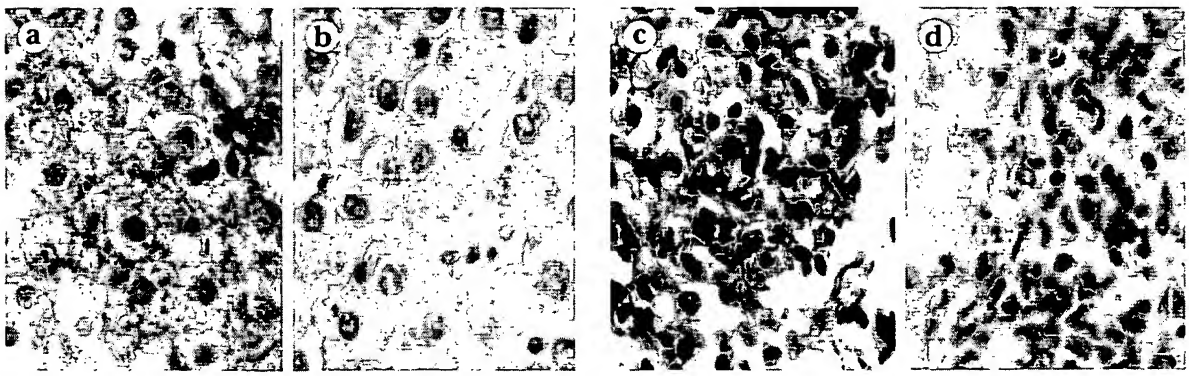

Figure 3. a) BAX expression in hepatocytes from HBsAg positive patient and, b) negative BAX immunostaining in hepatocytes from a patient with alcoholic hepatopathy, c) FAS expression in lymphocytes from HBsAg positive patient and, d) negative FAS immunostaining in lymphocytes from a patient with alcoholic hepatopathy.

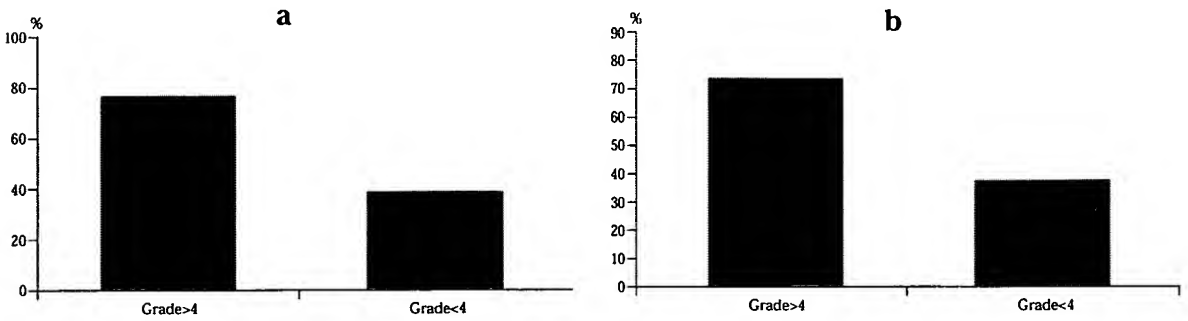

Figure 4. Percentage of HBsAg patients with increased, a) ALT, b) and AST, in relation to grade.

fore, based on our extensive experience, we believe that immunohistochemistry is the best choice of method by which we can support of our hypothesis. We have shown increased numbers of BAX positive hepatocytes in HbsAg-positive patients compared to the control groups suggesting that these cells may be susceptible to apoptosis. This is also supported by finding of higher TUNEL index of hepatocytes in HBsAg-positive patients. However, we have also shown that infiltrating lymphocytes from HBsAg positive cases more frequently express BAX and FAS. Taken together with the finding that the FAS-ligand is also expressed by hepatocytes, these results support the contention that apoptosis of CTLs induced by FAS-L bearing hepatocytes could be important in the persistence of infected hepatocytes. A similar mechanism of FAS bearing cells destruction which facilitate local tumor invasion was recently described in vitro by Yoong et al.[52] However, we did not find significant differences in the numbers of FAS-ligand expressing hepatocytes between patient groups. We might suggest that induction of FAS-ligand expression on hepatocytes could be a reaction not only to HBV infection but also to various non-specific agents.[21,33]

The infrequent expression of the anti-apoptotic protein, BCL-2, by hepatocytes and lymphocytes in the majority of cases, is further support that these cells may be susceptible to apoptosis. On the other hand, with the exception of the BAX protein, we did not test other members of BCL-2 family to validate this finding. Moreover apoptosis can be mediated in a BCL-2 independent fashion.[1] In addition, the high level of expression of PCNA in damaged liver cells suggests the beginning of liver regeneration. It must, however, be mentioned that the assessment of proliferative activity by Ki-67 analysis is more accurate, however estimation of proliferation by analysis of PCNA expression can also give valid results.[8] The absence of ICE expression in our series might suggest that this protein is not important in the apoptotic pathway of hepatocytes.

In summary, we have provided evidence to suggest that FAS/FAS-L interactions are important not only in the generation of liver cell damage in CHB but also potentially in the induction of apoptosis in CTLs leading to persistence of virus-infected hepatocytes. However, we cannot exclude the possibility that the survival of HBV-infected hepatocytes in CHB is due to other mechanisms like viral inhibition of apoptosis triggered by CD40/Fas interactions[2] or defects of downstream factors involved in the apoptotic cascade, such as DNAase enzymes and/or other caspases.

Acknowledgements

This work was supported by the GACR No. 301/96/KO47, and by the Grant of MSTM No. VS 96154 and No. J14/98 151100001.

References

1. *Adams JM, Cory S:* The Bcl -2 protein family: arbiters of cell survival. Science 281:1322-26, 1998.
2. *Afford SC, Randhawa S, Eliopoulos AG, et al:* CD40 activation induces apoptosis in cultured human hepatocytes via induction of cell surface fas ligand expression and amplifies fas-mediated hepatocyte death during allograft rejection. J Exp Med 189:441-6, 1999.
3. *Ando K, Guidotti LG, Wirth S, et al:* Class I-restricted cytotoxic T lymphocytes are directly cytopathic for their target cells in vivo. J Immunol. 152:3245-3253, 1994.
4. *Bellgrau D, Gold D, Selawry H, et al.* A role for CD95 ligand in preventing graft rejection. Nature 377: 630-632, 1995
5. *Berke G:* The CTL's kiss of death Cell 81:9-12, 1995.
6. *Beutler B, van Huffel C:* Unraveling function in the TNF ligand and receptor families. Science 264:667-668, 1994.
7. *Dayan CM:* FasL expression on epithelial cells: the Botazzo-Feldmann hypothesis revisited. Immunology Today 18:203, 1997.
8. *Dervan PA, Magee HM, Buckley C, et al:* Proliferating cell nuclear antigen counts in formalin-fixed paraffin-embedded tissue correlate with Ki-67 in fresh tissue. Am J Clin Pathol 97 (Suppl. 1): S21-S28, 1992.
9. *Ehrmann J jr, Jezdinská V, Ehrmann J, et al:* Immunohistochemical study of the expression of BCL-2, PCNA and p53 proteins in the patients with hepatitis B. The pilot study. Acta Univ Palacki Olomuc, Fac Med 10:83-85, 1996.
10. *Enari M, Hug H, Nagata S:* Involvement of an ICE-like protease in FAS-mediated apoptosis. Nature 375:78-81, 1995.
11. *Ferrari C, Penna A, Bertoletti A, et al.* Hepatitis B virus-specific immune response: from antigen recognition to liver damage. Forum 6:203-216, 1996.

12.[1]*French LE, Tschopp J:* Thyroiditis and hepatitis: FAS on the road to disease. Nature Medicine 3:387-388, 1997.
13.[1]*Galle PR, Hofmann WJ, Walczak H, et al:* Involvement of the CD 95 (APO-1/Fas) receptor and ligand in liver damage. J Exp Med 182:1223-30, 1995.
14.[1]*Golstein P:* Controlling cell death. Science 275:1081-1082, 1997.
15.[1]*Griffith TS, Brunner T, Fletcher SM, et al:* Fas ligand-induced apoptosis as a mechamism of immune privilege. Science 270:1189-1192, 1995.
16.[1]*Guidotti LG, Borrow P, Hobbs MV et al:* Viral cross talk: intracellular inactivation of the hepatitis B virus during an unrelated viral infection of the liver. Immunology 93:4589-4594, 1996.
17.[1]*Guidotti LG, Chisari FV:* The transgenic mouse model of hepatitis B virus infection. Forum 6:189-200, 1996.
18.[1]*Guidotti LG, Ishikawa T, Hobbs MV et al:* Intracellular inactivation of the hepatitis B virus by cytotoxic T lymphocytes. Immunity 4:25-26, 1996.
19.[1]*Guilhot S, Miller T, Cornman G, et al:* Apoptosis induced by tumor necrosis factor in rat hepatocyte cell lines expressing hepatitis B virus. Am J Pathol 148:801-814, 1996.
20.[1]*Hahne M, Rimoldi D, Schröter M, et al:* Melanoma cell expression of FAS (Apo-1/CD95) ligand : implications for tumor immune escape. Science 274:1363-1366, 1996.
21.[1]*Hiramatsu N, Hayashi A, Katayama K, et al:* Immunohistochemical detection of Fas antigen in liver tissue of patients with chronic hepatitis C. Hepatology 19:1354-1359, 1994.
22.[1]*Chisari F:* Hepatitis B virus transgenic mice: insights into the virus and disease. Hepatology 22:1316-1325, 1995.
23.[1]*Ishak K, Baptista A, Bianchi L, et al:* Histological grading and staging of chronic hepatitis. J Hepatol 22:696-699, 1995.
24.[1]*Kondo T, Suda T, Fukuyama H, et al:* Essential roles of the FAS ligand in the development of hepatitis. Nature Medicine 3:409-413, 1997.
25.[1]*Koziel MJ:* Immunology of viral hepatitis. Am J Med 100:98-109, 1996.
26.[1]*Kroemer G:* The proto-oncogene Bcl-2 and its role in regulating apoptosis. Nature Medicine 3:614-620, 1997.
27.[1]*Lacronique V Mignon A, Fabre A, et al:* Bcl-2 protects from lethal hepatic apoptosis induced by an anti-Fas antibody in mice. Nature Medicine 2:80-86, 1996.
28.[1]*Liu CC, Walsh CM, Young JDE:* Perforin: structure and function. Immunol Today 16:194-201, 1995.
29.[1]*Luo KX, Zhu YF, Zhang LX, et al:* In situ investigation of Fas/FasL expression in chronic hepatitis B infection and related liver diseases. J Viral Hepat 4:303-7, 1997.
30.[1]*Los M, Van de Craen M, Penning LC, et al:* Requirement of an ICE/CED-3 protease for FAS/APO-1-mediated apoptosis. Nature 375:81-83, 1995.
31.[1]*Marinos G, Torre F, Chokshi S, et al:* Induction of T-helper cell response to hepatitis B core antigen in chronic hepatitis B: a major factor in activation of the host immune response to the hepatitis B virus. Hepatology 22:1040-1049, 1995.
32.[1]*Mochizuki K, Hayashi N, Hiramatsu N, et al:* Fas antigen expression in liver tissues of patients with chronic hepatitis B. J Hepatology 24:1-7, 1996.
33.[1]*Muschen M, Warskulat U, Douillard P, et al:* Regulation of CD95 (APO-1/Fas) receptor and ligand expression by lipopolysaccharide and dexamethasone in parenchymal and non-parenchymal rat liver cells. Hepatology 27:200-208, 1998.
34.[1]*Nagata S, Golstein P:* The FAS death factor. Science 267:1449-1456, 1995.
35.[1]*Nakamoto Y, Guidotti LG, Pasquetto V, et al:* Differential target cell sensitivity to CTL-activated death pathways in hepatitis B virus transgenic mice. J Immunol 158:5692-7, 1997.
36.[1]*Paroli M, Nisini R, Accapezzato D, et al:* Viral escape from the immune system's control. Forum 6:122-127, 1996.
37.[1]*Patel T, Gores GJ, Kaufmann SH:* The role of proteases during apoptosis. FASEB J 10:587-597, 1996.
38.[1]*Peters M:* Actions of cytokines on the immune response and viral interactions: an overview. Hepatology 23:909-916, 1996.
39.[1]*Reed JC:* Double identity for proteins of the Bcl-2 family. Nature 387:773-776, 1997.
40.[1]*Rehermann B, Lau D, Hoofnagle JH, et al:* Cytotoxic T lymphocyte responsiveness after resolution of chronic hepatitis B virus infection. J Clin Invest 7:1655-1665, 1996.
41.[1]*Romero R, Lavine JE:* Cytokine inhibition of the hepatitis B virus core promoter. Hepatology 23:17-23, 1996.
42.[1]*Ryo K, Kamogawa Y, Ikeda I, et al:* FAS and FAS ligand strongly expressed in liver of fulminant hepatitis patients. Hepatology 22: AASLD Abstracts: 230 A, 1995.
43.[1]*Shibata S, Kyuwa S, Lee S, Toyota Y, et al:* Apoptosis induced in mouse hepatitis virus infected cells by a virus specific CD8+ cytotoxic lymphocyte clone. J Virol 68:7540-7545, 1994.
44.[1]*Schaff Z, Lotz G, Schulte-Herman R:* Pathomorphological characteristic and pathogenesis of viral hepatitis. Pathology Oncology Research 2:132-143, 1996.
45.[1]*Smyth MJ, Trapani JA:* Granzymes: exogenous proteinases that induce target cell apoptosis. Immunology Today 16:202-206, 1995.
46.[1]*Strand S, Hofmann WJ, Hug H, et al:* Lymphocyte apoptosis induced by CD95 (Apo-1/Fas) ligand-expressing tumor cells – a mechanism of immune evasion? Nature Medicine 2:1361-1366, 1996.
47.[1]*Streilein JW:* Unraveling immune privilege. Science 270:1158-1159, 1995.
48.[1]*Tang DG, Porter AT:* Apoptosis: a current molecular analysis. Pathology Oncology Research 2:117-131, 1996.
49.[1]*Vaux DL:* Ways around rejection. Nature 377:576-577, 1995.
50.[1]*Williams N:* Tumor cells fight back to beat immune system. Science 274:1362-1363, 1996.
51.[1]*Yoffe B, Noonan CA:* Hepatitis B virus – new and evolving issues. Dig Dis Sciences 37:1-9, 1992.
52.[1]*Yoong KF, Afford SC, Randhawa S, et al:* DH: Fas/Fas ligand interaction in human colorectal hepatic metastases: A mechanism of hepatocyte destruction to facilitate local tumor invasion. Am J Pathol 154:693-703, 1999.

Am J Physiol Heart Circ Physiol 283: H1634–H1644, 2002.
First published June 20, 2002; 10.1152/ajpheart.01073.2001.

Pyruvate improves redox status and decreases indicators of hepatic apoptosis during hemorrhagic shock in swine

PAUL D. MONGAN, JOHN CAPACCHIONE, SHANDA WEST, JOHN KARAIAN, DAWN DUBOIS, RYAN KENEALLY, AND PUSHPA SHARMA
Department of Anesthesiology, Uniformed Services University of the Health Sciences, Bethesda, Maryland 20814

Received 19 December 2001; accepted in final form 5 June 2002

Mongan, Paul D., John Capacchione, Shanda West, John Karaian, Dawn Dubois, Ryan Keneally, and Pushpa Sharma. Pyruvate improves redox status and decreases indicators of hepatic apoptosis during hemorrhagic shock in swine. *Am J Physiol Heart Circ Physiol* 283: H1634–H1644, 2002. First published June 20, 2002; 10.1152/ajpheart.01073.2001.—Previous studies have shown that the liver is the first organ to display signs of injury during hemorrhagic shock. We examined the mechanism by which pyruvate can prevent liver damage during hemorrhagic shock in swine anesthetized with halothane. Thirty minutes after the induction of a 240-min controlled arterial hemorrhage targeted at 40 mmHg, hypertonic sodium pyruvate (0.5 $g \cdot kg^{-1} \cdot h^{-1}$) was infused to achieve an arterial concentration of 5 mM. The volume and osmolality effects of pyruvate were matched with 10% saline (HTS) and 0.9% saline (NS). Although the peak hemorrhage volume increased significantly in both the pyruvate and HTS group, only the pyruvate treatment was effective in delaying cardiovascular decompensation. In addition, pyruvate effectively maintained the NADH/NAD redox state, as evidenced by increased microdialysate pyruvate levels and a significantly lower lactate-to-pyruvate ratio. Pyruvate also prevented the loss of intracellular antioxidants (GSH) and a reduction in the GSH-to-GSSG ratio. These beneficial effects on the redox environment decreased hepatic cellular death by apoptosis. Pyruvate significantly increased the ratio of Bcl-Xl (antiapoptotic molecule)/Bax (proapoptotic molecule), prevented the release of cytochrome *c* from mitochondria, and decreased the fragmentation of caspase 3 and poly(ADP ribose) polymerase (DNA repair enzyme). These beneficial findings indicate that pyruvate infused 30 min after the onset of severe hemorrhagic shock is effective in maintaining the redox environment, preventing the loss of the key antioxidant GSH, and decreasing early apoptosis indicators.

glutathione; redox state; caspases

DESPITE ADVANCES IN THE EARLY CARE of trauma victims over the past two decades, multiple organ failure (MOF) continues to be a major factor in the morbidity and mortality that occurs after resuscitation from hemorrhagic shock (16). While there are numerous factors that influence the development of MOF, there is increasing evidence that hepatic dysfunction plays a central role (21, 24, 42, 43). Experimental studies have shown that despite acute aggressive resuscitation, there is a consistent depression in microvascular blood flow that results in hypoperfusion and progressive hepatic dysfunction (32, 42, 43). This suggests that despite the restoration of global oxygen delivery, additional pharmacological therapies are needed to prevent or reverse ongoing hepatotoxicity. However, the precise mechanisms of hepatocellular dysfunction after severe hemorrhagic shock are not well defined. Some investigators have shown that the reduction in immunological mediators, such as tumor necrosis factor-α, improves outcome indicators (23, 41). Others have shown that there is severe hepatic energy depletion during hemorrhagic shock and that improvement in the hepatocellular energy state reduces liver dysfunction (7, 38, 40). Overall, these studies show that outcome after resuscitation is dependent on many factors.

Changes in the cellular redox environment and its ability to mediate oxidative stress during ischemia and reperfusion are major contributing factors in cellular injury and can induce cell death by either apoptosis or necrosis (11, 12, 26). While necrosis results from overwhelming cellular deenergization, recent studies suggest that the final common pathway for liver dysfunction after hemorrhagic shock is apoptosis (24). The induction of apoptosis results from transient opening of the mitochondrial permeability transition pore (MPTP) with the release of cytochrome *c*, further generation of oxidative stress, release of intracellular Ca^{2+}, and activation of a cascade of cysteine protease including caspase 3 (22, 25, 39). While numerous factors have been shown to mediate the increased open state probability of the MPTP, evidence suggest that changes in the redox state provide an early signaling mechanism for apoptosis (14, 22, 25, 39).

In this study, we sought to determine whether changes in the cellular redox environment were associated with apoptosis indicators. To test our hypothesis, we examined the ability of pyruvate to decrease the early indicators of hepatic apoptosis in a swine model

Address for reprint requests and other correspondence: P. D. Mongan, Dept. of Anesthesia, Uniformed Services Univ. of the Health Sciences, 4301 Jones Bridge Road, Bethesda, MD 20814 (E-mail: pmongan@usuhs.mil).

The costs of publication of this article were defrayed in part by the payment of page charges. The article must therefore be hereby marked "*advertisement*" in accordance with 18 U.S.C. Section 1734 solely to indicate this fact.

of severe controlled hemorrhagic shock. Pyruvate enhancement of the cellular redox environment can occur from one or more of the following mechanisms: *1*) direct neutralization of free radicals, *2*) alteration of the cytoplasmic NADH/NAD redox state, and/or *3*) enhancement of the intracellular glutathione antioxidant system. All of these could reduce opening of the MPTP and decrease apoptosis.

METHODS

After Institutional Animal Care and Use Committee approval, 24 adolescent Yorkshire swine (*Sus scrofa*) were randomized to receive either an intravenous infusion of 30% sodium pyruvate ($n = 8$), 10% NaCl ($n = 8$, osmotic control), or 0.9% NaCl ($n = 8$, volume control) 30 min after the start of controlled arterial hemorrhage. All animals were cared for according to the United States Department of Agriculture Animal Welfare Act and the National Institutes of Health *Guide for the Care and Use of Laboratory Animals*.

Animal Preparation and Monitoring

Anesthesia and hemodynamic monitoring procedures. The swine were fasted overnight with free access to water. In the morning, they were sedated with an intramuscular injection of ketamine (10 mg/kg) and anesthetized with halothane by nose cone to facilitate tracheal intubation. During surgical preparation, anesthesia was maintained with halothane (1.0–1.5% end tidal concentration) while the animals spontaneously ventilated 25% oxygen-75% nitrogen through a semiclosed circle system (Narkomed 2B, North American Drager; Telford, PA). Inspired and expired oxygen, carbon dioxide, and halothane concentrations were continuously monitored (M1026A Gas Analyzer and 68 Clinical Monitor, Hewlett-Packard; Andover, MD). The right external jugular vein was isolated, an 8.5-Fr introducer sheath was inserted, and a continuous thermodilution cardiac output pulmonary artery catheter was advanced through the sheath to measure pulmonary artery pressure and cardiac output (QVue, Abbott Critical Care; North Chicago, IL). Both femoral arteries and a femoral vein were isolated and cannulated with 8.5-Fr introducer sheaths. A micromanometer (MPC-500, Millar Instruments; Houston, TX) was inserted into the right femoral artery sheath and advanced to the midthoracic aorta for the measurement of mean arterial pressure (MAP). The second femoral artery sheath was used for controlled arterial hemorrhage, and the femoral vein was used for infusions. Physiological data were displayed on an eight-channel Hewlett-Packard model 68 clinical monitor.

Liver microdialysis. After instrumentation for physiological monitoring, a right subcostal incision was made. The animals were placed in the right lateral position, and the middle lobe of the liver was exposed. Two microdialysis probes (CMA 20, polycarbonate fiber length 10 mm; diameter 0.5 mm; 20,000-Da molecular cutoff) were inserted into the liver 2 and 3 cm caudate to the gallbladder at a distance of 3 cm from the liver edge. These probes were perfused with 0.9% NaCl at 2 μl/min using a precision, multisyringe pump (CMA 102, CMA/Microdialysis; Acton, MA). After the liver was repositioned in the abdominal cavity, the wound edges were infiltrated with bupivacaine (0.5%, 15 ml). Plastic wrap was used to restrict the intestines to the abdominal cavity, and the entire area was the area covered with plastic wrap to prevent desiccation.

Experimental Protocols

Computer-controlled arterial hemorrhage. One hour before the initiation of hemorrhage, and the expired halothane concentration was reduced to 0.8% with the animals spontaneously ventilating. Controlled arterial hemorrhage was automated to insure reproducibility. In brief, a customized computer protocol (LabView 5, National Instruments; Austin, TX) monitored the MAP and through a proportional control feedback algorithm controlled the speed and direction of a partial occlusion roller pump (MasterFlex Digital Console Drive, Cole-Parmer Instruments; Chicago, IL) that was connected to a femoral arterial cannula. At the start of the hemorrhage period, the computer program initiated blood withdrawal to decrease the MAP to 40 mmHg over 10 min. During hemorrhage, the blood was stored in a closed reservoir primed with sodium citrate (1.66 g) and porcine heparin (3,000 units) to inhibit clot formation. After the initial 10-min rapid hemorrhage, the program maintained the MAP at 40 mmHg either by withdrawal or by reinfusion of the hemorrhage blood as necessary. During the protocol, the volume of blood in the reservoir was gravimetrically measured (Sartorius LA4200, Sartorius; Edgewood, NY), and the data output was stored on computer hard disk with the time-stamped MAP. During isobaric-controlled arterial hemorrhage, the transition from compensated to decompensated hemorrhagic shock was recorded as the time when continued infusion of the hemorrhage volume (HV) was necessary to maintain the target MAP of 40 mmHg. The peak HV (PHV), which represents the maximum blood volume weighed in storage reservoir, is measured immediately before the time of decompensation. With the exception of the protocol infusions of pyruvate, 10% NaCl, or 0.9% NaCl, only the blood withdrawn to induce hypotension was administered to maintain the MAP at 40 mmHg. During the decompensatory phase of hemorrhagic shock, if all the HV was reinfused, no further therapy was used to support the MAP. Death was defined as a MAP <10 mmHg with cessation of spontaneous respiratory effort.

Pyruvate, 0.9% NaCl, and 10% NaCl infusion protocols. To determine the efficacy of pyruvate administered after the onset of hemorrhagic shock, the animals were block randomized to one of three treatment groups. *Group 1* was administered a 100 mg/kg bolus of 30% sodium pyruvate (pH 7.4) via the femoral vein, followed by 0.5 $g \cdot kg^{-1} \cdot h^{-1}$ for the duration of the protocol. In *groups 2* and *3*, a matched volume of 10% or 0.9% NaCl was bolused and infused to control for the osmolarity and volume effects of the hypertonic sodium pyruvate.

Analytic sampling procedures. Microdialysis samples were continuously collected over 30-min periods (60-μl aliquots) by an automated microfraction collector (CMA142, CMA/Microdialysis), and all analytic tests were performed within 1 h (lactate and pyruvate). One hour after insertion of the microdialysis probes, arterial blood was sampled every 30 min for measurement of pH, base excess, blood gases, and hemoglobin (IL 1610 and IL 682 CoOximeter, Instrumentation Laboratories; Lexington, KY). Heparinized blood samples for laboratory analysis were obtained every 30 min and immediately centrifuged.

Liver tissue sampling. At 0, 60, 120, and 240 min after the start of shock (H_0, H_{60}, H_{120}, and H_{240}, respectively), tissue samples were obtained from the liver for analysis. Liver tissue was taken from the edge of the left lobe and rapidly immersed in liquid isopentane at −90°C. Bleeding was controlled by application of thrombin, collagen matrix, and di-

rect pressure. After being frozen, the tissue was transferred to chilled cryovials and stored at −80°C for future analysis.

Analytic Methods

Microdialysis calibration procedures. In vitro relative recovery for each microdialysis probe was determined in triplicate before and after each experiment. The probes were immersed in a calibration standard solution at 38.5°C and perfused with 0.9% NaCl. The calibration standards were lactate (10 mM) and pyruvate (2 mM) in double-distilled deionized water. The concentrations of the nondialyzed standards were compared with the concentrations of the in vitro microdialysis samples to determine the relative recovery for each component. The relative recovery for each compound was used to estimate the in vivo extracellular concentration of the components in the immediate vicinity of the probes.

Lactate and pyruvate analysis. Lactate and pyruvate levels were measured in the plasma and microdialysate samples. These analyses were performed with a CMA 600 Analyzer (CMA/Microdialysis). This instrument performs an automated enzymatic conversion of lactate or pyruvate to H_2O_2. Peroxidase catalyses a reaction between H_2O_2 and other substrates to form the red-violet-colored quinonediimine. The rate of formation of the quinonediimine is measured at 546 nm and is proportional to the lactate and pyruvate concentrations.

Glutathione analysis. Frozen liver tissue samples were pulverized with porcelain mortars under liquid nitrogen, and GSH and GSSG were determined spectrophotometrically as previously described (36). In brief, 50 mg of frozen, pulverized tissue were homogenized with perchloric acid (1 N $HClO_4$) + 2 mM EDTA in Eppendorf tubes chilled in a Polar Block II cooling device (−20°C, Boekel Scientific; Feasterville, PA) using a Tissue Tearor (Biospec Products; Racine, WI). After centrifugation (5,000 *g*, 5 min at 0°C), the supernatant was neutralized with 2.0 M KOH and 0.3 M MOPS and centrifuged to remove the $KClO_4$ precipitate, and an aliquot assayed for GSH by the glyoxalase I reaction. *S*-lactoyl GSH formation was determined at 240 nm. For the determination of GSSG, pulverized liver was homogenized with 1 N $HClO_4$ with 2 mM EDTA and 50 mM *N*-ethyl maleimide (NEM). The NEM was added to trap the GSH and prevent its conversion to GSSG. After neutralization of the supernatant and removal of $KClO_4$, NEM was removed by anion exchange chromatography (QAE Sephadex). The GSSG eluent was concentrated with an evaporator, and its amount was determined spectrophotometrically at 340 nm.

NADPH and NADP analysis. NADP and NADPH were determined by reverse-phase HPLC analysis as previously described (4). In brief, to insure optimal recovery, NADP content was determined after acid extraction and NADPH was determined after alkaline extraction from frozen pulverized liver tissue. Extracts were equilibrated to a pH between 6 and 7, and 25 μl were automatically injected into a heated (35°C) Waters Symmetry Shield RP-18 column (4.6 × 150) by a refrigerated (4°C) autosampler (Waters 2690 Separations Module, Waters Associates; Milford, MA). The injectate was eluted with a 0.1 M KH_2PO_4-acetonitrile (2.5–25% vol/vol) buffer gradient. The chromatograms and absorbance data from the photodiode array (Water 996, Waters Associates) were recorded and analyzed using the Millenium 32 software (Waters Associates). Peak identification and quantification were accomplished by matching the spectral signal of the peaks, peak purity, and peak areas to the spectral signal and peak areas generated for the injected standards.

Assessment of Apoptosis [Bcl-Xl, Bax, Cytochrome c, Caspase 3, and Poly(ADP-Ribose) Polymerase Fragmentation]

Tissue preparation. Cell death by apoptosis was examined by Western immunoblotting in cell lysates or cytosolic preparations from liver tissue. In brief, pulverized frozen samples of liver tissue were lysed in 1:10 (wt/vol) ice-cold lysis buffer consisting of 25 mg/ml PBS, 230 mg/ml PMSF, 1 μg/ml leupeptin, and 1 μg/ml aprotinin in 1% Triton X-100. After brief sonication, samples were centrifuged at 1,000 *g*. The pellet S10 or cell lysate was used for the immunostaining with caspase 3 and poly(ADP-ribose) polymerase (PARP) antibodies. Liver cytosol was prepared by spinning the cell lysate at 100,000 *g* in a Beckman ultracentrifuge (TL-100). The supernatant S100 or cytosol was removed and used for immunostaining with Bcl-Xl, Bax, and cytochrome *c* antibodies.

Detection of Bcl-Xl, Bax, and cytochrome c. Cytosolic protein (25 μg) was lysed in sample buffer [62.5 mmol Tris·HCl (pH 6.8), 2% SDS, 10% glycerol, 5% β-mercaptoethanol, and 0.005% bromophenol blue] and subjected to SDS-polyacrylamide gel electrophoresis using minigel equipment (Bio-Rad). Ten percent polyacrylamide gels were used for analysis of Bcl-Xl and Bax expression, and 14% gels were used for cytochrome *c*. After electrophoresis, proteins were transferred to nitrocellulose membranes using miniblot equipment. Nonspecific proteins were blocked in 5% nonfat dried milk in Tris-buffered saline (TBS) containing 0.05% Tween 20 (TBS-T). Primary antibodies were diluted in blocking buffer and incubated with the blots for 1 h. Bcl-Xl, Bax, and cytochrome *c* (mouse monoclonal antibody at 1:500) were used. Blots were washed thoroughly with TBS-T and incubated in secondary antibody (peroxidase-conjugated goat anti-mouse, diluted 1:2,000 in blocking buffer) for 1 h. After a final wash in TBS-T, horseradish peroxidase was detected using ECL reagent (Amersham).

Caspase 3 and PARP fragmentation. Cell lysates from the liver were denatured in Laemmli sample buffer with 6 M urea for PARP and no urea for caspase 3. HL 60 cell extracts treated with etoposide to undergo apoptosis (BioMol; Plymouth Meeting, PA) were used as positive controls for the presence of the 85-kDa fragment of PARP. Proteins were resolved on 10% SDS gel and transferred to nitrocellulose membranes. For detection of caspase 3, the membrane was incubated with primary mouse monoclonal antibody from Oncogene (Gaithersburg, MD). Intact and fragmented PARP was detected by probing the membrane with primary mouse monoclonal antibody (1:2,000, BioMol), which detects both intact PARP (116 kDa) and the apoptosis-associated fragment (85 kDa). The membranes were then incubated with secondary antibody directed toward goat anti-mouse IgG (1:2,000). Negative controls were performed by omitting primary antibody as well as probing with actin. Chemiluminescence was detected by autoradiography, and the integrated optical density (OD) of the protein bands was measured using the Scion Image program.

Data Presentation and Statistics

All data are presented as means ± SE. To avoid spurious results due to multiple testing, differences within groups over the course of the experiment were determined by repeated-measures ANOVA. Differences between groups for nonrecurring measurements were assessed using ANOVA. Differences between groups over the course of the experiment were determined using a two-way ANOVA for one factor (dependent variable) over time. Within- and between-group testing

was accompanied by a Tukey's honestly significant difference multiple-range test to correct for the multiple comparisons. Proportions were evaluated using McNemar's test of proportions. Values were considered statistically different when $P < 0.05$ after correction for multiple comparisons. Error bars in the figures represent SE.

RESULTS

The animal weights were similar in the pyruvate and 10% and 0.9% NaCl groups (31.8 ± 0.9, 32.4 ± 1.1, and 31.1 ± 1.3 kg, respectively). Thirty minutes after the start of controlled arterial hemorrhage, the bolus and infusion of pyruvate raised the arterial pyruvate concentration from 0.09 ± 0.01 mM at H_{30} to 4.43 ± 0.63 mM at H_{60}. In the 10% and 0.9% NaCl groups, the pyruvate levels at H_{30} were 0.11 ± 0.02 and 0.13 ± 0.2 mM and increased to only 0.39 ± 0.03 and 0.45 ± 0.06 mM, respectively, during hemorrhage.

Hemodynamic and Hemorrhage-Related Parameters

MAP was similar in all groups before the start of the controlled arterial hemorrhage (99.6 ± 2.7, 100.5 ± 3.4, and 101.7 ± 1.0 mmHg) in the pyruvate, 10%, and 0.9% NaCl groups. Because of the automation of the hemorrhage protocol, there were no differences between the groups in the time to reach the target MAP of 40 mmHg or the variability in the MAP. However, there was a significant difference in the PHV in the pyruvate and 10% NaCl treatment groups (45.8 ± 1.2 and 42.3 ± 0.6 ml/kg) compared with the 0.9% NaCl group (34.8 ± 0.9 ml/kg, $P < 0.05$). Although there was a significant increase in the PHV in both the pyruvate and 10% NaCl groups, only the pyruvate treatment was effective in delaying cardiovascular decompensation as evidenced by the increased time to PHV (94 ± 5 vs. 73 ± 6 and 70 ± 4 min, $P < 0.05$). In addition to the delay in the decompensatory phase of hemorrhagic shock in the pyruvate group, there were significant differences in the cardiovascular profiles during the last 2 h of the hemorrhage that affected the rate of hemorrhage volume reinfusion. As detailed in Table 1, at H_{180}, both the 10% and 0.9% NaCl groups had a decrease in heart rate (HR) and were unable to increase the cardiac index despite the reinfusion of a larger amount of the HV. This decrement in cardiovascular function resulted in complete reinfusion of the HV in four animals in the both the 10% and 0.9% NaCl groups, progressive decreases in the MAP, and death. This profile indicates significantly compromised cardiovascular function. In contrast, despite the smaller amount of HV return, the pyruvate-treated animals had no decreases in HR, had greater augmentation of the cardiac index, and suffered only one animal death throughout the protocol. Thus the pyruvate treatment

Table 1. *Hemorrhage volume and physiological measurements*

	Time								
	H_0	H_{30}	H_{60}	H_{90}	H_{120}	H_{150}	H_{180}	H_{210}	H_{240}
n									
Pyruvate	8	8	8	8	8	8	8	8	7
10% NaCl	8	8	8	8	8	7	6	4	4
0.9% NaCl	8	8	8	8	8	7	6	6	4
HV, ml/kg									
Pyruvate	0	26.6 ± 1.7	41.2 ± 1.8	43.6 ± 1.6	42.3 ± 1.8	34.6 ± 1.7	29.1 ± 2.1	22.6 ± 1.9	18.5 ± 2.9
10% NaCl	0	25.9 ± 1.1	39.5 ± 1.4	38.5 ± 1.8	35.3 ± 1.7*	25.1 ± 1.8*	17.2 ± 2.4*	9.4 ± 2.3*	7.9 ± 4.2
0.9% NaCl	0	26.3 ± 1.2	33.5 ± 1.3*	31.8 ± 0.9*	27.1 ± 1.2*	20.6 ± 2.0*	16.1 ± 2.8*	10.2 ± 2.6*	8.2 ± 3.1
HR, beats/min									
Pyruvate	125 ± 9	212 ± 10	253 ± 9	252 ± 7	248 ± 8	251 ± 8	246 ± 6	245 ± 9	242 ± 8
10% NaCl	133 ± 11	204 ± 8	247 ± 12	249 ± 8	246 ± 7	234 ± 12	217 ± 10*	205 ± 7*	197 ± 11*
0.9% NaCl	135 ± 8	208 ± 11	250 ± 7	251 ± 6	245 ± 9	229 ± 10	212 ± 11*	209 ± 11*	190 ± 12*
MAP, mmHg									
Pyruvate	99.6 ± 2.7	40.4 ± 0.1	40.2 ± 0.1	40.0 ± 0.1	39.9 ± 0.3	39.7 ± 0.3	39.4 ± 0.3	39.4 ± 9	39.1 ± 1.2
10% NaCl	100.5 ± 3.4	40.3 ± 0.2	39.9 ± 0.1	39.4 ± 0.8	39.2 ± 0.2	39.4 ± 0.3	38.2 ± 0.7	38.5 ± 1.7	27.1 ± 4.9*
0.9% NaCl	101.7 ± 1.0	40.3 ± 0.2	40.1 ± 0.1	39.9 ± 0.1	38.7 ± 0.5	39.8 ± 0.2	38.8 ± 0.2	38.6 ± 0.7	32.4 ± 2.9
CVP, mmHg									
Pyruvate	1.4 ± 1.0	−5.7 ± 0.9	−6.2 ± 1.1	−6.7 ± 1.1	−6.5 ± 1.0	−5.6 ± 0.9	−5.3 ± 0.8	−5.2 ± 0.9	−4.9 ± 0.9
10% NaCl	1.1 ± 0.9	−5.5 ± 1.1	−6.1 ± 0.9	−6.4 ± 0.9	−5.7 ± 1.1	−5.0 ± 1.2	−4.1 ± 1.2	−4.1 ± 1.1	−3.8 ± 1.2
0.9% NaCl	1.4 ± 0.7	−5.9 ± 0.7	−6.1 ± 1.0	−6.2 ± 0.9	−5.8 ± 1.2	−5.1 ± 1.1	−4.7 ± 1.0	−3.8 ± 0.9	−3.5 ± 0.9
CI, $ml \cdot kg^{-1} \cdot min^{-1}$									
Pyruvate	178.2 ± 12.8	66.3 ± 4.2	48.4 ± 4.2	41.5 ± 3.6	45.0 ± 2.7	54.6 ± 3.3	61.2 ± 3.6	69.5 ± 5.1	70.8 ± 4.7
10% NaCl	174.5 ± 15.6	61.6 ± 4.7	49.1 ± 4.7	37.8 ± 3.4	39.2 ± 2.9	44.9 ± 4.3	45.8 ± 3.7*	44.6 ± 4.5*	46.2 ± 5.1*
0.9% NaCl	184.8 ± 8.1	67.3 ± 3.5	50.3 ± 4.4	35.5 ± 3.3	38.1 ± 2.4	42.4 ± 4.1	46.6 ± 5.6*	43.3 ± 5.8*	39.5 ± 1.3*
SV, ml/beat									
Pyruvate	45.2 ± 2.8	11.4 ± 1.6	6.2 ± 0.9	4.7 ± 0.5	5.5 ± 0.5	6.4 ± 0.4	7.8 ± 0.6	8.4 ± 0.8	9.1 ± 1.0
10% NaCl	44.9 ± 3.2	11.8 ± 1.7	6.6 ± 0.8	4.6 ± 0.8	5.1 ± 0.5	6.1 ± 0.7	6.9 ± 0.5	7.6 ± 0.9	8.3 ± 0.7
0.9% NaCl	47.1 ± 3.1	12.3 ± 1.5	6.9 ± 0.6	4.8 ± 0.4	5.6 ± 0.5	6.2 ± 0.6	7.4 ± 0.7	8.4 ± 0.9	8.6 ± 0.9

Data are presented as means ± SE; *n* = no. of swine. The initial hemodynamic measurements were made immediately before the start of the controlled arterial hemorrhage. Subscripted numbers refer to minutes. The pyruvate, 10% NaCl (osmotic control), or 0.9% NaCl (volume control) treatments were started 30 min after the start of hemorrhage (H_{30}). HV, hemorrhage volume; HR, heart rate; MAP, mean arterial pressure; CVP, central venous pressure; CI, cardiac index; SV, stroke volume. *$P < 0.05$ compared with the pyruvate group for the time-matched data.

delayed the onset of the decompensatory stage of hemorrhagic shock by increasing the time to PHV. In addition, during decompensation, the pyruvate-treated animals had a greater tolerance to the prolonged hypotension during hemorrhagic shock, as indicated by a more favorable cardiac function than the 10% and 0.9% NaCl groups.

Osmolality and Acid Base Parameters

Table 2 shows that there were significant increases and decreases in osmolality and hemoglobin, respectively, in the pyruvate and 10% NaCl groups. The changes were similar in those groups and significantly different compared with the 0.9% NaCl group. This indicates that the delay in cardiovascular decompensation in the pyruvate group was not related to either the volume or osmotic effects of the treatment. After the first 30 min of hemorrhage, all groups had *1*) similar increases in lactate and the lactate-to-pyruvate ratio and *2*) decreases in base excess (Table 2). However, after the initiation of the pyruvate or NaCl treatments, there were significant differences between the groups for the remainder of the protocol. After H_{30} in the NaCl groups, there were continued significant increases in lactate and the lactate-to-pyruvate ratio and decreases in base excess and pH. In comparison, although the pyruvate treatment caused lactate to increase two times higher than the other groups, the lactate-to-pyruvate ratio, the more relevant indicator of metabolic stress, decreased to one-half the initial value. In addition, the pyruvate administration prevented the magnitude of changes in acid-base parameters that occurred in the other groups.

Pyruvate Effects on Liver Microdialysis Lactate-to-Pyruvate Ratio

Figure 1 illustrates the differences between the treatment groups and the microdialysate lactate-to-pyruvate ratio measurements. The lactate, pyruvate, and lactate-to-pyruvate ratio was similar in both groups before (H_0) and 30 min after the start of hemorrhage (H_{30}; before treatment). However, the pyruvate infusion increased the microdialysate pyruvate levels from 0.07 to 1.62 mM during the experiment compared with the increases to 0.15 and 0.13 mM in the 10% and 0.9% NaCl animals, respectively ($P < 0.05$). Compared with the NaCl control groups, this rise in pyruvate resulted in a significantly lower and stable lactate-to-pyruvate ratio until the end of the protocol (H_{240}).

Pyruvate Effects on GSH/GSSG and NADP/NADPH

Figure 2 depicts the results of the GSH/GSSG levels and ratios in the groups during hemorrhagic shock. Basal levels of GSH and GSSG were similar in

Table 2. *Osmolality, hemoglobin, lactate, and acid-base status*

	Time								
	H_0	H_{30}	H_{60}	H_{90}	H_{120}	H_{150}	H_{180}	H_{210}	H_{240}
n									
Pyruvate	8	8	8	8	8	8	8	8	7
10% NaCl	8	8	8	8	8	7	6	4	4
0.9% NaCl	8	8	8	8	8	7	6	6	4
Osmolality, meq/l									
Pyruvate	271±3	270±3	297±5	308±4	311±5	316±5	318±4	320±4	325±5
10% NaCl	269±3	269±2	299±5	309±4	309±4	319±5	320±5	324±6	327±6
0.9% NaCl	268±3	266±3	266±3*	267±2*	267±3*	268±3*	270±3*	270±3*	269±5*
Hemoglobin, g/dl									
Pyruvate	9.6±0.1	8.7±0.2	7.5±0.2	6.7±0.2	6.9±0.3	7.0±0.3	7.1±0.3	7.1±0.3	7.1±0.3
10% NaCl	9.9±0.1	8.9±0.2	7.4±0.2	6.6±0.2	6.9±0.3	7.0±0.3	7.0±0.3	7.2±0.4	7.4±0.5
0.9% NaCl	9.7±0.1	8.6±0.2	8.7±0.3*	9.0±0.4*†	9.7±0.5*†	9.9±0.4*†	9.8±0.4*†	9.8±0.3*†	9.9±0.4*†
Lactate, mM									
Pyruvate	1.2±0.2	3.1±0.2	12.3±1.6	19.6±0.9	26.4±1.1	27.9±0.8	28.2±1.0	29.6±1.1	30.9±1.5
10% NaCl	1.2±0.1	3.2±0.2	6.6±1.4*	11.4±1.1*	12.5±1.0*	13.2±1.0*	14.1±0.6*	14.7±0.7*	13.2±1.1*
0.9% NaCl	1.1±0.1	3.3±0.3	7.0±1.3*	10.8±0.8*	11.5±0.6*	11.9±0.5*	13.3±0.4*	14.2±0.6*	12.0±1.0*
Lactate/pyruvate									
Pyruvate	14.2±1.3	25.9±4.2	4.7±0.5	4.4±0.4	4.8±0.4	5.1±0.6	5.2±0.5	5.8±0.6	6.0±0.7
10% NaCl	13.6±1.6	26.6±4.4	34.8±3.7*	36.9±3.8*	37.2±3.6*	39.7±3.1*	37.3±2.3*	35.4±2.1*	36.2±2.5*
0.9% NaCl	13.5±1.4	24.6±3.7	31.5±2.1*	33.2±2.4*	34.7±3.3*	33.1±2.7*	33.0±2.6*	34.2±1.4*	33.2±1.5*
Base excess, meq/l									
Pyruvate	4.4±0.6	−1.4±0.4	−1.8±1.0	−2.1±1.6	−1.7±1.4	−1.5±1.9	0.7±2.1	4.7±2.6	5.1±2.2
10% NaCl	4.8±0.8	−1.1±0.9	−5.9±1.5	−11.4±2.1*	−13.7±2.0*	−17.7±1.2*	−17.0±1.0*	−17.3±1.5*	−16.4±2.7*
0.9% NaCl	4.4±0.6	−0.9±0.5	−5.4±1.1	−10.1±1.3*	−11.9±1.0*	−13.6±1.2*	−14.5±1.2*	−14.4±1.5*	−14.9±2.1*
pH									
Pyruvate	7.41±0.01	7.38±0.02	7.37±0.04	7.38±0.06	7.39±0.04	7.38±0.05	7.39±0.06	7.41±0.03	7.42±0.05
10% NaCl	7.43±0.01	7.40±0.02	7.35±0.03	7.25±0.04	7.18±0.05*	7.14±0.04*	7.10±0.05*	7.14±0.07*	7.14±0.08*
0.9% NaCl	7.42±0.01	7.41±0.02	7.36±0.02	7.26±0.03	7.24±0.06*	7.20±0.04*	7.17±0.04*	7.16±0.06*	7.17±0.05*

Data are presented as means±SE; *n* = no. of swine. The initial measurements were made immediately before the start of the controlled arterial hemorrhage. The pyruvate, 10% NaCl, or 0.9% NaCl treatments were started 30 min after the start of hemorrhage (H_{30}). *$P < 0.05$ compared with the pyruvate group for the time-matched data; †$P < 0.05$ compared with the 10% NaCl group for the time-matched data.

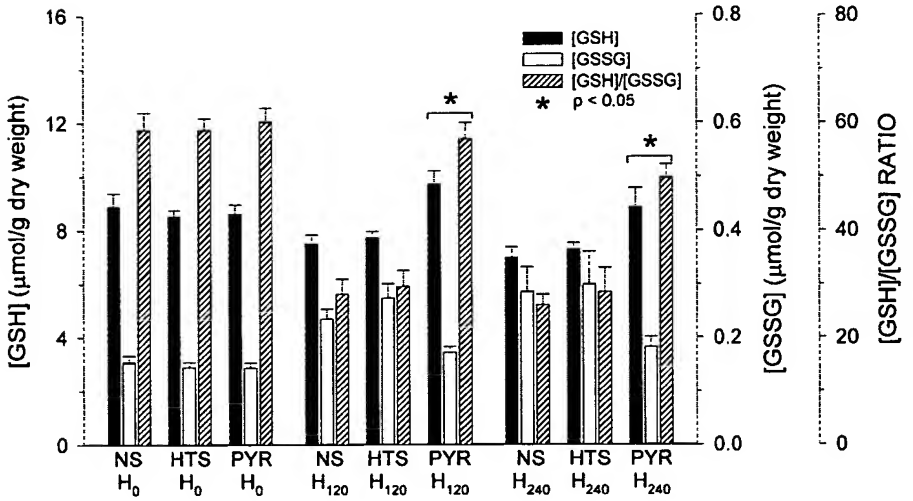

Fig. 1. Beneficial effects of pyruvate administration on GSH and diminution of the GSH-to-GSSG ratio (GSH/GSSG) during controlled arterial hemorrhage. At both 120 and 240 min after the start of shock (H_{120} and H_{240}), the pyruvate-treated animals had significantly higher GSH content and GSH/GSSG compared with the 10% NaCl (HTS) and 0.9% NaCl (NS)-treated animals.

all groups. Compared with the 10% and 0.9% NaCl animals, pyruvate maintained significantly higher levels of the intracellular antioxidant GSH at both H_{120} and H_{240}. Subsequently, the GSH-to-GSSG ratio in the pyruvate group was only slightly reduced at H_{240}, whereas there was a loss of total glutathione and a 50–60% reduction in GSH-to-GSSG ratio at both H_{120} and H_{240} in the other groups. Evaluation of NADP and NADPH levels showed that NADPH was similar at baseline in all the pyruvate and 10% and 0.9% NaCl animals (0.31 ± 0.01, 0.32 ± 0.02, and 0.32 ± 0.01 μM/g dry wt). Whereas the NADPH levels decreased similarly at H_{240} in the 10% and 0.9% NaCl animals (0.24 ± 0.02 and 0.26 ± 0.02 μM/g dry wt), the NADPH levels in the pyruvate animals were increased to 0.41 ± 0.03 μM/g dry wt at H_{240} and the NADPH-to-NADP ratio was increased by 1.5–2 times during the infusion of pyruvate. These findings are important because regeneration of GSH is carried out by the enzyme glutathione reductase, which requires the cofactor NADPH.

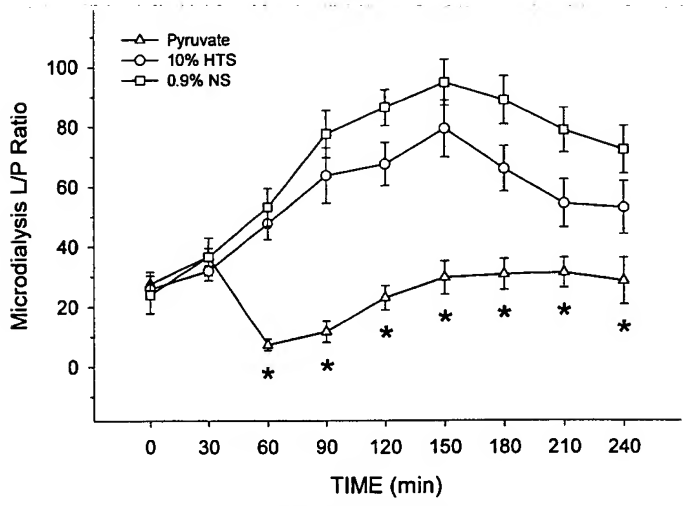

Fig. 2. Changes in the microdialysis lactate-to-pyruvate ratio (L/P) during the protocol. The increase in the 10% and 0.9% NaCl animals were due to a rapid and significant increase in lactate.

Pyruvate Effects on Apoptosis-Related Parameters

As shown in Table 3, the OD of Bcl-Xl in the pyruvate-treated group was significantly higher than that in the 10% NaCl or 0.9% NaCl groups ($P < 0.05$, $n = 8$). On the other hand, Bax expression was slightly lower in the pyruvate-treated group ($P > 0.05$). To further characterize the balance between Bcl-Xl and Bax in liver tissue, the Bcl-Xl-to-Bax ratio was calculated using the mean OD in autoradiographs after immunoblotting. At H_{240}, the pyruvate-treated animals had a significant higher ratio of Bcl-Xl to Bax compared with the 10% and 0.9% NaCl animals (1.63 vs. 0.35 and 0.59, respectively, $P < 0.05$). Representative examples are presented in Fig. 3. This difference is significant because the Bcl-Xl-to-Bax ratio is a significant factor in the induction of apoptosis by preventing mitochondrial depolarization and blocking the release of cytochrome *c*. Thus it represents the functional relevant checkpoint for the regulation of apoptosis. This increased Bcl-Xl-to-Bax ratio is consistent with the absence of cytochrome *c* detection in the pyruvate-treated animals compared with the consistent detection in all the 10% and 0.9% NaCl animals.

Table 3. *Differential expression of Bcl-Xl and Bax in treatment groups*

Treatment	Bcl-Xl	Bax	Bcl-Xl
Pyruvate	1.53 ± 0.22*	0.94 ± 0.17	1.63*
0.9% NaCl	0.77 ± 0.11	1.29 ± 0.19	0.59
10% NaCl	0.47 ± 0.06	1.36 ± 0.21	0.35

Numbers indicate means ± SE of optical density (OD) from each treatment group, which consisted of 8 animals. Expression of Bcl-Xl and Bax was measured in liver tissue obtained at 240 min after the start of controlled arterial hemorrhagic shock in animals treated with pyruvate, 0.9% NaCl, or 10% NaCl. Cellular cytosolic preparations from liver tissue were subjected to SDS-PAGE, and Western blot was performed using the monoclonal anti-Bcl-Xl or anti-BAX and a peroxidase-conjugated secondary antibody. In negative controls, primary antibodies were omitted. Ponceau staining in membranes indicated an equal amount of protein loaded per lane (data not shown). *$P < 0.05$ compared with the other groups.

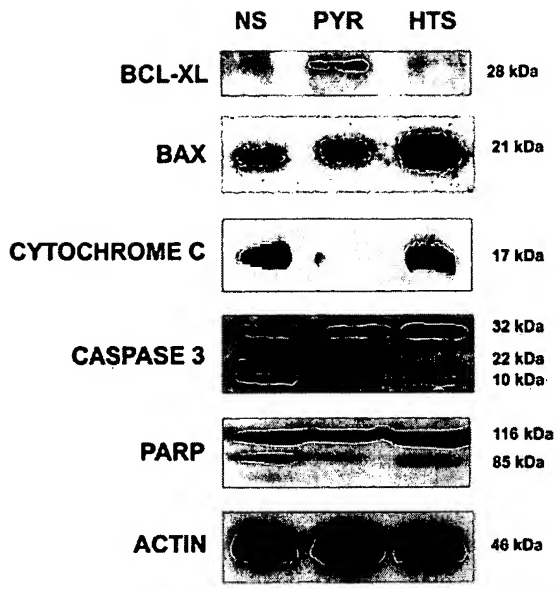

Fig. 3. Representative Western blots of the effects of pyruvate administration on critical indicators of hepatic apoptosis. Liver samples were obtained 240 min after the start of hemorrhagic shock or after complete infusion of the shed blood volume if/when complete cardiac collapse was imminent. The immunoblots demonstrate the increase in Bcl-Xl with similar Bax bands. Cytochrome *c* was not detectible in the pyruvate sample. Finally, there was increased activation of caspase 3 and poly(ADP-ribose) polymerase (PARP) fragmentation in the 10% and 0.9% NaCl animals.

Further evidence for the beneficial effect of pyruvate in decreasing apoptosis indicators during the prolonged period of hemorrhagic shock is presented in Table 4 and Fig. 3. As shown in the representative immunoblot in Fig. 3, cytochrome *c* was detected in the cytosolic fractions of the 10% and 0.9% NaCl groups and not in the pyruvate-treated animals. The activation of caspase 3 in cell extracts from liver samples in 10% and 0.9% NaCl groups is indicated by the increased detection of caspase 3 subunits. The 32-kDa proenzyme of caspase 3 is cleaved at specific aspartate residues to generate two smaller active subunits (21 and 10 kDa), which oligomerize to form an active protease complex. At H_{240}, the OD of 32-kDa protein was 0.81 ± 0.03, 0.64 ± 0.1, and 0.43 ± 0.02 in the pyruvate, 10% NaCl, and 0.9% NaCl animals. The OD of the active subunit of 21 kDa was 0.02 ± 0.01, 0.54 ± 0.1, and 0.41 ± 0.11 in the pyruvate, 10% NaCl, and 0.9% NaCl animals. This data represents only 3% activation of caspase 3 in the pyruvate group compared with 40% and 56% of the total caspase 3 in the 10% and 0.9% NaCl groups. These findings are not surprising because the release of cytochrome *c* is involved in the execution phase of apoptotic cell death via cytoplasmic proteolytic cascades that lead to caspase 3 activation. Another important process involved in apoptosis is the cleavage of PARP. At H_{240}, liver tissue from 10% and 0.9% NaCl animals exhibited significantly lower amounts of intact PARP (116 kDa, 2.63 ± 0.16 and 2.94 ± 0.33, $n = 8$) compared with the pyruvate-treated group (3.27 ± 0.27, $n = 8$, $P < 0.05$). The OD of fragmented PARP (85 kDa) was 1.5%, 26%, and 28% of the total PARP in the pyruvate, 10% NaCl, and 0.9% NaCl groups, respectively.

DISCUSSION

The present study indicates that infusion of pyruvate (5 mM) 30 min after the onset of severe controlled hemorrhagic shock suggests that pyruvate attenuated the initiation and execution phase of apoptotic cell death. This is indicated by the decreased release of cytochrome *c* from the mitochondria and reduced fragmentation of caspase 3 and PARP in the pyruvate liver samples obtained after the 4-h period of hypotension. This beneficial effect of pyruvate could be secondary to *1*) the alteration in the cytosolic redox state, as indicated by the microdialysate lactate-to-pyruvate ratio; *2*) the maintenance of a stable hepatic redox environment, as indicated by the GSH-to-GSSG ratio; *3*) maintenance of total glutathione content by the prevention of GSH efflux; and/or *4*) by limiting the hypotension induced changes in acid-base parameters.

We have previously shown that pyruvate treatment during controlled arterial hemorrhage prevents cardiovascular decompensation, delays the onset of the decompensatory phase of hemorrhagic shock, and significantly prolongs survival (29, 30). In this study, although there was no difference in the PHV between the pyruvate and 10% NaCl treatments, we again observed a delay in the onset of the decompensatory phase of shock as indicated by the longer time before the start of the HV to maintain the MAP in the pyru-

Table 4. *Caspase 3 and PARP immunoblot signal intensity*

Protein	Pyruvate	0.9% NaCl	10% NaCl
Intact caspase 3 (32 kDa)	0.81 ± 0.03*	0.43 ± 0.02	0.64 ± 0.16
Activated caspase 3 (21 kDa)	0.02 ± 0.01*	0.54 ± 0.10	0.41 ± 0.11
Total caspase 3 (32 + 21 kDa)	0.83 ± 0.17	0.97 ± 0.21	1.05 ± 0.62
%Activated caspase 3 [(21/32 kDa)100]	3%*	56%	40%
Intact PARP (116 kDa)	3.27 ± 0.27	2.94 ± 0.33	2.63 ± 0.16
Fragmented PARP (85 kDa)	0.05 ± 0.03*	1.15 ± 0.08	0.93 ± 0.05
Total PARP (116 + 85 kDa)	3.32 ± 0.63	4.09 ± 0.92	3.56 ± 0.41
%PARP fragmentation [(85 kDa/116)100]	1.5%*	28%	26%

Number indicate mean ± SE of OD from each treatment group, which consisted of 8 animals. Activation of caspase 3 and fragmentation of poly(ADP-ribose) polymerase (PARP) was measured in liver tissue obtained at 240 min after the start of controlled arterial hemorrhagic shock in animals treated with pyruvate, 0.9% NaCl, or 10% NaCl. Whole cell lysates from liver tissue were subjected to SDS-PAGE, and Western blot was performed using the monoclonal anti-caspase 3 or anti-PARP and a peroxidase-conjugated secondary antibody. In negative controls, primary antibodies were omitted. Ponceau staining in membranes indicated an equal amount of protein loaded per lane (data not shown). *$P < 0.05$ compared with the other groups.

vate group. While there are several metabolic and cardiovascular mechanisms that may be responsible for this observation, this salutary effect cannot be attributed to differences in volume status because of the similar changes in osmolality and hemoglobin in these two groups during the protocol.

In addition to the delay in the decompensatory phase of hemorrhagic shock, pyruvate administration during controlled arterial hemorrhagic shock improved key measures of cellular redox environment, antioxidant reserve, and indicators of cellular apoptosis. Cells die via two pathways: necrosis or apoptosis (programmed cell death). Necrosis is a form of cell death that is caused by physical, chemical, or osmotic damage with consecutive disruption of internal and external membranes, leading to cell swelling and lysis with release of cytoplasmic material. In contrast, apoptosis is an innate cellular program of cell death. Apoptosis is regulated by energy-dependent mechanisms that involve a cascade of biochemical events resulting in cell shrinkage, chromatin condensation, DNA fragmentation, and ultimately cell death. While there are significant differences in these two types of cell death, during ischemia they are a continuum of damage that occurs secondary to the duration of the increase in the open state of the MPTP (1, 14, 17, 22). While the open state probability of the MPTP increases with higher concentrations of Ca^{2+} in the mitochondria, the sensitivity can be increased by changes in the redox state, oxidative stress, and adenine nucleotide depletion (15). During apoptosis, opening of the MPTP is insufficient to result in complete mitochondrial failure. However, it is sufficient to cause mitochondrial swelling and cytochrome *c* release. The release of cytochrome *c* subsequently activates the apoptotic cascade and eventually causes cell death.

Whereas pyruvate has been documented to have beneficial myocardial functional effects secondary to metabolic alterations, Kerr et al. (19) has shown that the ability of pyruvate to decrease the open state probability of the MPTP during ischemia-reperfusion is unrelated to its metabolic enhancing effects. During ischemia, two redox-sensitive mechanisms have been implicated in the increased open state probability of the MPTP. The first is sensitive to decreases in GSH and the second is sensitive to an increase in the NADH-to-NAD ratio.

Glutathione is the major thiol-disulfide redox buffer of the cell. The redox pair GSH/GSSG provides a large pool of reducing equivalents and is thus not only an indicator of the redox state of the cell but the redox environment/buffering capacity of the cell as well. If there is insufficient NADPH to regenerate GSH, there is an overall shift in the redox state to a more positive potential. If this shift is not corrected by the regeneration of GSH, GSSG is exported to compensate for the deleterious shift in the redox state (34). Thus efflux of glutathione from the cell with subsequent loss of total content is an indicator of oxidative stress.

In previous evaluations, pyruvate has been observed to decrease apoptosis during oxidant stress (5, 19). One of the potential mechanisms for the decrease in apoptosis markers in this study is the ability of pyruvate to favorably alter these indicators of the cytosolic redox environment. Pyruvate administration has been shown to improve the NADH-to-NAD ratio and GSH-to-GSSG ratio, the key endogenous defense mechanism against oxidative stress (18, 36). Whereas the changes in the NADH-to-NAD ratio are affected through the conversion of pyruvate to lactate, the effect on GSH-to-GSSG ratio occurs when citric acid intermediates are increased through mitochondrial carboxylation of pyruvate. The elevated citrate concentration inhibits phosphofructokinase and diverts glycolytic flux into the hexose monophosphate shunt, the principal source of cytosolic NADPH (36). GSH is regenerated from oxidized glutathione disulfide, GSSG is generated by glutathione reductase, and NADPH is the source of the reducing equivalents for this reaction. In this current study, pyruvate administration increased the NADPH-to-NADP ratio, maintained the GSH-to-GSSG ratio, and prevented decreases in the GSH pool. While these findings have been observed in endothelial cell culture and isolated heart preparations, this is the first study to link these changes in the cytosolic redox environment and a decrease in apoptosis markers. From the data presented, it is apparent that the administration of pyruvate during hemorrhagic shock had several beneficial effects on cellular function and reduced multiple measures of apoptosis. One beneficial effect of pyruvate in preventing the apoptosis is the favorable maintenance of the hepatic GSH-to-GSSG ratio and prevention of a decrease in total glutathione content throughout the study. Other studies performed during hemorrhagic shock and hypoxia have shown that the hepatic GSH-to-GSSG ratio is reduced and there is an efflux of glutathione content from the liver (20). This was prevented by the administration of pyruvate in the current study. In addition, other studies have shown a temporal link between decreases in GSH and the GSH-to-GSSG ratio and activation of caspase 3 and PARP fragmentation (44). Isolated rat hepatocytes with moderate depletion of GSH results in apoptosis, and cardiomyocyte apoptosis has been shown to be regulated by redox-sensitive transcription factors (27, 31). These studies in concert with our data support the concept that deleterious alterations in the cytosolic thiol redox state results in activation of factors leading to apoptosis.

In addition to improving the thiol redox state of the hepatic tissue, pyruvate administration also improved the microdialysis lactate-to-pyruvate ratio, an indicator of the NADH/NAD cytosolic redox state. The marked increase in the lactate-to-pyruvate ratio in the 0.9% and 10% NaCl swine is an indicator of an increase in NADH and the cytosolic NADH-to-NAD ratio. When considering the redox pairs NADPH/NADP and NADH/NAD, pyruvate causes distinctly opposite but beneficial effects. NADPH is a reductive cofactor that serves as an electron donor in the regeneration of GSH. However, in the cytosol, pyruvate administration decreases the NADH-to-NAD ratio via

the conversion of pyruvate to lactate. In this instance, NAD serves as a sink for electrons and functions to reduce oxidative stress (34). Both of these changes help to maintain a favorable reduction of the cytosol, thus decreasing oxidative signaling for an increased open state probability of the MPTP. As opposed to the increase in lactate and NADH during hemorrhagic shock, the decrease in the lactate-to-pyruvate ratio by pyruvate indicates a favorable change in the NADH-to-NAD ratio with a reduction in the redox potential. Compared with the beneficial effects of pyruvate, increases in the NADH-to-NAD ratio in hepatocytes through the use of NADH-generating substrates (ethanol and lactate) increases cytotoxicity despite maintenance of cellular ATP content (31). Both of these effects are important because increases in the NADH-to-NAD ratio and depletion of GSH have been implicated in decreases of the Bcl-Xl-to-Bax ratio, release of cytochrome *c*, and signaling of the execution phase of apoptosis (11, 26).

Another major difference between the groups during the experiment was the attenuation of the changes in acid-base measurements in the pyruvate group. There are two potential causes for this effect. First, pyruvate metabolism is associated with a natural consumption of hydrogen ions. Second, the administration of sodium pyruvate causes marked decrease in serum chloride (21). Sodium pyruvate administration increase sodium from ≈140 to 165 meg/dl and causes a decrease in Cl from ≈100 to 90 meq/dl. In contrast, the hypertonic NaCl solution increased both the serum Na from ≈140 to 170 meg/dl and the Cl from ≈100 to 125 meq/dl. While the impact of the hyperchloremia due to the 10% hypertonic saline on acid-base parameters appears to be negligible compared with the normal saline control (Table 2), the impact of the hypochloremia on the alkalinization effect in the pyruvate group is unknown. However, the impact of these changes on apoptosis in vivo is unclear. In vitro studies of the relationship between acidosis and apoptosis provide conflicting results (9, 10, 37). Furthermore, the effects of other methods of systemic alkalinization were not evaluated because the use of bicarbonate or Carbicarb has not been shown to be beneficial in improving outcome during hemorrhagic shock (2, 3). Even so, the administration of other metabolizable alkalinizing agents such as sodium acetate or sodium β-hydroxybutyrate may help delineate the impact of the pyruvate-induced serum chloride changes on acid-base parameters and indicators of cellular compromise.

While the exact mechanism for pyruvate favorably altering early indicators of apoptosis cannot be determined from the current experiments, changes in the redox state are known to play a major role in the initiation phase of apoptosis. In addition to the known beneficial changes in the MPTP by pyruvate, the redox sensitive antiapoptotic protein Bcl-Xl also blocks the release of cytochrome *c*. Decreasing the release of cytochrome *c* is important because cytochrome *c* irreversibly commits the cell to death by activating caspase 3 and the degradation phase of apoptosis. Activation of caspase 3 has been linked to the proteolytic cleavage of cellular substrates including PARP, a strong indicator of apoptosis (6, 13, 35). Although some studies have shown that Bcl2 and Bcl-Xl are equally effective in preventing apoptosis, others have suggested that overexpression of Bcl-Xl is more important in the protection of apoptosis induced by ischemia-reperfusion (8, 46). In accordance with these observations, an increase in Bcl-Xl protein in the pyruvate-treated group suggests that apoptosis in liver cells caused by hemorrhagic shock can be prevented by the use of pyruvate.

In this study, favorable changes in the Bcl-Xl-to-Bax ratio and the prevention of release of cytochrome *c* from mitochondria were apparent in pyruvate-treated animals. Our data further substantiate that pyruvate can prevent apoptosis by inhibiting the cleavage of caspase 3 because the OD of the cleaved 21-kDa protein was significantly less in the pyruvate-treated group than the 0.9% and 10% NaCl animals. Subsequently, PARP cleavage was reduced when compared with the 0.9% and 10% NaCl groups of animals.

In recent years, evidence has accumulated that increased production of free radicals and apoptosis is a main factor in liver dysfunction after hemorrhagic shock (33). Hepatic apoptosis has been demonstrated in animals subjected to ischemia-reperfusion damage and has been shown to impair hepatocyte function (33). The significance of apoptosis-mediated cell death in the generation of MOF during hemorrhagic shock has been closely examined in a murine model of hemorrhage and resuscitation. In comparing mice genetically deficient in PARP with wild-type mice, the results indicate that PARP activation was associated with hepatic dysfunction and decreases survival. However, this damaging sequence of events was not seen in PARP-deficient mice with hemorrhagic shock (24). In addition, other studies of rats undergoing hemorrhagic shock and resuscitation have shown that the prevention of PARP activation decreases hepatic damage and dysfunction (28, 45). In our study, PARP fragmentation was significantly prevented by pyruvate administration compared with the 0.9% and 10% NaCl groups of swine. This decrease in PARP fragmentation suggests that pyruvate therapy may also help to ameliorate or even prevent the hepatocellular dysfunction that occurs after hemorrhagic shock and resuscitation.

In summary, we demonstrated that pyruvate delays cardiovascular decompensation and decreases early indicators of hepatic apoptosis in this swine model of severe isobaric hemorrhagic shock. Furthermore, this study suggests that the protection offered by exogenous pyruvate could be related to alteration in the cytosolic redox state, acid-base status, or improvement in antioxidant reserves.

This work was supported in part by the Office of Naval Research and the Office of Research and Development, Medical Research Service, Department of Veterans Affairs, and in part by the Division of Surgery, Walter Reed Army Institute of Research.

The opinions or assertions contained herein are the private views of the authors and are not to be construed as reflecting the views of

the Department of the Army, the Department of Defense, or the Department of Veterans Affairs.

REFERENCES

1. **Andreyev A and Fiskum G.** Calcium induced release of mitochondrial cytochrome *c* by different mechanisms selective for brain versus liver. *Cell Death Differ* 6: 825–832, 1999.
2. **Beech JS, Nolan KM, Iles RA, Cohen RD, Williams SC, and Evans SJ.** The effects of sodium bicarbonate and a mixture of sodium bicarbonate and carbonate ("Carbicarb") on skeletal muscle pH and hemodynamic status in rats with hypovolemic shock. *Metabolism* 43: 518–522, 1994.
3. **Benjamin E, Oropello JM, Abalos AM, Hannon EM, Wang JK, Fischer E, and Iberti TJ.** Effects of acid-base correction on hemodynamics, oxygen dynamics, and resuscitability in severe canine hemorrhagic shock. *Crit Care Med* 22: 1616–1623, 1994.
4. **Bernocchi P, Ceconi C, Cargnoni A, Pedersini P, Curello S, and Ferrari R.** Extraction and assay of creatine phosphate, purine, and pyridine nucleotides in cardiac tissue by reversed-phase high-performance liquid chromatography. *Anal Biochem* 222: 374–379, 1994.
5. **Borle AB and Stanko RT.** Pyruvate reduces anoxic injury and free radical formation in perfused rat hepatocytes. *Am J Physiol Gastrointest Liver Physiol* 270: G535–G540, 1996.
6. **Boulares AH, Zoltoski AJ, Contreras FJ, Yakovlev AG, Yoshihara K, and Smulson ME.** Regulation of DNAS1L3 endonuclease activity by poly(ADP-ribosyl)ation during etoposide-induced apoptosis. Role of poly(ADP-ribose) polymerase-1 cleavage in endonuclease activation. *J Biol Chem* 277: 372–378, 2002.
7. **Chang CG, Van Way CW, Dhar A, Helling T, and Hahn Y.** The use of insulin and glucose during resuscitation from hemorrhagic shock increases hepatic ATP. *J Surg Res* 92: 171–176, 2000.
8. **Clem RJ, Cheng EH, Karp CL, Kirsch DG, Ueno K, Takahashi A, Kastan MB, Griffin DE, Earnshaw WC, Veliuona MA, and Hardwick JM.** Modulation of cell death by Bcl-XL through caspase interaction. *Proc Natl Acad Sci USA* 95: 554–559, 1998.
9. **D'Arcangelo D, Facchiano F, Barlucchi LM, Melillo G, Illi B, Testolin L, Gaetano C, and Capogrossi MC.** Acidosis inhibits endothelial cell apoptosis and function and induces basic fibroblast growth factor and vascular endothelial growth factor expression. *Circ Res* 86: 312–318, 2000.
10. **Ding D, Moskowitz SI, Li R, Lee SB, Esteban M, Tomaselli K, Chan J, and Bergold PJ.** Acidosis induces necrosis and apoptosis of cultured hippocampal neurons. *Exp Neurol* 162: 1–12, 2000.
11. **Domenicotti C, Paola D, Vitali A, Nitti M, d'Abramo C, Cottalasso D, Maloberti G, Biasi F, Poli G, Chiarpotto E, Marinari UM, and Pronzato MA.** Glutathione depletion induces apoptosis of rat hepatocytes through activation of protein kinase C novel isoforms and dependent increase in AP-1 nuclear binding. *Free Radic Biol Med* 29: 1280–1290, 2000.
12. **Fernandes RS and Cotter TG.** Apoptosis or necrosis: intracellular levels of glutathione influence mode of cell death. *Biochem Pharmacol* 48: 675–681, 1994.
13. **Galvez A, Morales MP, Eltit JM, Ocaranza P, Carrasco L, Campos X, Sapag-Hagar M, Diaz-Araya G, and Lavandero S.** A rapid and strong apoptotic process is triggered by hyperosmotic stress in cultured rat cardiac myocytes. *Cell Tissue Res* 304: 279–285, 2001.
14. **Halestrap AP, Doran E, Gillespie JP, and O'Toole A.** Mitochondria and cell death. *Biochem Soc Trans* 28: 170–177, 2000.
15. **Halestrap AP, Kerr PM, Javadov S, and Woodfield KY.** Elucidating the molecular mechanism of the permeability transition pore and its role in reperfusion injury of the heart. *Biochim Biophys Acta* 1366: 79–94, 1998.
16. **Heckbert SR, Vedder NB, Hoffman W, Winn RK, Hudson LD, Jurkovich GJ, Copass MK, Harlan JM, Rice CL, and Maier RV.** Outcome after hemorrhagic shock in trauma patients. *J Trauma* 45: 545–549, 1998.
17. **Hirsch T, Susin SA, Marzo I, Marchetti P, Zamzami N, and Kroemer G.** Mitochondrial permeability transition in apoptosis and necrosis. *Cell Biol Toxicol* 14: 141–145, 1998.
18. **Kashiwagi A, Nishio Y, Asahina T, Ikebuchi M, Harada N, Tanaka Y, Takahara N, Taki H, Obata T, Hidaka H, Saeki Y, and Kikkawa R.** Pyruvate improves deleterious effects of high glucose on activation of pentose phosphate pathway and glutathione redox cycle in endothelial cells. *Diabetes* 46: 2088–2095, 1997.
19. **Kerr PM, Suleiman MS, and Halestrap AP.** Reversal of permeability transition during recovery of hearts from ischemia and its enhancement by pyruvate. *Am J Physiol Heart Circ Physiol* 276: H496–H502, 1999.
20. **Khan S and O'Brien P.** Rapid and specific efflux of glutathione before hepatocyte injury induced by hypoxia. *Biochem Biophys Res Commun* 238: 320–322, 1997.
21. **Kobelt F, Schreck U, and Henrich HA.** Involvement of liver in the decompensation of hemorrhagic shock. *Shock* 2: 281–288, 1994.
22. **Kroemer G, Dallaporta B, and Resche-Rigon M.** The mitochondrial death/life regulator in apoptosis and necrosis. *Annu Rev Physiol* 60: 619–642, 1998.
23. **Leist M, Gantner F, Bohlinger I, Tiegs G, Germann PG, and Wendel A.** Tumor necrosis factor-induced hepatocyte apoptosis precedes liver failure in experimental murine shock models. *Am J Pathol* 146: 1220–1234, 1995.
24. **Liaudet L, Soriano FG, Szabo E, Virag L, Mabley JG, Salzman AL, and Szabo C.** Protection against hemorrhagic shock in mice genetically deficient in poly(ADP-ribose)polymerase. *Proc Natl Acad Sci USA* 97: 10203–10208, 2000.
25. **Marchetti P, Castedo M, Susin SA, Zamzami N, Hirsch T, Macho A, Haeffner A, Hirsch F, Geuskens M, and Kroemer G.** Mitochondrial permeability transition is a central coordinating event of apoptosis. *J Exp Med* 184: 1155–1160, 1996.
26. **Marchetti P, Decaudin D, Macho A, Zamzami N, Hirsch T, Susin SA, and Kroemer G.** Redox regulation of apoptosis: impact of thiol oxidation status on mitochondrial function. *Eur J Immunol* 27: 289–296, 1997.
27. **Maulik N, Sasaki H, Addya S, and Das DK.** Regulation of cardiomyocyte apoptosis by redox-sensitive transcription factors. *FEBS Lett* 485: 7–12, 2000.
28. **McDonald MC, Mota-Filipe H, Wright JA, Abdelrahman M, Threadgill MD, Thompson AS, and Thiemermann C.** Effects of 5-aminoisoquinolinone, a water-soluble, potent inhibitor of the activity of poly (ADP-ribose) polymerase on the organ injury and dysfunction caused by haemorrhagic shock. *Br J Pharmacol* 130: 843–850, 2000.
29. **Mongan PD, Capacchione J, Fontana JL, West S, and Bunger R.** Pyruvate improves cerebral metabolism during hemorrhagic shock. *Am J Physiol Heart Circ Physiol* 281: H854–H864, 2001.
30. **Mongan PD, Fontana JL, Chen R, and Bunger R.** Intravenous pyruvate prolongs survival during hemorrhagic shock in swine. *Am J Physiol Heart Circ Physiol* 277: H2253–H2263, 1999.
31. **Niknahad H, Khan S, and O'Brien PJ.** Hepatocyte injury resulting from the inhibition of mitochondrial respiration at low oxygen concentrations involves reductive stress and oxygen activation. *Chem Biol Interact* 98: 27–44, 1995.
32. **Remmers DE, Wang P, Cioffi WG, Bland KI, and Chaudry IH.** Chronic resuscitation after trauma-hemorrhage and acute fluid replacement improves hepatocellular function and cardiac output. *Ann Surg* 227: 112–119, 1998.
33. **Sasaki H, Matsuno T, Nakagawa K, Matsuoka J, and Tanaka N.** Superoxide induces hepatocyte apoptosis during the early phase of reperfusion after murine liver ischemia. *Transplant Proc* 30: 2958–2959, 1998.
34. **Schafer FQ and Buettner GR.** Redox environment of the cell as viewed through the redox state of the glutathione disulfide/glutathione couple. *Free Radic Biol Med* 30: 1191–1212, 2001.
35. **Soldani C, Lazze MC, Bottone MG, Tognon G, Biggiogera M, Pellicciari CE, and Scovassi AI.** Poly(ADP-ribose) polymerase cleavage during apoptosis: when and where? *Exp Cell Res* 269: 193–201, 2001.
36. **Tejero-Taldo MI, Caffrey JL, Sun J, and Mallet RT.** Antioxidant properties of pyruvate mediate its potentiation of beta-

adrenergic inotropism in stunned myocardium. *J Mol Cell Cardiol* 31: 1863–1872, 1999.
37. **Thangaraju M, Sharma K, Leber B, Andrews DW, Shen SH, and Srikant CB.** Regulation of acidification and apoptosis by SHP-1 and Bcl-2. *J Biol Chem* 274: 29549–29557, 1999.
38. **Van Way CW, Dhar A, Reddy R, Evans L, Wogahn B, and Helling TS.** Changes in adenine nucleotides during hemorrhagic shock and reperfusion. *J Surg Res* 66: 159–166, 1996.
39. **Vieira HL, Haouzi D, El Hamel C, Jacotot E, Belzacq AS, Brenner C, and Kroemer G.** Permeabilization of the mitochondrial inner membrane during apoptosis: impact of the adenine nucleotide translocator. *Cell Death Differ* 7: 1146–1154, 2000.
40. **Wang P, Ba Z, Dean R, and Chaudry I.** ATP-$MgCl_2$ restores the depressed hepatocellular function and hepatic blood flow following hemorrhage and resuscitation. *J Surg Res* 50: 368–374, 1991.
41. **Wang P, Ba ZF, Morrison MH, Ayala A, and Chaudry IH.** Mechanism of the beneficial effects of pentoxifylline on hepatocellular function after trauma hemorrhage and resuscitation. *Surgery* 112: 451–458, 1992.
42. **Wang P, Hauptman JG, and Chaudry IH.** Hemorrhage produces depression in microvascular blood flow which persists despite fluid resuscitation. *Circ Shock* 32: 307–318, 1990.
43. **Wang P, Hauptman JG, and Chaudry IH.** Hepatocellular dysfunction occurs early after hemorrhage and persists despite fluid resuscitation. *J Surg Res* 48: 464–470, 1990.
44. **Wang TG, Gotoh Y, Jennings MH, Rhoads CA, and Aw TY.** Lipid hydroperoxide-induced apoptosis in human colonic CaCo-2 cells is associated with an early loss of cellular redox balance. *FASEB J* 14: 1567–1576, 2000.
45. **Watts JA, Grattan RM, Whitlow BS, and Kline JA.** Activation of poly(ADP-ribose) polymerase in severe hemorrhagic shock and resuscitation. *Am J Physiol Gastrointest Liver Physiol* 281: G498–G506, 2001.
46. **Yang Z, Zingarelli B, and Szabo C.** Effect of genetic disruption of poly (ADP-ribose) synthetase on delayed production of inflammatory mediators and delayed necrosis during myocardial ischemia-reperfusion injury. *Shock* 13: 60–66, 2000.

Review Article

Wien Klin Wochenschr (2002) 114/15–16: 671–677

wiener klinische wochenschrift
the middle european journal of medicine
Printed in Austria

Tubular apoptosis in the pathophysiology of renal disease

Peter Hauser and **Rainer Oberbauer**

Abteilung für Nephrologie, Universitätsklinik für Innere Medizin, Universität Wien, Vienna, Austria

Summary. Apoptosis of renal tubular epithelial cells plays a major role in acute renal failure. Several external and internal signals can induce apoptosis, which is then effectuated via several pathways. These pathways are either the FAS/FAS-L pathway and downstream MAPK (mitogen-activated protein kinases) and JNK (c-Jun N-terminal kinase) signal transduction, or the RANK/RANK-L (receptor activator of NFkB) pathway via activation of the caspase cascade. Other pathways, especially for apoptosis induction by toxins, include the mitochondrial permeability transition pore activation and Bcl-2 superfamily member differential regulation. An important final, irreversible branch of these pathways is the release of cytochrome c from the mitochondria, leading to nuclear fragmentation.

Therapeutic interventions of acute tubular injury focus on the prevention of apoptosis by either modulation of the balance of the bcl-2 family or by selectively blocking angiotensin receptors. It is not clear yet, which receptor blockade or combination of receptor blockers are most effective in apoptosis prevention.

In chronic renal failure, tubular apoptosis has been found in biopsies from polycystic kidneys, but not in a quantitatively meaningful amount in other chronic human renal diseases. On the other hand, given the short half-life of apoptotic cells of few hours, even low numbers over time might turn out to be important modulators of chronic kidney disease, which are characterized by tubular cell loss. Potential therapeutic interventions to prevent tubular apoptosis in chronic renal disease include angiotensin system inhibition, whereby the angiotensin II AT2 receptor blockade seems more promising in apoptosis inhibition than the inhibition of other receptor subtypes.

Key words: Angiotensin II, apoptosis, necrosis, renal failure.

Introduction

Cellular death is the main issue in ischemic acute and chronic renal failure. At least two pathophysiologically distinctly different forms of cell death, apoptosis and necrosis exist. Where necrosis represents a chaotic breakdown of irreversibly damaged cells, apoptosis is a highly choreographed process of removing isolated cells, leaving the surrounding tissue unaltered. Because of these highly structured pathways, therapeutic interventions are increasingly performed in order to prevent and treat acute as well as chronic renal tubular cell damage. Reviews covering similar topics are listed as references [1–3]. Although improvements in the course of progression and treatment of chronic renal failure have been achieved over the last decades, no such success was accomplished in the treatment or prevention of acute renal failure [4]. Morbidity and mortality of acute renal failure have remained nearly unchanged over the last three decades. The reasons are manifold, but the lack of understanding of the pathophysiological events during cell death on the molecular level might have contributed to this disappointing fact. Without the detailed knowledge of these processes, it is impossible to invent a specific treatment.

It has only recently been appreciated that not only necrosis, but also apoptosis of renal tubule cells play an important role in this setting [5]. Although there are fundamental differences between these two processes, some initial molecular pathways are shared between these two forms of cell death. A number of researchers even propose that these two events represent the margins of a common corridor of cellular fatality. As an example, mild cellular depletion of energy providing adenosine triphosphate (ATP) causes apoptosis, whereas profound ATP depletion leads to necrosis [6, 7]. Kerr and Wyllie first described apoptosis in liver cells [8]. Unlike necrosis, apoptosis is an active, energy consuming and highly choreographed process, which leads to the removal of dying cells without inflammation. Individual, lethally injured cells are removed from tissue, leaving the neighbouring cells unaffected. This is one of the key differences from necrosis, which usually affects an entire cluster or compound of cells and is associated with an inflammatory response. The main differences between these two processes are illustrated in Table 1. Although the term programmed cell death (PCD) is widely used synonymously for apoptosis, emerging evidence suggests that PCD should be reserved for the planned removal of cells in embryogenesis or physiological growth and organization of normally growing tissue. Thus the term PCD is not used in this review to describe the designed removal of lethally injured tubule cells.

Apoptosis

On a morphological basis, apoptosis can be described as the slow fade of injured cells, causing no alter-

Table 1. Differences between apoptosis and necrosis

Apoptosis	Necrosis
Programmed, choreographed active removal of unwanted cells (suicide)	Passive process, which affects clusters of lethally injured adjacent cell (murder)
Morphology	
Phosphatidylserin externalisation, cytoplasmic budding and blebbing, nuclear and cytoplasmic condensation, internucleosomal DNA fragmentation	Plasma membrane disruption, cytoplasmic swelling, lysis of cells and inflammation
Appearance of membrane bound cell segments (apoptotic bodies)	
Time course	
< 12 hours (similar in many types of cells)	Immediately after severe injury

ation to the surrounding tissue. This was in fact, the reason why this planned removal of cells was termed apoptosis. The Greek word "ptosis", as used for the drooping of the upper eyelid, describes the slow and harmonic down fall of leaves from a tree. This analogy was well chosen because on a morphological basis, apoptotic cells seem to be removed from the tissue in a silent and harmonical way, leaving the surrounding tissue unaltered. Conversely, necrosis represents a chaotic breakdown of injured cells, which massively influence the neighbouring tissue. Local inflammation and alteration of the neighbouring cells are the consequence of cellular disintegrity of lysed cells.

1. Morphology of apoptotic cell death

One of the first events in cells prone to apoptosis, is the externalisation of the membrane bound phosphatidylserin, which can be identified by the ligation to Annexin V. Following this externalisation, cytoplasmic budding and blebbing, as well as cytoplasmic condensation occur, but leave cellular organelles intact. At the same time, nuclear shrinkage and lateralization arise. The internucleosomal DNA fragmentation represents one of the final events in apoptosis, taking place just before the cellular remains are phagocytosed. The internucleosomal fragmentation can be stained and visualized by the TUNEL technique (terminal deoxynucleotidyl transferase biotin-dUTP nick end labeling). It has been estimated that the duration of this evolutionary conserved process takes only few hours from apoptosis induction until disappearance of the cell [9].

2. Pro- and antiapoptotic stimuli

Apoptosis of cells can be triggered by external and internal factors. External stimuli can be the withdrawal of growth factors as evidenced by the culture of tubule cells in serum free media, some drugs or temporary ischemia. Addition of insulin, insulin like growth factor (IGF), hepatocyte growth factor (HGF) or epidermal growth factor (EGF) can rescue some apoptotic cells, which have been subjected to nutritional deprivation. Internal apoptotic stimuli are ligation of cell surface molecules, such as members of the TNF superfamily to their ligand. This event has been found to induce apoptosis in renal cells. Among the most prominent members of the TNF family are FAS and FAS-ligand, TNF-α and TNF-receptor [10, 11]. They signal via the caspase system, which consists of at least 14 members in mammalian cells and represents one of the final apoptotic pathways. Caspases are proteases; so far more than 40 different protein substrates have been identified. Among these substrates is a nuclease, which causes an internucleosomal cleavage and fragmentation of DNA, one of the hallmarks of apoptosis. However, this DNA fragmentation is not specific for apoptosis, as similar events have been described to occur in necrosis.

There are many other external stimuli that have been shown to induce apoptosis in renal cells. Examples are toxins such as: actinomycin B, cisplatin, doxorubicin, shigatoxin; immunosuppressive drugs such as: immunophyllins, thiazide diuretics or even high doses of flouroquinolone antibiotics [12–18]. Reactive oxygen radicals, mercury and cadmium are capable of apoptosis induction but the list is far away from being complete [19–21]. Wang and co-workers demonstrated that transfection and overexpression of FAS-L in renal tubule cells, did not lead to an increased susceptibility to apoptosis after lipopolysaccaride stiumulation. The transfected tubule cells however, induced apoptosis of activated leukocytes [22].

Internal apoptotic stimuli – intracellular signal transduction: Similar to the complement cascade, where a classical and alternative pathway has been described, apoptosis can occur by using one of several pathways. As mentioned above, the caspase cascade can be activated, leading to cleavage of substrates until the final effector caspases 3, 6 and 7 are activated leading ultimately to apoptosis. There is a mitogen-activated protein kinases pathway (MAPK), which transduces a signal from receptor tyrosine kinases (RTKs), through the MAP kinase (MAPK) cascade, leading to a change in gene expression patterns and/or apoptosis, for example, via JNK (c-Jun N-terminal kinase) and bcl-2 members. Other internal apoptosis pathways consist of tumor suppressor gene activation and inhibition in cell cycle progression. The cells either return to the G0 phase or commit apoptosis. Besides the described signaling pathway, several other trails for apoptosis induction have been discovered [3].

3. Mitochondria and activation of caspases

For many stimuli, the final process of apoptosis induction is mediated via the mitochondrial release of cytochrome c and caspase activation, leading to DNA fragmentation. Once this has happened, there is no rescue and the cell is prone to die. The bcl-2 superfamily consists of pro- and antiapoptotic members, which are bound to the mitochondrial membrane. By heterodimerization, pro- and antiapoptotic members are balanced, thereby preventing the opening of the mitochondrial permeability transition pore and the cytochrome c release. If the proapoptotic members such as bax, bcl-xS or bak are produced in excess compared to the antiapoptotic members such as bcl-2 itself, bcl-xL or bik however, the permeability pore will open and cytochrome c will be released [23–26]. This has been shown, for example, for cisplatin induced tubular apoptosis [27].

A simplified cartoon of the current understanding of the apoptosis cascade and the several possible pathways is given in Fig. 1.

Acute renal failure

Apoptotic death of tubule epithelial cells has been studied in various forms of acute renal failure [28]. Sheridan et al. and Rana et al. recently reviewed the potential interventions to prevent and treat apoptotic tubular cell death in acute renal failure [29, 30]. Among the best-studied and clinically most relevant forms of acute renal failure is acute ischemic injury, which will be highlighted in this paper. Many investigators used rodent models to study the morphological and molecular events of tubular apoptosis after renal reperfusion injury. They all found a significant increase of tubular apoptosis after reperfusion [10, 11, 31–37]. We used a rat model of unilateral nephrectomy and contralateral cross clamping of the renal artery, because it more closely resembles the clinical situation of ischemic acute renal failure (ARF). ARF in humans predominantly occurs in patients with pre-existing renal impairment and thus reduced nephron numbers. The time points we investigated were: one hour, one day, seven days and twenty weeks after reperfusion [37]. Apoptosis of tubular cells peaked at one day and was still present after seven days, but not after twenty weeks. Proliferation of sub-lethally injured cells occurred as quickly as one day after the insult, decreased after one week, but reoccurred at twenty weeks, where cystic dilation and an increase of whole kidney weight was observed. Another reason for using the model of uninephrectomy and contralateral ischemia is that it closely resembles the most frequent clinical situation of ARF; the posttransplant ARF.

In the clinical situation of renal transplantation, an initially healthy donor kidney is subjected to warm ischemia during harvesting and about 30 minutes during anastomosis preparation. During cold ischemic preservation, no apoptosis can occur, because at 4 °C all active cell processes cease. Posttransplant ARF occurs in 20 to 40% of cases, and represents the most prevalent risk factor for reduced long-term graft survival [38, 39]. Ojo and coworkers analysed the USRDS data of 42,000 patients after renal transplantation between 1992 and 1998. The relative risk of reduced transplant survival was calculated to be 1.99 in allograft recipients with ARF [40]. Therefore, a parameter which can predict the subsequent development of ARF, would be helpful in the clinical setting since special measures could be undertaken in those patients at risk. These interventions would include the delayed use of calcineurin antagonist, for example. On a morphological and demographic base, such a marker does not exist. We were able to demonstrate however, that the number of apoptotic cells found in donor kidney biopsies, which were obtained before transplantation into the recipients,

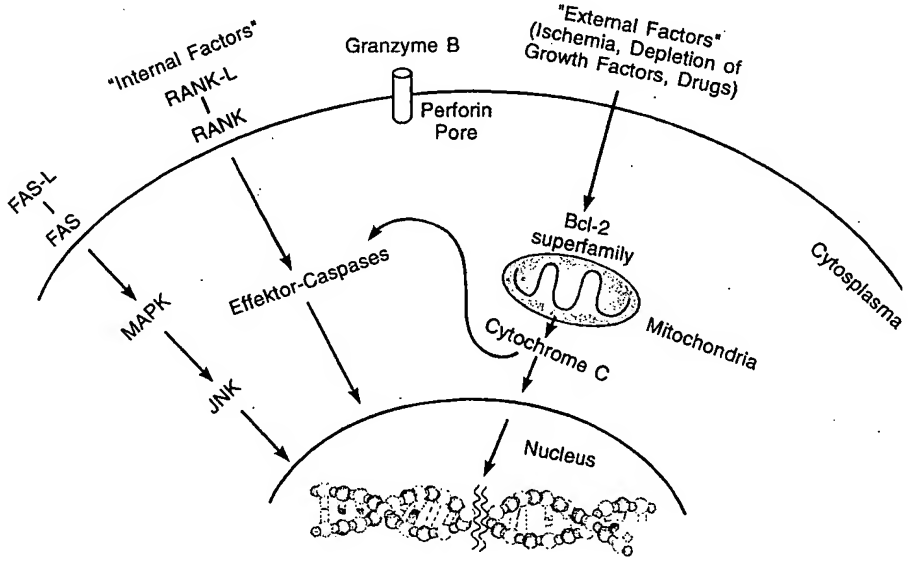

Fig. 1. Apoptosis cascade, "internal" and "external" induction of apoptosis. This drawing represents a very simplified version of the complex interactions and manifold pathways involved in apoptosis induction and execution. Only the best described regulators and pathways are illustrated. The internucleosomal cleavage of DNA represents the final, irreversible pathway of cellular apoptosis. *FAS* CD95 (L-ligand); *RANK* receptor activator of NFkB (L-ligand); *MAPK* mitogen-activated protein kinases

was significantly higher in those patients with subsequent ARF [41]. We furthermore observed a misbalance of the bcl-2 members. The antiapoptotic bcl-2 was down-regulated in those tubule cells, which were undergoing apoptosis.

Interventions to prevent tubular apoptosis in acute renal failure

A reasonable approach towards prevention of apoptotic cell death is the external supplementation of bcl-2 peptide or suppression of the proapoptotic members of the bcl-2 family. To test this hypothesis, we designed artificial peptides of the bcl-2 family, namely bcl-2 itself, bax and bak, and injected them into renal tubular cells [9, 42]. The antiapoptotic members, such as bcl-2, prevented tacrolimus induced cell death, bax and bak induced apoptosis after microinjection. A FITC labelled control peptide was ineffective in either apoptosis prevention or induction (Fig. 2 adapted from AJPysiol). It has been shown by other investigators, that bcl-2 and bcl-xL over-expression can exert antiapoptotic activity in glioma cells [43]. Cheng and co-workers found similar results in bcl-2 transfected tubule cells after H2O2 induction of apoptosis [44]. Since this is a feasible approach in renal transplantation, where the manipulation of the kidney can be performed *ex vivo*, it is certainly not easily practicable in native renal ARF. Therefore other antiapoptotic approaches need to be tested. Dai and colleagues transfected tubule cells with HGF and were able to demonstrate that this single transfection could ameliorate the severity of folic acid induced acute renal failure and promoted regeneration. Expression of HGF transgene activated protein kinase B/Akt and preserved Bcl-xL protein expression *in vivo* [45].

One of the methods could be the use of selective angiotensin II AT 2 receptor blockers. In this issue of the journal we were able to show that physiological concentrations of angiotensin II can cause apoptosis in cultured human tubule cells [46]. This effect is mediated via the AT2 receptor, since a specific blockade of this receptor using the drug PD123319 inhibited the angiotensin II induced apoptosis, whereas the addition of the specific angiotensin II AT1 receptor was ineffective in apoptosis prevention. Hruska and co-workers did not find a preventive effect of the ACE inhibitor perindopril in ureteral obstruction [47] Other researches have shown reduced apoptosis of tubule cells by using angiotensin converting enzyme inhibitors or angiotensin II AT1 blocker [48, 49]. An overview of the different studies is given in Table 2. Possible explanations for the discrepancies between the findings of these studies are discussed in the following section of chronic renal failure.

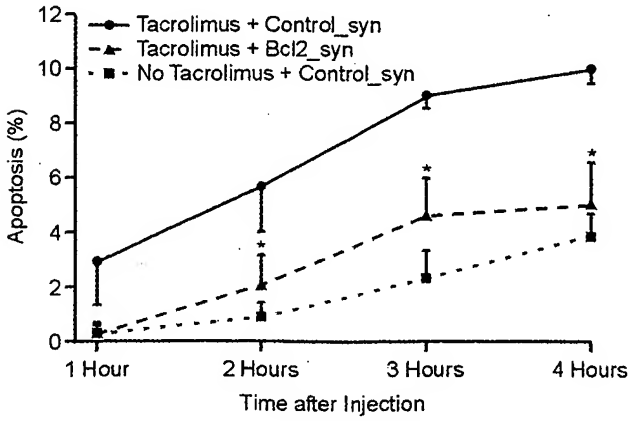

Fig. 2. Microinjection of synthetically derived BH4 domain of the bcl-2 peptide into renal proximal tubule epithelial cells prevented tacrolimus induced apoptosis. The microinjection of a nonsense control peptide was ineffective in apoptosis prevention (with permission from Am J Physiol [9])

Chronic renal failure

Apoptosis of tubule cells in chronic renal failure is not as prominent as in acute renal failure. However, several studies described tubular apoptosis to be a key feature of progressing renal insufficiency. Woo reported the detection of DNA fragmentation in glomeruli, in cyst walls, and in both cystic and non-cystic tubules of polycystic kidneys but not in kidneys from patients with IgA nephropathy, nephrosclerosis, focal glomerulosclerosis or diabetic nephropathy [50]. The author speculated that tubular apoptosis contributes to the progressive deteriorating nature of polycystic kidney disease. The limitation of these findings is the definition of apoptosis solely by DNA fragmentation. It is therefore not surprising, that no apoptosis was found in the other chronic kidney diseases investigated.

It has been shown in animal models, as well as in biopsies from human kidneys, that ureteral obstruction causes tubular apoptosis. Truong et al. found caspase 3 significantly up-regulated and concluded that among other caspases, which regulate apoptosis of tubular and interstitial cells in obstructive uropathy, caspase 3 is especially important for the execution of apoptosis [51]. There are reports in animal models that apoptosis of podocytes occurs in TGF-β transgenic mice and might contribute to their deletion in progressive glomerulosclerosis. The kinase Smad7 served as amplifier of TGF-β [52].

The effects of angiotensin II and the angiotensin receptor, with respect to apoptosis regulation in chronic kidney disease, are not clear now. In an experimental study by Aizawa and colleagues, angiotensin II infusion caused apoptosis in tubule cells of rats, but the infusion of norepinephrin to achieve similar elevation in blood pressure did not lead to apoptosis [53]. This effect was paralleled by a sevenfold increase of bax protein. Interestingly, angiotensin II induced apoptosis could be completely blocked by the AT1 blocker losartan, but not by hydralazin. On the other hand, the AT1 blocker was ineffective but the AT2 blocker most potent in prevention of angiotensin II induced apoptosis in the cell culture study by Weidekamm et al. [46]. This discrepancy in findings might be explained by a blood pressure reduction by losartan in the *in vivo* experiments, compared to the *in vitro* study by Weidekamm et al. It has been shown previously, that blood pressure per se can induce apoptosis of renal cells [54]. Kelly and co-workers showed apoptosis of tubule cells in the streptozotozin model of diabetes in rats, which was associated with up-regulation of TGF-β and suppression of epidermal growth factor (EGF) [48]. The ACE inhibitor perindopril as well as the AT1 blocker

Table 2. Studies investigating the differential effects of angiotensin receptor subtypes on apoptosis of tubule epithelial cells

Study	Involvement of angiotensin receptors		References
	AT1	AT2	
In vitro study of human renal proximal tubule cells		•	[46]
In vivo rat model of unilateral obstruction		•	[56, 57]
In vitro rat model of angiotensin II/norepinephrin infusion	•	•	[49, 53]
Calcineurin antagonist induced apoptosis *in vitro* and *in vivo*	•		[9, 58]

valsartan reduced the number of apoptortic cells, but probably via suppression of TGF-β and normalization of EGF. The same group however, showed that the AT2 receptor is expressed in adult rat kidney and that it promotes cell proliferation and apoptosis. Given this dual mode of action, it is very likely that many pathways downstream of the angiotensin receptor subtypes are involved in these processes. This might be another explanation for the heterogeneous findings with regards to angiotension II stimulation as well as apoptosis and proliferation. Table 2 summarizes the published data on the effect of either AT1 or AT2 receptor blockade on apoptosis. Bonnet and colleagues published a detailed review about this subject [55].

Conclusions

Apoptotic cell death contributes to renal tubular cell fade in acute as well as in chronic renal disease. The regulation of the processes and pathways has been studied more thoroughly in acute renal failure. The Bcl-2 superfamily plays a key role in the apoptosis effector phase. Therefore therapeutic and preventive interventions in acute renal failure focus on the differential regulation and iatrogenic suppression or overexpression of the pro- and antiapoptotic Bcl-2 members respectively. In chronic renal failure, the absolute amount of tubule cells which died by apoptosis in a defined time frame is hard to estimate, but the contribution of tubular apoptosis to the progression of renal failure is widely accepted. Among other signal transduction pathways, angiotensin II receptors seem to play a main role in the differential regulation of this process. Therefore, selective angiotensin II receptor antagonists are under heavy investigation in the prevention of tubular apoptosis in various forms of progressive renal failure.

Sources of support

Else Kröner Fresenius Stiftung, Germany, and the Bürgermeisterfonds of the city of Vienna, Austria.

References

1. Lieberthal W, Koh JS, Levine JS (1998) Necrosis and apoptosis in acute renal failure. Semin Nephrol 18: 505–518
2. De Broe ME (2001) Apoptosis in acute renal failure. Nephrol Dial Transplant 16: 23–26
3. Ueda N, Kaushal GP, Shah SV (2000) Apoptotic mechanisms in acute renal failure. Am J Med 108: 403–415
4. Druml W (1999) Nothing new in treatment of acute renal failure? Wien Klin Wochenschr 111: 126–128
5. Ueda N, Shah SV (2000) Tubular cell damage in acute renal failure-apoptosis, necrosis, or both. Nephrol Dial Transplant 15: 318–323
6. Wiegele G, Brandis M, Zimmerhackl LB (1998) Apoptosis and necrosis during ischaemia in renal tubular cells (LLC-PK1 and MDCK). Nephrol Dial Transplant 13: 1158–1167
7. Allen J, Winterford C, Axelsen RA, Gobe GC (1992) Effects of hypoxia on morphological and biochemical characteristics of renal epithelial cell and tubule cultures. Ren Fail 14: 453–460
8. Kerr JF, Wyllie AH, Currie AR (1972) Apoptosis: a basic biological phenomenon with wide-ranging implications in tissue kinetics. Br J Cancer 26: 239–257
9. Peherstorfer E, Mayer B, Böhm S, Lukas A, Hauser P, Mayer G, et al (2002) Effects of microinjection of synthetic Bcl-2 family member domain peptides on apoptosis of renal tubular epithelial cells. Am J Physiol Renal Physiol (in press)
10. Nagata S, Golstein P (1995) The Fas death factor. Science 267: 1449–1456
11. Baker SJ, Reddy EP (1998) Modulation of life and death by the TNF receptor superfamily. Oncogene 17: 3261–3270
12. Shinozaki M, Hirahashi J, Lebedeva T, Liew FY, Salant DJ, Maron R, et al (2002) IL-15, a survival factor for kidney epithelial cells, counteracts apoptosis and inflammation during nephritis. J Clin Invest 109: 951–960
13. Kaushal GP, Kaushal V, Hong X, Shah SV (2001) Role and regulation of activation of caspases in cisplatin-induced injury to renal tubular epithelial cells. Kidney Int 60: 1726–1736
14. van de Water B, Houtepen F, Huigsloot M, Tijdens IB (2001) Suppression of chemically induced apoptosis but not necrosis of renal proximal tubular epithelial (LLC-PK1) cells by focal adhesion kinase (FAK). Role of FAK in maintaining focal adhesion organization after acute renal cell injury. J Biol Chem 276: 36183–36193
15. Kiyokawa N, Taguchi T, Mori T, Uchida H, Sato N, Takeda T, et al (1998) Induction of apoptosis in normal human renal tubular epithelial cells by Escherichia coli Shiga toxins 1 and 2. J Infect Dis 178: 178–184
16. Cheng CH, Hsieh CL, Shu KH, Chen YL, Chen HC (2002) Effect of calcium channel antagonist diltiazem and calcium ionophore A23187 on cyclosporine A-induced apoptosis of renal tubular cells. FEBS Lett 516: 191–196
17. Loffing J, Loffing-Cueni D, Hegyi I, Kaplan MR, Hebert SC, Le Hir M, et al (1996) Thiazide treatment of rats provokes apoptosis in distal tubule cells. Kidney Int 50: 1180–1190
18. Dharnidharka VR, Nadeau K, Cannon CL, Harris HW, Rosen S (1998) Ciprofloxacin overdose: acute renal failure with prominent apoptotic changes. Am J Kidney Dis 31: 710–712

19. Lieberthal W, Triaca V, Koh JS, Pagano PJ, Levine JS (1998) Role of superoxide in apoptosis induced by growth factor withdrawal. Am J Physiol 275: F691–702
20. Duncan-Achanzar KB, Jones JT, Burke MF, Carter DE, Laird HE, 2nd (1996) Inorganic mercury chloride-induced apoptosis in the cultured porcine renal cell line LLC-PK1. J Pharmacol Exp Ther 277: 1726–1732
21. Shibutani M, Mitsumori K, Niho N, Satoh S, Hiratsuka H, Satoh M, et al (2000) Assessment of renal toxicity by analysis of regeneration of tubular epithelium in rats given low-dose cadmium chloride or cadmium-polluted rice for 22 months. Arch Toxicol 74: 571–577
22. Wang Y, Yi S, Tay YC, Feng X, Kairaitis L, Harris DC (2002) Transfection of tubule cells with Fas ligand causes leukocyte apoptosis. Kidney Int 61: 1303–1311
23. Chittenden T, Harrington EA, O'Connor R, Flemington C, Lutz RJ, Evan GI, et al (1995) Induction of apoptosis by the Bcl-2 homologue Bak. Nature 374: 733–736
24. Gobe G, Zhang XJ, Willgoss DA, Schoch E, Hogg NA, Endre ZH (2000) Relationship between expression of Bcl-2 genes and growth factors in ischemic acute renal failure in the rat. J Am Soc Nephrol 11: 454–467
25. Oltvai ZN, Milliman CL, Korsmeyer SJ (1993) Bcl-2 heterodimerizes in vivo with a conserved homolog, Bax, that accelerates programmed cell death. Cell 74: 609–619
26. Oltvai ZN, Korsmeyer SJ (1994) Checkpoints of dueling dimers foil death wishes. Cell 79: 189–192
27. Park MS, De Leon M, Devarajan P (2002) Cisplatin induces apoptosis in LLC-PK1 cells via activation of mitochondrial pathways. J Am Soc Nephrol 13: 858–865
28. Schwarz C, Gruber U, Oberbauer R (2000) Pathophysiology of acute renal failure at the cellular level. Wien Klin Wochenschr 112: 5–15
29. Sheridan AM, Bonventre JV (2000) Cell biology and molecular mechanisms of injury in ischemic acute renal failure. Curr Opin Nephrol Hypertens 9: 427–434
30. Rana A, Sathyanarayana P, Lieberthal W (2001) Role of apoptosis of renal tubular cells in acute renal failure: therapeutic implications. Apoptosis 6: 83–102
31. Schumer M, Colombel MC, Sawczuk IS, Gobe G, Connor J, O'Toole KM, et al (1992) Morphologic, biochemical, and molecular evidence of apoptosis during the reperfusion phase after brief periods of renal ischemia. Am J Pathol 140: 831–838
32. Nakajima T, Miyaji T, Kato A, Ikegaya N, Yamamoto T, Hishida A (1996) Uninephrectomy reduces apoptotic cell death and enhances renal tubular cell regeneration in ischemic ARF in rats. Am J Physiol 271: F846–853
33. Yin T, Sandhu G, Wolfgang CD, Burrier A, Webb RL, Rigel DF, et al (1997) Tissue-specific pattern of stress kinase activation in ischemic/reperfused heart and kidney. J Biol Chem 272: 19943–19950
34. Nogae S, Miyazaki M, Kobayashi N, Saito T, Abe K, Saito H, et al (1998) Induction of apoptosis in ischemia-reperfusion model of mouse kidney: possible involvement of Fas. J Am Soc Nephrol 9: 620–631
35. Raafat AM, Murray MT, McGuire T, DeFrain M, Franko AP, Zafar RS, et al (1997) Calcium blockade reduces renal apoptosis during ischemia reperfusion. Shock 8: 186–192
36. Beeri R, Symon Z, Brezis M, Ben-Sasson SA, Baehr PH, Rosen S, et al (1995) Rapid DNA fragmentation from hypoxia along the thick ascending limb of rat kidneys. Kidney Int 47: 1806–1810
37. Oberbauer R, Schwarz C, Regele HM, Hansmann C, Meyer TW, Mayer G (2001) Regulation of renal tubular cell apoptosis and proliferation after ischemic injury to a solitary kidney. J Lab Clin Med 138: 343–351
38. van Valenberg PL, Hoitsma AJ, Tiggeler RG, Berden JH, van Lier HJ, Koene RA (1987) Mannitol as an indispensable constituent of an intraoperative hydration protocol for the prevention of acute renal failure after renal cadaveric transplantation. Transplantation 44: 784–788
39. Hall BM, Tiller DJ, Duggin GG, Horvath JS, Farnsworth A, May J, et al (1985) Post-transplant acute renal failure in cadaver renal recipients treated with cyclosporine. Kidney Int 28: 178–186
40. Ojo AO, Hanson JA, Meier-Kriesche H, Okechukwu CN, Wolfe RA, Leichtman AB, et al (2001) Survival in recipients of marginal cadaveric donor kidneys compared with other recipients and wait-listed transplant candidates. J Am Soc Nephrol 12: 589–597
41. Oberbauer R, Rohrmoser M, Regele H, Muhlbacher F, Mayer G (1999) Apoptosis of tubular epithelial cells in donor kidney biopsies predicts early renal allograft function. J Am Soc Nephrol 10: 2006–2013
42. Siehs C, Oberbauer R, Mayer G, Lukas A, Mayer B (2002) Discrete simulation of regulatory homo- and heterodimerization in the apoptosis effector phase. Bioinformatics 18: 67–76
43. Sawada M, Nakashima S, Banno Y, Yamakawa H, Takenaka K, Shinoda J, et al (2000) Influence of Bax or Bcl-2 overexpression on the ceramide-dependent apoptotic pathway in glioma cells. Oncogene 19: 3508–3520
44. Ichimiya M, Chang SH, Liu H, Berezesky IK, Trump BF, Amstad PA (1998) Effect of Bcl-2 on oxidant-induced cell death and intracellular Ca2+ mobilization. Am J Physiol 275: C832–839
45. Dai C, Yang J, Liu Y (2002) Single injection of naked plasmid encoding hepatocyte growth factor prevents cell death and ameliorates acute renal failure in mice. J Am Soc Nephrol 13: 411–422
46. Weidekamm C, Hauser P, Hansmann C, Schwarz C, Klingler C, Mayer G, et al (2002) Effects of AT1 and AT2 receptor blockade on angiotensin II induced apoptosis of human renal proximal tubular epithelial cells. Wien Klin Wochenschr 114: 725–729
47. Hruska KA, Guo G, Wozniak M, Martin D, Miller S, Liapis H, et al (2000) Osteogenic protein-1 prevents renal fibrogenesis associated with ureteral obstruction. Am J Physiol Renal Physiol 279: F130–143
48. Kelly DJ, Cox AJ, Tolcos M, Cooper ME, Wilkinson-Berka JL, Gilbert RE (2002) Attenuation of tubular apoptosis by blockade of the renin-angiotensin system in diabetic Ren-2 rats. Kidney Int 61: 31–39
49. Cao Z, Kelly DJ, Cox A, Casley D, Forbes JM, Martinello P, et al (2000) Angiotensin type 2 receptor is expressed in the adult rat kidney and promotes cellular proliferation and apoptosis. Kidney Int 58: 2437–2451
50. Woo D (1995) Apoptosis and loss of renal tissue in polycystic kidney diseases. N Engl J Med 333: 18–25
51. Truong LD, Choi YJ, Tsao CC, Ayala G, Sheikh-Hamad D, Nassar G, et al (2001) Renal cell apoptosis in chronic obstructive uropathy: the roles of caspases. Kidney Int 60: 924–934
52. Schiffer M, Bitzer M, Roberts IS, Kopp JB, ten Dijke P, Mundel P, et al (2001) Apoptosis in podocytes induced by TGF-beta and Smad7. J Clin Invest 108: 807–816
53. Aizawa T, Ishizaka N, Kurokawa K, Nagai R, Nakajima H, Taguchi J, et al (2001) Different effects of angiotensin II and catecholamine on renal cell apoptosis and proliferation in rats. Kidney Int 59: 645–653

54. Orlov SN, Tremblay J, Deblois D, Hamet P (2002) Genetics of programmed cell death and proliferation. Semin Nephrol 22: 161–171
55. Bonnet F, Cao Z, Cooper ME (2001) Apoptosis and angiotensin II: yet another renal regulatory system? Exp Nephrol 9: 295–300
56. Morrissey JJ, Klahr S (1999) Effect of AT2 receptor blockade on the pathogenesis of renal fibrosis. Am J Physiol 276: F39–45
57. Ma J, Nishimura H, Fogo A, Kon V, Inagami T, Ichikawa I (1998) Accelerated fibrosis and collagen deposition develop in the renal interstitium of angiotensin type 2 receptor null mutant mice during ureteral obstruction. Kidney Int 53: 937–944
58. Thomas SE, Andoh TF, Pichler RH, Shankland SJ, Couser WG, Bennett WM, et al (1998) Accelerated apoptosis characterizes cyclosporine-associated interstitial fibrosis. Kidney Int 53: 897–908

(Received April 2, 2002, accepted after revision June 3, 2002)

Correspondence: Rainer Oberbauer, M.D., Abteilung für Nephrologie und Dialyse, Universitätsklinik für Innere Medizin III, Währinger Gürtel 18–20, A-1090 Vienna, Austria,
E-mail: rainer.oberbauer@akh-wien.ac.at

Kidney International, Vol. 60 (2001), pp. 1765–1776

Caspase-3 and apoptosis in experimental chronic renal scarring

BIN YANG, A. MEGUID EL NAHAS, GRAHAM L. THOMAS, JOHN L. HAYLOR, PHILIP F. WATSON, BART WAGNER, and TIMOTHY S. JOHNSON

Sheffield Kidney Institute, Division of Clinical Sciences, and Department of Histopathology, Northern General Hospital Trust, Sheffield University, Sheffield, England, United Kingdom

Caspase-3 and apoptosis in experimental chronic renal scarring.

Background. Caspase-3 is a member of the caspase enzyme family, having a central role in the execution of apoptosis. However, the significance of Caspase-3 in the inappropriate and excessive apoptosis that contributes to the progression of non-immune–mediated renal scarring has not been established.

Methods. Kidneys from sham-operated and subtotal nephrectomized (SNx) rats were harvested on days 7, 15, 30, 60, 90 and 120 post-surgery. These were analyzed for apoptosis (in situ end labeling of DNA, light and electron microscopy), Caspase-3 activity (fluorometric substrate cleavage assay), protein and mRNA (Western and Northern blotting), as well as distribution (immunohistochemistry), inflammation (ED-1 immunohistochemistry) and fibrosis (Masson's Trichrome staining).

Results. Apoptosis, inflammation and fibrosis gradually increased in glomeruli, tubules and interstitium of SNx rats. Caspase-3 was mainly located in damaged tubules, but also was found in some glomerular and interstitial cells. Little or no staining was noted in sham-operated kidneys. In SNx kidneys, Caspase-3 activity was significantly increased from day 30 and peaked on day 120 (2.5-fold). This resulted from increases in the 17 and 24 kD active protein subunits. The 32 kD precursor was increased at all time points (1861% on day 120, $P < 0.01$). Caspase-3 changes were transcription-dependent with the 2.7 kb caspase-3 mRNA significantly increased at all time points (287% on day 120). Caspase-3 activity was a better predictor of apoptosis (Std β coefficient = 0.347, $P < 0.05$) than Caspase-3 proteins or mRNA; however, Caspase-3 at all levels correlated with apoptosis, inflammation and fibrosis (all $P < 0.01$).

Conclusions. Up-regulation of apoptosis in remnant kidneys is likely to be Caspase-3-dependent as it is associated with increases in Caspase-3 at the activity, protein and mRNA levels. Therefore, Caspase-3 is a potential therapeutic target for the modification of renal cell apoptosis and subsequently renal fibrosis.

Apoptosis plays a dual role in the evolution of renal scarring with potential beneficial and harmful influences [1]. The resolution of renal inflammatory changes depends to a large extent on the apoptosis of infiltrating inflammatory cells in addition to their migration out of the kidneys when the initial insult has subsided [2]. On the other hand, inappropriate regulation of apoptosis may lead to an ongoing proliferation of these cells within the kidneys leading to the initiating and progression of renal fibrosis [1]. The harmful side of apoptosis in relation to renal scarring pertains to the deletion by this programmed cell death process of intrinsic renal cells [3, 4]. Such a mechanism has been put forward to explain experimental progressive glomerulosclerosis [3, 4] and tubular atrophy [5] and the ensuing tubulointerstitial fibrosis.

This has been postulated in the remnant kidney model of renal scarring in rats, where ongoing deletion of glomerular cells through apoptosis was instrumental in the progression of glomerulosclerosis [3]. In the same model, we have demonstrated the progressive increase in apoptosis of tubular and interstitial cells, thus contributing to tubular atrophy and the associated renal fibrosis [6].

While it is clear that apoptosis is associated with the progression of chronic experimental and clinical renal diseases [3–6], questions remain as to the causal link and the precise mechanisms and mediators linking programmed cell death with renal fibrosis. The identification of key mediators involved in apoptosis and renal scarring may allow for therapeutic interventions based on their manipulations and aimed at inhibiting renal atrophy, fibrosis and scarring.

An increasing body of evidence suggests that caspases (cysteine proteases) play an essential role in both the regulation and execution phases of apoptotic cell death and act upstream of DNA fragmentation [7, 8]. To date, a family of 14 different caspases has been identified that play a role in both inflammation and apoptosis [8]. They are all produced as inactive precursors (zymogens) that are processed into the large and small active subunits [9]. Caspases are highly specific with an absolute requirement for cleavage after aspartic acid, while individual caspase recognize different tetrapeptide motifs, which might explain their individual substrate specificity [8]. Caspases have diverse functions, with members of this

Key words: programmed cell death, inflammation, subtotal nephrectomy, kidney lesions, tubular atrophy, fibrosis, inflammation.

Received for publication March 8, 2001
and in revised form June 18, 2001
Accepted for publication June 20, 2001

family playing essential roles in both initial signaling events (Caspase-8, Caspase-9) and the downstream proteolytic cleavages (Caspase-3) [7, 8]. Caspase-3 (CPP32, YAMA or apopain) is thought to be key executor of apoptosis and is activated via the mitochondrial (Bcl-2/Bax, Caspase-9), death receptor (Fas/FasL, Caspase-8), or endoplasmic reticulum (Caspase-12) routes [7, 10]. Protease inhibitors, including macromolecular and peptide-based inhibitors of caspases, are highly effective in preventing apoptotic cell death in both in vitro and in vivo models of apoptosis [8, 11].

We have recently observed changes of Caspase-3 in an immune-mediated glomerulonephritis model of renal scarring [12]. This suggested that Caspase-3 is associated with apoptosis, inflammation and fibrosis, and highlighted it as a potential therapeutic target for preventing renal scarring. However, there are no data concerning changes of Caspase-3 during the progression of renal scarring in non-immune–mediated chronic renal scarring. With that in mind, we have measured Caspase-3 activity, protein and mRNA levels throughout the 120-day course of renal scarring in rats submitted to extensive renal ablation, and correlated the observed changes with those of apoptosis, inflammation and fibrosis during the progression of the disease.

METHODS

Experimental animals and protocol

Male Wistar rats (Sheffield University strain) weighing 250 to 300 g were subjected to subtotal (5/6) nephrectomy (SNx). Rats were housed at constant temperature (20°C) and humidity (45%) on a 12-hour light/dark cycle. They were fed ad libitum on standard laboratory rat chow (Lab Sure Ltd., March, Cambridge, UK) and had free access to tap water. Subtotal nephrectomy was undertaken in 32 rats as a one-step procedure: left 2/3 nephrectomy through the ligation and ablation of the kidney upper and lower poles as well as a right uninephrectomy [13]. Rats were sacrificed in groups (N = 4 to 6) at days 7, 15, 30, 60, 90 and 120 after SNx. Sham-operated rats (N = 29) were used as controls, being sacrificed at the same time points as those with SNx. Rats were housed in metabolic cages for 24 hours prior to sacrifice to facilitate urine collection. All the experiments were carried out according to the rules and regulations laid down by the Home Office (Animal Scientific Procedure Act 1986, UK).

Removed kidney tissue was fixed in formal calcium [4% (wt/vol) paraformaldehyde and 2% (wt/vol) calcium chloride, pH 7.4] and paraffin-embedded for histological and immunohistochemical examination. For electron microscopy, small tissue blocks were fixed in 2.5% (vol/vol) glutaraldehyde solution in phosphate buffer (pH 7.4). Snap-frozen tissues were stored in liquid nitrogen for Caspase-3 activity, protein and mRNA analyses. Serum creatinine concentration (standard autoanalyzer techniques) and 24-hour urinary protein excretion (Biuret method) were determined in each group at all time points.

Estimation of renal scarring

The extent of renal scarring following SNx was determined by two authors who were blinded to the experimental code according to a previously published arbitrary scale [14–16]. Using a ×200 magnification, sections stained with Masson's Trichrome were scored as follows. For glomerulosclerosis, a normal glomerulus scored 0; mild glomerulosclerosis (GS) affecting up to 25% of the glomerular tuft scored 1; moderate GS affecting between 25% and 50% of the tuft scored 2; and severe GS affecting in excess of 50% of the tuft scored 3. Tubulointerstitial scarring was defined and scored as: normal tubules with approximately 1000 tubule cells per ×200 magnification field and no expansion of the interstitium scored 0; mild tubular atrophy (TA), with approximately 800 tubular cells per field and interstitial edema or fibrosis (IF) affecting up to 25% of the section scored 1; moderate TA with tubular cell number approximately 600 per field and IF affecting 25% to 50% of the section scored 2; and severe TA with tubular cell number approximately 400 per field, IF exceeding 50% of the section scored 3. To determine the level of tubular atrophy, tubular cells per ×200 magnification field were counted. The data were collected from a minimum series of 12 randomly selected fields in the cortex, or such number of fields until 30 glomeruli had been counted.

In situ end-labeling for the detection of apoptotic cells

In formal calcium-fixed and paraffin-embedded 4 μm sections, fragmented nuclear DNA was labeled in situ with digoxigenin-deoxyuridine (dUTP) by terminal deoxynucleotidyl transferase (TdT), using the ApopTag™ Plus peroxidase kit (Appligene Oncor, Illkirch, France) according to the manufacturer's instructions [6, 17]. Briefly, after deparaffinization and hydration, sections were digested by incubation with 15 μg/mL proteinase K for 15 minutes at 37°C. Endogenous peroxidase was inactivated by 2% (vol/vol) H_2O_2 in phosphate-buffered saline (PBS). The sections were then immersed in TdT reaction buffer, and incubated with TdT and digoxigenin-dUTP for 60 minutes at 37°C. The slides were transferred to stop buffer at 37°C for 30 minutes to terminate the reaction. The sections were incubated with the antidigoxigenin-peroxidase complex for 30 minutes at 37°C and developed by using the 3′-amino-9-ethylcarbazole (AEC) substrate kit (Vector Laboratories, Peterborough, UK) and counterstained with hematoxylin. For negative controls, slides were incubated in TdT buffer without TdT. For biochemically induced positive controls, slides were pre-

treated with 10 μg/mL of DNAse I (Sigma, Poole, UK) in DNA buffer.

For each experimental animal, more than 30 glomerular cross-sections and 20 high power (×400) fields of tubulointerstitium were examined blinded to the experimental code by two authors. The number of in situ end labeling (ISEL) positive-staining nuclei per glomerulus (Gapo), per 400 tubular cells (Tapo), or per interstitial field (Iapo) was determined, respectively. ISEL of DNA, while associated with apoptosis, also can be seen in necrotic (nonspecific DNA degradation) and mitotic (transient DNA strand break) cells. To substantiate the specificity of our results, apoptosis was confirmed by light microscopic evaluation of the characteristic morphological features; only strongly positive ISEL cells with observable morphological features of apoptosis such as shrunken cells with condensed nuclei surrounded by a narrow cytoplasmic halo were counted [4, 6, 18, 19].

Evaluation of distribution of Caspase-3 and cellular inflammation (ED-1) by immunostaining

Localization of Caspase-3 and ED-1 (a specific monocyte/macrophage marker) was performed in paraffin-embedded kidney tissues by immunohistochemistry using a standard avidin-biotin peroxidase complex technique as described previously [15]. ED-1 immunostaining was analyzed to evaluate the cellular inflammation. Sections were pretreated with 0.25% or 0.125% (wt/vol) trypsin at 37°C for 10 minutes. A polyclonal rabbit anti-human Caspase-3 antibody (Pharmingen, San Diego, CA, USA) recognizing the 32 and 17 kD Caspase-3 subunits with no cross reactivity against other caspase family members (manufacturer's specification) or a monoclonal mouse anti-rat ED1 antibody (Serotec Ltd., Oxford, UK) were diluted 1:100 or 1:50 and then applied overnight at 4°C in a humid atmosphere. Thereafter, the sections were stained by an avidin-biotinylated HRP procedure using a commercially available kit (ABC Elite, Vector Laboratories). AEC was used as the substrate. Finally, sections were counterstained with hematoxylin and mounted in Glycergel (Dako, Glostrup, Denmark). Negative control sections were incubated with normal mouse IgG or normal rabbit serum at the same protein concentration as the primary antibody. The immunohistochemical staining pattern of ED-1 was semiquantitatively assessed using the same counting system as with the ISEL staining.

Double staining for both apoptosis and Caspase-3, ED-1 or α-smooth muscle actin

Double immunohistochemical staining was undertaken on paraffin sections. ISEL was carried out as described above. Before application of the anti-digoxigenin antibody, sections were pre-incubated with blocking serum for 30 minutes, labeled with the anti Caspase-3, anti-ED-1 or anti-α-smooth muscle actin (α-SMA; monoclonal mouse anti-human α-SMA, diluted 1:250; Dako) antibodies at 4°C overnight. The α-SMA antibody was used to detect myofibroblasts typically expressing a high immunostaining for this cytoskeletal protein [20]. Sections were labeled with biotinylated secondary anti-mouse or -rabbit IgG at 37°C for 30 minutes, with alkaline phosphatase streptavidin for another 30 minutes and developed with Fast Red TR/Naphthol AS-MX solution (Sigma) to produce a bright pink color. Subsequently, anti-digoxigenin peroxidase antibody was applied to the sections and revealed by the addition of diaminobenzidine to provide positive staining as a yellow/brown color. Control sections were incubated with non-immune normal mouse IgG or normal rabbit serum in place of primary antibody and with the omission of TdT enzyme as ISEL controls.

Detection of Caspase-3 activity in renal tissue

The modified Fluorometric CaspACE™ Assay System (Promega, Cambridge, UK) was used to detect the activity of Caspase-3 in tissue. Kidney tissue (20 to 50 mg) from control and SNx rats was ground in liquid nitrogen using a pestle and mortar. A 1:9 (wt/vol) tissue:buffer extract was prepared in Tris/acetate buffer, pH 7.5, at 30°C [21]. The extract was centrifuged at 12,000 × g for 10 minutes and supernatant was collected. A volume of supernatant equivalent to 100 μg protein was assayed for Caspase-3 activity by the ability to cleave the florigenic substrate Ac-DEVD-AMC. The specificity of the assay was determined using the Caspase-3 inhibitor Ac-DEVD-CHO by adding to the sample 30 minutes before the substrate. Proteolytic cleavage of the substrates was monitored in a fluorescence microplate reader (SOFTmax PRO; Molecular Devices Corp., Sunnyvale, CA, USA) using an excitation wavelength of 360 nm and an emission wavelength of 460 nm. The fluorescence intensity was calibrated with standard concentrations of AMC, and the Caspase-3 activity calculated from the slope of the recorder trace and expressed in picomols per minute per μg of protein at 30°C.

Measurement of tissue Caspase-3 protein level

Tissue level of Caspase-3 protein was determined by immunoprobing of Western blots. Ten percent (wt/vol) tissue homogenate was prepared in the STE buffer [0.32 mol/L sucrose, 5 mmol/L Tris, 2 mmol/L ethylenediaminetetraacetic acid (EDTA), 1 mmol/L phenylmethylsulfonyl fluoride (PMSF), 5 mmol/L benzamidine and 20 μg/mL leupeptin], then centrifuged at 4°C, 14,000 × g for 10 minutes. Twenty micrograms of protein from the supernatant was separated on a 15% (wt/vol) poly acrylamide denaturing gel and then electro-blotted onto Hybond-C nitrocellulose membranes (Amersham Life Science, Little Chalfont, UK). Membranes were blocked by the addition of 3% (wt/vol) bovine serum albumin

(BSA) in 0.1% (vol/vol) Tween 20 TBS (TTBS) at 4°C overnight before being probed with a polyclonal rabbit anti-rat full-length Caspase-3 (Santa Cruz Biochemicals, Santa Cruz, CA, USA) at 1:2,000 dilution in TTBS buffer at room temperature for two hours. Primary antibody binding was revealed using an anti-rabbit peroxidase conjugate (Dako) diluted at 1:2,000 in TTBS buffer for one hour and the ECL chemiluminescent detection system (Amersham Life Science). Recombinant Caspase-3 (17 kD and 12 kD subunits; Sigma) was used to verify antibody efficacy under experimental conditions. Developed films were semiquantitatively analyzed by volume density using a Bio-Rad GS-690 scanning densitometer and Molecular Analyst version 4 software (Bio-Rad Laboratories Ltd, Hertfordshire, UK). Translation size was determined by comparison to protein molecular weight markers (Bio-Rad Laboratories Ltd.) using the same analysis package.

Northern blot analysis of Caspase-3 mRNA

Northern blot analysis was carried on the snap-frozen kidney tissues. Total RNA was extracted using the TRIzol® reagent (Life Technologies BRL, Paisley, UK) and quantified by scanning spectrophotometer at 260 nm. Fifteen micrograms of total RNA were electrophoresed on a 1% (wt/vol) agarose/3-(N-Morpholino) propane sulfonic acid (MOPS)/formaldehyde gel. RNA was then transferred to a nylon membrane (Hybond-N, Amersham Life Science) by capillary blotting using 20 × SSC and cross-linked to the nylon filter using a UV crosslinker (Amersham Life Science) at 70 mJ/cm^2 energy [22, 23].

To produce a Caspase-3 cDNA probe, Caspase-3 exonic DNA was amplified from rat cDNA by the polymerase chain reaction (PCR) using the following previously published primers: 5′-sense ATGGACAACAACGAA ACCTCCGTG, 3′-antisense CCACTCCCAGTCATTC CTTTAGTG [24]. Amplification reactions were performed with 100 μmol/L of each dNTP in amplification buffer (containing 1.5 mmol/L $MgCl_2$) and 1 unit Taq polymerase at 85°C for five minutes, before 20 picomoles of primers were added. Thirty-nine cycles of amplification were completed using the following conditions: 94.6°C for one minute, 48°C for one minute, 72°C for two minutes. The 850 bp PCR product was cloned into the pCR®2.1 vector (Invitrogen, UK). Following bacterial amplification and plasmid purification, the Caspase-3 insert was excised with BstXI and EcoRV, separated by electrophoresis on a 1.5% (wt/vol) agarose TAE gel and purified using Prep-A-Gene DNA Purification Systems (Bio-Rad Laboratories Ltd., Hertfordshire, UK). Product confirmation was by restriction mapping using EcoRI and KpnI [12]. Purified cDNA was random primed with ^{32}P-labeled dCTP (NEN, USA) using the Prime-a-Gene® Labeling System (Promega). Unincorporated label was removed using a Sephadex® G-50 NICK™ column (Pharmacia Biotech, UK).

Prehybridization and hybridization were performed using the Church buffer system (0.5 mol/L sodium phosphate and 7% SDS) at 65°C [25]. The filter was washed three times in church wash buffer (40 mmol/L sodium phosphate, 1% SDS) at 65°C for 20 minutes and then exposed to Kodak Biomax MS film for 24 hours. Autoradiographs were quantitatively analyzed by scanning volume density using a Bio-Rad GS-690 densitometer and Molecular Analyst version 4 analysis software (Bio-Rad Laboratories Ltd.). Optical density values for Caspase-3 were corrected for loading using the housekeeping gene cyclophilin [12, 26]. Results were expressed as percentage of control sample mRNA densities. Transcript size was determined by comparison to RNA molecular weight markers (Promega) using the same analysis package and by visual comparison to the ribosomal RNA subunits.

Statistical analysis

Results are expressed as mean ± standard error of the mean (SEM). The statistical difference was assessed by a single factor variance (ANOVA) or the Student t test. Linear correlation analysis using GraphPad InStat (GraphPad Software Inc., San Diego, CA, USA) and multiple linear regression analysis using SSPS (SPSS Inc., Chicago, IL, USA) were applied to determine the correlation and association between parameters. $P < 0.05$ was considered to be significant.

RESULTS

Renal function and histology studies

Proteinuria in SNx rats was significantly raised from day 30 (SNx 40.4 ± 8.0 mg/24 h vs. Sham 9.3 ± 0.7 mg/24 h, $P < 0.05$) while serum creatinine was significantly raised from day 7 (SNx 68.5 ± 5.8 μmol/L vs. Sham 33.8 ± 3.1 μmol/L). Both reached maximum levels on day 120 (proteinuria, SNx 256.8 ± 56.8 mg/24 h vs. Sham 7.4 ± 0.8 mg/24 h; serum creatinine, SNx 140.6 ± 36.5 μmol/L vs. Sham 40.0 ± 1.4 μmol/L; Table 1). Significant evidence of GS (0.22 ± 0.10), TA (936 ± 26 tubular cells per ×200 field) and IF (0.32 ± 0.13 at ×200 field) following SNx was noted from day 7 and progressively increased thereafter. Maximum changes were recorded on day 120 after SNx with GS reaching 1.86 ± 0.15, TA at 613.62 ± 47.54 tubular cells per ×200 field and an IF score of 1.93 ± 0.24 at ×200 field (Table 1). This indicated the progressive renal insufficiency and a moderate degree of renal scarring as previously documented in our earlier studies using this model [6].

Detection of apoptotic cells

Using ISEL, very few apoptotic cells were noted in the glomeruli, tubules and interstitium of sham-operated

Table 1. Changes with time in renal fibrosis, apoptosis and inflammation in the kidneys of rats submitted to subtotal nephrectomy (SNx)

Days		UP *mg/24 h*	S_{Cr} *μmol/L*	GS	TA	IF	Gapo	Tapo	Iapo	Ged-1	Ied-1
7	SNc	6.5 ± 0.7	33.8 ± 3.1	ND	1000 ± 0	ND	0.02 ± 0.01	0.09 ± 0.01	0.17 ± 0.02	0.17 ± 0.07	2.02 ± 0.19
	SNx	16.9 ± 4.5[a]	68.5 ± 5.8[a]	0.22 ± 0.10[b]	936 ± 26[b]	0.32 ± 0.13[b]	0.06 ± 0.02	1.08 ± 0.24[b]	0.43 ± 0.05[c]	1.50 ± 0.43[a]	4.08 ± 0.69[a]
15	SNc	9.3 ± 2.7	42.6 ± 2.4	ND	1000 ± 0	ND	0.01 ± 0.01	0.09 ± 0.01	0.14 ± 0.04	0.19 ± 0.07	1.86 ± 0.41
	SNx	16.7 ± 2.8	84.2 ± 7.9[a]	0.18 ± 0.06[b]	943 ± 12[b]	0.27 ± 0.06[b]	0.07 ± 0.02[a]	0.92 ± 0.08[b]	0.46 ± 0.06[b]	6.86 ± 0.84[c]	9.60 ± 1.50[c]
30	SNc	9.3 ± 0.7	53.8 ± 4.2	ND	1000 ± 0	ND	0.03 ± 0.01	0.06 ± 0.02	0.18 ± 0.02	0.22 ± 0.13	2.05 ± 0.41
	SNx	40.4 ± 8.0[a]	78.7 ± 6.4[a]	0.34 ± 0.05[b]	892 ± 13[b]	0.54 ± 0.06[b]	0.12 ± 0.03[a]	1.09 ± 0.22[b]	0.73 ± 0.10[b]	4.08 ± 0.20[b]	10.50 ± 1.91[b]
60	SNc	7.7 ± 2.1	42.5 ± 1.8	ND	996 ± 4	0.02 ± 0.02	0.02 ± 0.01	0.10 ± 0.01	0.18 ± 0.03	0.15 ± 0.15	1.98 ± 0.37
	SNx	131.1 ± 23.0[a]	107.4 ± 28.5	0.73 ± 0.13[b]	763 ± 49[b]	1.18 ± 0.25[b]	0.10 ± 0.01[c]	1.66 ± 0.14[c]	0.85 ± 0.12[b]	7.50 ± 1.66[b]	17.40 ± 3.23[c]
90	SNc	9.9 ± 1.1	53.4 ± 5.6	ND	1000 ± 0	ND	0.02 ± 0.01	0.08 ± 0.01	0.21 ± 0.04	0.46 ± 0.15	3.74 ± 0.75
	SNx	234.1 ± 45.4[a]	111.2 ± 19.9[a]	1.67 ± 0.16[c]	653 ± 39[c]	1.73 ± 0.20[c]	0.21 ± 0.04[b]	2.09 ± 0.53[b]	0.96 ± 0.31[a]	12.80 ± 2.65[c]	21.80 ± 3.65[c]
120	SNc	7.4 ± 0.8	40.0 ± 1.4	ND	1000 ± 0	ND	0.03 ± 0.02	0.06 ± 0.02	0.11 ± 0.03	0.48 ± 0.16	3.98 ± 0.83
	SNx	256.8 ± 56.8[a]	140.6 ± 36.5[a]	1.86 ± 0.15[c]	613 ± 48[c]	1.93 ± 0.24[c]	0.25 ± 0.04[c]	2.77 ± 0.44[c]	1.04 ± 0.25[b]	15.90 ± 3.64[c]	27.40 ± 4.78[c]

Data represent mean ± SEM. Statistical significance when compared to respective control.

Abbreviations are: SNc, sham-operated ($N = 4$); SNx, subtotally nephrectomized ($N = 6$); UP, proteinuria; S_{Cr}, serum creatinine; GS, glomerulosclerosis; TA, tubular atrophy; IF, interstitial edema or fibrosis; Gapo, apoptotic cells per glomerulus; Tapo, apoptotic cells per 400 tubular cells; Iapo, apoptotic cells per ×400 field; Ged1, ED-1 positive-staining cells per glomerulus; Ied1, ED-1 positive-staining cells per ×400 field.

[a] $P < 0.05$, [b] $P < 0.01$, [c] $P < 0.005$ and ND, not detectable

rats. Remnant kidneys demonstrated a significant and gradual increase in positively stained nuclei in the glomeruli from day 15 (SNx 0.07 ± 0.02 vs. Sham 0.01 ± 0.01 per glomerulus), in the tubules from day 7 (SNx 1.08 ± 0.24 vs. Sham 0.09 ± 0.01 per 400 tubular cells) and in the interstitium from day 7 (SNx 0.43 ± 0.05 vs. Sham 0.17 ± 0.02 per interstitial field at ×400) until the end of the time course. Maximum changes were seen at day 120 for apoptosis in glomeruli (SNx 0.25 ± 0.04 vs. Sham 0.03 ± 0.02), tubules (SNx 2.77 ± 0.44 vs. Sham 0.06 ± 0.02 cell per 400 tubular cells) and interstitium (SNx 1.04 ± 0.25 vs. Sham 0.11 ± 0.03 cell per interstitial field at ×400; Table 1). The highest rates of apoptosis were in the sclerotic glomeruli (Fig. 1A), dilated or atrophied tubules (Fig. 1B) and expanded interstitium (Fig. 1C). In positive control sections treated with DNAse I before the TdT reaction, nearly all of the cells stained, but most of positive nuclei showed normal shape, and no cytoplasmic condensation. No staining was present in the negative control sections using buffer lacking TdT (data not shown). Electron microscopy confirmed apoptotic cells with distinct morphological motifs (Fig. 2).

Distribution of Caspase-3 and detection of cellular inflammatory ED-1

There was no or very faint Caspase-3 immunostaining in sham-operated kidneys (Fig. 1D). In contrast, Caspase-3 staining was seen in dilated tubules (Fig. 1E), damaged glomerular capsule and a few glomerular cells (Fig. 1E), the loop of Henle (Fig. 1F) and interstitial cells (Fig. 1G) of remnant kidneys. Some Caspase-3 positive cells had the typical morphological features of apoptosis (Fig. 1G).

In kidneys from sham-operated rats, a small number of ED-1 positive cells were seen in the glomeruli (0.28 ± 0.12 per glomerulus) and interstitium (2.61 ± 0.49 per ×400 field; Fig. 1J). In contrast, ED-1 staining cells were gradually and significantly increased throughout the experimental time course in SNx kidneys with a peak on day 120 in the glomeruli (15.90 ± 3.64 per glomerulus) and interstitium (27.40 ± 4.78 per ×400 field; Table 1). ED-1+ cells were distributed in inflamed or sclerotic glomeruli (Fig. 1K), expanded interstitium (Fig. 1L) and dilated tubular lumens (Fig. 1M).

Double staining for ED-1, α-SMA and Caspase-3 with apoptosis

Double staining cells of Caspase-3 and ISEL were noted in glomerular cells (Fig. 1H) and atrophied tubular cells (Fig. 1I). In remnant kidneys ED-1 and ISEL double-staining, positive cells were found in inflamed interstitium (Fig. 1N) and glomeruli (not shown). Some cells stained positively for both apoptosis (ISEL) and α-SMA in the interstitium (Fig. 1O).

Caspase-3 activity

There was a gradual increase in Caspase-3 protease activity in SNx rat kidneys at all time points compared with the controls reaching significance by day 30 and reaching a peak on day 120 (2.5-fold of control; Fig. 3). The specific and competitive tetrapeptide inhibitor of Caspase-3, Ac-DEVD-CHO, almost fully inhibited the Caspase-3 activity in the assays, demonstrating assay specificity (data not shown).

Tissue level of Caspase-3 protein

Western blot analysis showed a considerable variation in Caspase-3 levels in animals from the same experimental groups in this study (Fig. 4). However, the magnitude of the observed changes was statistically significant. The 17 kD Caspase-3 active subunit was significantly increased from day 30 onwards in SNx kidneys with maxi-

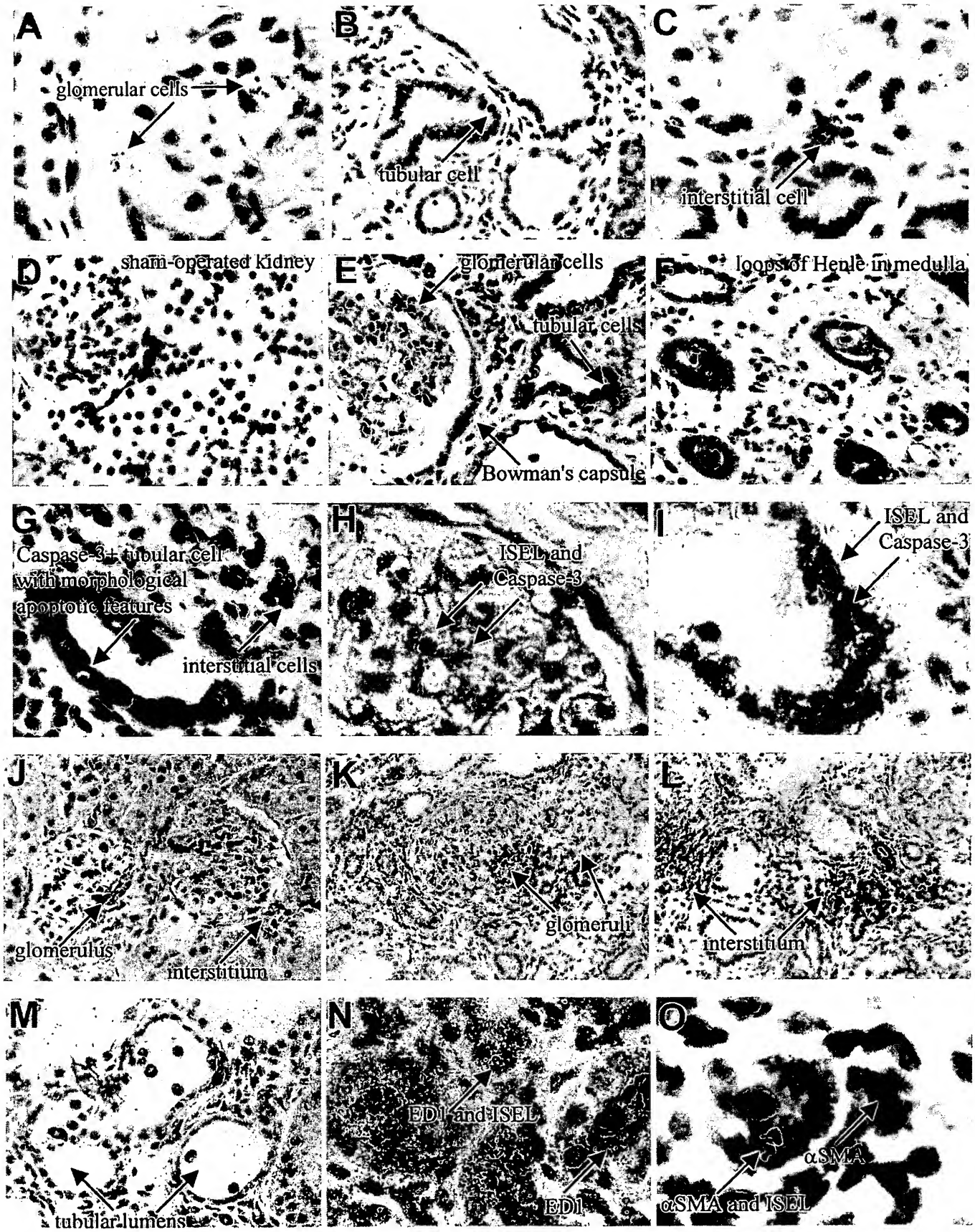
A
glomerular cells
B
tubular cell
C
interstitial cell
D
sham-operated kidney
E
glomerular cells
tubular cells
Bowman's capsule
F
loops of Henle in medulla
G
Caspase-3+ tubular cell with morphological apoptotic features
interstitial cells
H
ISEL and Caspase-3
I
ISEL and Caspase-3
J
glomerulus
interstitium
K
glomeruli
L
interstitium
M
tubular lumens
N
ED1 and ISEL
ED1
O
αSMA
αSMA and ISEL

mal expression on day 120 (1942% of control). A 24 kD band also representing a Caspase-3 active subunit was gradually and significantly increased at all time points, reaching a peak on day 120 (921% of control). The 29 kD Caspase-3 processing intermediate was present in all kidneys throughout the time course. The 32 kD precursor of Caspase-3 was significantly increased as early as day 7 (747%), peaked on day 60 (2704%), and then dropped with time until day 120 (1861% of control). This was in contrast with the continuous increase of both 17 kD and 24 kD active subunits (Fig. 4).

To validate antibody reactivity, Western blots were performed utilizing recombinant active Caspase-3 protein. The full length Caspase-3 antibody strongly bound with 12 and 17 kD recombinant Caspase-3 proteins (Fig. 4).

Expression of Caspase-3 mRNA

Northern blot analysis revealed the expression of a Caspase-3 mRNA transcript at 2.7 kb (Fig. 5). In comparison with the control rat kidneys, the level of Caspase-3 mRNA was significantly increased at all time points, and reaching a peak at day 120 (287% of control; Fig. 5).

Correlation between apoptosis, inflammation, fibrosis and Caspase-3

Cellular apoptosis in glomeruli, tubules and interstitium closely correlated with inflammation ($r = 0.403$, 0.820 and 0.732, $P < 0.01$), as well as with GS, TA and IF ($r = 0.871$, -0.873 and 0.773, $P < 0.01$ [28]). Cellular inflammation also positively correlated with GS, TA and IF ($r = 0.679$, -0.698 and 0.698, $P < 0.01$). Multiple regression analysis showed that apoptosis was more closely associated with GS and TA (Std β coefficients = 0.531 and -0.723, respectively, $P < 0.01$) than inflammation or proliferation and interstitial inflammation was more closely related with IF (Std β coefficients = 0.458, $P < 0.01$) than apoptosis and proliferation (refer previous data [6]).

There were close associations between the expression of Caspase-3 activity and proteins (17 kD, $r = 0.512$ and 24 kD, $r = 0.440$, $P < 0.01$; and 32 kD, $r = 0.302$, $P < 0.05$); proteins and mRNA (17 kD, $r = 0.634$; 24 kD, $r = 0.637$; and 32 kD, $r = 0.583$, all $P < 0.01$); and activity and mRNA ($r = 0.698$, $P < 0.01$). The Caspase-3 at different levels positively correlated with overall apoptosis (activity, $r = 0.589$, 17 kD, $r = 0.530$; 24 kD, $r = 0.573$; and 32 kD, $r = 0.577$; and mRNA, $r = 0.642$, all $P < 0.01$), inflammation (activity, $r = 0.722$; 17 kD, $r = 0.642$; 24 kD, $r = 0.621$; and 32 kD, $r = 0.544$; and mRNA, $r = 0.805$, all $P < 0.01$) and fibrosis (activity, r = 0.728; 17 kD, $r = 0.679$; 24 kD, $r = 0.711$; and 32 kD, $r = 0.589$; and mRNA, $r = 0.818$, all $P < 0.01$). Among Caspase-3 activity, protein and mRNA, multiple regression analysis showed that Caspase-3 activity was the best predictor of apoptosis (Std β coefficient = 0.347, $P < 0.05$) and Caspase-3 mRNA was a better predictor of inflammation and fibrosis (Std β coefficient = 0.435 and 0.394 respectively, $P < 0.01$).

DISCUSSION

Subtotal nephrectomy in rats is a non-immune mediated experimental model of chronic renal scarring [27]. Previously we described a progressive and sustained increase in the number of apoptotic cells in the glomeruli, tubules and interstitium in this model, with maximal apoptosis detected in sclerotic glomeruli, atrophied tubules and expanded interstitium [6]. Further studies in this model have demonstrated that apoptosis is likely to be influenced by the interplay between Bax (pro-apoptotic antigen) and Bcl-2 (anti-apoptotic antigen) with changes at both the mRNA and protein levels [28]. An increase in Bax coupled with a decreased level of Bcl-2 was shown to have strong associations with the changes in apoptosis and the progression of renal scarring [28]. In this study, we extended our observations to encompass Caspase-3, which is thought to be a key enzyme for the execution of the apoptotic program [7, 8]. There is a clear up-regulation of Caspase-3 activity that is dependent on changes not only at the translation and transcription levels, but also by post-translational modification of the latent precursor. Multiple regression analysis demonstrated that Caspsase-3 activity was the best predictor of apoptosis and strongly correlated with its protein and mRNA levels. Furthermore, we have highlighted changes in Caspase-3 that are consistent with variations in apoptosis, inflammation and fibrosis over the time course.

The caspase enzyme family, and in particular Caspase-3, has a central role in the execution of apoptosis that results in the phenotype of apoptosis. Caspase-3 is translated as an inactive 32 kD precursor that is proteolytically processed to become a functionally active enzyme [29–32].

Fig. 1. (*A–C*) Positive apoptotic cells (indicated by arrows) in glomeruli (A, ×400), tubules (B, ×200) and interstitium (C, ×400) of subtotally nephrectomized (SNx) kidneys by ApopTag staining. (*D–I*) Caspase-3 immunostaining in sham-operated (D, ×200) and remnant kidneys (E–G) within the dilated tubules (E, ×200; G, ×400), glomerulus (E), loops of Henle (F, ×200) and interstitial cells (G). (H and I) Double staining of Caspase-3 (bright pink) with ISEL (brown) in the glomerulus (H, ×800) and atrophied tubule (I, ×800) in the remnant kidney with dark brown indicating composite staining. (*J–M*) ED-1 positive cells in the glomerulus and interstitium of sham-operated rat kidney (J, ×200), and in glomeruli, interstitium (K and L, ×100) and tubular lumen of remnant kidneys (M, ×200). (*N* and *O*) Double staining of ISEL (brown) with ED-1 (bright pink) (N, ×400) and α-smooth muscle actin (α-SMA; bright pink; O, ×1000) in the interstitium of SNx kidneys.

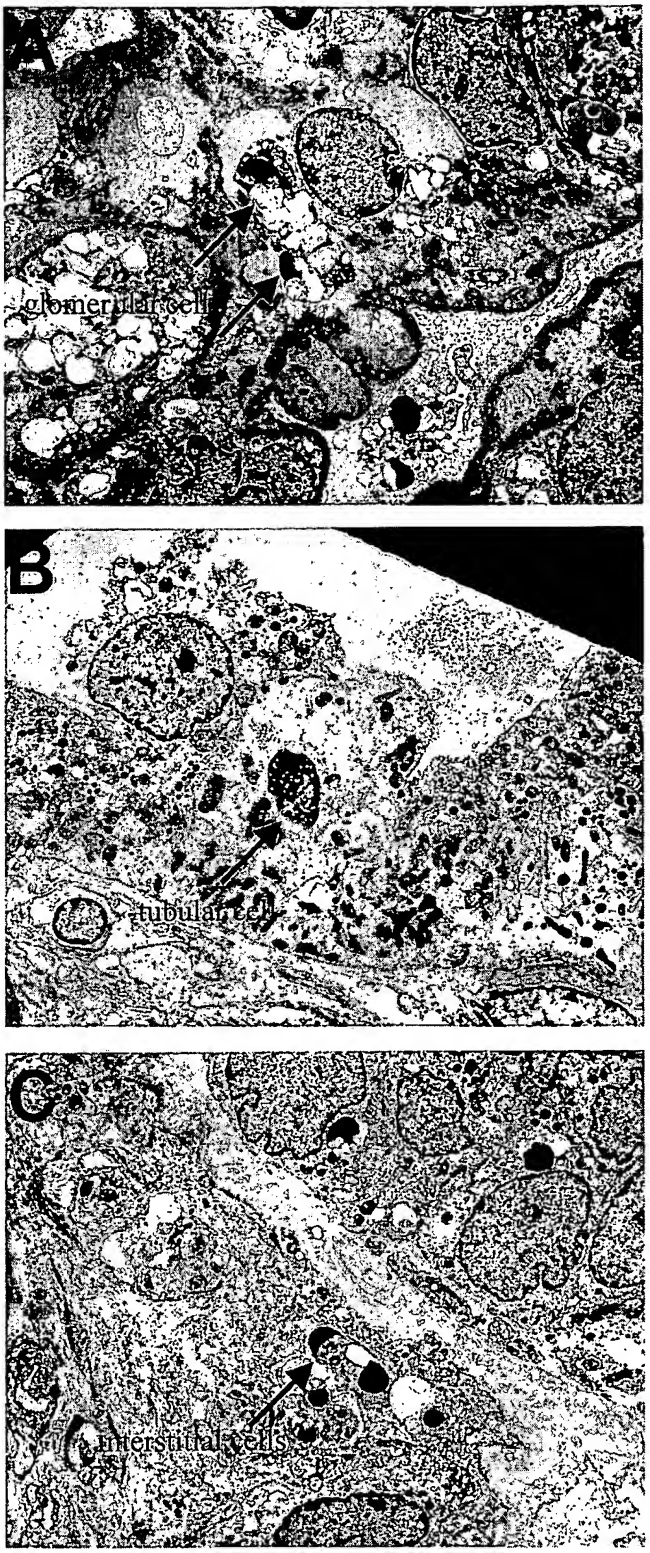

Fig. 2. Positive apoptotic cells (indicated by arrows) in glomeruli (*A*, ×8829), tubules (*B*, ×11142) and interstitium (*C*, ×6858) of SNx kidneys by electron microscopy.

Activation of Caspase-3 requires two proteolytic cleavage events. Removal of the NH_2 terminal pro-domain generating a 29 kD processing intermediate that is subsequently cleaved into 17 kD and 11 kD or 12 kD subfragments [30–32]. However, other active fragments, such as 24, 20 and 18 kD, have also been reported [12, 24, 33]. These subfragments then heterodimerize to form the activated protease [31, 32].

In this SNx model, Western blot analysis of remnant kidneys showed significant increases in both the 17 kD and 24 kD subunits representing active Caspase-3. The appearance of the active Caspase-3 fragments correlated well with the changes in enzyme activity. However, while elevated, Caspase-3 mRNA did not increase in line with the Caspase-3 activity. Thus, the changes in activity due to the increases in 17 kD and 24 kD proteins would appear to be a consequence of changes in level of activation of the 32 kD Caspase-3 precursor, rather than solely down to an increased transcriptional rate. This also explains the decrease in 32 kD protein at the latter time points in spite of a continuing up-regulation of the mRNA levels, suggesting this de novo Caspase-3 precursor is immediately processed to the smaller active forms when apoptosis is at its highest. Furthermore, the levels of 32 kD Caspase-3 protein are not wholly consistent with the changes of Caspase-3 mRNA level at earlier time points. The steadily increasing levels of the 32 kD protein up to day 60 in comparison to the static elevation in mRNA level indicates that changes in mRNA stability or alteration to the rate of translation also may be important in Caspase-3 production.

Immunolocalization of Caspase-3 in rat kidneys has previously proved difficult with a few studies restricted to analysis of human tissues [34, 35]. Here for the first time, we have been able to localize Caspase-3 in paraffin-embedded rat kidney by pretreating sections with a high concentration of trypsin and applying an anti-human full-length Caspase-3 antibody. This revealed no or very faint Caspase-3 positive immunostaining in sham-operated kidneys. Given the substantial levels of Caspase-3 protein and mRNA detectable in normal kidneys (assumption made on band development time in Western and Northern blotting analysis) this would be consistent with a low expression of Caspase-3 in many cells falling below the threshold for immunohistochemical detection. In contrast within remnant kidneys, there was a strong Caspase-3 staining especially in damaged tubules, but also within some glomerular and interstitial cells. This staining pattern is consistent with that of ISEL, which in combination with double staining provides direct evidence for the involvement of Caspase-3 in apoptosis in this model of renal scarring. While the location allows identification of tubular cells as producers of Caspase-3, it is not directly evident from our study that cell types in the glomeruli and interstitium have elevated Caspase-3. These may be

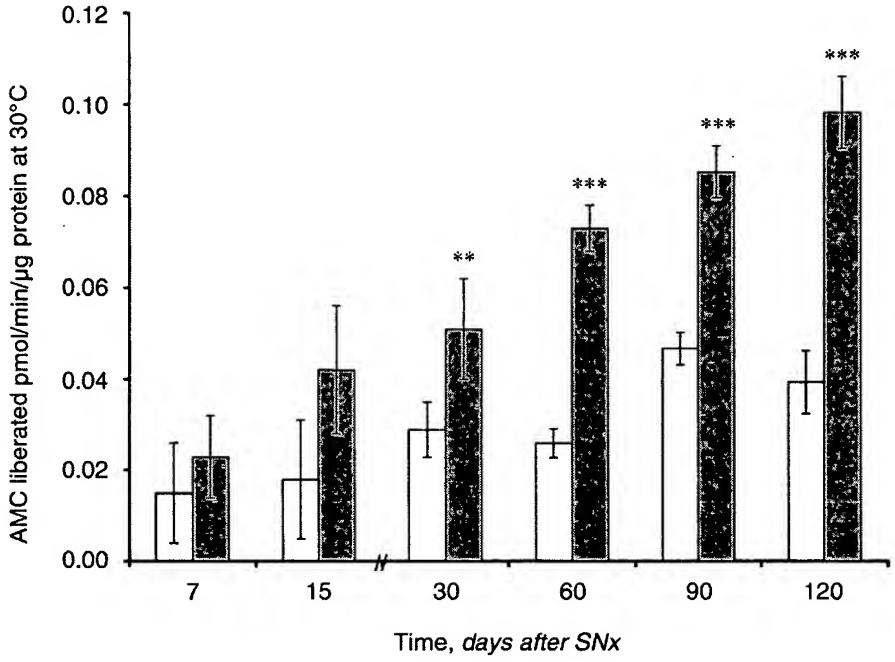

Fig. 3. Activity of Caspase-3 in kidney tissues assayed by the fluorometric measurement of AMC cleaved from a specific Caspase-3 substrate. Symbols are: (□) control; (■) SNx. Data represent mean ± SEM. $N = 4$ for control and $N = 6$ for SNx. $^{**}P < 0.01$; $^{***}P < 0.001$ compared with the control kidneys.

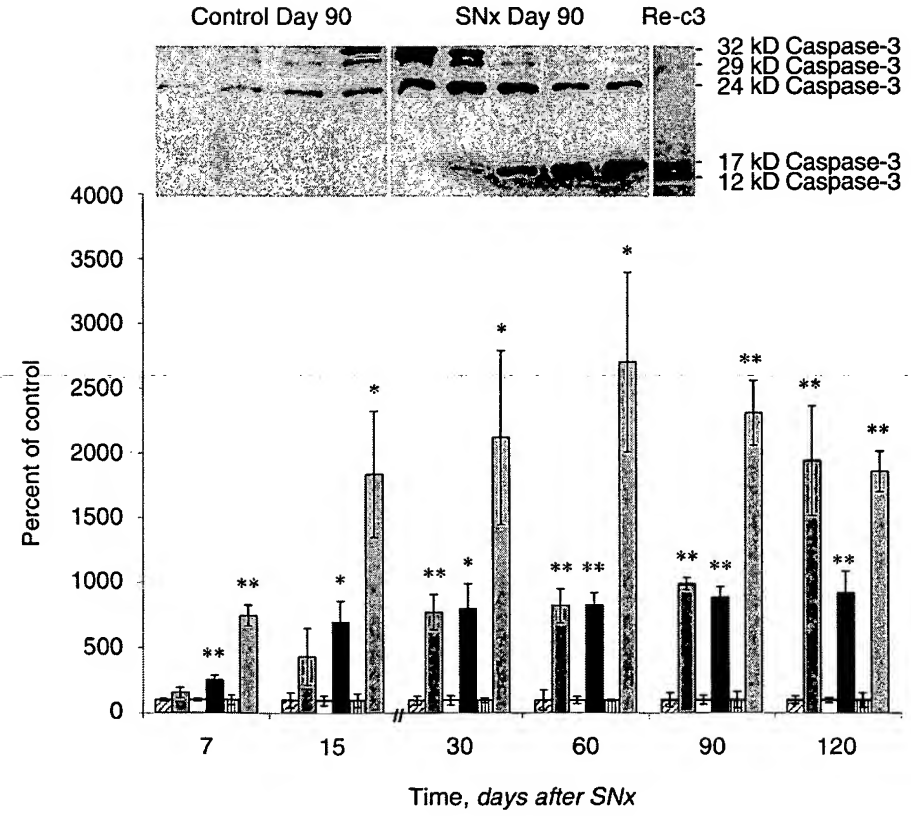

Fig. 4. Western blot analysis for Caspase-3 protein in SNx kidneys on day 7, 15, 30, 60, 90 and 120. A 17 kD band and a 24 kD band, representing the Caspase-3 active subunit; a 29 kD, representing processing intermediate of Caspase-3; a 32 kD band, representing the precursor of Caspase-3. Re-c3: 5 ng recombinant Caspase-3. Symbols are: (▨) control; (■) 17 kD; (□) control; (■) 24 kD; (▥) Control; (▣) 32 kD. Data represent the mean percentage change in volume density compared to the average control value (mean ± SEM). $N = 4$ for control, $N = 5$ for SNx. $^{*}P<0.05$; $^{**}P<0.01$ compared with the control kidneys.

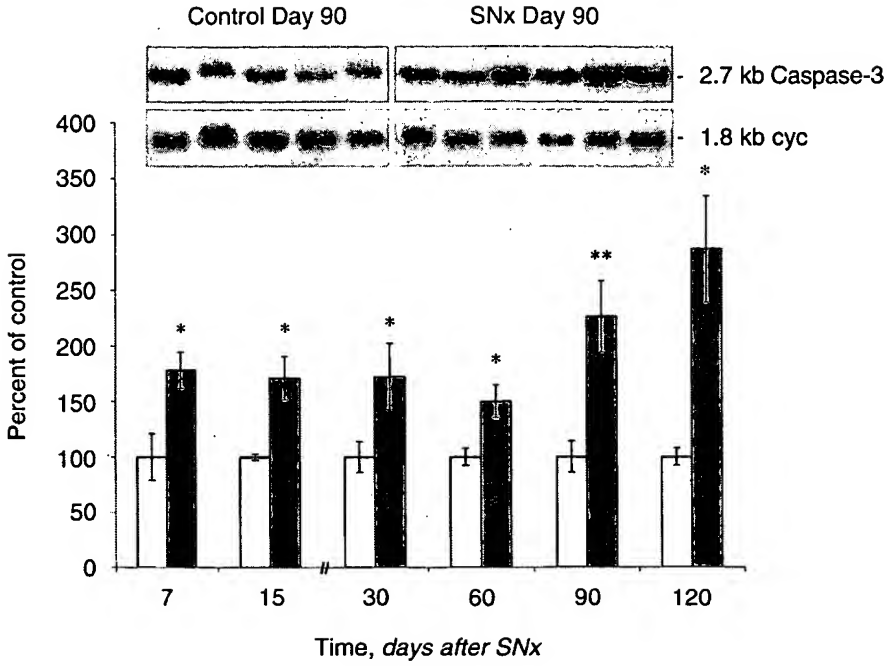

Fig. 5. Tissue level of Caspase-3 mRNA by Northern blot analysis in SNx rat kidneys. Autoradiographs at the top show 2.7 kb Caspase-3 mRNA transcript and the bottom, cyclophilin 1.8 kb transcript. The histogram shows the volume density analysis of autoradiographs corrected for loading using cyclophilin. Data represent the mean percentage change in volume density compared to the average control value (mean ± SEM). $N = 4$ for control and $N = 6$ for SNx. $^{*}P < 0.05$; $^{**}P < 0.01$ compared with the control kidneys.

either resident renal cells or inflammatory cells. Double staining for cell markers appears to be a solution, although markers such as ED-1 and α-SMA are rapidly lost once the apoptotic pathway has commenced. Given that most Caspase-3 positive cells are likely to be at some stage in the apoptotic program and requirement of strong trypsinization for Caspase-3 immunostaining, then the co-localization of a specific cell marker with Caspase-3 has obvious problems. However, we have had some success double-staining ISEL-positive cells with ED-1 or α-SMA, which by inference suggests that most cells expressing Caspase-3 would be monocytes or myofibroblasts in the glomeruli and interstitium.

Other immunohistochemical studies using the same Caspase-3 antibody in normal human kidneys showed strong positive staining in renal tubule epithelium with little or no Caspase-3 immunoreactivity in the glomeruli [35]. The higher tubular staining in normal human kidneys may well represent differences between species; however, it equally could be due to greater sensitivity of the antibody for human than rat Caspase-3. Studies describing changes in Caspase-3 staining in human scarred tissue remain to be performed. However, when this is done it will be interesting to note if the considerable Caspase-3 staining within the glomeruli and interstitium seen in this experimental model also are evident, as they undoubtedly contribute significantly to the Caspase-3 pool.

The predominantly Caspase-3 tubular epithelial staining pattern combined with the positive double staining of Caspase-3 and ISEL clearly implicates Caspase-3 in tubular cell apoptosis and tubular atrophy. Caspase-3 also has been reported to be involved in the pathogenesis of other renal injury models associated with apoptosis. For instance, it was found to be up-regulated at both mRNA and total protein levels during reperfusion in a rat model of acute renal ischaemia [24]. In addition, increased Caspase-3 activity was reported following the administration of nephrotoxic doses of cyclosporine A in salt-depleted rats [36].

The staining profile of Caspase-3 reported here is similar to that reported for Bax in remnant kidneys, especially in dilated tubules, sclerotic glomeruli and fibrotic interstitial areas [28]. This indicates that Bax and Caspase-3 may have a coordinating role in the processing of apoptotic cell death. Caspase-3 is potentially the most important effector enzyme in apoptosis, providing a common pathway for death receptor (Fas/FasL), mitochondria-dependent (Bax/Bcl-2 related) or endoplasmic reticulum-mediated apoptosis [7, 10, 37]. In light of our previous findings of changes in the Bax/Bcl-2 ratio in this model [28], it seems likely that Caspase-3 activation may be linked with the changes of Bax/Bcl-2.

While our results clearly implicate Caspase-3 in apoptosis associated with progressive renal scarring, it is important to note that Caspase-3 also is involved in the inflammation as indicated by the positive correlation between the Caspase-3 activity, proteins, mRNA and cellular inflammation in remnant kidneys. While the remnant kidney model of renal scarring is not initiated by an immune response, the progression of fibrosis has been associated with the severity of the late interstitial inflammatory infiltrate [27, 38]. This was supported in our study by the strong association between the severity of the monocytic interstitial infiltrate and interstitial fibro-

sis. In addition, we noted that this inflammatory monocytic (ED-1+) infiltrate paralleled the gradual increase of apoptosis in glomeruli, tubules and interstitium. Such a persistent inflammation may favor a microenvironment for uncontrolled apoptosis of renal cells. This not only may be due to the direct action of various inflammatory cells to instigate apoptosis through cell to cell contact [39], but also due to the inevitable changes in cytokines and growth factors that accompany inflammatory cells. Many of these, such as transforming growth factor-β1 [40–41] and tumor necrosis factor-α (TNF-α) [42], are highly influential on apoptotic rates.

The pivotal role of Caspase-3 in the apoptosis machinery makes it an attractive target to regulate apoptosis-related cell death. In vitro, the induction of apoptosis in mouse proximal tubule cells by cisplatin has been inhibited by Ac-Asp-Glu-Val-Asp-H, a known Caspase-3 inhibitor [43]. Application of this therapeutic approach in vivo is clearly more problematic, although has met with some success despite fears relating to the potential tumorigenic consequences of inhibiting apoptosis. For example, elevated apoptosis of hepatic parenchymal cells during endotoxemia (TNF-α mediated) was prevented by injection of Z-VAD, a strong Caspase-3 inhibitor [44]. It has been also been reported that the administration of B-D-FMK (a pan caspase inhibitor) was neuro-protective when given by intra-cerebral or systemic injection after cerebral hypoxia-ischemia [45]. More recently, it has been reported Z-VAD-FMK reduced the Caspase-3 activity and prevented the early onset of not only renal apoptosis, but also inflammation and tissue injury in a mouse model of renal ischemia [46]. Given these findings a similar blockade of Caspase-3 in progressive renal scarring may provide a novel therapeutic approach to the treatment of renal scarring by controlling inappropriate apoptosis of renal cells.

In conclusion, we have demonstrated, to our knowledge for the first time, significant increases in Caspase-3 at the activity, protein and mRNA levels, which coincide with elevated apoptosis in a non-immune mediated chronic renal fibrosis model. During the SNx time course, the increase of Caspase-3 activity was associated with the elevated precursor and active Caspase-3 proteins, which resulted from the increase of Caspase-3 mRNA transcription indicating the requirement for de novo synthesis of Caspase-3. Caspase-3 activity was a good predictor of apoptosis occurrence associated with GS and TA. The manipulation of Caspase-3 could therefore be a therapeutic target for prevention renal cell deletion by uncontrolled apoptosis and the subsequent renal fibrosis.

ACKNOWLEDGMENTS

The authors would like to thank the National Kidney Research Fund, the Northern General Hospital NHS Trust Research Committee, the Sheffield Kidney Research Foundation and the Sheffield Kidney Patients Association for their financial support of this study. Part of this work was presented in abstract form at the 33rd American Society of Nephrology meeting, Toronto, Ontario, Canada, October 2000.

Reprint requests to Bin Yang, M.D., Sheffield Kidney Institute, Northern General Hospital, The University of Sheffield, Herries Road, Sheffield S5 7AU, England, United Kingdom.
E-mail: Bin.Yang@Sheffield.ac.uk

REFERENCES

1. Savill J, Smith J, Sarraf C, *et al*: Glomerular mesangial cells and inflammatory macrophages ingest neutrophils undergoing apoptosis. *Kidney Int* 42:924–936, 1992
2. Baker AJ, Mooney A, Hughes J, *et al*: Mesangial cell apoptosis: The major mechanism for resolution of glomerular hypercellularity in experimental mesangial proliferative nephritis. *J Clin Invest* 94: 2105–2116, 1994
3. Sugiyama H, Kashihara N, Makino H, *et al*: Apoptosis in glomerular sclerosis. *Kidney Int* 49:103–111, 1996
4. Shimizu A, Masuda Y, Kitamura H, *et al*: Apoptosis in progressive crescentic glomerulonephritis. *Lab Invest* 74:941–951, 1996
5. Truong LD, Petrusevska G, Yang G, *et al*: Cell apoptosis and proliferation in experimental chronic obstructive uropathy. *Kidney Int* 50:200–207, 1996
6. Thomas GL, Yang B, Wagner BE, *et al*: Cellular apoptosis and proliferation in experimental renal fibrosis. *Nephrol Dial Transplant* 13:2216–2226, 1998
7. Rudel T: Caspase inhibitors in prevention of apoptosis. *Herz* 24: 236–241, 1999
8. Thornberry NA, Rano TA, Peterson EP, *et al*: A combinatorial approach defines specificities of members of the caspase family and granzyme B. Functional relationships established for key mediators of apoptosis. *J Biol Chem* 272:17907–17911, 1997
9. Rotonda J, Nicholson DW, Fazil KM, *et al*: The three-dimensional structure of apopain/CPP32, a key mediator of apoptosis. *Nat Struct Biol* 3:619–625, 1996
10. Nakagawa T, Zhu H, Morishima N, *et al*: Caspase-12 mediates endoplasmic-reticulum-specific apoptosis and cytotoxicity by amyloid-β. *Nature* 403:98–103, 2000
11. Thornberry NA: The caspase family of cysteine proteases. *Br Med Bull* 53:478–490, 1997
12. Yang B, Johnson TS, Thomas GL, *et al*: Apoptosis and Caspase-3 in experimental anti-glomerular basement membrane nephritis. *J Am Soc Nephrol* 12:485–495, 2001
13. Muchaneta Kubara EC, El Nahas AM: Myofibroblast phenotypes expression in experimental renal scarring. *Nephrol Dial Transplant* 12:904–915, 1997
14. Johnson TS, Griffin M, Thomas GL, *et al*: The role of transglutaminase in the rat subtotal nephrectomy model of renal fibrosis. *J Clin Invest* 99:2950–2960, 1997
15. El Nahas AM: Growth factors and glomerular sclerosis. *Kidney Int* 41(Suppl 36):S15–S20, 1992
16. Muchaneta Kubara EC, Sayed Ahmed N, El Nahas AM: Subtotal nephrectomy: a mosaic of growth factors. *Nephrol Dial Transplant* 10:320–327, 1995
17. Gavrieli Y, Sherman Y, Ben Sasson SA: Identification of programmed cell death in situ via specific labeling of nuclear DNA fragmentation. *J Cell Biol* 119:493–501, 1992
18. Saraste A: Morphologic criteria and detection of apoptosis. *Herz* 24:189–195, 1999
19. Gobé G, Zhang XJ, Willgoss DA, *et al*: Relationship between expression of Bcl-2 genes and growth factors in ischemic acute renal failure in the rat. *J Am Soc Nephrol* 11:454–467, 2000
20. Zhang G, Moorhead PJ, El Nahas AM: Myofibroblasts and the progression of experimental glomerulonephritis. *Exp Nephrol* 3: 308–318, 1995
21. Haycock JW, Falkous G, Maltin CA, *et al*: Effect of prednisone on protease activities and structural protein levels in rat muscles in vivo. Clin Chim Acta 249:47–58, 1996
22. Shehata M, Cope GH, Johnson TS, *et al*: Cyclosporine enhances the expression of TGF-beta in the juxtaglomerular cells of the rat kidney. *Kidney Int* 48:1487–1496, 1995

23. JOHNSON TS, SKILL NJ, EL NAHAS AM, *et al*: Transglutaminase transcription and antigen translocation in experimental renal scarring. *J Am Soc Nephrol* 10:2146–2157, 1999
24. KAUSHAL GP, SINGH AB, SHAH SV: Identification of gene family of caspases in rat kidney and altered expression in ischemia-reperfusion injury. *Am J Physiol* 274:F587–F595, 1998
25. SHIFMAN MI, STEIN DG: A reliable and sensitive method for nonradioactive Northern blot analysis of nerve growth factor mRNA from brain tissues. *J Neurosci Methods* 59:205–208, 1995
26. DOUTHWAITE JA, JOHNSON TS, HAYLOR JL, *et al*: Effects of transforming growth factor-β1 on renal extracellular matrix components and their regulating proteins. *J Am Soc Nephrol* 10:2109–2119, 1999
27. EL NAHAS AM, PARASKEVAKOU H, ZOOB S, *et al*: Effect of dietary protein restriction on the development of renal failure after subtotal nephrectomy in rats. *Clin Sci* 65:399–406, 1983
28. YANG B, JOHNSON TS, THOMAS GL, *et al*: The expression of apoptosis-related genes and proteins in experimental chronic renal scarring. *J Am Soc Nephrol* 12:275–288, 2001
29. THORNBERRY NA: Interleukin-1 beta converting enzyme. *Methods Enzymol* 244:615–631, 1994
30. SCHLEGEL J, PETERS I, ORRENIUS S, *et al*: CPP32/apopain is a key interleukin 1 beta converting enzyme-like protease involved in Fas-mediated apoptosis. *J Biol Chem* 271:1841–1844, 1996
31. FERNANDES-ALNEMRI T, LITWACK G, ALNEMRI ES: CPP32, a novel human apoptotic protein with homology to Caenorhabditis elegans cell death protein Ced-3 and mammalian interleukin-1 beta-converting enzyme. *J Biol Chem* 269:30761–30764, 1994
32. SABBATINI P, HAN J, CHIOU SK, *et al*: Interleukin 1 beta converting enzyme-like proteases are essential for p53-mediated transcriptionally dependent apoptosis. *Cell Growth Differ* 8:643–653, 1997
33. ARMSTRONG RC, AJA TJ, HOANG KD, *et al*: Activation of the CED3/ICE-related protease CPP32 in cerebellar granule neurons undergoing apoptosis but not necrosis. *J Neurosci* 15:553–562, 1997
34. KRAJEWSKI S, GASCOYNE RD, ZAPATA JM, *et al*: Immunolocalization of the ICE/Ced-3-family protease, CPP32 (Caspase-3), in non-Hodgkin's lymphomas, chronic lymphocytic leukemias, and reactive lymph nodes. *Blood* 89:3817–3825, 1997
35. KRAJEWSKA M, WANG HG, KRAJEWSKI S, *et al*: Immunohistochemical analysis of in vivo patterns of expression of CPP32 (Caspase-3), a cell death protease. *Cancer Res* 57:1605–1613, 1997
36. SHIHAB FS, ANDOH TF, TANNER AM, *et al*: Expression of apoptosis regulatory genes in chronic cyclosporine nephrotoxicity favors apoptosis. *Kidney Int* 56:2147–2159, 1999
37. COHEN GM: Caspases: The executioners of apoptosis. *Biochem J* 326:1–16, 1997
38. FUJIHARA CK, DE LOURDES NORONHA I, MALHEIROS DM, *et al*: Combined mycophenolate mofetil and losartan therapy arrests established injury in the remnant kidney. *J Am Soc Nephrol* 11:283–290, 2000
39. MIX JE, ZETTL UK, ZIELASEK J, *et al*: Apoptosis induction by macrophage-derived reactive oxygen species in myelin-specific T cells requires cell-cell contact. *Neuroimmunol* 95:152–156, 1999
40. EDDY AA: Experimental insights into the tubulointerstitial disease accompanying primary glomerular lesions. *J Am Soc Nephrol* 5: 1273–1287, 1994
41. BURSCH W, OBERHAMMER F, JIRTLE RL, *et al*: Transforming growth factor-beta 1 as a signal for induction of cell death by apoptosis. *Br J Cancer* 67:531–536, 1993
42. ORTIZ A, LORZ C, GONZÁLEZ CUADRADO S, *et al*: Cytokines and Fas regulate apoptosis in murine renal interstitial fibroblasts. *J Am Soc Nephrol* 8:1845–1854, 1997
43. FUKUOKA K, TAKEDA M, KOBAYASHI M, *et al*: Distinct interleukin-1beta-converting enzyme family proteases mediate cisplatin- and staurosporine-induced apoptosis of mouse proximal tubule cells. *Life Sci* 62:1125–1138, 1998
44. JAESCHKE H, FISHER MA, LAWSON JA, *et al*: Activation of Caspase-3 (CPP32)-like proteases is essential for TNF-alpha-induced hepatic parenchymal cell apoptosis and neutrophil-mediated necrosis in a murine endotoxin shock model. *J Immunol* 160:3480–3486, 1998
45. CHENG Y, DESHMUKH M: DCosta A, *et al*: Caspase inhibitor affords neuroprotection with delayed administration in a rat model of neonatal hypoxic-ischemic brain injury. *J Clin Invest* 101:1992–1999, 1998
46. DAEMEN MA, VAN'T VEER C, DENECKER G, *et al*: Inhibition of apoptosis induced by ischemia-reperfusion prevents inflammation. *J Clin Invest* 104:541–549, 1999